Novel Synthesis, Characterization and Properties of Graphene Nanoplatelets Reinforced Cu-Ni Alloy Matrix Composites

THESIS

Submitted in partial fulfilment of the requirements for the degree of

DOCTOR OF PHILOSOPHY

by

PINGALE AJAY DADABHAU

Under the Supervision of

Dr. Sachin U. Belgamwar
&
Prof. Jitendra S. Rathore

BITS Pilani
Pilani Campus

BIRLA INSTITUTE OF TECHNOLOGY & SCIENCE, PILANI

PILANI-333031, RAJASTHAN, INDIA

2022

BIRLA INSTITUTE OF TECHNOLOGY AND SCIENCE, PILANI

CERTIFICATE

This is to certify that the thesis titled **"Novel Synthesis, Characterization and Properties of Graphene Nanoplatelets Reinforced Cu-Ni Alloy Matrix Composites"** submitted by **Pingale Ajay Dadabhau** ID No **2017PHXF0408P** for award of Ph.D. of the institute embodies original work done by him under our supervision.

Signature of Co- Supervisor
Prof. Jitendra S. Rathore
Associate Professor,
Mechanical Engineering Department,
Birla Institute of Technology and Science, Pilani,
Rajasthan-333031, India
Date:

Signature of Supervisor
Dr. Sachin U. Belgamwar
Assistant Professor,
Mechanical Engineering Department,
Birla Institute of Technology and Science, Pilani,
Rajasthan-333031, India
Date:

Acknowledgement

My heartfelt and foremost gratitude is expressed to my supervisor **Dr. Sachin U. Belgamwar** and co-supervisor **Prof. Jitendra S. Rathore**, for welcoming me onboard on this stimulating research and for being the best supervisors I could ever wish for. I express my sincere thanks to **Dr. Sachin U. Belgamwar** for introducing me to this fascinating research on metal and alloy matrix nanocomposites. I offer my respectful obeisance unto the lotus feet of my both supervisors for all his valuable guidance, excellent direction, everlasting encouragement and inspiration given to me without which the present work would not have been possible. It was indeed my privilege to work under the supervision of the supervision of both. Their expertise in presenting the scientific work added scientific value in my thesis.

I am immensely thankful to **Prof. Souvik Bhattacharyya**, Vice-Chancellor, BITS Pilani, and **Prof. Sudhir Kumar Barai**, Director, BITS Pilani, Pilani Campus for their support and blessings. I express my gratitude to **Prof. S. K. Verma** (Dean, Administration, BITS Pilani, Pilani Campus) for his kind support. I also express my sincere thanks to **Prof. Shamik Chakraborty**, Associate Dean, Academic-Graduate Studies & Research Division (AGSRD) for his motivation, constant support and encouragement. I thank **Prof. Srikanta Routroy**, Head of the Department of Mechanical Engineering for his valuable support and guidance. I am highly indebted to **Prof. Navin Singh**, Associate Dean, Student Welfare Division, for his encouragement and suggestions.

I express sincere thanks to **Dr. Venkatesh K. P.**, DRC convener, Department of Mechanical Engineering. I pay my heartfelt gratitude to my DAC members **Prof. P. Srinivasan** and **Prof. Sharad Shrivastava** for their valuable suggestions and for sparing their valuable time for departmental evaluation of this thesis. I would also like to acknowledge all faculty members as well as non-academic staff of Department of Mechanical Engineering for their support, encouragement and cooperation. It is my pleasure to acknowledge the individuals who have contributed to the evolution of this work.

I owe my gratitude to fellow research scholars of Mechanical Engineering Department for their constant support. I would like to thank and appreciate my dearest friends Ayush Owhal, Harsh Sharma, Diplesh Gautam, Pradnya Chabbi, Ashish Khare, Naveen P.T, Shital Patil and Shrikant Pawar for their support. Words cannot do justice to the support, love and affection I have received during this research work from my parents **Shri Dadabhau Pingale** and **Sau Leelabai Pingale** and my brother **Mr. Vijay Pingale**. Last but not the least, I pray and thank the Almighty for showering HIS divine blessings and giving me an inner strength and patience.

Ajay D. Pingale

Abstract

Nowadays, the nanoparticle reinforced alloy-based composites are emerging materials for structural applications in automobile, marine, aerospace and chemical industries due to their high strength-to-weight ratio, good corrosion resistance and wear resistance properties. Cu-Ni alloys are widely applied as a coating material for several industrial applications due to their good strength, high wear and corrosion resistance. The addition of nickel in copper can improve mechanical strength and corrosion resistance properties. At present, Cu-Ni alloy coatings are widely employed in heat exchangers, marine hardware, condensers and piping in seawater systems. The performance of Cu-Ni alloy coatings is usually associated with their microstructure, composition and surface characteristics. Therefore, many researchers all over the globe are taking efforts to enhance the properties of Cu-Ni alloy by the reinforcement of nanoparticles.

A significant amount of research on Cu-Ni alloy-based composite coatings using electrodeposition method has been carried out. However, very few literatures are available on the fabrication of Cu-Ni alloy-based composites using the powder metallurgy method. Also, a more efficient method needs to be developed for facile, low cost and bulk production of Cu-Ni alloy-based composites. Cu-Ni alloy-based composites prepared using graphene as a reinforcing element through the electrodeposition method suggest a most simple and economical way to improve the overall properties.

Towards realization of this newer material, in this thesis we focused on synthesis of (i) Cu-Ni/Gr composite coatings by electro-co-deposition method and (ii) Cu-Ni/Gr composites by a modified electro-co-deposition method followed by powder metallurgy method. To achieve the objective of the proposed research, the thesis is divided into seven chapters. Some of the salient features of these chapters are as follows:

In Chapter 1, a brief introduction of composites, classification of composites, nanomaterials, nanomaterial reinforced composites and need of Cu-Ni/Gr composites have been discussed. The aim of the present work is also discussed at the end of the chapter.

In Chapter 2, different techniques for the fabrication of Cu-Ni alloy-based composites have been discussed thoroughly for their merits and demerits with respect to Cu-Ni alloy-based composites.

The effect of various process parameters, bath composition and type of reinforcing elements have been discussed in detail. Also, detail review of mechanical, tribological and electrical properties of the Cu-Ni alloy-based composites is carried out and arranged chronologically to study the evolution of the composites. the scope of the present work towards designing of newer method is discussed at the end of this chapter.

In chapter 3, the synthesis of Cu-Ni/Gr composite has been discussed in two different forms. 1. Electro-co-deposition of Cu-Ni/Gr coating on the metallic substrate 2. Synthesis of Cu-Ni/Gr composites in the powder form by using a modified electrochemical-co-deposition method which is a simple, economical and suitable for bulk production of Cu-Ni/Gr composite powder.

In chapter 4, the detailed study of surface morphology, elemental composition, and microstructure of Cu-Ni/Gr composite coatings prepared by electro-co-deposition method and Cu-Ni/Gr composite powder prepared by a modified electro-co-deposition method have been carried out.

In chapter 5, details of the mechanical, tribological and corrosion properties of Cu-Ni/Gr composite coatings prepared by electro-co-deposition method are explained. Also, the mechanical, tribological and corrosion properties of Cu-Ni/Gr composites plates prepared from the samples of the powder synthesized by modified electro-co-deposition method and followed by powder metallurgy method are discussed.

In chapter 6, the effect of electrolysis parameters and graphene nanoplatelets concentration on mechanical and corrosion properties of Cu-Ni/Gr composite coatings prepared by the electro-co-deposition method has been discussed. Also, the effect of electrolysis parameters on mechanical and corrosion properties of Cu-Ni/Gr composites plates prepared from the samples of the powder fabricated using a modified electrochemical-co-deposition method followed by the conventional powder metallurgy method has been discussed. The set of experiments is performed based on the design developed by the Taguchi method.

In Chapter 7, the overall conclusions and future scope of the present study have been discussed.

Table of Contents

CONTENTS

List of Figures

List of Tables

Chapter 1
Introduction

The need for superior mechanical, tribological, electrical, optical, and corrosion properties has resulted in extensive research work in the development of metal matrix composites (MMCs). MMCs have been extensively used in several industries such as aerospace, chemical, automobile and marine due to their enhanced mechanical and physical properties [1]–[3]. MMCs are composites embedding reinforcement into a metal matrix to obtain desirable functional properties which are not offered by conventional unreinforced monolithic metal or metal alloy counterparts. MMCs have been fabricated using different methods such as powder metallurgy, electrodeposition, chemical vapor deposition, physical vapor deposition, plasma spraying, and thermal spraying [4]–[6]. However, electrodeposition and powder metallurgy methods are most extensively employed to fabricate MMCs [7]. Several reinforcing elements such as graphene, carbon nanotubes, Al_2O_3, TiO_2, SiC, and Y_2O_3 have been added into a metal matrix [8]. Especially, graphene reinforced MMCs have attracted lots of attention due to their extraordinary properties such as mechanical strength, hardness, wear, and corrosion resistance, thermal and electrical conductivity, and creep resistance [9], [10]. In graphene reinforced MMCs, Cu, Ti, Ni, Zn, Mg, and Al or their alloys have been employed as matrix [11].

Copper and its alloys are well known for their remarkable properties such as good electrical and thermal conductivities, mechanical strength, corrosion resistance, and aesthetic appearance, thus expanding their applications in machinery, electronic, transport and marine industries [12]. Among all these alloys, Cu-Ni alloys are widely applied as a coating material for several industrial applications due to their excellent strength, wear resistance and corrosion resistance properties [13]. The addition of nickel in copper can improve the mechanical strength and corrosion resistance properties. Cu-Ni alloy coatings are widely employed in heat exchangers, marine hardware, condensers, and piping in seawater systems [14]. The performance of Cu-Ni alloy coatings is usually associated with their microstructure, composition, and surface characteristics. Therefore, many researchers all over the globe are making efforts to enhance the properties of Cu-Ni alloy coatings.

The properties of material surfaces exposed to mechanical and corrosive environments have been enhanced by applying Cu-Ni alloy coating rather than enhancing the properties

of the entire material. To enhance the mechanical and corrosion properties of Cu-Ni alloy coating, many researchers have focused on the addition of reinforcement particles in the Cu-Ni alloy coating. Cu-Ni alloy matrix composite coatings are promising to increase the lifetime of engineering components in harsh conditions. This chapter describes a brief introduction of composites and the problem statement investigated in this thesis.

1.1 Composite

Composite materials are materials made from two or more different constituent materials, with properties that are significantly different from the properties of constituent materials. In far back as 1200 B.C, Egyptians and Hebrews have fabricated synthetic composite by the addition of straw as reinforcement in bricks to enhance their mechanical properties. Wattle and daub is 6000 years old synthetic composite material and has been used in many historic buildings. Fiberglass is the first modern composite material and is extensively used in car bodies, building panels, sports equipment and boat hulls. Drivers for improved composite materials are weight reduction, cost reduction as well as to improve performance by enhancing resistance to fatigue, corrosion, and mechanical damage. To meet the requirement of a particular application, the composite material can be fabricated by selecting an appropriate reinforcing element and matrix material. Composite materials include reinforced concrete, reinforced plastics, ceramic matrix composite, metal matrix composites, plywood, etc. Composite materials have been commonly used for bridges, buildings and structural material for storage tanks and bathtubs. Also, composite materials have been used for industrial applications due to their high strength, less expensive, or lightweight than traditional materials. Currently, composite materials are widely employed in advanced engineering applications such as sensing, computation, communication, and actuation.

1.1.1 Matrix

In composite material, the matrix serves different functions such as transfer load between the reinforcement, binds the reinforcement, provides the composite component its net shape and protects the reinforcement from mechanical and environmental damage. A composite matrix may be ceramic, polymer, metal, or carbon. The polymer matrix is widely used in aerospace applications due to its good mechanical, electrical, and chemical properties. Ceramic and metal matrices are widely used in automobile and aerospace

applications due to their high mechanical strength. The carbon matrix is commonly used in high-temperature applications due to its superior thermal resistance.

1.1.2 Reinforcement

The reinforcement element is generally used to enhance the desired properties of the matrix material. Reinforcements are categorized into different groups: whiskers, short fibers, continuous fibers, platelets, and particles. The enhancement in the properties of the composites depends upon the type of reinforcement, the orientation of reinforcement and the geometry of reinforcement. The roles of reinforcement are to carry the load from the matrix and strengthen the composite by improving its overall properties. Reinforcements are also used for the special purpose of resistance to corrosion, heat resistance, heat conduction, improve the strength and provide rigidity. As per the functional requirements, a specific reinforcement could be selected for the fabrication of composites.

1.2 Classification of Composites

A composite material consists of two basic parts: Matrix and reinforcement. Composite materials can be classified by their matrix type. A composite matrix may be ceramic, polymer, metal, or carbon. Therefore, a composite material could be categorized as ceramic matrix composites (CMCs), polymer matrix composites (PMCs), carbon-carbon composites (CCCs), or metal matrix composites (MMCs) [15].

1.2.1 Ceramic matrix composites

Ceramic matrix composites (CMCs) are composite materials and key materials for advanced energy systems. They generally consist of ceramic fibers or whiskers reinforced in a ceramic matrix, developing a ceramic fiber-reinforced material. CMCs have been developed to overcome the brittleness problem of unreinforced ceramic materials. SiC/SiC, C/C, Al_2O_3/Al_2O_3, and C/SiC are the most commonly used CMCs in several industrial applications. Applications for CMCs are being considered for the recirculating fan, Gas-fired radiant, burner tubes, canned motor, filtration, and heat exchanger [16].

1.2.2 Polymer matrix composites

Polymer matrix composites (PMCs) are composite materials comprised of a specific type of fiber, bound together by the polymer matrix to accomplish desired properties. The fiber of PMCs consists of aramid, glass fiber, and graphite. PMCs are easy to fabricate compared to metal-matrix, ceramic-matrix, and carbon-matrix. PMCs have many

advantages such as good abrasion and corrosion resistance, lightweight, high strength, and high stiffness along the direction of reinforcement. Nowadays, PMCs are widely used in automobiles, aircraft, marine structures, and other moving structures [17].

1.2.3 Carbon-carbon composites

Carbon-carbon composites (CCCs) are consist of graphitic carbon fiber reinforced carbon matrix. CCCs are commonly used for high strength and modulus of rigidity. Also, these composites are lightweight and can withstand up to 3000 °C. CCCs are widely used in aircraft, rocket nozzles, space shuttle nose tip, F1-racing cars and train brakes due to their remarkable properties such as high thermal and abrasion resistance, high electrical conductivity, low density and high strength [18].

1.2.4 Metal matrix composites

Metal matrix composites (MMCs) are composite materials synthesized by incorporating various reinforcing phases in the metal matrix. MMCs are the potential contestants for operation in complex service conditions such as marine, nuclear power plants, automobile, chemical and infrastructure. In MMCs, the main matrix materials may be Ni, Cu, Al, Mg, and Ti. The main reinforcements used are alumina, carbide, and silicon. MMCs with lightweight and high strength have been developed for satellites, aircraft, missiles, jet engines, and high-speed machinery. Presently, MMC is used in diesel engine piston developed by Toyota, which shows high wear resistance and high-temperature strength [17]. MMCs are most commonly used in several engineering applications. Presently, particulate reinforced MMCs have attracted considerable attention from researchers worldwide due to their low cost, ease of synthesis, and near-isometric enhancement in the overall properties. Also, the incorporation of nanoparticles in the metal matrix has shown significant enhancement in the mechanical, tribological, electrical, tribological, optical, and corrosion properties of the resulting composite. In the next section, a brief introduction to some reinforcing nanomaterials and the significance of the nanosize effect are discussed.

1.3 Nanomaterials

Nanotechnology and nanoscience fields have attracted considerable research interest due to their wide range of applications and numerous benefits in several engineering sectors. Nanoparticles are defined as particulate matter with at least one dimension is less than 100 nm [19]. When the scale of the material is within the range of 1-100 nm, the properties of

the material may change so abruptly so that the material may have some outstanding properties. Nanomaterials differs in properties from their macro counterpart. Many natural nanoparticles are present in the volcano dust, soil, seawater spills, humid matter, colloidal clay, soil, and atmosphere on the earth [20]. Nanomaterials synthesized by nanotechnology have superior flexibility, strength, and surface-to-volume ratio. Atoms present on the surface of nanoparticles are quite active compared to other atoms. The powder form of nanoparticles can be used as a catalyst or solid fuel in the rocket [21]. Nanoparticles are being widely used in electronics, optics, medicine, chemistry, agricultural, food industries, and automobile industries [22].

Graphene, carbon nanotube (CNT), and c60 fullerene are 2-, 1- and 0-dimensional nanomaterials, respectively, and their properties are not similar to macroscopic carbon materials. The unexpected properties of nanocarbon have a novel scientific field that can drastically change our lifestyle. Among the various types of nanoparticles, graphene nanoplatelets have been paid special attention (Figure 1.1).

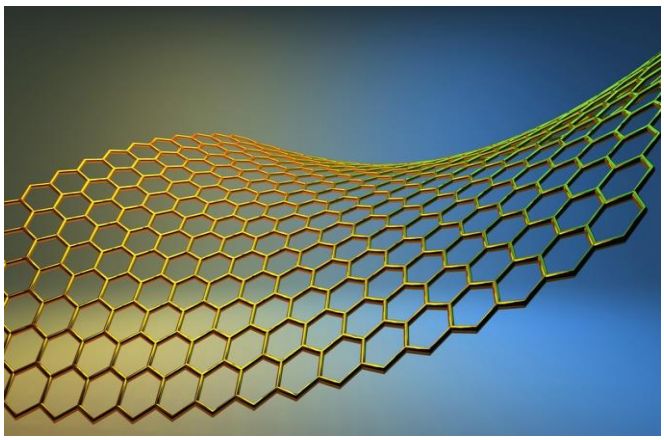

Figure 1.1: Graphene structure of the single two-dimensional hexagonal sheet of carbon atoms[1]

Graphene is a one-atom-thick planar sheet of sp^2 hybridized carbon atoms arranged in a crystal lattice and yet stronger than diamond [23]. In 2004, graphene was firstly isolated from graphite by the mechanical exfoliation method [24]–[27]. To date, various methods to produce graphene have been developed, such as exfoliation and cleavage, thermal chemical vapor deposition, plasma-enhanced chemical vapor deposition, thermal decompositions, electrochemical method, and pulsed-laser scribing [28]. Graphene has

[1] https://newatlas.com/graphene-inexpensive-electronics-university-glasgow/40508/

achieved immense research interest in recent years due to its outstanding properties, such as large theoretical specific surface area, excellent electrical conductivity, and high mechanical strength [29]. It's remarkable electronic, mechanical, optical, electrochemical, and thermal properties compared with other carbon materials, which makes it a promising material in electrical, chemical and automobile industrial applications [30], [31]. Graphene has superior properties such as high fracture toughness (125 GPa), super charge-carrier mobility (200,000 $cm^2V^{-1}s^{-1}$), high Young's modulus (1 TPa), extreme thermal conductivity (5,000 $Wm^{-1}K^{-1}$) and higher fracture toughness of 125 GPa [32]–[35]. Graphene has been widely used in electronic industries due to its superior carrier mobility (up to 350,000 $cm^2\ V^{-1}\ s^{-1}$) and high optical transparency (97.7%) [36], [37].

The advantage of graphene over CNT using in the composites includes high-pressure processing result in damage of CNT structure; the possibility of graphene to disperse uniformly in the metal matrix without agglomeration; short CNT serve as a good reinforcing element however, not suitable for wear applications, CNT forms only point to point contact however, graphene has strong interfacial bonding, fracture strengthening is more in graphene composites because of its planar geometry and high aspect ratio [38]. These extraordinary properties make graphene an ideal reinforcing material for the composites, for possible enhancement in mechanical, tribological and corrosion properties of the resulting composite. To have the advantage of their extraordinary properties at the bulk level, scientists are exploring the possibility of preparing composites, termed as graphene reinforced composites, which are detailed in the next section.

1.4 Composite reinforced with graphene

Metal matrix composites have shown increased strength compared to conventional materials [39]–[42]. Recently, several authors have fabricated graphene reinforced metal composites for metals like Al [43]–[49], Cu [33]–[49], Mg [63]–[67], Ni [68] and Ti [63]. Different research groups have been developed different processing routes for graphene reinforced metal matrix composites like powder metallurgy, casting, electroless deposition, melting and solidification, thermal spray, laser deposition, electrochemical deposition, sol-gel, and other novel routes [69]. Electrodeposition and powder metallurgy methods are extensively used for the synthesis of graphene reinforced composites owing to several advantages over the other conventional processes [5], [40], [70], [71].

There are two approaches for the synthesis of graphene metal matrix composites that have been developed to enhance the mechanical, tribological, and corrosion properties. In the first approach, graphene reinforced composites are formed through uniform dispersion of graphene. However, in the second approach, graphene reinforced composites are developed by forming layered structures by alternate deposition of graphene and metal matrix [35], [54], [72], [73]. Graphene is very light in weight and cannot be dissolved in water, and it can be dispersed uniformly in a plating solution using a surfactant [74], [75]. The strong graphene coupling to the metal matrix particles caused highly increase in the thermal conductivity [76]–[78]. Recently graphene gained extensive interest in electrochemistry field and has many applications in various sectors like biosensors [79], supercapacitors [80], transparent electrodes [81]–[85], sensors [86]–[88], nanoscale electronic devices [89], and field emission devices [90] and filler materials [91], [92].

Owing to the outstanding properties of graphene, it is believed that it could significantly improve the performance of composites. Also, graphene is ideal to be an efficient reinforcing element to achieve high-quality metal matrix composite coatings.

1.5 Need for Cu-Ni/Graphene composites

A wide range of objects, be they components, tools, sub-assemblies, machines, or entire plants are made from different types of materials. In most cases, the lifetime of these materials is strongly affected by external factors and the operational environment. The surface of the components is usually damaged due to the mechanical interaction between the surfaces of the components in contact with each other as well as electrochemical reactions with the environment [93]. The surface of the component is the most vulnerable site for different forms of attacks, including chemical, mechanical, thermal, or electrochemical. Such types of attacks may be present individually or in combination and lead to damaging changes at the surface. The damaging changes at the surface arise due to oxidation, erosion, electrochemical corrosion, scaling, cavitation, weathering, microbiological damage, and wear. The recognition that one might protect a surface from operational and environmental conditions by applying a metallic, organic or inorganic coating, so extending the life of not just the surface but also the entire component.

Nowadays, deterioration of active metals such as Al, Mg, and Fe under the influence of wear and corrosion is a serious problem faced by marine, automobile and chemical industries [94]. Among these active metals, mild steel is extensively used due to its good

mechanical strength, low cost and durability. The rate of wear and corrosion can be controlled using some approaches such as a change in the surrounding environment, selection of materials and use of metallic coatings. Among these approaches use of metallic coating is the most acceptable approach [95]. The efficiency of metallic components that are exposed to corrosion and wear is possible to improve by applying pure and alloy coatings.

Alloy deposition is an old technique and same scientific principles as individual metals electrodeposition [96]. The interest in the utilization of alloy coating is increased due to the wide range of possible alloy combinations and the related possible applications. Alloy coatings have superior properties in certain composition ranges than those of individuals metal coatings. They can be harder, better resistance against corrosion, stronger and tougher, more wear resistance and superior in magnetic properties.

Copper is alloyed with different elements and mainly classified into three groups: bronzes, brasses, and copper-nickel alloys [39]. Some of the industrial applications of Cu-Ni alloy are shown in Figure 1.2. Copper-nickel alloy coatings are more popular due to their better corrosion resistance in seawater and remarkable physical properties such as high density, high melting point and high strength [97]. Cu-Ni alloy coatings, in addition to automobile and marine applications, find several applications in gas, oil, and chemical industries [12], [98]–[102].

Graphene is a novel nanomaterial having excellent mechanical, chemical, electrical and thermal properties [32], [89], [103]–[107]. In the last decade, graphene reinforced metal composites have attracted the extensive interest of researchers. Many researchers have reported to fabricate graphene reinforced composites for different metal such as Al [108], [109], Cu [9], [54], [110], Mg [64], [65], [67], Ni [111]–[113] and Ag [114]. The reinforcement of graphene improved the chemical, electrical, mechanical, tribological and corrosion properties of metal matrix [54], [113], but graphene reinforced alloy composites are less studied.

Currently, many different methods are adopted to prepare graphene reinforced metal composites coatings, such as electrodeposition and powder metallurgy [35], [115]. Electrodeposition is an economical and simplest process to fabricate metal composite coatings. Also, the properties of prepared composites coatings can be controlled by

optimizing the process parameters such as pH, current density, temperature, reinforcement concentration, and bath composition [116]–[118].

Figure 1.2: Some of the industrial applications of Cu-Ni alloy

Over the past few years, Cu-Ni alloy coatings have attracted considerable scientific and industrial interest [119]. The addition of nickel to copper coating reduces the coefficient of thermal expansion, and improves its resistance to corrosion, cavitation, and erosion in all kinds of water [120]. Due to this, Cu-Ni alloy coatings are widely used to reduce corrosion and wear rate. Hence, it finds large number of applications in piping, condensers and heat exchangers in seawater system, desalination plants, marine hardware, boat hulls, oil rigs and platforms, seawater intake screens, fish farming cages, etc [14], [97], [102], [121]–[123]. Also, Cu-Ni alloy components are used in bearing fasteners, gears, pump and valve trim, bolting, Shafts, bearing bushes, forgings, firewater systems and hydraulic tubing.

The incorporation of graphene can improve the properties of Cu-Ni alloy as they may improve the corrosion or wear resistance. To prepare high-performance the Cu-Ni matrix composite, the main challenges are to improve the dispersion of graphene nanoplatelets

and the interfacial interaction between the Cu-Ni matrix and graphene nanoplatelets. A strong interaction between the graphene nanoplatelets and the Cu-Ni matrix is important to transfer stress across the interface, thereby significantly affects the mechanical properties. The main aim of the present work is to enhance the properties of Cu-Ni/Gr composite by improving the dispersion and the interaction between the graphene nanoplatelets and the Cu-Ni matrix.

Employing incorporation of graphene nanoplatelets in the Cu-Ni matrix seen to be interesting, since graphene nanoplatelets can affect on mechanical, tribological and corrosion properties. Therefore, it is necessary to fabricate Cu-Ni/Gr composite, which would improve the mechanical, tribological and corrosion properties of engineering components by using the electrodeposition method.

Among many issues and challenges, the present thesis addresses the uniform dispersion aspect of graphene in the Cu-Ni matrix to enhance the mechanical, tribological and corrosion properties of Cu-Ni/Gr composites. The next chapter presents a detailed review of the different Cu-Ni matrix composite synthesis processes and the properties of the Cu-Ni alloy matrix composite achieved by various methods. Based on the literature review and discussion, the problem statement addressed in this thesis is formed and presented.

References

[1] W. . Chen, J. . Tu, L. . Wang, H. . Gan, Z. . Xu, and X. . Zhang, “Tribological application of carbon nanotubes in a metal-based composite coating and composites,” *Carbon N. Y.*, vol. 41, no. 2, pp. 215–222, Feb. 2003, doi: 10.1016/S0008-6223(02)00265-8.

[2] Z. Hu *et al.*, “Graphene-reinforced metal matrix nanocomposites - A review,” *Mater. Sci. Technol. (United Kingdom)*, vol. 32, no. 9, pp. 930–953, 2016, doi: 10.1080/02670836.2015.1104018.

[3] S. R. Bakshi, D. Lahiri, and A. Agarwal, “Carbon nanotube reinforced metal matrix composites - a review,” *Int. Mater. Rev.*, vol. 55, no. 1, pp. 41–64, 2010, doi: 10.1179/095066009X12572530170543.

[4] D. Janas and B. Liszka, “Copper matrix nanocomposites based on carbon nanotubes or graphene,” *Mater. Chem. Front.*, pp. 22–35, 2017, doi: 10.1039/C7QM00316A.

[5] M. Rashad, F. Pan, A. Tang, M. Asif, and M. Aamir, “Synergetic effect of graphene nanoplatelets (GNPs) and multi-walled carbon nanotube (MW-CNTs) on mechanical properties of pure magnesium,” *J. Alloys Compd.*, vol. 603, pp. 111–118, 2014, doi: 10.1016/j.jallcom.2014.03.038.

[6] K. Shirvanimoghaddam *et al.*, “Carbon fiber reinforced metal matrix composites: Fabrication processes and properties,” *Compos. Part A Appl. Sci. Manuf.*, vol. 92, pp. 70–96, 2017, doi: 10.1016/j.compositesa.2016.10.032.

[7] P. Hidalgo-Manrique, X. Lei, R. Xu, M. Zhou, I. A. Kinloch, and R. J. Young, “Copper/graphene composites: a review,” *J. Mater. Sci.*, vol. 54, no. 19, pp. 12236–12289, 2019, doi: 10.1007/s10853-019-03703-5.

[8] M. Alizadeh and H. Safaei, “Characterization of Ni-Cu matrix, Al2O3 reinforced nano-composite coatings prepared by electrodeposition,” *Appl. Surf. Sci.*, vol. 456, pp. 195–203, Oct. 2018, doi: 10.1016/j.apsusc.2018.06.095.

[9] K. Chu and C. Jia, “Enhanced strength in bulk graphene-copper composites,” *Phys. status solidi*, vol. 211, no. 1, pp. 184–190, Jan. 2014, doi: 10.1002/pssa.201330051.

[10] F. Chen, J. Ying, Y. Wang, S. Du, Z. Liu, and Q. Huang, “Effects of graphene

content on the microstructure and properties of copper matrix composites," *Carbon N. Y.*, vol. 96, pp. 836–842, 2016, doi: 10.1016/j.carbon.2015.10.023.

[11] H. G. Prashantha Kumar and M. Anthony Xavior, "Graphene reinforced metal matrix composite (GRMMC): A review," *Procedia Eng.*, vol. 97, pp. 1033–1040, 2014, doi: 10.1016/j.proeng.2014.12.381.

[12] I. Baskaran, T. S. N. Sankara Narayanan, and A. Stephen, "Pulsed electrodeposition of nanocrystalline Cu–Ni alloy films and evaluation of their characteristic properties," *Mater. Lett.*, vol. 60, no. 16, pp. 1990–1995, Jul. 2006, doi: 10.1016/j.matlet.2005.12.065.

[13] C. R. Thurber *et al.*, "Metal Matrix Composite Coatings of Cupronickel Embedded with Nanoplatelets for Improved Corrosion Resistant Properties," *Int. J. Corros.*, vol. 2018, pp. 1–11, Jun. 2018, doi: 10.1155/2018/5250713.

[14] C. R. Thurber *et al.*, "Electrodeposition of 70-30 Cu–Ni nanocomposite coatings for enhanced mechanical and corrosion properties," *Curr. Appl. Phys.*, vol. 16, no. 3, pp. 387–396, Mar. 2016, doi: 10.1016/j.cap.2015.12.022.

[15] M. K. Surappa, "Microstructure evolution during solidification of DRMMCs (discontinuously reinforced metal matrix composites): State of art," *J. Mater. Process. Technol.*, vol. 63, no. 1–3, pp. 325–333, 1997, doi: 10.1016/S0924-0136(96)02643-X.

[16] W. Krenkel, *Ceramic Matrix Composites: Fiber Reinforced Ceramics and their Applications*. Wiley, 2008. [Online]. Available: https://books.google.co.in/books?id=j81hCENfG60C

[17] U. S. C. Office of Technology Assesment, *Advanced materials by design.* U.S. Government Printing Office, 1988. [Online]. Available: https://books.google.co.in/books?id=cuIh1Qb7xc8C

[18] G. Savage, G. Savage, and G. M. Savage, *Carbon-Carbon Composites*. Chapman & Hall, 1993. [Online]. Available: https://books.google.co.in/books?id=_qF2BD9sI-wC

[19] C. M. Hussain, *Nanomaterials in Chromatography: Current Trends in Chromatographic Research Technology and Techniques*. Elsevier Science, 2018. [Online]. Available: https://books.google.co.in/books?id=64RfDwAAQBAJ

[20] H. A. Khan and I. A. Arif, *Toxic Effects of Nanomaterials*. Bentham Science, 2012. [Online]. Available: https://books.google.co.in/books?id=v700zEYcY3gC

[21] D. Shi, *Nanomaterials and Devices*. Elsevier Science, 2014. [Online]. Available: https://books.google.co.in/books?id=OER0AwAAQBAJ

[22] S. Kanchi and S. Ahmed, *Green Metal Nanoparticles: Synthesis, Characterization and their Applications*. Wiley, 2018. [Online]. Available: https://books.google.co.in/books?id=LmatDwAAQBAJ

[23] M. Skoda, I. Dudek, A. Jarosz, and D. Szukiewicz, "Graphene: One Material, Many Possibilities—Application Difficulties in Biological Systems," *J. Nanomater.*, vol. 2014, pp. 1–11, 2014, doi: 10.1155/2014/890246.

[24] J. Park *et al.*, "3D structure of individual nanocrystals in solution by electron microscopy," *Science (80-.).*, vol. 349, no. 6245, pp. 290–295, Jul. 2015, doi: 10.1126/science.aab1343.

[25] A. K. Geim, "Graphene: Status and Prospects," *Science (80-.).*, vol. 324, no. 5934, pp. 1530–1534, Jun. 2009, doi: 10.1126/science.1158877.

[26] A. K. Geim, "Nobel Lecture: Random walk to graphene," *Rev. Mod. Phys.*, vol. 83, no. 3, pp. 851–862, Aug. 2011, doi: 10.1103/RevModPhys.83.851.

[27] K. S. Novoselov, "Nobel Lecture: Graphene: Materials in the Flatland," *Rev. Mod. Phys.*, vol. 83, no. 3, pp. 837–849, 2011, doi: 10.1103/RevModPhys.83.837.

[28] W. Choi, I. Lahiri, R. Seelaboyina, and Y. S. Kang, "Synthesis of Graphene and Its Applications: A Review," *Crit. Rev. Solid State Mater. Sci.*, vol. 35, no. 1, pp. 52–71, Feb. 2010, doi: 10.1080/10408430903505036.

[29] M. J. Allen, V. C. Tung, and R. B. Kaner, "Honeycomb Carbon: A Review of Graphene," *Chem. Rev.*, vol. 110, no. 1, pp. 132–145, Jan. 2010, doi: 10.1021/cr900070d.

[30] M. S. Fuhrer, C. N. Lau, and A. H. MacDonald, "Graphene: Materially Better Carbon," *MRS Bull.*, vol. 35, no. 4, pp. 289–295, Apr. 2010, doi: 10.1557/mrs2010.551.

[31] V. Singh, D. Joung, L. Zhai, S. Das, S. I. Khondaker, and S. Seal, "Graphene based materials: Past, present and future," *Prog. Mater. Sci.*, vol. 56, no. 8, pp. 1178–1271, Oct. 2011, doi: 10.1016/j.pmatsci.2011.03.003.

[32] C. Lee, X. Wei, J. W. Kysar, and J. Hone, “Measurement of the Elastic Properties and Intrinsic Strength of Monolayer Graphene,” *Science (80-.).*, vol. 321, no. 5887, pp. 385–388, Jul. 2008, doi: 10.1126/science.1157996.

[33] S. Graphene, A. A. Balandin, S. Ghosh, W. Bao, and I. Calizo, “Superior Thermal Conductivity of,” *Nano*, 2008.

[34] K. I. Bolotin *et al.*, “Ultrahigh electron mobility in suspended graphene,” *Solid State Commun.*, vol. 146, no. 9–10, pp. 351–355, 2008, doi: 10.1016/j.ssc.2008.02.024.

[35] J. Wang, Z. Li, G. Fan, H. Pan, Z. Chen, and D. Zhang, “Reinforcement with graphene nanosheets in aluminum matrix composites,” *Scr. Mater.*, vol. 66, no. 8, pp. 594–597, Apr. 2012, doi: 10.1016/j.scriptamat.2012.01.012.

[36] R. R. Nair *et al.*, “Fine Structure Constant Defines Visual Transparency of Graphene,” *Science (80-.).*, vol. 320, no. 5881, pp. 1308–1308, Jun. 2008, doi: 10.1126/science.1156965.

[37] L. Banszerus *et al.*, “Ultrahigh-mobility graphene devices from chemical vapor deposition on reusable copper,” *Sci. Adv.*, vol. 1, no. 6, p. e1500222, Jul. 2015, doi: 10.1126/sciadv.1500222.

[38] M. Anthony Xavior and H. G. Prashantha Kumar, “Processing and Characterization Techniques of Graphene Reinforced Metal Matrix Composites (GRMMC); A Review,” *Mater. Today Proc.*, vol. 4, no. 2, pp. 3334–3341, 2017, doi: 10.1016/j.matpr.2017.02.220.

[39] A. D. Pingale, S. U. Belgamwar, and J. S. Rathore, “Effect of Graphene Nanoplatelets Addition on the Mechanical, Tribological and Corrosion Properties of Cu–Ni/Gr Nanocomposite Coatings by Electro-co-deposition Method,” *Trans. Indian Inst. Met.*, vol. 73, no. 1, pp. 99–107, Jan. 2020, doi: 10.1007/s12666-019-01807-9.

[40] H. Yang, X. Guo, N. Birbilis, G. Wu, and W. Ding, “Tailoring nickel coatings via electrodeposition from a eutectic-based ionic liquid doped with nicotinic acid,” *Appl. Surf. Sci.*, vol. 257, no. 21, pp. 9094–9102, 2011, doi: 10.1016/j.apsusc.2011.05.106.

[41] W. Zhai *et al.*, “Investigation of mechanical and tribological behaviors of

multilayer graphene reinforced Ni3Al matrix composites," *Compos. Part B Eng.*, vol. 70, pp. 149–155, 2015, doi: 10.1016/j.compositesb.2014.10.052.

[42] N. V. Ponraj *et al.*, "Effect of milling on dispersion of graphene nanosheet reinforcement in different morphology copper powder matrix," *Surfaces and Interfaces*, vol. 9, no. June, pp. 260–265, 2017, doi: 10.1016/j.surfin.2017.10.006.

[43] S. Dixit, A. Mahata, D. R. Mahapatra, S. V. Kailas, and K. Chattopadhyay, "Multi-layer graphene reinforced aluminum – Manufacturing of high strength composite by friction stir alloying," *Compos. Part B Eng.*, vol. 136, no. August 2017, pp. 63–71, 2018, doi: 10.1016/j.compositesb.2017.10.028.

[44] R. Ranjan, N. K. Singh, A. P. Jaiswal, and V. Bajpai, "Metal matrix nano composites using graphene nano platelets indented on copper particles in aluminium matrix," *Adv. Mater. Lett.*, vol. 9, no. 09, pp. 652–655, 2018, doi: 10.5185/amlett.2018.2078.

[45] M. Kostecki, J. Woźniak, T. Cygan, M. Petrus, and A. Olszyna, "Tribological Properties of Aluminium Alloy Composites Reinforced with Multi-Layer Graphene—The Influence of Spark Plasma Texturing Process," *Materials (Basel).*, vol. 10, no. 8, p. 928, Aug. 2017, doi: 10.3390/ma10080928.

[46] B. L. Dasari, M. Morshed, J. M. Nouri, D. Brabazon, and S. Naher, "Mechanical properties of graphene oxide reinforced aluminium matrix composites," *Compos. Part B Eng.*, vol. 145, no. January, pp. 136–144, 2018, doi: 10.1016/j.compositesb.2018.03.022.

[47] P. Ashwath and M. A. Xavior, "The Effect of Ball Milling & Reinforcement Percentage on Sintered Samples of Aluminium Alloy Metal Matrix Composites," *Procedia Eng.*, vol. 97, pp. 1027–1032, 2014, doi: 10.1016/j.proeng.2014.12.380.

[48] S. J. Niteesh Kumar, R. Keshavamurthy, M. R. Haseebuddin, and P. G. Koppad, "Mechanical Properties of Aluminium-Graphene Composite Synthesized by Powder Metallurgy and Hot Extrusion," *Trans. Indian Inst. Met.*, vol. 70, no. 3, pp. 605–613, 2017, doi: 10.1007/s12666-017-1070-5.

[49] P. Hidalgo-Manrique *et al.*, "Microstructure and mechanical behaviour of aluminium matrix composites reinforced with graphene oxide and carbon nanotubes," *J. Mater. Sci.*, vol. 52, no. 23, pp. 13466–13477, 2017, doi: 10.1007/s10853-017-1450-6.

[50] G. Xie, M. Forslund, and J. Pan, “Direct Electrochemical Synthesis of Reduced Graphene Oxide (rGO)/ Copper Composite Films and Their Electrical / Electroactive Properties,” *ACS Appl. Mater. Interfaces*, vol. 6, pp. 7444–7455, 2014, doi: 10.1021/am500768g.

[51] D. B. Xiong *et al.*, “Graphene-and-Copper Artificial Nacre Fabricated by a Preform Impregnation Process: Bioinspired Strategy for Strengthening-Toughening of Metal Matrix Composite,” *ACS Nano*, vol. 9, no. 7, pp. 6934–6943, 2015, doi: 10.1021/acsnano.5b01067.

[52] P. Sadowski, K. Kowalczyk-Gajewska, and S. Stupkiewicz, “Classical estimates of the effective thermoelastic properties of copper-graphene composites,” *Compos. Part B Eng.*, vol. 80, pp. 278–290, 2015, doi: 10.1016/j.compositesb.2015.06.007.

[53] X. Liu *et al.*, “In-situ synthesis of graphene nanosheets coated copper for preparing reinforced aluminum matrix composites,” *Mater. Sci. Eng. A*, vol. 709, no. August 2017, pp. 65–71, 2018, doi: 10.1016/j.msea.2017.10.030.

[54] J. Hwang *et al.*, “Enhanced Mechanical Properties of Graphene/Copper Nanocomposites Using a Molecular-Level Mixing Process,” *Adv. Mater.*, vol. 25, no. 46, pp. 6724–6729, Dec. 2013, doi: 10.1002/adma.201302495.

[55] L. Wang *et al.*, “Graphene-copper composite with micro-layered grains and ultrahigh strength,” *Sci. Rep.*, vol. 7, no. 1, p. 41896, Mar. 2017, doi: 10.1038/srep41896.

[56] D. Zhang and Z. Zhan, “Strengthening effect of graphene derivatives in copper matrix composites,” *J. Alloys Compd.*, vol. 654, pp. 226–233, 2016, doi: 10.1016/j.jallcom.2015.09.013.

[57] K. Jagannadham, “Thermal conductivity of copper-graphene composite films synthesized by electrochemical deposition with exfoliated graphene platelets,” *Metall. Mater. Trans. B Process Metall. Mater. Process. Sci.*, vol. 43, no. 2, pp. 316–324, 2012, doi: 10.1007/s11663-011-9597-z.

[58] C. Ayyappadas, A. Muthuchamy, A. Raja Annamalai, and D. K. Agrawal, “An investigation on the effect of sintering mode on various properties of copper-graphene metal matrix composite,” *Adv. Powder Technol.*, vol. 28, no. 7, pp. 1760–1768, Jul. 2017, doi: 10.1016/j.apt.2017.04.013.

[59] R. Song, “Study on Graphene Reinforced Copper Contact Material,” *MATEC Web Conf.*, vol. 100, p. 04010, Mar. 2017, doi: 10.1051/matecconf/201710004010.

[60] K. Jagannadham, “Orientation dependence of thermal conductivity in copper-graphene composites,” *J. Appl. Phys.*, vol. 110, no. 7, 2011, doi: 10.1063/1.3641640.

[61] Y. Peng, Y. Hu, L. Han, and C. Ren, “Ultrasound-assisted fabrication of dispersed two-dimensional copper/reduced graphene oxide nanosheets nanocomposites,” *Compos. Part B Eng.*, vol. 58, pp. 473–477, 2014, doi: 10.1016/j.compositesb.2013.10.036.

[62] X. Wangl, Q. Wangl, Y. Hul, L. Tanl, and J. Cail, “Copper and graphene composite material prepared by electrodeposition and its potential application for 3D integration,” pp. 1672–1675, 2017.

[63] M. Rashad *et al.*, “Effect of graphene nanoplatelets (GNPs) addition on strength and ductility of magnesium-titanium alloys,” *J. Magnes. Alloy.*, vol. 1, no. 3, pp. 242–248, 2013, doi: 10.1016/j.jma.2013.09.004.

[64] M. Rashad *et al.*, “Development of magnesium-graphene nanoplatelets composite,” *J. Compos. Mater.*, vol. 49, no. 3, pp. 285–293, Feb. 2015, doi: 10.1177/0021998313518360.

[65] M. Rashad, F. Pan, M. Asif, and X. Chen, “Corrosion behavior of magnesium-graphene composites in sodium chloride solutions,” *J. Magnes. Alloy.*, vol. 5, no. 3, pp. 271–276, Sep. 2017, doi: 10.1016/j.jma.2017.06.003.

[66] M. Rashad, F. Pan, M. Asif, and A. Tang, “Powder metallurgy of Mg-1%Al-1%Sn alloy reinforced with low content of graphene nanoplatelets (GNPs),” *J. Ind. Eng. Chem.*, vol. 20, no. 6, pp. 4250–4255, 2014, doi: 10.1016/j.jiec.2014.01.028.

[67] M. Rashad, F. Pan, H. Hu, M. Asif, S. Hussain, and J. She, “Enhanced tensile properties of magnesium composites reinforced with graphene nanoplatelets,” *Mater. Sci. Eng. A*, vol. 630, pp. 36–44, Apr. 2015, doi: 10.1016/j.msea.2015.02.002.

[68] C. M. P. Kumar, T. V. Venkatesha, and R. Shabadi, “Preparation and corrosion behavior of Ni and Ni-graphene composite coatings,” *Mater. Res. Bull.*, vol. 48,

no. 4, pp. 1477–1483, 2013, doi: 10.1016/j.materresbull.2012.12.064.

[69] R. Casati and M. Vedani, "Metal Matrix Composites Reinforced by Nano-Particles—A Review," *Metals (Basel).*, vol. 4, no. 1, pp. 65–83, 2014, doi: 10.3390/met4010065.

[70] E. Rudnik, L. Burzyńska, Ł. Dolasiński, and M. Misiak, "Electrodeposition of nickel/SiC composites in the presence of cetyltrimethylammonium bromide," *Appl. Surf. Sci.*, vol. 256, no. 24, pp. 7414–7420, 2010, doi: 10.1016/j.apsusc.2010.05.082.

[71] S. A. Lajevardi and T. Shahrabi, "Effects of pulse electrodeposition parameters on the properties of Ni-TiO2 nanocomposite coatings," *Appl. Surf. Sci.*, vol. 256, no. 22, pp. 6775–6781, 2010, doi: 10.1016/j.apsusc.2010.04.088.

[72] L. Y. Chen *et al.*, "Novel nanoprocessing route for bulk graphene nanoplatelets reinforced metal matrix nanocomposites," *Scr. Mater.*, vol. 67, no. 1, pp. 29–32, 2012, doi: 10.1016/j.scriptamat.2012.03.013.

[73] Z. Li *et al.*, "Uniform dispersion of graphene oxide in aluminum powder by direct electrostatic adsorption for fabrication of graphene/aluminum composites," *Nanotechnology*, vol. 25, no. 32, 2014, doi: 10.1088/0957-4484/25/32/325601.

[74] C. Song, D. Wu, F. Zhang, P. Liu, Q. Lu, and X. Feng, "Gemini surfactant assisted synthesis of two-dimensional metal nanoparticles/graphene composites," *Chem. Commun.*, vol. 48, no. 15, p. 2119, 2012, doi: 10.1039/c2cc16890a.

[75] M. Lotya, P. J. King, U. Khan, S. De, and J. N. Coleman, "High-Concentration, Surfactant- Stabilized Graphene Dispersions," *ACS Nano*, vol. 4, no. 6, pp. 3155–3162, 2010, doi: 10.1021/nn1005304.

[76] K. M. F. Shahil and A. A. Balandin, "Graphene-multilayer graphene nanocomposites as highly efficient thermal interface materials," *Nano Lett.*, vol. 12, no. 2, pp. 861–867, 2012, doi: 10.1021/nl203906r.

[77] K. M. F. Shahil and A. A. Balandin, "Thermal properties of graphene and multilayer graphene: Applications in thermal interface materials," *Solid State Commun.*, vol. 152, no. 15, pp. 1331–1340, 2012, doi: 10.1016/j.ssc.2012.04.034.

[78] V. Goyal and A. A. Balandin, "Thermal properties of the hybrid graphene-metal nano-micro-composites: Applications in thermal interface materials," *Appl. Phys.*

Lett., vol. 100, no. 7, 2012, doi: 10.1063/1.3687173.

[79] Y. Zhou *et al.*, "Electrostatic self-assembly of graphene-silver multilayer films and their transmittance and electronic conductivity," *Carbon N. Y.*, vol. 50, no. 12, pp. 4343–4350, 2012, doi: 10.1016/j.carbon.2012.04.069.

[80] Y. Dai *et al.*, "Fabrication of self-binding noble metal/flexible graphene composite paper," *Carbon N. Y.*, vol. 50, no. 12, pp. 4648–4654, 2012, doi: 10.1016/j.carbon.2012.05.053.

[81] B. G. Choi, J. Hong, W. H. Hong, P. T. Hammond, and H. Park, "Facilitated Ion Transport in All-Solid- State Flexible Supercapacitors," *ACS Nano*, vol. 5, no. 9, pp. 7205–7213, 2011.

[82] K. Zhang, L. L. Zhang, X. S. Zhao, and J. Wu, "Graphene/polyaniline nanofiber composites as supercapacitor electrodes," *Chem. Mater.*, vol. 22, no. 4, pp. 1392–1401, 2010, doi: 10.1021/cm902876u.

[83] G. Jo *et al.*, "Large-scale patterned multi-layer graphene films as transparent conducting electrodes for GaN light-emitting diodes," *Nanotechnology*, vol. 21, no. 17, p. 175201, Apr. 2010, doi: 10.1088/0957-4484/21/17/175201.

[84] L. Tang, Y. Wang, Y. Li, H. Feng, J. Lu, and J. Li, "Preparation, Structure, and Electrochemical Properties of Reduced Graphene Sheet Films," *Adv. Funct. Mater.*, vol. 19, no. 17, pp. 2782–2789, Sep. 2009, doi: 10.1002/adfm.200900377.

[85] K. S. Kim *et al.*, "Large-scale pattern growth of graphene films for stretchable transparent electrodes," *Nature*, vol. 457, no. 7230, pp. 706–710, 2009, doi: 10.1038/nature07719.

[86] N. Hu *et al.*, "Gas sensor based on p-phenylenediamine reduced graphene oxide," *Sensors Actuators, B Chem.*, vol. 163, no. 1, pp. 107–114, 2012, doi: 10.1016/j.snb.2012.01.016.

[87] J. C. Reed, H. Zhu, A. Y. Zhu, C. Li, and E. Cubukcu, "Graphene-enabled silver nanoantenna sensors," *Nano Lett.*, vol. 12, no. 8, pp. 4090–4094, 2012, doi: 10.1021/nl301555t.

[88] X. Huang *et al.*, "Reduced graphene oxide–polyaniline hybrid: Preparation, characterization and its applications for ammonia gas sensing," *J. Mater. Chem.*, vol. 22, no. 42, p. 22488, 2012, doi: 10.1039/c2jm34340a.

[89] A. K. Geim and K. S. Novoselov, “The rise of graphene,” *Nat. Mater.*, vol. 6, no. 3, pp. 183–191, Mar. 2007, doi: 10.1038/nmat1849.

[90] M. A. Raza, A. Westwood, A. Brown, N. Hondow, and C. Stirling, “Characterisation of graphite nanoplatelets and the physical properties of graphite nanoplatelet/silicone composites for thermal interface applications,” *Carbon N. Y.*, vol. 49, no. 13, pp. 4269–4279, 2011, doi: 10.1016/j.carbon.2011.06.002.

[91] J. Yan *et al.*, “Preparation of a graphene nanosheet/polyaniline composite with high specific capacitance,” *Carbon N. Y.*, vol. 48, no. 2, pp. 487–493, 2010, doi: 10.1016/j.carbon.2009.09.066.

[92] N. Hu *et al.*, “A Facile Route for the Large Scale Fabrication of Graphene Oxide Papers and Their Mechanical Enhancement by Cross-linking with Glutaraldehyde,” *Nano-Micro Lett.*, vol. 3, no. 4, pp. 215–222, 2011, doi: 10.1007/BF03353675.

[93] N. Kanani, *Electroplating: Basic Principles, Processes and Practice*. Elsevier Science, 2004. [Online]. Available: https://books.google.co.in/books?id=Ii1e-pp1pq0C

[94] B. Ranjith and G. P. Kalaignan, “Ni–Co–TiO2 nanocomposite coating prepared by pulse and pulse reversal methods using acetate bath,” *Appl. Surf. Sci.*, vol. 257, no. 1, pp. 42–47, 2010, doi: https://doi.org/10.1016/j.apsusc.2010.06.029.

[95] R. A. Shakoor, R. Kahraman, U. S. Waware, Y. Wang, and W. Gao, “Properties of Electrodeposited Ni-B-ZrO2 Composite Coatings,” *Int. J. Electrochem. Sc.*, vol. 10, pp. 2110–2119, 2015.

[96] M. Schlesinger and M. Paunovic, *Modern Electroplating*. Wiley, 2011. [Online]. Available: https://books.google.co.in/books?id=j3OSKTCuO00C

[97] D. Goranova, G. Avdeev, and R. Rashkov, “Electrodeposition and characterization of Ni-Cu alloys,” *Surf. Coatings Technol.*, vol. 240, pp. 204–210, 2014, doi: 10.1016/j.surfcoat.2013.12.014.

[98] S. Mohan and N. Rajasekaran, “Influence of electrolyte pH on composition, corrosion properties and surface morphology of electrodeposited Cu–Ni alloy,” *Surf. Eng.*, vol. 27, no. 7, pp. 519–523, 2011, doi: 10.1179/026708410x12786785573472.

[99] E. Pellicer *et al.*, “Surface & Coatings Technology A comparison between fi ne-grained and nanocrystalline electrodeposited Cu – Ni fi lms . Insights on mechanical and corrosion performance,” *Surf. Coat. Technol.*, vol. 205, no. 23–24, pp. 5285–5293, 2011, doi: 10.1016/j.surfcoat.2011.05.047.

[100] U. Sarac, R. M. Öksüzoğlu, and M. C. Baykul, “Deposition potential dependence of composition, microstructure, and surface morphology of electrodeposited Ni-Cu alloy films,” *J. Mater. Sci. Mater. Electron.*, vol. 23, no. 12, pp. 2110–2116, 2012, doi: 10.1007/s10854-012-0709-6.

[101] S. K. Ghosh, A. K. Grover, G. K. Dey, and M. K. Totlani, “Nanocrystalline Ni-Cu alloy plating by pulse electrolysis,” *Surf. Coatings Technol.*, vol. 126, no. 1, pp. 48–63, 2000, doi: 10.1016/S0257-8972(00)00520-X.

[102] P. Q. Dai, C. Zhang, J. C. Wen, H. C. Rao, and Q. T. Wang, “Tensile Properties of Electrodeposited Nanocrystalline Ni-Cu Alloys,” *J. Mater. Eng. Perform.*, vol. 25, no. 2, pp. 594–600, Feb. 2016, doi: 10.1007/s11665-016-1881-2.

[103] A. A. Balandin *et al.*, “Superior Thermal Conductivity of Single-Layer Graphene,” *Nano Lett.*, vol. 8, no. 3, pp. 902–907, Mar. 2008, doi: 10.1021/nl0731872.

[104] S. Liu, K. Chen, Y. Fu, S. Yu, and Z. Bao, “Reduced graphene oxide paper by supercritical ethanol treatment and its electrochemical properties,” *Appl. Surf. Sci.*, vol. 258, no. 13, pp. 5299–5303, Apr. 2012, doi: 10.1016/j.apsusc.2012.02.023.

[105] S. Liu, J. Ou, Z. Li, S. Yang, and J. Wang, “Layer-by-layer assembly and tribological property of multilayer ultrathin films constructed by modified graphene sheets and polyethyleneimine,” *Appl. Surf. Sci.*, vol. 258, no. 7, pp. 2231–2236, Jan. 2012, doi: 10.1016/j.apsusc.2011.09.011.

[106] Y.-H. Ding *et al.*, “Surface adhesion properties of graphene and graphene oxide studied by colloid-probe atomic force microscopy,” *Appl. Surf. Sci.*, vol. 258, no. 3, pp. 1077–1081, Nov. 2011, doi: 10.1016/j.apsusc.2011.09.005.

[107] A. Siokou, F. Ravani, S. Karakalos, O. Frank, M. Kalbac, and C. Galiotis, “Surface refinement and electronic properties of graphene layers grown on copper substrate: An XPS, UPS and EELS study,” *Appl. Surf. Sci.*, vol. 257, no. 23, pp. 9785–9790, Sep. 2011, doi: 10.1016/j.apsusc.2011.06.017.

[108] R. Pérez-Bustamante, D. Bolaños-Morales, J. Bonilla-Martínez, I. Estrada-Guel, and R. Martínez-Sánchez, "Microstructural and hardness behavior of graphene-nanoplatelets/aluminum composites synthesized by mechanical alloying," *J. Alloys Compd.*, vol. 615, no. S1, pp. S578–S582, Dec. 2014, doi: 10.1016/j.jallcom.2014.01.225.

[109] S. Rengifo, C. Zhang, S. Harimkar, B. Boesl, and A. Agarwal, "Tribological Behavior of Spark Plasma Sintered Aluminum-Graphene Composites at Room and Elevated Temperatures," *Technologies*, vol. 5, no. 1, p. 4, Jan. 2017, doi: 10.3390/technologies5010004.

[110] X. Gao *et al.*, "Mechanical properties and thermal conductivity of graphene reinforced copper matrix composites," *Powder Technol.*, vol. 301, pp. 601–607, Nov. 2016, doi: 10.1016/j.powtec.2016.06.045.

[111] A. Jabbar *et al.*, "Electrochemical deposition of nickel graphene composite coatings: effect of deposition temperature on its surface morphology and corrosion resistance," *RSC Adv.*, vol. 7, no. 49, pp. 31100–31109, 2017, doi: 10.1039/C6RA28755G.

[112] J. Jiang, X. He, J. Du, X. Pang, H. Yang, and Z. Wei, "In-situ fabrication of graphene-nickel matrix composites," *Mater. Lett.*, vol. 220, no. March, pp. 178–181, Jun. 2018, doi: 10.1016/j.matlet.2018.03.039.

[113] G. Yasin *et al.*, "Synthesis of spheres-like Ni/graphene nanocomposite as an efficient anti-corrosive coating; effect of graphene content on its morphology and mechanical properties," *J. Alloys Compd.*, vol. 755, pp. 79–88, Jul. 2018, doi: 10.1016/j.jallcom.2018.04.321.

[114] R. Gao *et al.*, "Paper-like graphene-Ag composite films with enhanced mechanical and electrical properties," *Nanoscale Res. Lett.*, vol. 8, no. 1, p. 32, 2013, doi: 10.1186/1556-276X-8-32.

[115] D. Kuang, L. Xu, L. Liu, W. Hu, and Y. Wu, "Graphene-nickel composites," *Appl. Surf. Sci.*, vol. 273, pp. 484–490, 2013, doi: 10.1016/j.apsusc.2013.02.066.

[116] G. Brankovic, V. M. Maksimovic, and N. D. Nikolic, "Effect of the anodic current density on copper electrodeposition in the hydrogen co-deposition range by the reversing current (RC) regime," *J. Electroanal. Chem.*, vol. 661, pp. 309–316, 2011, doi: 10.1016/j.jelechem.2011.08.006.

[117] T. N. Ostanina, A. A. Uritskaya, V. M. Rudoi, N. I. Ostanin, and O. V Ryabova, “Effect of pH on the electrodeposition kinetics of copper from acetate and sulfosalicylate complex solutions,” *Russ. Chem. Bull.*, vol. 63, no. 7, pp. 1498–1503, Jul. 2014, doi: 10.1007/s11172-014-0626-3.

[118] D. Zhang and Z. Zhan, “Preparation of graphene nanoplatelets-copper composites by a modified semi-powder method and their mechanical properties,” *J. Alloys Compd.*, vol. 658, pp. 663–671, Feb. 2016, doi: 10.1016/j.jallcom.2015.10.252.

[119] M. Metikoš-Huković, R. Babić, I. Škugor Rončević, and Z. Grubač, “Corrosion resistance of copper-nickel alloy under fluid jet impingement,” *Desalination*, vol. 276, no. 1–3, pp. 228–232, 2011, doi: 10.1016/j.desal.2011.03.056.

[120] V. Zin, K. Brunelli, and M. Dabalà, “Characterization of Cu-Ni alloy electrodeposition and synthesis of nanoparticles by pulsed sonoelectrochemistry,” *Mater. Chem. Phys.*, vol. 144, no. 3, pp. 272–279, 2014, doi: 10.1016/j.matchemphys.2013.12.028.

[121] K. Ngamlerdpokin and N. Tantavichet, “Electrodeposition of nickel-copper alloys to use as a cathode for hydrogen evolution in an alkaline media,” *Int. J. Hydrogen Energy*, vol. 39, no. 6, pp. 2505–2515, 2014, doi: 10.1016/j.ijhydene.2013.12.013.

[122] P. Calleja, J. Esteve, P. Cojocaru, L. Magagnin, E. Vallés, and E. Gómez, “Developing plating baths for the production of reflective Ni–Cu films,” *Electrochim. Acta*, vol. 62, pp. 381–389, Feb. 2012, doi: 10.1016/j.electacta.2011.12.049.

[123] J. Ahmed *et al.*, “Bimetallic Cu-Ni nanoparticles of varying composition (CuNi3, CuNi, Cu3Ni),” *Colloids Surfaces A Physicochem. Eng. Asp.*, vol. 331, no. 3, pp. 206–212, 2008, doi: 10.1016/j.colsurfa.2008.08.007.

Chapter 2

Literature Review

Chapter 1 showed that Cu-Ni alloy matrix composites are beneficial in several industrial applications to overcome the existing challenges. This chapter summarizes the latest progress in the fabrication of Cu-Ni composites and provides an insight into the fabrication of Cu-Ni alloy matrix composites through electrodeposition and powder metallurgy methods. The gaps in research and the scope of future research are discussed in detail at the end of the chapter.

2.1. Introduction

As the frontier of modern technology and science spread out into more complex and sophisticated fields, the operating system tackles harsh working conditions. Therefore, modern technology quests for systems with high performance in extreme and often an adverse working environment. The material surface is the most vulnerable site for different forms of attacks, including mechanical, electrochemical, chemical and thermal. As these attacks proceed, the degradation of material surfaces is initiated and leads to damaging changes at the material surface. The damages mainly due to the corrosion and wear attack at the material surface are not recoverable. Therefore, the protection of the material surface is very important. The degradation of material surfaces can be decreased by applying a surface coating or changing the entire material of the part that will lessen the effect of given working conditions and surrounding environment and extending the service life, not just the surface but the entire equipment. However, the application of a protective coating is more feasible and economical than changing the entire material of the part. Thus, surface modification technologies have found a wide range of applications in several engineering industries to protect the material surface from corrosion and wear. The selection of the suitable coating technique depends upon many factors including, application, economics, feasibility, etc. Cu-Ni alloy parts and Cu-Ni alloy coatings have been widely used in most engineering applications due to their unique physical and mechanical property. However, in order to enhance their performance in harsh working conditions, reinforcing elements have been added to them. Therefore, in the next section, we have discussed the several fabrication methods which are used in the fabrication of Cu-Ni alloy composites.

2.2. Fabrication Methods

Several fabrication methods such as chemical vapor deposition, electrodeposition, physical vapor deposition, plasma spraying, and thermal spraying have been developed over the past few years to enhance the structure and properties of the MMCs. However, electrodeposition and powder metallurgy methods are most widely employed for the synthesis of Cu-Ni alloy composites (Figure 2.1). Electrodeposition method has been used to synthesize Cu-Ni alloy and Cu-Ni alloy composite coatings to protect the base material from harsh working conditions. However, powder metallurgy has been used for the synthesis of Cu-Ni alloy and Cu-Ni alloy composites.

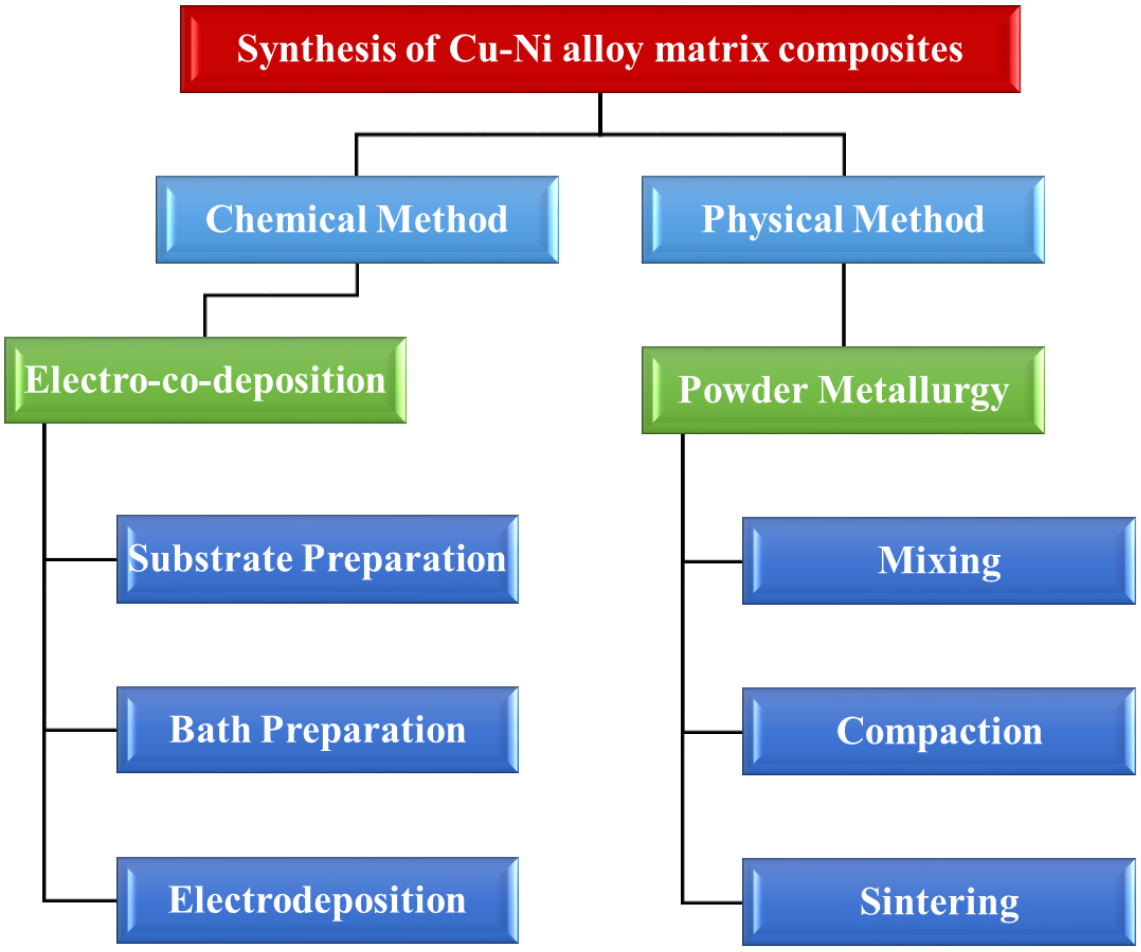

Figure 2.1: Methods for the synthesis of Cu-Ni alloy matrix composites

2.3. Electro-co-deposition Method

Among the different surface coating techniques, the electrodeposition technique is widely used due to the low capital and operating cost, easy to operate, and comparatively fast for

the fabrication of the coating compared to other methods. The electrodeposition technique has long been known and employed for developing decorative as well as wear and corrosion-resistant surface. Generally, the electrodeposition setup consists of electrodes (cathode and anode), plating bath has electrolyte-containing metal ions, and a power supply unit. The electrolyte bath can be aqueous, organic, or fused salt, and it must be conductive. At least two electrodes are required for the electrodeposition process. One electrode acts as a cathode or substrate on which deposition is desired, and another electrode acts as an anode, which helps maintain the concentration of metal ions in the electrolyte bath. The electrodeposition can be carried out using direct current (D.C) at a constant voltage (potentiostatic deposition), D.C at constant current (galvanostatic deposition), and pulse current. The electrodeposition technique is very suitable for the synthesis of different metallic coatings because of a wide range of properties for coatings can be accomplished by selecting appropriate electrolysis parameters. Electrodeposition of metal and alloy coatings is carried out by the reduction of metal ions on the cathode surface. The electrodeposited coating can enhance electrical conductivity, thermal conductivity, solderability, and corrosion and wear resistance of the substrate material.

2.3.1 Electrodeposition of Cu and Cu-Ni alloy coating

Pure Cu and Cu alloys are widely used in automobile, chemical, electrical, mechanical and marine applications for a variety of merits such as high strength and good corrosion and wear resistance. Cu coating has a widespread application in the manufacturing of electronic devices because of high electromigration resistance, superior electric and thermal conductivity, and excellent mechanical and chemical characteristics [1]. Also, Cu is used in some medical applications owing to its excellent anti-bacterial properties [2]. To increase the utilization of pure Cu, it is strengthened by work hardening or by the addition of alloying elements. Copper is alloyed with different metals and mainly classified into Cu-Zn [3], Cu-Sn [4], and Cu-Ni [5]. Among all these alloys, Cu-Ni alloys have outstanding anti-fouling and anticorrosion properties in seawater and thus have been extensively used in marine applications such as heat exchanger tubes, ship pipes, boiler parts, pump impellers, conduits, pump bodies and components, boat hulls, valve bodies, seawater condensers, pipe fittings, oil rigs and platforms, seawater intake screens, fish farming cages and other ship hardware [6]. Some of the most used Cu-Ni alloys consist of copper with 30 % nickel and copper with 10 % nickel. In the year 1920s, a 70-30 copper-nickel alloy was fabricated for the application in naval condensers. A 90-10 copper-nickel

alloy was first manufactured in the year 1950s, in the beginning, it was used for seawater piping and is now the more widely used alloy [7]. The addition of nickel into copper can enhance its tensile strength, ductility, thermal conductivity, and thermal expansion as well as improve its resistance to corrosion, cavitation, and erosion in all kinds of water. The alloy also shows excellent corrosion resistance to fatigue and stress corrosion cracking [8]. The chemical industry uses cast products, tubes and sheets made of copper-nickel alloys in oil refineries industries for the applications of impeller wheels, valves and pump bodies, fittings, and piping for the salt environment and other highly corrosive solutions, for heat exchangers, agitators and mixers, pressure and other vessels, cooling devices, autoclaves and many other types of equipment. The food processing industry uses copper-nickel alloys for agitators, multistage evaporators, feed water boilers, sugar refineries, piping and apparatus for fruit sieves, mixers and presses, food packaging [9].

Cu-Ni alloy coatings are extensively used in automobile, chemical, marine, and mechanical applications because of their superior resistance against corrosion in seawater, durability and good strength [10]. Also, Cu-Ni alloy coatings are preferred in the condenser, heat exchangers, microelectronics, and pipeline in marine environments [11]–[13]. The 70-30 Cu-Ni alloy has high strength and excellent corrosion resistance in many oxidizing and reducing gas environments, seawater, and alkaline and acidic media than the 90-10 Cu-Ni alloy coating, hence more widely used [9]. Also, 70-30 Cu-Ni alloy coating has higher hardness than 90-10 Cu-Ni alloy coating due to the higher concentration of nickel [7].

2.3.2 Mechanism of Cu-Ni electrodeposition

The mechanisms of Cu-Ni alloy electrodeposition are presented in Figure 2.2. The figure gives an idea of the different aspects involved in the selection of operational conditions and bath composition. The standard reduction potentials of copper and nickel are +0. 34 V and -0.25 V, respectively, which considerably differ from each other [9]. Hence, in the electrolyte bath, the concentration of Ni^{2+} is usually kept higher than that of Cu^{2+} and a complexing agent is also added, thus allowing the co-deposition of Cu and Ni on the cathode surface. For instance, the work of Pellicer et al. [14] shows that the nickel content in the Cu-Ni alloy coating is increased with an increase in current density. Also, at a low current density deposition rate of copper is higher than the deposition rate of nickel; hence, Cu-Ni alloy coating is rich in copper color. However, at a higher current density, the

deposition rate of nickel is higher than the deposition rate of copper, hence Cu-Ni alloy coating is rich with nickel color [15]. Usually, Cu and Ni anode plates are used in Cu-Ni alloy coating deposition to maintain the concentration of Cu and Ni ions in the electrolyte bath during the electrodeposition process.

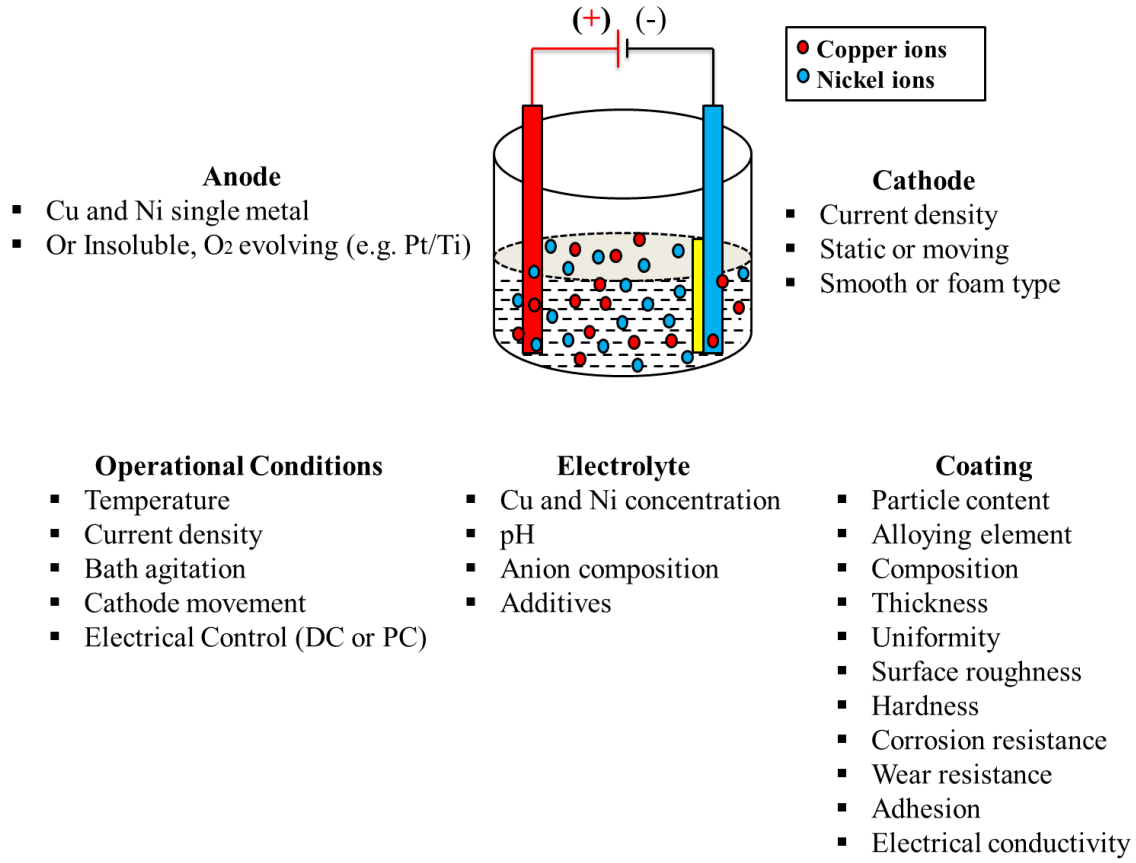

Figure 2.2: Electrodeposition of Cu-Ni alloy coating and different aspects involved in the selection of operational conditions and bath composition

The electrodeposition reactions of Cu-Ni alloy coating have been modeled as follows:

In case of a soluble anode, Cu and Ni ions are formed at the anode surface (Eq. (2.1) & Eq. (2.2))

$$Cu + 2e^- = Cu^{2+} \quad (2.1)$$

$$Ni + 2e^- = Ni^{2+} \quad (2.2)$$

In the case of insoluble anode such as Pt/Ti, oxygen is evolved at the anode (Eq. (2.3))

$$2H_2O + 4e^- = O_2 + 4H^+ \quad (2.3)$$

At the cathode, Cu and Ni ions are discharged simultaneously to form Cu-Ni alloy coating (Eq. (2.4) & Eq. (2.5)):

$$Cu^{2+} + 2e^{-} = Cu \quad (2.4)$$

$$Ni^{2+} + 2e^{-} = Ni \quad (2.5)$$

$$2H^{+} + 2e^{-} = H_2 \quad (2.6)$$

Equation (2.6) shows the hydrogen evaluation reaction that occurs during the electrodeposition process at the cathode surface, which results in a decrease in local pH and current efficiency and an increase in porosity of the coating. This is due to the increased in H_2 bubbles on the coating surface, in case of surfactant is not used or cathode movement is fixed.

2.3.3 Bath used in electrodeposition of Cu-Ni alloy coating

For electrodeposition of Cu-Ni alloy and composite coatings, different types of baths have been used, such as chloride, sulfate (Watt- type), and sulfamate baths. A survey of the literature for the bath composition for electrodeposition of Cu-Ni alloy and composite coatings is shown in Table 2.1.

2.3.3.1 Chloride bath

Usage of chloride baths in the electrodeposition of Cu-Ni coatings has been reported in very few studies [16]–[18]. The basic composition of a chloride bath consists of copper chloride and nickel chloride. Boric acid, sodium citrate, sodium dodecyl sulfate, and saccharin are commonly used as supporting agent. The presence of Cl^- due to the addition of Ni chloride to the electrolyte causes dissolution of Ni anodes and increases the conductivity of the solution. In electroplating bath in which the non-consumable anodes are used, the absence of chlorides will be favorable [19]. The coatings prepared in chloride-based baths are rough and loose surfaces with several defects and cracks, which would result in low corrosion resistance. A chloride bath can be used to increase the ductility of nanocrystalline materials for several industrial applications. However, its deposits have high internal stress [16]. Deng et al. [17] have described the electrodeposition of Cu-Ni alloy in 1-ethyl-3-methylimidazolium dicyanamide ionic liquid (EMI-DCA IL) containing anhydrous nickel chloride and copper chloride. It was found that the metal ions concentration in the electrolyte bath and the deposition potential had an

impact on the compositions of the Cu-Ni alloy coating. Also, EMI-DCA IL is difficult to synthesis, costly, and can have an adverse effect on human health and the environment. Recently, Wang et al. [18] fabricated the Cu-Ni alloy coating by electrodeposition method from a eutectic-based ionic liquid containing nickel chloride hexahydrate and copper chloride dihydrate and investigated the electrodeposition effect on the compositions, microstructures and corrosion resistances of Cu-Ni alloy coatings. The results showed that the deposition current density significantly influenced the compositions, microstructures, and corrosion resistance of Cu-Ni alloy coatings.

2.3.3.2 Watts-type (sulfate) bath

The watts type baths are one of the most popular baths in electrodeposition methods. The watts type bath was invented by O. P. watts about 100 years ago. The Cu-Ni coatings prepared from watts type baths have been studied in earlier research. Sulfate-based baths are extensively used baths in the industry due to its economic aspects. This bath consists of copper sulfate, nickel sulfate, and supporting agents. Copper sulfate and nickel sulfate are the main sources of Cu and Ni ions. Sodium citrate is used as a complexing agent to stabilize the electrolyte system, and boric acid is employed to adjust the pH of the electrolyte solution. To avoid an insoluble citrate complex forming and precipitating out of the solution, the pH value of the citrate bath is restricted [20]. Citrate type bath has several advantages such as less maintenance, easy to use, low cost, low corrosion of equipment and its deposits have low internal stress compared to other baths. However, deposits from this bath have high tensile strength and hardness. Ghosh et al. [9] synthesized the Cu-Ni alloy coating by pulse electrodeposition method from citrate bath containing copper sulfate, nickel sulfate, and supporting agents. It was found that the pulse parameters and operating conditions had a significant effect on the composition, current efficiency, and quality of the Cu-Ni alloy coatings. Baskaran et al.[15] have investigated the structural, morphology, thermal characteristics and magnetic properties of Cu-Ni alloy coatings using the pulse electrodeposition method. They observed that the lattice constant decreases and the saturation magnetization increase with the increase in Ni content of the Cu–Ni alloy coating. The watts bath with or without organic additives is most commonly employed [21], [22]. Among several organic additives, saccharine is commonly added as a stress-relieving and grain refining agent [23], [24]. In fact, saccharine performs these functions well for many metals and alloys deposited from a variety of baths. Pellicer et al. [14] have reported the nanocrystalline Cu–Ni films with a variable composition prepared by

electrodeposition method using saccharine-containing baths. The study shows that the addition of saccharine in watts type bath results in larger hardness and elastic recovery and better wear resistance due to the reduction in the crystallite size of the film.

2.3.3.3 Sulfamate bath

A survey of the literature shows that there are very few studies available for Cu-Ni alloy coatings electrodeposition in sulfamate baths. The basic composition of the sulfamate bath consists of nickel sulfamate, copper acetate and sodium citrate. Sulfamate, citrate and acetate are selected as being less hazardous substances to the environment [25]. In most of the studies to facilitate simultaneous deposition of Cu and Ni ions, sodium citrate was used as a complexing agent [26], [27], also it acts as a buffering [28], brightening [29] and leveling agent [30], thus eliminating the need of bath additives. Sulfamate bath has several advantages, such as excellent stability for temperatures by up to 60°C and different pH ranges from 2 to 4 [31]–[33]. The sulphamate baths can operate at high concentration and high current effectively. The properties of sulfamate deposits such as hardness, thermal conductivity, ductility, mechanical strength, internal stress, microstructure, porosity, roughness, density, specific heat that can be affected by operating conditions and impurities [34].The sulphamate baths are used for many engineering applications due to the high deposition rate, low residual stress, excellent dimensional corrections and high throwing power. However, the sulfamate bath has disadvantages that hydrolysis is generated and sulfamate exists as an intermediate like azodisulfonate. It is reported that a higher concentration of Ni sulfamate decreases the hydrolysis but improves the production of the impurities such as azodisulfonate. Several impurities such as sulfite, sulfate, persulfate and azodisulfonate could be produced in a sulphamate bath. However, among these impurities, azodisulfonate is the main source of sulfur in the deposit, which reduces the compressive stresses and ductility of the deposit [35], [36].

2.3.3.4 Lactate bath

The Ni–Cu alloy thin films prepared from an environmentally friendly lactate bath have been studied [37]. This bath is composed of nickel sulfate, copper sulfate, lactic acid and supporting agents. Lactic acid has been used as a complexing agent. Lactic acid is cheap, easily available and nontoxic in nature [38]. Smooth, compact and bright Ni–Cu alloy thin films have been successfully obtained using a lactic acid-based electrolyte bath. Cathodic

polarization measurements revealed that the amount of Ni in the deposit is less than its amount in the bath, demonstrating that the deposition of Ni–Cu alloy is of a regular type [39]. It is also reported that the cathodic efficiency is high and mainly depends on temperature, pH and the applied current density. The deposited Ni-Cu alloy films consist of a single solid solution phase with FCC structure. The obtained crystallite sizes for deposited Ni-Cu alloy films are lying between 12-25 nm. Also, it is observed that the increase in the temperature of the electrolyte bath leads to an increase in the crystallite size of the Ni-Cu alloy film.

2.3.3.5 Glycine bath

The glycine has been used as a complexing agent in the electro-co-deposition of alloy coatings including Zn-Co-Cu, Co-Ni-Mo, Cu-Co, Zn-Co and Zn-Ni to achieve high-quality deposits [40]. Also, it acts as a buffering agent and stabilizes the pH of electrolyte during the deposition process of metals and alloys. Cu-Ni alloy coatings have been synthesized using a glycine bath by varying pH of electrolyte and bath composition to investigate the mechanism which controls the elemental composition of Cu-Ni alloy coatings [41]. This bath is composed of nickel sulfate, copper sulfate, glycine acid and NaOH. NaOH was used to adjust the pH of the electrolyte bath. The elemental composition study of deposited Cu-Ni alloy coatings showed that the electrolyte pH significantly affected the elemental composition of coatings. Ni content of deposited coating is higher at pH values of 5 and 6 mainly due to the similar reduction potential of Ni^{2+} and Cu^{2+}. At pH value 8, Ni content in the deposited coating is low due to the decrease in the formation of Ni^{2+}-glycine complex as compared to Cu^{2+}-glycine complex. TEM analysis along with EDS confirmed the uniform composition of coating at all positions.

Table 2.1: Bath composition and operating conditions employed for preparing Cu-Ni and Cu-Ni alloy composites

Coating	Bath composition	pH	Temperature (ºC)	Current density	Goal	Ref.
Cu-Ni	0.475 M $NiSO_4$, 0.125 M $CuSO_4$, 0.2 M $Na_3C_6H_5O_7$	9	20	2 A/dm^2 (PC)	Improving corrosion resistance and microhardness	[42]
Cu-Ni	0.7 M $NiSO_4$, 0.0125-0.04 M $CuSO_4$, 0.26 M $Na_3C_6H_5O_7$	-	-	0-0.2 A/cm^2 (PC)	Investigating the effect of rotation speed, bath composition and pulse parameters on the composition of Cu-Ni alloy film	[43]
Cu-Ni	0.1-0.5 M $NiSO_4$, 0.05 M $CuSO_4$, 0.25 M $Na_3C_6H_5O_7$	8	-	-1200 mV	Investigating the effect of Cu/Ni ratio on morphology, microstructure and corrosion properties of Cu-Ni alloy coatings.	[44]
Cu-Ni	0.7 M $Ni(SO_3NH_2)_2.4H_2O$ 0.025 M $CuSO_4.5H_2O$, 30g/L H_3BO_3 0.15 g/L $NaC_{12}H_{25}SO_4$	3.5	38 ± 0.2	-102 mA/cm^2 (PC)	Investigating the effect of pulses parameters on the morphology and mass transfer rate of Cu.	[45]
Cu-Ni	0.475-0.5 M $NiSO_4.7H_2O$, 0.10-0.125 M $CuSO_4.5H_2O$, 0.2-0.3 M $Na_3C_6H_5O_7$	9	40	20 A/dm^2 (PC)	Improving corrosion resistance and microhardness	[9]
Cu-Ni	0.02 M $NiSO_4.7H_2O$, 0.002 M $CuSO_4.5H_2O$, 0.2 M $Na_3C_6H_5O_7$	5	55 ± 1	2.5, 5, 7.5, 10, 15 & 20 A/dm^2 (PC)	Investigating the effect of duty cycle and current density on lattice constant and magnetic properties	[15]

Cu-Ni	184 g/L $NiSO_4.7H_2O$, 6.24 g/L $CuSO_4.5H_2O$, 87 g/L $Na_3C_6H_5O_7$, 0.5g/L $C_7H_5NO_3S$, 0.2 g/L $NaC_{12}H_{25}SO_4$	4.5	30	0.210 V	Improving corrosion resistance in a chloride medium	[14]
Cu-Ni	2.0 M $Ni(SO_3NH_2)_2.4H_2O$ 0.01-0.04 M $CuSO_4.5H_2O$, 0.5 M H_3BO_3	2, 2.6 & 3.3	23	−1.7 V	Investigating the effect of electrolyte pH and Cu concentration on the microstructure of Cu-Ni alloy films	[46]
Cu-Ni	0.07 M $NiSO_4.7H_2O$, 0.0014 M $CuSO_4.5H_2O$, 0.04 M H_3BO_3	3.5 ± 1	25	-1.2, -1.4, -1.6 & -1.8 V	Investigating the effect of deposition potential on morphological and structural properties of Cu-Ni alloy films	[47]
Cu-Ni	0-0.5 M $Ni(H_2NSO_3)_2.4H_2O$ 0-0.025 M $(CH_3COO)_2Cu.H_2O$ 0-0.25 M $Na_3C_6H_5O_7.2H_2O$	3, 4, 5 & 6	25	-1.5 - 0.5 V	Developing plating baths to produce reflective Cu-Ni films	[25]
Cu-Ni	174 g/L $NiSO_4.7H_2O$, 16 g/L $CuSO_4.5H_2O$, 87 g/L $Na_3C_6H_5O_7$, 0.5g/L $C_7H_5NO_3S$, 0.2 g/L $NaC_{12}H_{25}SO_4$	4.5	30	0.25 V	Improving corrosion resistance and hardness	[48]
Cu-Ni	0.07 M $NiSO_4.7H_2O$, 0.0014 M $CuSO_4.5H_2O$, 0.04 M H_3BO_3	4.4 ± 0.2	25, 40, 55 & 70	-9 mA/cm^2 (DC)	Investigating the effect of electrolyte temperature on morphological and structural properties	[27]

Cu-Ni	0.2 M $NiSO_4.7H_2O$, 0.04 M $CuSO_4.5H_2O$, 0-0.2 M $Na_3C_6H_5O_7$	2, 2.5, 3 & 3.5	25	100 mA/cm^2 (PC)	Synthesis of Cu-Ni alloy nanoparticles using pulsed sonoelectrochemistry	[49]
Cu-Ni	0.2-0.8 M $NiSO_4.7H_2O$, 0.05-0.2 M $CuSO_4.5H_2O$, 0.2 M $Na_3C_6H_5O_7$	9	20	1 & 2 A/dm^2 (DC)	Investigating the effect of current density and bath composition on elemental composition and structure of coatings	[10]
Cu-Ni	0.02 M $NiSO_4.7H_2O$, 0.002 M $CuSO_4.5H_2O$, 0.2 M $Na_3C_6H_5O_7$	5	23	5, 10, 50, 100, 150 and 300 mA/cm^2 (DC or PC)	Improving electrocatalytic performance of the Cu-Ni alloy electrodes.	[50]
Cu-Ni	300 g/L $Ni(O_3SNH_2)_2$ 2.5-15 g/L $CuSO_4.5H_2O$, 20 g/L $NiCl_2$, 20g/L H_3BO_3, 80 g/L $Na_3C_6H_5O_7$, 2 g/L $C_7H_5NO_3S$, 0.1 g/L $NaC_{12}H_{25}SO_4$	4.5	50	2 A/dm^2 (PC)	Improving tensile ultimate and tensile strength of Cu-Ni alloys	[16]
Cu-Ni/MMT	0.32 M $Ni(NH_4)_2(SO_4)_2.6H_2O$ 0.06 M $CuSO_4.5H_2O$, 0.25 M $Na_3C_6H_5O_7$, MMT (0.05, 0.1, 0.2%), 2.0 M NaOH	6	25	-1.0 V	Improving mechanical and corrosion properties of 70:10 Cu-Ni alloy	[8]
Cu-Ni/Al_2O_3	105 g/L $NiSO_4.7H_2O$, 25 g/L $CuSO_4.5H_2O$, 59 g/L $Na_3C_6H_5O_7$ Al_2O_3 (0-30 g/L)	4	35	2 A/dm^2 (DC)	Improving microhardness, wear resistance and corrosion resistance	[51]

Cu-Ni/MMT	0.24 M $Ni(NH_4)_2(SO_4)_2.6H_2O$ 0.06 M $CuSO_4.5H_2O$, 0.25 M $Na_3C_6H_5O_7$, (0-0.15%) MMT, 2.0 M NaOH	6	25	-1.0 V	Improving hardness, shear strength and corrosion resistance properties of 90:10 Cu-Ni alloy	[7]
Ni-Cu/TiN	160 g/L $NiSO_4.7H_2O$, 15 g/L $CuSO_4.5H_2O$, 20 g/L H_3BO_3, 8 g/L TiN, 1 g/L $C_7H_5NO_3S$, 0.05 g/L $NaC_{12}H_{25}SO_4$	4.3 ± 0.2	50	2 and 4 A/dm^2 (PC)	Improving corrosion resistance by ultrasonic agitation	[52]
Ni-Cu-ZrO_2	70.96 g/L $NiSO_4.7H_2O$, 15 g/L $CuSO_4$, 42.6 g/L Na_2SO_4, 63 g/L Lactic acid (0-16 g/L) ZrO_2	8-9	30	6-20 mA/cm^2 (DC)	Improving microhardness and corrosion resistance properties	[53]
Ni-Cu/TiN-ZrO_2	160 g/L $NiSO_4.7H_2O$, 15 g/L $CuSO_4.5H_2O$, 20 g/L H_3BO_3, 6 g/L ZrO_2 , 4 g/L TiN, 1 g/L $C_7H_5NO_3S$, 0.05 g/L $NaC_{12}H_{25}SO_4$	4.2 ± 0.1	50 ± 1	3-6 A/dm^2 (PC)	Investigating effect of pulse parameters on surface morphology and microstructure of coatings and improving corrosion resistance	[54]
Cu–Ni–Cr	100 g/L $NiSO_4.7H_2O$, 5-20 g/L $CuSO_4.5H_2O$, 12 g/L $NiCl.7H_2O$, 25 g/L H_3BO_3, 120 g/L $Na_3C_6H_5O_7$, (0, 15, and 20 wt.%.) Cr	7	35	1 A/dm^2 (DC)	Improving oxidation resistance	[55]

Cu–Ni–Cr	100 g/L $NiSO_4.7H_2O$, 5-25 g/L $CuSO_4.5H_2O$, 12 g/L $NiCl.7H_2O$, 25 g/L H_3BO_3, 120 g/L $Na_3C_6H_5O_7$, (0, 15, and 20 wt.%.) Cr	7	35	0.5-2.0 A/dm^2 (DC)	Improving oxidation resistance	[56]
Ni-Cu-Y_2O_3	150 g/L $NiSO_4.7H_2O$, 30 g/L $CuSO_4.5H_2O$, 50 g/L $Na_3C_6H_5O_7$, 30 g/L H_3BO_3, 0.4 g/L $NaC_{12}H_{25}SO_4$, 1 g/L $C_7H_5NO_3S$, (0-5 g/L) Y_2O_3	4-5	60	3 A/dm^2 (DC)	Investigating the effect of Y_2O_3 on surface morphology and microstructure of coatings and improving corrosion resistance	[57]
Ni-Cu-SiC	300 g/L $NiSO_4.7H_2O$, 1.3 g/L $CuSO_4.5H_2O$, 19.4 g/L NH_4HF_2 35 g/L H_3BO_3, 0.4 g/L $NaC_{12}H_{25}SO_4$, (0, 10, 20 and 30 g/L) SiC	4.4-4.8	50	3 A/dm^2 (DC)	Improving hydrophobicity and corrosion resistance	[58]

2.3.4 Additives

In general, the addition of additives in the electrolyte bath can enhance the surface finish and properties of Cu-Ni alloy coatings [49]. The addition of small amount of additives in the electrolyte bath can enhance the quality and performance of the coating. Among several additives, sodium dodecyl sulfate as a surfactant, boric acid and sodium hydroxide as a buffering agent, saccharin as an internal stress reliever and grain refiner, and sodium citrate as a complexing agent are most the frequently used and listed in Table 2.2. Additives affect the elemental composition, crystallite size, microstructure and mechanical properties of the coating [25].

Table 2.2: Bath additives used in electrodeposition of Cu-Ni alloy coating

Additive	Formula	Performance	Ref.
Boric acid	H_3BO_3	Buffer	[27]
Sodium hydroxide	NaOH	Buffer	[8]
Saccharin	$C_7H_5NO_3S$	Grain refinement, surface roughness reducing, stress-reducing, enhancing the brightness and quality of coatings	[14]
Sodium dodecyl sulfate (SDS)	$NaC_{12}H_{25}SO_4$	Surfactant	[16]
Sodium citrate	$Na_3C_6H_5O_7$	Complexing agent	[51]

2.3.4.1 Boric acid

The boric acid is used as a buffering agent in sulfate and chloride baths in order to achieve high current efficiencies [59]. It is reported that the presence of boric acid has a significant effect on the composition of alloy coatings and leads to rising the amount of the less noble component in the alloy [60], [61]. The Cu-Ni alloy coatings have been deposited from different electrolyte baths containing boric acid [16], [27], [46], [47]. The presence of boric acid in the electrolyte bath buffers the pH and avoids pH increment on the cathode surface [62]. In the presence of boric acid, a more coherent and brighter deposit appearance can be achieved. Furthermore, the addition of boric acid in an electrolyte bath enhances the range of required current density in the electrodeposition process without hydroxide deposition as well as reduces the brittleness of coating.

2.3.4.2 Trisodium citrate

The electrodeposition of Cu-Ni coatings is generally carried out earlier using a different electrolyte bath containing trisodium citrate [15]. Trisodium citrate is used as a buffering agent in the electrodeposition process of Cu-Ni alloy coating. It helps to maintain the pH value of electrolyte near a chosen value and also to prevent the rapid change in the pH value of the electrolyte. It is reported that in the presence of citrate, the nobler component (Cu) is deposited at more negative potential compared to its actual standard electrode potential [10]. Many researchers investigated the electrodeposition of Cu-Ni alloy coating from a citrate-based electrolyte bath and studied the effects of current, pH, agitation, and temperature on the properties of Cu-Ni alloy deposits [44], [45]. Green et al. have reported that the Cu-Ni alloy films deposited from a citrate bath possess very high current efficiency [9]. It is reported that in the presence of a citrate electrolyte bath, Ni and Cu deposition is charge-transfer-controlled and mass-transfer-controlled. Also, with increasing the current density, Cu ions concentration at the surface of the cathode electrode decreases, whereas Ni deposition is enhanced, which results in Ni-rich deposits [63]. Many studies have shown that the trisodium citrate can be used as an adjuvant or stabilizer effectively in the composite coatings to enhance the structural properties stability and dispersibility [64]. Nowadays, citrate baths have been considered for electrodeposition of composite coatings in which boric acid is replaced by citric acid [65], [66]. The main role of trisodium citrate in the electrodeposition of Cu-Ni alloy coating is to decrease the large difference in the standard reduction potentials of nickel (-0.25 V) and copper (+0.34 V) to favor the simultaneous electrodeposition of copper and nickel [14]. Trisodium citrate is the most suitable for Cu-Ni alloy coatings because of its low toxicity; its ability to develop excellent deposit with stress-free Ni-rich alloys with very high current efficiency and also it can act as a buffering, leveling and brightening agent, thus eliminating the need for other bath additives [67]. It is found that an increase in trisodium citrate concentration in the electrolyte bath results in an increase in the content of copper in the deposit [9]. In the electrolyte bath, citrate forms complexes with nickel and copper, but the percentage of nickel complexes formation is lower than copper complexes. Also, increasing the concentration of trisodium citrate in the electrolyte bath results in a moderate shift of the nickel deposition onset [67]. Trisodium citrate is suitable for adjusting the elemental composition of the deposited alloy and at a high concentration of citrate in the electrolyte bath leads to Cu enriched alloy. Also, it acts as a capping agent, which helps to stabilize

the grain size of deposits [49]. Also, it is reported that trisodium citrate promotes the nucleation sites and nucleation rate in the electrodeposition process [68].

2.3.4.3 Saccharin

In the deposition of several metals and alloys, saccharine has been added to the electrolyte bath as an additive agent. It is well known that the presence of saccharine in the electrolyte bath leads to a reduction in the crystallite size and suppressing the dendrite growth of the deposit. It is reported that the standard reduction potential of nickel shifts toward more positive values due to the presence of saccharin in the electrolyte bath. Also, with increasing the concentration of saccharin in the electrolyte bath, the size of crystals gets smaller and more compact, which is caused due to the inhibitory effect of the adsorbed species (saccharin) on the reduction of the nickel ion on the surface of the cathode [69]. The addition of saccharine not affects the solution stability as well as the deposition process and no significant variation in the film composition of the deposits has been observed. However, it improves the deposit quality by inhibiting the stress or reducing tensile stress and increasing the planarity [67]. According to some studies, in the case of Cu-Ni alloy deposition, the stabilized potential of the galvanostatic curves shifted towards more negative values due to the addition of saccharine in the electrolyte bath, which leads to enhancing reduction of Ni ions. Also, saccharine is responsible for higher hardness and elastic recovery and excellent wear resistance of Cu-Ni alloy coatings [14].

2.3.5 Electrodeposition methods

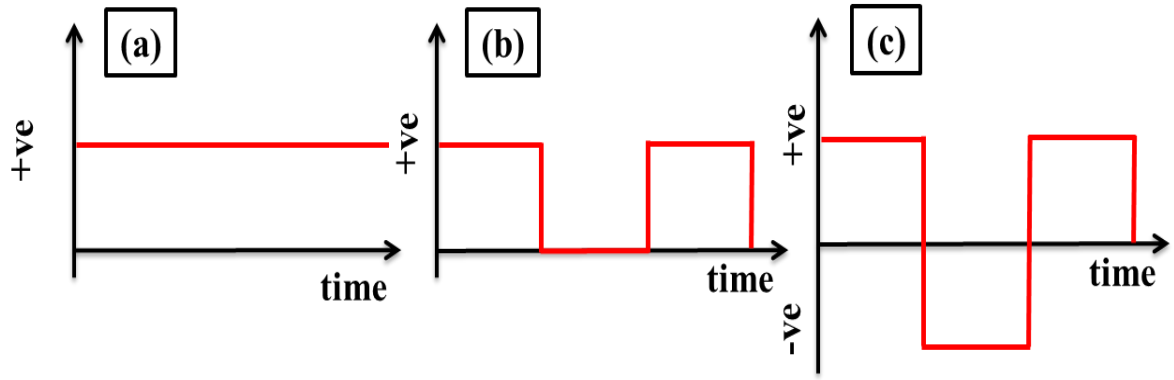

Figure 2.3: The schematic representation of different modes of current density for electrodeposition (a) DC, (b) PC and (c) PRC

Electrodeposition technique is more attractive for the synthesis of composite thin films as being the simplest and economical process as compared to other techniques [14], [70]–

[72]. Electrodeposition of pure metals, alloys, and their composites thin films is generally carried out using direct current (DC). Furthermore, in the electrodeposition technique, by changing the current type, different composite thin films could be synthesized with more even distribution of reinforcing elements in the metal matrix, higher content of particle reinforcement, and decreased crystallite sizes of the metal matrix as compared to those usually obtained under DC technique [71], [73], [74]. In recent years, in addition to DC electrodeposition technique, pulse current (PC) and pulse reverse current (PRC) electrodeposition techniques have been used for the synthesis of composite thin films. Figure 2.3 shows different modes of the electrodeposition process. PC and PRC electrodeposition techniques have received more attention in comparison to the conventional DC electrodeposition technique [75]. In PC and PRC electrodeposition method, applied potential, duty cycle, cathodic/anodic pulses, and pulse waveform can be controlled to improve the surface morphology, microstructure, elemental composition, crystallite size, mechanical and wear properties of resulting composite thin films [76]–[79]. The DC, PC and PRC electrodeposition techniques have been employed to develop various alloy thin films such as Ni-Fe [80], Ni-P [81], Ni-W [82], Ni-Cr [83], and Cu-Ni [15] alloy thin films.

2.3.5.1 DC electrodeposition

DC electrodeposition method is widely used in the electrodeposition of metal and alloy coatings. DC electrodeposition method has been used to fabricate Cu-Ni alloy coatings and their properties such as surface morphology, microstructure, elemental composition, internal stress, microhardness, corrosion behavior, and magnetic performance have been studied in detail [10], [27], [49], [50]. The inclusion of ferromagnetic Ni into the copper film, the film shifts from diamagnetic to ferromagnetic in nature. The saturation magnetization increases with the increase in nickel content of the Cu–Ni alloy film. Cu-Ni alloy films have shown enhanced performance in magnetic microactuators for MEMS [84]. In DC electrodeposition method, constant electrical current is continuously supplied for the deposition process. DC electrodeposition method has several attractive advantages such as economical, ease of operation and high throughput.

2.3.5.2 PC electrodeposition

The modification of DC electrodeposition method is done by the use of current interruption known as pulsed electrodeposition, where not only the current but also

potential can be varied. The enhanced hardness, wear resistance and corrosion resistance properties can be achieved as it is possible to get non-dendritic, coherent deposits at much higher current densities than with the straight direct currents. Pulse plating improves the deposit properties such as finer grain size, plating thickness distribution, hardness, porosity, ductility and electrical conductivity. In the PC electrodeposition method, pulses are rectangular shapes and current and potential, which are periodic manner reaches zero. During the electrodeposition process, the instantaneous energy related to a pulse current is higher than that of direct current, resulting in the reduction of metal ions at an extremely high over-potential. When the current reaches zero, the discharge ion concentration near the cathode electrode gets restore to its initial value, and subsequently, the concentration polarization disappears [85]. PC electrodeposition can be affected by bath composition, process parameters, peak current density, pulse On-time (Ton) and off-time (Toff). The duty cycle and pulse frequency are the main pulse variables, which can be used for the optimization of the electrodeposition process. Duty cycle and pulse frequency are measured using equations (2.7) and (2.8), respectively:

$$Pulse\,duty\,cycle = \left(\frac{T_{on}}{(T_{on} + T_{off})} \right) \times 100 \tag{2.7}$$

$$Pulse\ frequency = \left(\frac{1}{(T_{on} + T_{off})} \right) \tag{2.8}$$

Also, the average current density can be calculated using equation (2.9) as follows:

$$Average\,current\,density = Pulse\,duty\,cycle \times Pulse\,peak\,current\,density \tag{2.9}$$

In general, the advantages of pulse current electrodeposition over direct current electrodeposition are summarized as follows:

1. Higher rate of deposition due to increased permissible current densities.
2. Higher density of deposits with low porosity
3. Better control on the composition and microstructure of coatings.
4. Higher entrapment of reinforcing element in the deposits.
5. Enhancement in the purity of deposits due to the reduction of impurities deposition in the deposit.
6. Reduced internal stress in deposits.
7. Increased Ni content in the case of Cu-Ni alloy electrodeposition.
8. Reduction in hydrogen evolution.
9. Reduce or eliminate the need of additional additive agents.
10. Reduction in the surface roughness and crystallite size of the deposits.

Significant research work in the field of PC electrodeposition of Cu-Ni alloy coatings has been carried out to obtain a better quality of deposits [9], [15], [16], [42], [43], [45], [49], [50], [86]. Ghosh et al. [9] have reported that by appropriately adjusting the pulse parameters, the smooth and coherent surface finish of the Ni-Cu alloy coating can be achieved. Also, the microhardness value of PC electrodeposited Ni-Cu alloy coating was higher than that of the DC electrodeposited Ni-Cu alloy coating.

2.3.5.3 PRC electrodeposition

PRC electrodeposition is a bipolar process where anodic and cathodic pulses are mixed. In this method, the polarity of a DC (including cathodic and anodic currents) is continually reversed. PRC electrodeposition has several advantages, such as a simple, economical, and scalable method that provides homogenous dispersion of reinforcing elements throughout the matrix and exhibiting good mechanical and corrosion properties [87]. PRC electrodeposition method has been used for the synthesis of Cu-Ni alloy coatings [9], [43], [44]. Also, it is reported that the internal stress in the PRC electrodeposited is minimum than that of the DC electrodeposited coating due to the reduction in the hydrogen gas evaluation in the cathode surface.

2.3.6 Electrodeposition parameters of Cu-Ni alloy

2.3.6.1 Electrolyte composition (metal ratio of the bath)

Several works [9], [10], [49], [88], [89] studied the effect of copper concentration on the surface morphology, microstructure, elemental composition, thickness, microhardness and corrosion properties of Cu-Ni alloy coatings. As the copper concentration is increased, the copper content in the deposit is decreased and crystallite size is decreased [89]. Also, the surface roughness of Cu-Ni films increases with increasing the Cu concentration in the electrolyte bath [46]. The microhardness of Cu-Ni alloy coating is decreased with the increase in the copper concentration in the electrolyte bath due to the increase in the Cu content and decrease in the Ni content [9]. It is found that the corrosion resistance of Cu-Ni alloy coating is enhanced with an increase in the content of Ni in the coating [88].

2.3.6.2 Current density

It has been shown that the electrodeposition and operating conditions have a significant effect on the properties of electrodeposited coatings. Current density plays a key role in the electrodeposition of metal and alloy coatings alloy due to its excellent control on the

surface morphology, elemental composition, microstructure, electrode kinetics and rate of deposition of metal ions. According to previous studies, the deposition of Cu is diffusion-controlled and the deposition of Ni is activation controlled. During electrodeposition of Cu-Ni alloy coating, with an increase in current density tends to increment of cathodic overpotential, therefore, enhancement in the activation reaction on the cathode electrode surface, which results in the increase in the Ni content and decrease in the Cu content in the deposit. According to several studies, the increase in the applied deposition current density results in an increase in the Cu content and a decrease in the Ni content of the coating [9], [42], [43]. This is mainly due to the much more rapid increase in the partial current of Ni deposition compared to the partial current for Cu deposition. In the case of a mass-transfer controlled metal deposition process, the obtained deposits have powdery or dendritic structure. At high current density deposition, the deposits have a minimum content of Cu, which results in a smooth, uniform, and bright surface of the coating. Similarly, at low current density, the content of Cu in the deposit is more tends to the nodular surface morphology of the coating [43].

The thickness of Cu-Ni alloy coating obtained at a higher current density is higher than that of the coating deposited at a lower current density. This behavior suggests that the higher current density results in higher current efficiency [14]. The crystallite size of the Cu-Ni alloy coating decreases with an increase in the deposition current density due to the decrease in the lattice constant. The relationship between saturation magnetization of the Cu–Ni alloy coatings and applied deposition current density has also been explained. The saturation magnetization of Cu- Ni alloy coating is increased with an increase in the current density[15]. This is due to the increase in Ni content in the coating with an increase in current density. It is well-known that nickel is ferromagnetic and copper is diamagnetic, thereby the Cu–Ni alloy coating with high Cu content exhibits diamagnetic nature and the Cu–Ni alloy coating with high Ni content exhibits ferromagnetic nature [90]. The ferromagnetic nature increases with an increase in Ni content of the Cu-Ni alloy coating [91]. Nickel would be mechanically harder than pure Cu and Cu-Ni alloy. It should be noted that an increasing current density of up to a certain limit leads to an increase in the hardness of Cu-Ni alloy coating [14]. The hardness of Cu-Ni alloy coating is increased with an increase in the nickel content in the deposit, which is mainly due to the solid solution strengthening and reduction in the crystallite size of the coating [63].

2.3.6.3 Electrolyte agitation

The electrolyte agitation is one of the most important parameters in the electrodeposition process of metal and alloy coatings because it can significantly affect the elemental composition, cost of production, and properties of deposits. For laboratory investigations, magnetic stirrer is employed for stirring of the electrolyte solution during the electrodeposition process [19]. The effect of electrolyte bath stirring has also been studied for the electrodeposition of Cu-Ni alloy coatings [9], [92], [93]. In the presence of a citrate bath, the reduction of cupric species is diffusion-controlled during the Cu-Ni alloy deposition. It should be noted that with increasing electrolyte stirring tends to increase in the mass transfer of Cu ions in the electrolyte bath, thereby the copper content in the deposit increases. Also, in the stirring condition, a metallic, reddish-brown coating was obtained and without stirring condition, a nonmetallic and black powdery coating was obtained [92]. The crystallite size of the coating is increased with the increase in the stirring speed; thereby, this condition results in the less compact surface morphology and reduction in the Ni deposition [9].

2.3.6.4 Electrolyte pH

Electrolyte pH is a key system factor that has a significant effect on microstructure, surface morphology, elemental composition, mechanical and corrosion properties of metal and alloy coatings. The electrodeposition of Cu-Ni alloy coatings have been carried out with different electrolyte pH values [41], [46], [49], [67], [94]. According to previous studies, the electrodeposition of Cu-Ni alloy coatings has been performed in the acidic as well as alkaline range. The Cu content of the Cu-Ni alloy coating increases with increasing electrolyte pH. It is reported that at a low pH value, there is a formation of a low degree of a complex, which results in a quick supply of metal ions towards the cathode surface [41]. Hence, the surface roughness of Cu-Ni alloy coating increases with a decrease in the electrolyte pH. The crystallite size of the Cu-Ni alloy coating increases with an increase in the pH value due to the increase in the copper content in the deposit [46].

2.3.6.5 Temperature

In order to achieve the desired properties of the electrodeposited coatings, the correct control of the operating temperature is very important. The operating temperature has a significant effect on the surface morphology, elemental composition, microstructure and quality of the coatings. The effect of operating temperature on the electrodeposition of Cu-

Ni alloy coating has been studied [9], [27], [94]. As we know, copper is deposited under diffusion control (i.e., under limiting current condition). The rate of diffusion of cupric species increases with an increase in the operating temperature of the electrolyte bath. It has been found that, in the electrodeposition of Cu-Ni alloy coating, as the operating temperature increased from 25 to 40 ºC, the content of Cu in the deposit rapidly increased and further increased in the operating temperature did not have a significant effect on the copper content. This trend showed that the current efficiency also increased with an increase in the operating temperature of the electrolyte bath [9]. Silaimani et al. [94] reported the enhancement in the corrosion current of Cu-Ni alloy coating due to the change in the growth of surface morphology structure from 2D to 3D caused due to the increase in the operating temperature from 20 and 30 ºC. Sarac et al. [41] reported the electrodeposition of Ni-Cu film at different electrolyte temperatures. They have shown that the crystallite size and the nickel in the Ni-Cu alloy film are decreased with the increment of the operating temperature of the electrolyte bath.

2.3.7 Properties of electrodeposited Cu-Ni alloy

Copper is more ductile than nickel and is widely used in electrical applications due to high electrical and thermal conductivity. Cu and Ni belong to f.c.c. structure with a molar mass of 63.54 and 58.9 u and density 8.96 and 8.9 $g.cm^{-3}$. Some important properties of Cu and Ni are listed in Table 2.3.

Table 2.3 Important properties of pure Cu and Ni

Properties	Copper	Nickel
Atomic number	29	28
Molar mass (u)	63.54	58.69
Electron configuration	[Ar] 3d10 4s1	[Ar] 3d8 4s2 or [Ar] 3d9 4s1
Density ($g.cm^{-3}$)	8.96	8.9
Crystal structure	f.c.c.	f.c.c.
Melting point (°C)	1085	1455
Boiling point (°C)	2562	4946
Young's modulus (GPa)	128	200
Electrical resistivity (nΩ.m)	63.54	69.3
Magnetic ordering	Paramagnetic	Ferromagnetic
Thermal conductivity (W/(m.K))	398	90.9

2.3.7.1 Microstructure

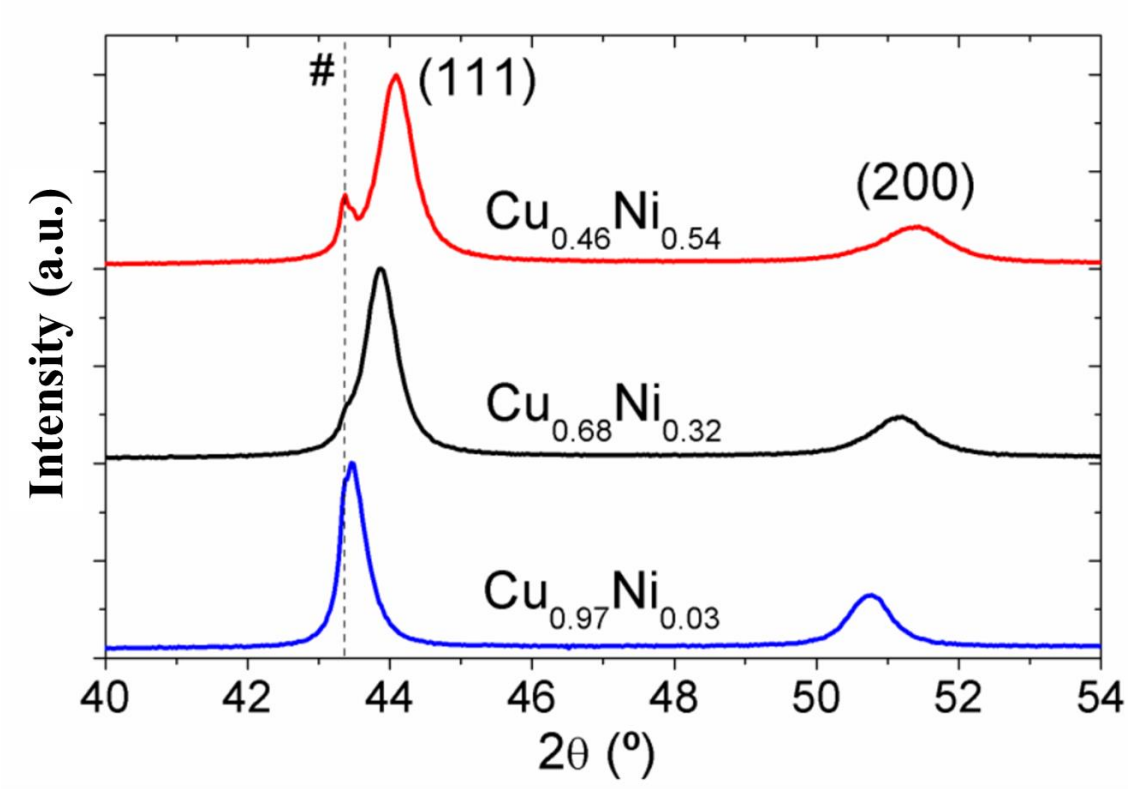

Figure 2.4: XRD patterns in the 40º-54º 2θ region of Cu-Ni samples with dissimilar copper content. The peak denoted by # belongs to the Cu seed layer [48]

The XRD pattern of Cu-Ni alloy film with various copper content is shown in Figure 2.4 [48]. All deposited films are showed peaks corresponding to the plane (111) and (200). From Figure 2.4, it is observed that as the copper content decreased, diffraction peaks are shifted towards a higher 2θ angle. The shifting of peaks towards a higher 2θ angle is mainly due to the increase in the lattice parameter. It was also reported that the lattice parameter of pure Cu (0.3614 nm) is higher than a pure nickel (0.3523 nm). Thus as the Cu content in the alloy increases, there is lattice expansion within the alloy takes place [9]. It is noticeable that Cu-Ni films with higher copper content exhibited a larger crystallite size. The XRD pattern of Cu-Ni alloy does not show a characteristic peak related to pure Cu and pure nickel, which confirms the formation of a solid solution of Cu and Ni atoms [15]. Cu and Ni both have FCC structure, and both have almost similar atomic sizes. Therefore, the Cu-Ni alloy is known as an isomorphous binary alloy, which means the two metals are completely soluble in one another and have one type of crystal structure [8]. The crystallite size of Cu-Ni alloy usually is in the nanometer; however, crystallite size can be varied by changing process parameters and bath compositions.

2.3.7.2 Mechanical properties

Pellicer et al. [14] have reported that the hardness of Cu-Ni alloy is increased with an increase in the nickel content of Cu-Ni alloy coating. This is associated with a decrease in the crystallite size of the coating due to the decrease in lattice parameter caused due to increase in nickel content. The higher hardness is usually expected for smaller crystallite sizes because the propagation of dislocations is easily hindered by a large number of grain boundaries. Varea et al. [48] have shown that the mechanical properties such as young's modulus, hardness and wear resistance can be varied by varying the deposit composition and are superior for moderate copper content. Eva Pellicer et al. [63] have prepared Cu-Ni alloy films by varying alloy composition and reported their mechanical properties. It was observed that the penetration depth was lower for the higher nickel content of Cu-Ni alloy film. This observation confirmed that the Cu-Ni alloy coating with higher nickel content is harder as compared to the lower nickel content Cu-Ni alloy coating. The Cu-Ni alloy coatings with higher hardness are necessary for structural components in MEMS applications.

2.3.7.3 Magnetic properties

The effect of various current densities on the magnetic properties of Cu-Ni alloys has been studied [15]. Copper is diamagnetic and nickel is ferromagnetic. Cu-Ni alloy with a higher percent of Cu is expected to diamagnetic and higher nickel content is expected to ferromagnetic. The vibrating sample magnetometer (VSM) study is used to evaluate the magnetic properties of Cu-Ni alloy coatings. The obtained results showed that the coatings prepared at 2.5 and 5.0 A/dm^2 are diamagnetic; the one prepared at 7.5 A/dm^2 is weakly ferromagnetic; however, those prepared at 10, 15 and 20 A/dm^2 are ferromagnetic. Results revealed that the magnetization of Cu-Ni alloy increases with the increase in nickel content. Similarly, Pellicer et al. [63] demonstrated that the saturation magnetization and coercivity values of Cu-Ni alloy coatings gradually increase with the increase in the Ni content.

2.3.7.4 Corrosion behavior

The polarization curve method is widely used for the evaluation of corrosion resistance of Cu-Ni alloy coatings. Cu-Ni alloy exhibits good corrosion resistance and it depends upon the composition alloy. Few studies have been carried out to evaluate the corrosion

performance of Cu-Ni alloy coatings [9], [48]. Ghosh et al. [9] have reported that PC electrodeposited Cu-Ni alloy coating with 35.8 wt. % Cu shows higher corrosion resistance as compared to DC electrodeposited Cu-Ni alloy coating. Also, Varea et al. [48] have presented that the corrosion resistance of Cu-Ni alloy coating is superior as compared to pure Cu.

2.3.7.5 Wear behavior

Very few studies have been carried out on the wear properties of Cu-Ni alloy coatings [14], [48]. Wear characteristics of Cu-Ni alloy coatings are evaluated by depth-sensing nanoindentation technique. These studies revealed that the wear performance of Cu-Ni alloy coating increases with an increase in the nickel content of coatings. Also, they have reported that the wear resistance mainly depends upon the microstructure of the coating and is enhanced with a decrease in the crystallite size of the coating.

2.3.8 Cu-Ni alloy composite coatings

The Cu-Ni composite coatings fabricated by the electrodeposition method have been rarely studied. A few researchers have prepared Cu-Ni alloy matrix composite coatings based on Al_2O3, TiN, ZrO_2, Y_2O_3, Cr and layered silicate (MMT) using the electrodeposition method. The incorporation of the reinforcing element in the Cu-Ni matrix composite coatings can affect the mechanical, corrosion and tribological properties of the coating. Ceramic particles such as Al_2O_3, TiN, and ZrO_2 have been used in the synthesis of composite coatings due to their excellent mechanical properties like hardness and wear resistance. The addition of ceramic particles in the composite coatings resulted in increased hardness, wear, and corrosion resistance. During the deposition process, the presence of ceramic particles inhibits crystal growth and reduces the crystallite size of the composite coatings (Hall-Petch effect). Also, the increase in the concentration of ceramic particles in the electrolyte bath leads to an increase in the incorporation of ceramic particles in composite coatings up to a certain limit. The increase in ceramic particle content in the composite coating results in a subsequent increase in the required stress for the movement of dislocations, and hence, according to the Orowan mechanism, microhardness is increased [51]. Furthermore, the ceramic particles can enhance the wear properties of composite coatings. The ceramic particles act as a solid lubricant during the wear test and thus, reduce the friction coefficient of the composite coatings. Also, corrosion resistance of the ceramic particle reinforced composite coatings has been enhanced by providing a more

tortuous mean-free path of corrosion and a decrease in intergranular discontinuity by filling microholes, gaps, and cracks. Also, the addition of ceramic particles can alter the texture of the composite coating and covers the metallic surface of the matrix and thus, corrosion resistance is increased. The effect of the addition of reinforcing particles on the properties of Cu-Ni alloy composite coatings can be described as follows:

2.3.8.1 Effect of MMT nanoplatelets

The effects of different concentrations of MMT nanoplatelets in the electrolyte bath reinforcement on the durability, corrosion resistance, and mechanical properties of Cu-Ni coatings have been investigated. The incorporation of MMT in the Cu-Ni alloy matrix leads to a decrease in particle size of the resulting coating. Also, the AFM study showed that the incorporation of MMT particles in the Cu-Ni alloy matrix slightly increases the surface roughness of the coating. The hardness of the coating increases with MMT contents, while the content of MMT particles and the reduction in grain size caused by the embedding process have a considerable effect on hardness. The incorporation of MMT particles increased the corrosion resistance of the Cu-Ni alloy coating. This attributed to slowing the mean free path of corrosion due to the grain refinement and availability of more surface area offered by conducting MMT particles [7], [8].

2.3.8.2 Effect of Al_2O_3 nanoparticles

The effect of the additions of Al_2O_3 nanoparticles on the microhardness, wear resistance, and corrosion resistance of the Ni-Cu alloy coatings has been studied. According to obtained results, the microhardness and wear resistance of Ni-Cu/Al_2O_3 composite coating are increased about 2.4 and 3.75 times, respectively, than that of the pure Ni-Cu alloy coating. Results showed that the crystallite size of the pure Ni-Cu alloy coating is decreased from 37 nm to 16 nm by the incorporation of Al_2O_3. This is attributed to the role of Al_2O_3 nanoparticles in grain refinement by increasing active nucleation sites in the coating during the deposition process and thus prevents grain growth. Also, the incorporation of Al_2O_3 nanoparticles increased the microhardness of the coating from 331 HV to 570 HV. The wear rate for Ni-Cu/Al_2O_3 composite coatings was decreased with an increase in Al_2O_3 nanoparticles bath (up to 20 g/L) and then increased with a further increase in Al_2O_3 concentration in the electrolyte bath. This is ascribed to the role of Al_2O_3 nanoparticles to restrain the plastic deformation of the Ni-Cu alloy matrix. The addition of Al_2O_3 nanoparticles improved the values of corrosion potential and corrosion current

density, which shows enhanced corrosion resistance. The increase in corrosion resistance is attributed to the change in coating texture due to the incorporation of Al_2O_3 in the Ni-Cu alloy matrix Al_2O_3 [51].

2.3.8.3 Effect of TiN nanoparticles

Ni-Cu/TiN composite coatings have been prepared using ultrasonic-assisted electrodeposition from a citrate bath. The effects of current density on surface morphology, structural and electrochemical properties of Ni-Cu/TiN nanocomposite coatings have been investigated. The presence of TiN nanoparticles changes the texture of the Ni-Cu coating compared to pure Ni coating. The corrosion resistance of the Ni-Cu/TiN composite coating can be affected by ultrasonic agitation as well as current density. The incorporation of TiN particles into the Ni-Cu alloy matrix leads to an increase in surface roughness of Ni-Cu/TiN composite coating compared to Ni-Cu coating. The highest corrosion resistance for Ni-Cu/TiN composite coating was achieved at 5 A dm^{-2} [52].

2.3.8.4 Effect of ZrO_2 particles

ZrO_2 particles have been used in several composite coatings because the incorporation of ZrO_2 could enhance mechanical properties such as wear resistance and hardness. Ni-Cu/ZrO_2 composite coatings have been electrodeposited from a citrate bath and the effects of current density, duty cycle and their combination on corrosion performance of coating studied. According to the obtained results, the corrosion resistance and hardness of Ni-Cu/ZrO_2 composite coatings have been enhanced compared to pure Ni and Ni-Cu alloy coatings. The presence of ZrO_2 in the Ni-Cu alloy matrix results in an increase in microhardness about 100 HV compared to pure Ni-Cu alloy coating. The hardness of Ni-Cu/ZrO_2 composite coatings is increased with a decrease in the duty cycle. The corrosion study showed that the Ni-Cu/ZrO_2 composite coatings electrodeposited at a current density of 3 A dm^{-2}, a duty cycle of 80%, and a current density of 5 A dm^{-2}, duty cycle of 40% have higher corrosion resistance [53].

2.3.8.5 Effect of TiN-ZrO_2 particles

Ni-Cu/TiN-ZrO_2 nanocomposite coatings have been produced using the pulse electrodeposition method from s from a citrate bath. The effects of current density and duty cycle on the surface morphology, structural and corrosion properties of Ni-Cu/TiN-ZrO_2 nanocomposite coating have been studied. The incorporation of TiN and ZrO_2

nanoparticles in the Ni-Cu matrix changes the texture of the coating. The surface roughness of Ni-Cu/TiN-ZrO_2 nanocomposite coating is increased as compared to the pure Ni and Ni-Cu alloy coating. The crystallite size for this Ni-Cu/TiN-ZrO_2 nanocomposite was about 14-21 nm. The process parameters such as duty cycle, current density, and frequency have a slight effect on the crystallite size of the Ni-Cu/TiN-ZrO_2 nanocomposite coatings. The incorporation of TiN and ZrO_2 particles in the Ni-Cu matrix resulted in an improvement in the anti-corrosion performance of the resulting coating. The duty cycle and current density have a significant effect on the corrosion resistance of the Ni-Cu/TiN-ZrO_2 nanocomposite coating compared to frequency [54].

2.3.8.6 Effect of Cr nanoparticles

Cr nanoparticles have been widely used in composite coatings due to their high mechanical strength and outstanding electrical and thermal conductivity. Cu-Ni-Cr nanocomposite coatings have been produced by electro-co-deposition method using a citrate type bath [55], [56]. The presence of Cr nanoparticles leads to an improvement in the oxidation resistance of Cu-Ni alloy coating. The results show that Cu-Ni-Cr nanocomposite coating based on Cu/Ni ≈ 1 and as low as 15 wt. % Cr can form a protective chromia scale during a 20 h oxidation in air at 800 °C. The unique structure of the Cu-Ni-Cr nanocomposite helps in the fast formation of the Cr_2O_3 scale. Once Cr_2O_3 scale forms, the growth rate of the Cu and Ni oxides is decreased, results in the enhancement of the oxidation resistance [55].

2.3.8.7 Effect of Y_2O_3 nanoparticles

Y_2O_3 nanoparticles have been used in composite coatings due to their promising mechanical and anti-corrosive properties. Ni-Cu/Y_2O_3 nanocomposite coatings are prepared using the electrodeposition method to enhance the corrosion resistance performance in the marine environment [57]. Electrochemical impedance spectroscopy (EIS), Tafel polarization, and open circuit potential (OCP) measurements have been carried out to study the corrosion performance of coatings. The crystallite size of the Ni-Cu alloy coating is decreased due to the inclusion of Y_2O_3 nanoparticles. Also, the crystallite size of Ni-Cu/Y_2O_3 nanocomposite coatings decreases with an increase in the Y_2O_3 concentration in the electrolyte bath. The obtained results show that Ni-Cu-Y_2O_3 (4 g/L) nanocomposite coating exhibits higher resistance against corrosion mainly due to the

higher content of Y_2O_3 nanoparticles and the least microstructural defects such as pores, voids and micro-cracks.

2.3.8.8 Effect of SiC nanoparticles

SiC has been widely used in photo-induced wettable composite coatings due to a highly effective photocatalyst under UV or visible light irradiation. Ni-Cu-SiC composite coatings have been synthesized on the Mg-Li alloy using the electrodeposition method and stearic acid modification to enhance corrosion resistance and hydrophobicity [95]. Wettability transition test and corrosion test were carried out to analyze the coating samples. Surface wettability tests revealed that the contact angle for Ni-Cu-SiC composite coating was increased with an increase in SiC concentration in the electrolyte bath up to 20 g/L and decreased with further increase in SiC concentration in the electrolyte bath. Corrosion study showed that the high hydrophobic state of coatings results in enhancement in the corrosion resistance of coatings.

2.4. Powder Metallurgy Method

2.4.1 Introduction to powder metallurgy

Powder metallurgy is ideal for producing metallic components from metallic powders because of its several advantages, such as fine-grained microstructure and enhanced homogeneity in terms of distribution of alloying elements, phase distribution and grain size. Powder metallurgy is extensively used in the fabrication of MMCs because of its near-shape capability, simplicity and flexibility. Most graphene reinforced metal matrix (Al [96], Mg [97], Cu [98] and Ni [99]) composites are fabricated by using the powder metallurgy technique. Also, very few studies on graphene reinforced alloy matrix (Mg-Ti [100], Mg-Al [101]) composites have been reported. The powder metallurgy method basically involves four different steps to complete the process, as shown in Figure 2.5. The first step involves the preparation of powder. The second step involves mixing reinforcement with metal matrix powder, which is generally carried out using a ball, planetary, high enemy mill, etc. The third step involves the compaction of powder, which is generally done using a hydraulic press. The final step involves the sintering of compacts, which is carried out using a muffle furnace or induction furnace. Powders under 200 μm are generally used to produce metallic components. During sintering of metallic components, sintering temperature is kept below the melting temperature of metallic

powder. Also, inert atmosphere is necessary to avoid the oxidation of the metallic components during sintering process.

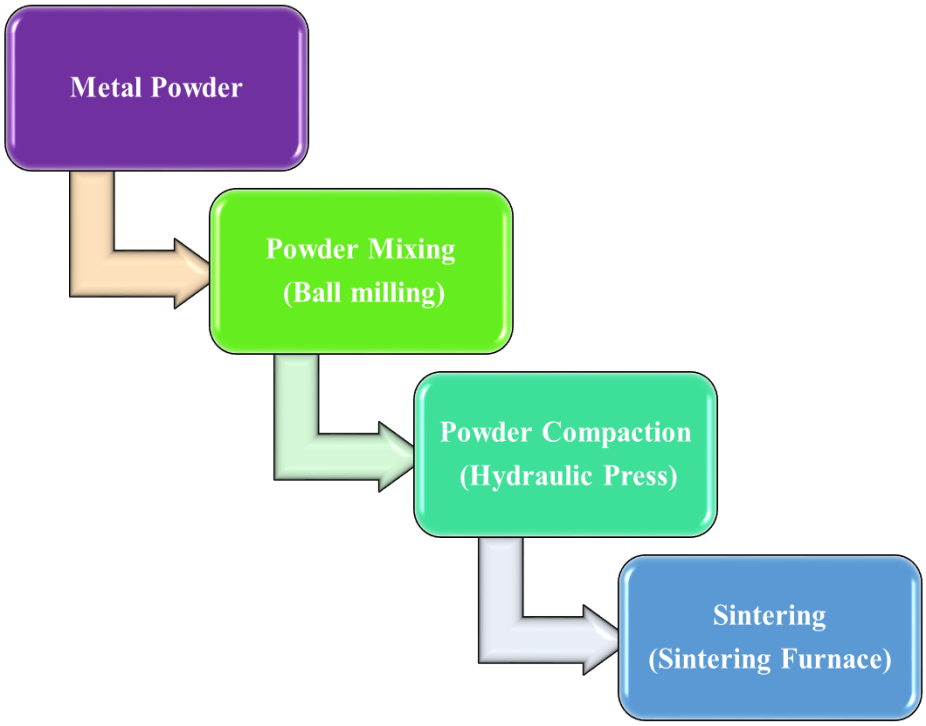

Figure 2.5: Processing route of powder metallurgy

2.4.2 Mixing

The composites powders have been synthesized by several mixing methods such as vortex mixing, sonication, magnetic stirring, mechanical alloying, ball milling and mechanical stirring [98], [102]–[108]. However, mechanical alloying is commonly used for powder processing to prepare alloy and composite materials. In this process initially, reinforcement and metallic powders are added in the desired proportion. After this, grinding of metallic powders and reinforcement is carried out using an attritor, planetary mill or shaker mill. An inert atmosphere is required to protect the metallic powder mixture from oxidation in the grinding mill. The energy milling process depends upon several process parameters such as the operating temperature, milling speed, milling time, milling atmosphere, design of ball mill and charge ratio. The intimate mixing of metallic powders and reinforcement is taken place at the atomic level due to the welding processes, deformation and repeating fracture during the milling process. Several process control agents (petroleum ether, stearic acid, etc.) have been used to avoid the agglomeration and sticking of metallic powder during the milling process. Process control agent is absorbed

on the metallic powder surface and decreases cold welding between impacted metallic particles. However, organic solvents (acetone, ethanol, etc.) are used in the ball milling process to prevent agglomeration of reinforcing elements such as graphene, CNT, etc. Before the consolidation process, vacuum rotary air-drying, vacuum infiltration, freeze-drying and evaporation drying are generally employed to remove organic solvent from the mixture. Tjong et al. [109] have reported that uniform dispersion of graphene in Cu matrix along with finer microstructure can be achieved with the help of the mechanical alloying process. However, some precautions related to processing parameters are necessary to avoid structural damage of graphene. Yue et al. [110] synthesized the graphene nanosheets reinforced Cu matrix composites using high energy ball milling and hot press sintering and observed that the size of Cu-graphene nanosheets powder decreases and the dispersion of graphene nanosheets in the Cu matrix enhances with an increase in ball milling time. However, the damage of graphene nanosheets increases with an increase in ball milling time. SEM images of Cu-GO 0.5 wt.% powders after ball-milling for different time is represented in Figure 2.6. From Figure 2.6, it is noticeable that with an increase in ball milling time, the shape of Cu-Go powders changes from flake-like to less granular. This change in the shape of Cu-Go powders is mainly due to the shearing effect of the balls. Also, from magnified images, it is clearly seen that the dispersion of GO nanosheets gradually is increased and the size of GO nanosheets is decreased with the increase in the ball milling time. After 5 hours milling process, GO nanosheets are absorbed on the surface of Cu powder. Cu-GO powder milled for 7 hours shows smaller size because of cold-working as a result of long-time shearing action.

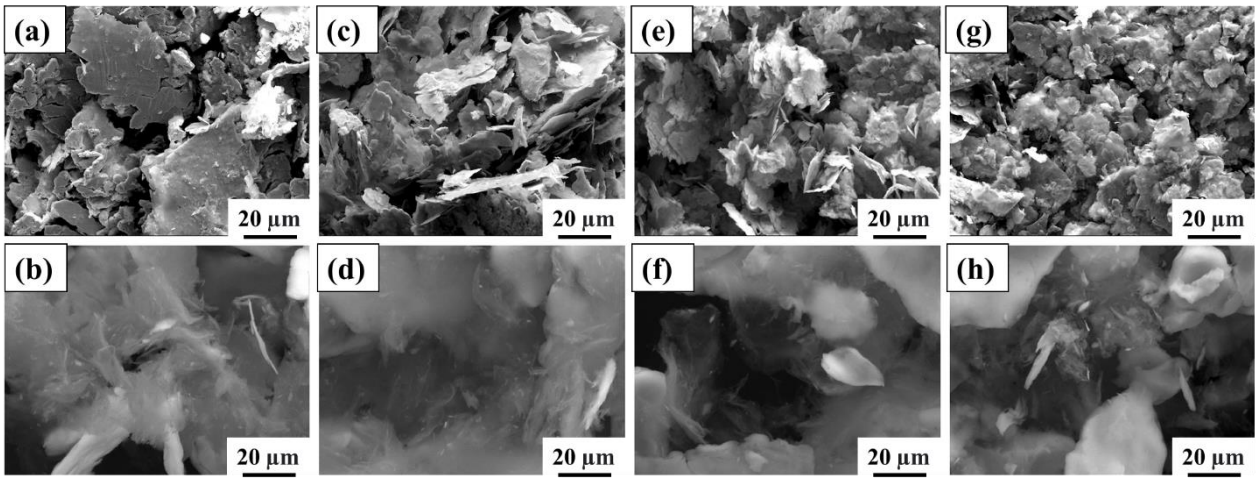

Figure 2.6: SEM images of Cu-0.5 wt.% GO powder after ball milling for (a, b) 1 hour, (c, d) 3 hours, (e, f) 5 hours and (g, h) 7 hours [110]

The degree of damage takes place to Go nanosheets can be determined using the intensity ratio of I_D/I_G. Figure 2.7 shows the Raman spectrum of Cu-GO 0.5 wt.% powders after ball milling for different times. From Figure 2.7, it is clearly seen that the ratio of I_D/I_G increases from 0.84 to 1.42 with an increase in ball milling time. Raman test result revealed that milling time should be appropriate to obtain a uniform dispersion of graphene in Cu matrix without damaging its structure.

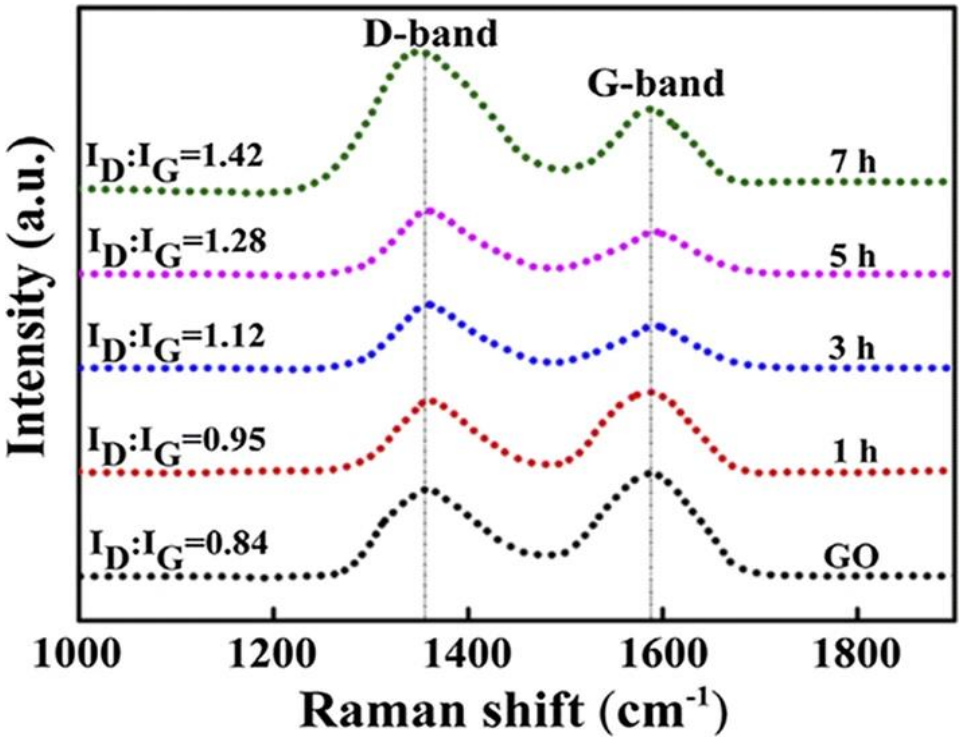

Figure 2.7: Raman spectra of Cu-0.5 wt.% GO powder after ball milling for different times [110]

Bakhshaei et al. [111] have fabricated Cu_{50}-Ni_{50}/CNT nanocomposite by the mechanical alloying method. First, Cu and Ni powder are mixed with equal quantity and then CNT are added to them. Then Cu-Ni alloy was reinforced with multi-walled carbon nanotubes using a ball milling. From the XRD analysis, it was confirmed that the formation of Cu_{50}-Ni_{50} alloy in 10 hours milled sample. The presence of CNT significantly affected the elemental composition and microstructure of Cu_{50}-Ni_{50}/CNT nanocomposite. Also, it was observed that decrease in crystalline size of Cu_{50}-Ni_{50}/CNT nanocomposites with an increase in milling time. The addition of CNTs to Cu-Ni powder enhances the work hardening and decreases the cold-welding rate of the powder particles during the ball milling, which resulted in a reduction in the particle size of the nanocomposite. The addition of CNT in Cu-Ni alloy decreases saturation magnetization and increases

coercivity than that of the Cu_{50}-Ni_{50} powder. Hence ball milling parameters need to be appropriate to obtain a uniform dispersion of CNT in the Cu-Ni alloy matrix while decreasing CNT structural damage.

2.4.3 Consolidation

Sintering method have been widely used to consolidate the metal, alloy and composite powders. In some research studies, green compacts are formed using a hydraulic press and sintered using a conventional or microwave furnace [96], [112], [113]. Microwave sintering is highly preferred compared to conventional sintering because it produces composites with much finer grain sizes due to quick heating.

Several researchers have reported hot pressing consolidation of metal, alloy and composite powders [114], [115]. Initially, the composite powder is filled in a graphite die and then simultaneous application of uniaxial pressure and heat is provided to obtain the consolidation of composite powder. Jiang et al. [116] have employed the powder metallurgy method to synthesize graphene nickel composites. They have used sucrose as a precursor of graphene then dispersed it into nickel powders to grow graphene. They have shown an improvement in the mechanical properties of composites and high load transfer from nickel matrix to graphene. During the high-temperature sintering process, carbon atoms segregate from the Ni matrix. Subsequently, graphene developed on the grain boundaries of Ni when the composite is cooled. The enhancement in the mechanical properties of Ni-graphene composite is mainly due to the decrease in foreign impurities, uniform dispersion of graphene and well-connected interfaces as a result of in-situ growth of graphene in bulk Ni matrix.

Wang et al. [117] investigated the Cu-graphene nanocomposites by powder metallurgy method. Initially, graphene is directly grown on Cu nanoparticle surface using chemical vapor deposition technique and then sintered at various temperatures to fabricate dense Cu-graphene nanocomposites. Cu-graphene nanocomposite is sintered using screwed graphite mold at 600, 650, 700, and 750 °C for 30 min. They observed that the hardness of the Cu-graphene nanocomposite prepared at 650 °C was 2.53 GPa, around 2.5 times higher than that of pure Cu. Also, the friction coefficient is reduced from 0.35 to 0.2. The enhancement in the properties of the Cu-graphene nanocomposite is attributed to the uniform dispersion of high-quality graphene into the Cu matrix.

There is a possibility of enhancement in mechanical, tribological and corrosion properties of Cu-Ni alloy matrix composites. Based upon the detailed literature review upon the synthesis of Cu-Ni alloy composites, research gaps have been determined and presented in the next section.

2.5. Gaps in Existing Research and Investigations

In chapter 1 and 2, we have reviewed the electrodeposition and powder metallurgy methods for the synthesis of Cu-Ni alloy matrix composites. In most of the research work, the synthesis of Cu-Ni alloy matrix composites has been carried out using electrodeposition method. From the literature review, a few significant gaps still exist in studies on the synthesis of Cu-Ni alloy matrix composite coatings. The following issues are figured out and addressed in this thesis and are detailed below:

1. Several reinforcing elements such as Al_2O_3, SiC, TiO_2, Y_2O_3, ZrO_2, TiN, MMT and Cr have been used to synthesize Cu-Ni alloy matrix composite coatings. However, the incorporation of ceramics can lead to problems with brittleness and delamination, resulting in short service life. Therefore, there is a need to explore a promising reinforcing element for fabricating Cu-Ni alloy matrix composite coatings.

Proposed Solution- Recently, graphene nanoplatelets have been identified as one of the best suitable reinforcing elements in the field of composite coating due to their outstanding chemical, tribological, electrical, mechanical, and corrosion properties [102], [118]. A lesser amount of uniformly distributed graphene nanoplatelets in the metal matrix can impart extraordinary mechanical, anti-corrosion and tribological properties. In the last decade, several researchers have fabricated graphene nanoplatelets reinforced composites for different metals such as Al [119], [120], Cu [98], [105], Mg [97], [121], Ni [116], [122] and Ag [123]. Currently, graphene nanoplatelets based composites are extensively used in several applications such as conductive ink pigment, paper sensors for electrochemical detection, electrochemical cells, alcohol oxidation, superconductors, adsorption and desorption of electrochemical energy, redox reactions [124]. The main disadvantages of graphene nanoplatelets are high cost, hydrophobicity difficult workability and small production rate [125]. In the past few decades, significant work has been carried out only on the electrodeposition of pure Cu-Ni alloy. Only a few attempts have been made to fabricate Cu-Ni alloy-based composite coatings to enhance the properties of Cu-Ni alloy further. However, graphene nanoplatelets reinforced Cu-Ni alloy

composite coatings have not been explored in the literature. Therefore, this research work proposes graphene nanoplatelets as a reinforcing element for the synthesis of Cu-Ni alloy matrix composite coatings.

2. For graphene-based composites, the enhancement in the properties depends upon the uniform dispersion of graphene in the metal matrix and structure of graphene. Several attempts have been made towards the improvement in the uniform dispersion of graphene without damaging its structure. Still, the uniform dispersion of graphene in the metal matrix without damaging its structure is a major challenge in the field of composite synthesis. Therefore, a method to overcome the above challenges needs to be investigated.

Proposed Solution- Nanoparticles agglomerates due to their high surface area to volume ratio. Several strategies were followed in the literature to disperse the nanoparticles in the metal matrix. To overcome the agglomeration of graphene nanoplatelets during electrodeposition process and avoid the damage of graphene nanoplatelets structure, this research is aimed to find an effective way, which can improve the mechanical, tribological and corrosion properties by providing a uniform dispersion of graphene nanoplatelets in the alloy metal matrix without damaging its structure.

3. A lot of the research work has been done on the Cu-Ni alloy matrix composite coatings using the electrodeposition method. The electrodeposition method limits the thickness of the composite up to 200 µm. No study has been there that reports a method for economical as well as scale-up and gives a huge amount of production for graphene nanoplatelets reinforced Cu-Ni alloy matrix composites.

Proposed Solution- A novel method for facile synthesis of graphene nanoplatelets reinforced Cu-Ni alloy matrix composites with improved mechanical, tribological and corrosion properties is proposed in this study. The method aids in providing a uniform dispersion of graphene nanoplatelets in the Cu-Ni alloy matrix without damaging its structure. The proposed method is a combination of the electrodeposition method and powder metallurgy method. This novel method enables bulk production of graphene nanoplatelets reinforced Cu-Ni alloy matrix composite in powder form.

Based on the existing knowledge and gaps in research, the following four objectives are designed:

1. Study of different fabrication methods for Cu-Ni alloy matrix composites to conclude about the most suitable method.

2. Synthesis of Cu-Ni/Gr composite coatings using electrodeposition method and bulk production of Cu-Ni/Gr composite powder using a novel method.
3. Study the effect on mechanical, tribological and corrosion properties of Cu-Ni/Gr composites by varying weight proportion of graphene nanoplatelets.
4. Optimization of process parameters with respect to improvement in mechanical and corrosion properties of Cu-Ni/Gr composites.

2.6. Organization of the Thesis

Cu-Ni alloys have been widely employed in several industries such as mechanical, automobile, chemical and marine due to their remarkable physical and mechanical properties. Currently, most efforts are focused on using Cu-Ni alloy matrix composite coatings in marine applications to improve their surface properties such as microhardness, corrosion and wear resistance through the incorporation of several reinforcing elements. A significant amount of research on Cu-Ni alloy matrix composite coatings using electrodeposition method has been carried out. Also, a more efficient method needs to be developed for facile, low cost and bulk production of Cu-Ni alloy matrix composites. Cu-Ni alloy matrix composites prepared using graphene as a reinforcing element through the electrodeposition method suggest a most simple and economical way to improve the overall properties.

In chapter 3, the synthesis of Cu-Ni/Gr composite has been discussed in two different forms. 1. Electro-co-deposition of Cu-Ni/Gr coating on the metallic substrate 2. Synthesis of Cu-Ni/Gr composites in the powder form by using a modified electrochemical-co-deposition method which is a simple, economical and suitable for bulk production of Cu-Ni/Gr composite powder.

In chapter 4, the detailed study of surface morphology, elemental composition, and microstructure of Cu-Ni/Gr composite coatings prepared by electro-co-deposition method and Cu-Ni/Gr composite powder prepared by a modified electro-co-deposition method have been carried out.

In chapter 5, details of the mechanical, tribological and corrosion properties of Cu-Ni/Gr composite coatings prepared by electro-co-deposition method are explained. Also, the mechanical, tribological and corrosion properties of Cu-Ni/Gr composites plates

prepared from the samples of the powder synthesized by modified electro-co-deposition method and followed by powder metallurgy method are discussed.

In chapter 6, the effect of electrolysis parameters and graphene nanoplatelets concentration on mechanical and corrosion properties of Cu-Ni/Gr composite coatings prepared by the electro-co-deposition method has been discussed. Also, the effect of electrolysis parameters on mechanical and corrosion properties of Cu-Ni/Gr composites plates prepared from the samples of the powder fabricated using a modified electrochemical-co-deposition method followed by the conventional powder metallurgy method has been discussed. The set of experiments is performed based on the design developed by the Taguchi method.

In Chapter 7, the overall conclusions and future scope of the present study have been discussed.

References

[1] C.-C. Chen, C.-H. Yang, Y.-S. Wu, and C.-E. Ho, "Depth-dependent self-annealing behavior of electroplated Cu," *Surf. Coatings Technol.*, vol. 320, pp. 489–496, Jun. 2017, doi: 10.1016/j.surfcoat.2016.11.057.

[2] W. R. Osório, A. Cremasco, P. N. Andrade, A. Garcia, and R. Caram, "Electrochemical behavior of centrifuged cast and heat treated Ti–Cu alloys for medical applications," *Electrochim. Acta*, vol. 55, no. 3, pp. 759–770, Jan. 2010, doi: 10.1016/j.electacta.2009.09.016.

[3] H. Li, S. Yu, J. Hu, and X. Yin, "Modifier-free fabrication of durable superhydrophobic electrodeposited Cu-Zn coating on steel substrate with self-cleaning, anti-corrosion and anti-scaling properties," *Appl. Surf. Sci.*, vol. 481, no. November 2018, pp. 872–882, Jul. 2019, doi: 10.1016/j.apsusc.2019.03.123.

[4] A. Banerjee, R. Kumar, M. Dutta, S. Bysakh, A. K. Bhowmick, and T. Laha, "Microstructural evolution in Cu–Sn coatings deposited on steel substrate and its effect on interfacial adhesion," *Surf. Coatings Technol.*, vol. 262, pp. 200–209, Jan. 2015, doi: 10.1016/j.surfcoat.2014.12.049.

[5] A. D. Pingale, S. U. Belgamwar, and J. S. Rathore, "Effect of Graphene Nanoplatelets Addition on the Mechanical, Tribological and Corrosion Properties of Cu–Ni/Gr Nanocomposite Coatings by Electro-co-deposition Method," *Trans. Indian Inst. Met.*, vol. 73, no. 1, pp. 99–107, Jan. 2020, doi: 10.1007/s12666-019-01807-9.

[6] P. Ferro, F. Bonollo, and A. Tiziani, "Laser welding of copper–nickel alloys: a numerical and experimental analysis," *Sci. Technol. Weld. Join.*, vol. 10, no. 3, pp. 299–310, 2005, doi: 10.1179/174329305X40615.

[7] C. R. Thurber *et al.*, "Metal Matrix Composite Coatings of Cupronickel Embedded with Nanoplatelets for Improved Corrosion Resistant Properties," *Int. J. Corros.*, vol. 2018, pp. 1–11, Jun. 2018, doi: 10.1155/2018/5250713.

[8] C. R. Thurber *et al.*, "Electrodeposition of 70-30 Cu–Ni nanocomposite coatings for enhanced mechanical and corrosion properties," *Curr. Appl. Phys.*, vol. 16, no. 3, pp. 387–396, Mar. 2016, doi: 10.1016/j.cap.2015.12.022.

[9] S. K. Ghosh, A. K. Grover, G. K. Dey, and M. K. Totlani, "Nanocrystalline Ni-Cu

alloy plating by pulse electrolysis," *Surf. Coatings Technol.*, vol. 126, no. 1, pp. 48–63, 2000, doi: 10.1016/S0257-8972(00)00520-X.

[10] D. Goranova, G. Avdeev, and R. Rashkov, "Electrodeposition and characterization of Ni-Cu alloys," *Surf. Coatings Technol.*, vol. 240, pp. 204–210, 2014, doi: 10.1016/j.surfcoat.2013.12.014.

[11] S. J. Yuan and S. O. Pehkonen, "Surface characterization and corrosion behavior of 70/30 Cu–Ni alloy in pristine and sulfide-containing simulated seawater," *Corros. Sci.*, vol. 49, no. 3, pp. 1276–1304, 2007, doi: https://doi.org/10.1016/j.corsci.2006.07.003.

[12] B. E. Torres Bautista *et al.*, "Effect of protein adsorption on the corrosion behavior of 70Cu–30Ni alloy in artificial seawater," *Bioelectrochemistry*, vol. 97, pp. 34–42, Jun. 2014, doi: 10.1016/j.bioelechem.2013.10.004.

[13] X. Zhu and T. Lei, "Characteristics and formation of corrosion product films of 70Cu–30Ni alloy in seawater," *Corros. Sci.*, vol. 44, no. 1, pp. 67–79, Jan. 2002, doi: 10.1016/S0010-938X(01)00041-5.

[14] E. Pellicer *et al.*, "A comparison between fine-grained and nanocrystalline electrodeposited Cu–Ni films. Insights on mechanical and corrosion performance," *Surf. Coatings Technol.*, vol. 205, no. 23–24, pp. 5285–5293, Sep. 2011, doi: 10.1016/j.surfcoat.2011.05.047.

[15] I. Baskaran, T. S. N. Sankara Narayanan, and A. Stephen, "Pulsed electrodeposition of nanocrystalline Cu–Ni alloy films and evaluation of their characteristic properties," *Mater. Lett.*, vol. 60, no. 16, pp. 1990–1995, Jul. 2006, doi: 10.1016/j.matlet.2005.12.065.

[16] P. Q. Dai, C. Zhang, J. C. Wen, H. C. Rao, and Q. T. Wang, "Tensile Properties of Electrodeposited Nanocrystalline Ni-Cu Alloys," *J. Mater. Eng. Perform.*, vol. 25, no. 2, pp. 594–600, Feb. 2016, doi: 10.1007/s11665-016-1881-2.

[17] M.-J. DENG, P.-C. LIN, I.-W. SUN, P.-Y. CHEN, and J.-K. CHANG, "Electrodeposition of Ni-Cu Alloys in an Air and Water Stable Room Temperature Ionic Liquid," *Electrochemistry*, vol. 77, no. 8, pp. 582–584, 2009, doi: 10.5796/electrochemistry.77.582.

[18] S. Wang *et al.*, "Electrodeposition mechanism and characterization of Ni-Cu alloy

coatings from a eutectic-based ionic liquid," *Appl. Surf. Sci.*, vol. 288, pp. 530–536, 2014, doi: 10.1016/j.apsusc.2013.10.065.

[19] V. Torabinejad, M. Aliofkhazraei, S. Assareh, M. H. Allahyarzadeh, and A. S. Rouhaghdam, "Electrodeposition of Ni-Fe alloys, composites, and nano coatings–A review," *J. Alloys Compd.*, vol. 691, pp. 841–859, Jan. 2017, doi: 10.1016/j.jallcom.2016.08.329.

[20] W. Schleich, "Typical Failures of CuNi 90 / 10 Seawater Tubing Systems and How to Avoid Them Effect of Alloying Elements," *Eng. Struct.*, vol. 2004, pp. 1–10, 2004.

[21] A. M. Rashidi and A. Amadeh, "The effect of current density on the grain size of electrodeposited nanocrystalline nickel coatings," *Surf. Coatings Technol.*, vol. 202, no. 16, pp. 3772–3776, 2008, doi: 10.1016/j.surfcoat.2008.01.018.

[22] A. M. Rashidi and A. Amadeh, "The effect of saccharin addition and bath temperature on the grain size of nanocrystalline nickel coatings," *Surf. Coatings Technol.*, vol. 204, no. 3, pp. 353–358, 2009, doi: 10.1016/j.surfcoat.2009.07.036.

[23] S. Guan and B. J. Nelson, "Electrodeposition of low residual stress CoNiMnP hard magnetic thin films for magnetic MEMS actuators," *J. Magn. Magn. Mater.*, vol. 292, pp. 49–58, 2005, doi: 10.1016/j.jmmm.2004.10.094.

[24] E. Gómez, E. Pellicer, and E. Vallés, "Microstructures of soft-magnetic cobalt-molybdenum alloy obtained by electrodeposition on seed layer/silicon substrates," *Electrochem. commun.*, vol. 6, no. 8, pp. 853–859, 2004, doi: 10.1016/j.elecom.2004.06.011.

[25] P. Calleja, J. Esteve, P. Cojocaru, L. Magagnin, E. Vallés, and E. Gómez, "Developing plating baths for the production of reflective Ni–Cu films," *Electrochim. Acta*, vol. 62, pp. 381–389, Feb. 2012, doi: 10.1016/j.electacta.2011.12.049.

[26] G. H. M. Saeed, S. Radiman, S. S. Gasaymeh, H. N. Lim, and N. M. Huang, "Mild Hydrothermal Synthesis of Ni – Cu Nanoparticles," no. May 2014, 2010, doi: 10.1155/2010/184137.

[27] U. Sarac and M. C. Baykul, "Morphological and microstructural properties of two-phase Ni–Cu films electrodeposited at different electrolyte temperatures," *J.*

Alloys Compd., vol. 552, pp. 195–201, Mar. 2013, doi: 10.1016/j.jallcom.2012.10.071.

[28] M. Pushpavanam and K. Balakrishnan, "Zinc-nickel alloy deposition in the presence of citrate ions," *J. Appl. Electrochem.*, vol. 26, no. 10, pp. 1065–1066, Oct. 1996, doi: 10.1007/BF00242202.

[29] M. Ishikawa, H. Enomoto, M. Matsuoka, and C. Iwakura, "Effect of some factors on electrodeposition of nickel-copper alloy from pyrophosphate-tetraborate bath," *Electrochim. Acta*, vol. 40, no. 11, pp. 1663–1668, 1995, doi: https://doi.org/10.1016/0013-4686(95)00084-R.

[30] A. R. Despić, V. D. Jović, and S. Spaić, "Electrochemical Formation of Laminar Deposits of Controlled Structure and Composition II. Dual Current Pulse Galvanostatic Technique," *J. Electrochem. Soc.*, vol. 136, no. 6, pp. 1651–1657, 1989.

[31] H. Zhang and S.-M. Park, "Studies on the anodic decomposition products of sulfamate," *J. Appl. Electrochem.*, vol. 24, no. 11, Nov. 1994, doi: 10.1007/BF00241319.

[32] H. Zhang and S. M. Park, "Studies on the anodic decomposition products of sulfamate," *J. Appl. Electrochem.*, vol. 24, no. 11, pp. 1182–1187, 1994, doi: 10.1007/BF00241319.

[33] S. Mohan and N. Rajasekaran, "Influence of electrolyte pH on composition, corrosion properties and surface morphology of electrodeposited Cu–Ni alloy," *Surf. Eng.*, vol. 27, no. 7, pp. 519–523, 2011, doi: 10.1179/026708410x12786785573472.

[34] N. V Mandich and D. W. Baudrand, "Troubleshooting electroplating installations: Nickel sulfamate plating systems," *Plat. Surf. Finish.*, vol. 89, pp. 68–76, 2002.

[35] D. J. Kim, Y. M. Roh, M. H. Seo, and J. S. Kim, "Effects of the peak current density and duty cycle on material properties of pulse-plated Ni–P–Fe electrodeposits," *Surf. Coatings Technol.*, vol. 192, no. 1, pp. 88–93, Mar. 2005, doi: 10.1016/j.surfcoat.2004.03.055.

[36] M. H. Seo, D. J. Kim, and J. S. Kim, "The effects of pH and temperature on Ni–Fe–P alloy electrodeposition from a sulfamate bath and the material properties of

the deposits," *Thin Solid Films*, vol. 489, no. 1–2, pp. 122–129, Oct. 2005, doi: 10.1016/j.tsf.2005.05.011.

[37] M. M. Kamel, Z. M. Anwer, I. T. Abdel-Salam, and I. S. Ibrahim, "Electrodeposition of nanocrystalline Ni-Cu alloy from environmentally friendly lactate bath," *Surf. Interface Anal.*, vol. 46, no. 7, pp. 442–448, Jul. 2014, doi: 10.1002/sia.5525.

[38] M. M. Kamel, "Anomalous codeposition of Co–Ni: alloys from gluconate baths," *J. Appl. Electrochem.*, vol. 37, no. 4, pp. 483–489, Mar. 2007, doi: 10.1007/s10800-006-9279-8.

[39] I.-W. Sun and P.-Y. Chen, "Electrodeposition of Alloys," in *Electrodeposition from Ionic Liquids*, Weinheim, Germany: Wiley-VCH Verlag GmbH & Co. KGaA, 2008, pp. 125–146. doi: 10.1002/9783527622917.ch5.

[40] İ. H. Karahan, "Effects of pH Value of the Electrolyte and Glycine Additive on Formation and Properties of Electrodeposited Zn-Fe Coatings," *Sci. World J.*, vol. 2013, pp. 1–7, 2013, doi: 10.1155/2013/273953.

[41] I. Mizushima, "Microstructure of Electrodeposited Cu-Ni Binary Alloy Films," *J. Electrochem. Soc.*, vol. 143, no. 6, p. 1978, 1996, doi: 10.1149/1.1836935.

[42] M. Cherkaoui, E. Chassaing, and K. Vu Quang, "Pulse plating of Ni-Cu alloys," *Surf. Coatings Technol.*, vol. 34, no. 3, pp. 243–252, Apr. 1988, doi: 10.1016/0257-8972(88)90116-8.

[43] S. Roy, "Effect of Corrosion on the Composition of Pulse-Plated Cu-Ni Alloys," *J. Electrochem. Soc.*, vol. 141, no. 6, p. 1509, 1994, doi: 10.1149/1.2054954.

[44] L. Bonou, Y. Massiani, and J. Crousier, "Electrodeposition and corrosion behaviour of copper-nickel alloys," *Br. Corros. J.*, vol. 29, no. 3, pp. 201–206, Jan. 1994, doi: 10.1179/000705994798267719.

[45] P. Bradley, S. Roy, and D. Landolt, "Pulse-plating of copper–nickel alloys from a sulfamate solution," *J. Chem. Soc., Faraday Trans.*, vol. 92, no. 20, pp. 4015–4019, 1996, doi: 10.1039/FT9969204015.

[46] M. Haciismailoglu and M. Alper, "Effect of electrolyte pH and Cu concentration on microstructure of electrodeposited Ni-Cu alloy films," *Surf. Coatings Technol.*, vol. 206, no. 6, pp. 1430–1438, 2011, doi: 10.1016/j.surfcoat.2011.09.010.

[47] U. Sarac, R. M. Öksüzoğlu, and M. C. Baykul, “Deposition potential dependence of composition, microstructure, and surface morphology of electrodeposited Ni-Cu alloy films,” *J. Mater. Sci. Mater. Electron.*, vol. 23, no. 12, pp. 2110–2116, 2012, doi: 10.1007/s10854-012-0709-6.

[48] A. Varea *et al.*, “Mechanical properties and corrosion behaviour of nanostructured Cu-rich CuNi electrodeposited films,” *Int. J. Electrochem. Sci.*, vol. 7, no. 2, pp. 1288–1302, 2012.

[49] V. Zin, K. Brunelli, and M. Dabalà, “Characterization of Cu-Ni alloy electrodeposition and synthesis of nanoparticles by pulsed sonoelectrochemistry,” *Mater. Chem. Phys.*, vol. 144, no. 3, pp. 272–279, 2014, doi: 10.1016/j.matchemphys.2013.12.028.

[50] K. Ngamlerdpokin and N. Tantavichet, “Electrodeposition of nickel-copper alloys to use as a cathode for hydrogen evolution in an alkaline media,” *Int. J. Hydrogen Energy*, vol. 39, no. 6, pp. 2505–2515, 2014, doi: 10.1016/j.ijhydene.2013.12.013.

[51] M. Alizadeh and H. Safaei, “Characterization of Ni-Cu matrix, Al2O3 reinforced nano-composite coatings prepared by electrodeposition,” *Appl. Surf. Sci.*, vol. 456, pp. 195–203, Oct. 2018, doi: 10.1016/j.apsusc.2018.06.095.

[52] B. Li, T. Mei, D. Li, and S. Du, “Ultrasonic-assisted electrodeposition of Ni-Cu/TiN composite coating from sulphate-citrate bath: Structural and electrochemical properties,” *Ultrason. Sonochem.*, vol. 58, no. May, 2019, doi: 10.1016/j.ultsonch.2019.104680.

[53] B. Li, T. Mei, D. Li, S. Du, and W. Zhang, “Structural and corrosion behavior of Ni-Cu and Ni-Cu/ZrO2 composite coating electrodeposited from sulphate-citrate bath at low Cu concentration with additives,” *J. Alloys Compd.*, vol. 804, pp. 192–201, 2019, doi: 10.1016/j.jallcom.2019.06.381.

[54] B. Li, S. Du, and T. Mei, “Pulse electrodepsoited Ni-Cu/TiN-ZrO 2 nanocomposite coating: microstructural and electrochemical properties,” *Mater. Res. Express*, vol. 6, no. 9, p. 096433, Jul. 2019, doi: 10.1088/2053-1591/ab31e9.

[55] Z. Huang, X. Peng, and F. Wang, “Preparation and oxidation of novel electrodeposited Cu-Ni-Cr nanocomposites,” *Oxid. Met.*, vol. 65, no. 3–4, pp. 223–236, 2006, doi: 10.1007/s11085-006-9017-y.

[56] Z. Huang, X. Peng, C. Xu, and F. Wang, “On the exclusive growth of external chromia scale on the novel electrodeposited Cu-Ni-Cr nanocomposites,” *J. Mater. Res.*, vol. 22, no. 11, pp. 3166–3177, 2007, doi: 10.1557/jmr.2007.0411.

[57] M. S. Safavi, M. Fathi, S. Mirzazadeh, A. Ansarian, and I. Ahadzadeh, “Perspectives in corrosion-performance of Ni–Cu coatings by adding Y 2 O 3 nanoparticles,” *Surf. Eng.*, vol. 0, no. 0, pp. 1–10, Jan. 2020, doi: 10.1080/02670844.2020.1715543.

[58] W. Tian, S. Li, B. Wang, X. Chen, J. Liu, and M. Yu, “Graphene-reinforced aluminum matrix composites prepared by spark plasma sintering,” *Int. J. Miner. Metall. Mater.*, vol. 23, no. 6, pp. 723–729, 2016, doi: 10.1007/s12613-016-1286-0.

[59] J. Vazquez-Arenas, L. Altamirano-Garcia, T. Treeratanaphitak, M. Pritzker, R. Luna-Sánchez, and R. Cabrera-Sierra, “Co–Ni alloy electrodeposition under different conditions of pH, current and composition,” *Electrochim. Acta*, vol. 65, pp. 234–243, Mar. 2012, doi: 10.1016/j.electacta.2012.01.050.

[60] W. C. Grande, “Electrodeposition of Thin Films of Nickel-Iron,” *J. Electrochem. Soc.*, vol. 140, no. 3, p. 675, 1993, doi: 10.1149/1.2056141.

[61] J. Horkans, “Effect of Plating Parameters on Electrodeposited NiFe,” *J. Electrochem. Soc.*, vol. 128, no. 1, p. 45, 1981, doi: 10.1149/1.2127385.

[62] B. V Tilak, A. S. Gendron, and M. A. Mosoiu, “Borate buffer equilibria in nickel refining electrolytes,” *J. Appl. Electrochem.*, vol. 7, no. 6, pp. 495–500, Nov. 1977, doi: 10.1007/BF00616760.

[63] E. Pellicer *et al.*, “Nanocrystalline Electroplated Cu-Ni: Metallic Thin Films with Enhanced Mechanical Properties and Tunable Magnetic Behavior,” *Adv. Funct. Mater.*, vol. 20, no. 6, pp. 983–991, Mar. 2010, doi: 10.1002/adfm.200901732.

[64] A. F. de Faria *et al.*, “Anti-adhesion and antibacterial activity of silver nanoparticles supported on graphene oxide sheets,” *Colloids Surfaces B Biointerfaces*, vol. 113, pp. 115–124, Jan. 2014, doi: 10.1016/j.colsurfb.2013.08.006.

[65] C. LI, X. LI, Z. WANG, and H. GUO, “Nickel electrodeposition from novel citrate bath,” *Trans. Nonferrous Met. Soc. China*, vol. 17, no. 6, pp. 1300–1306,

Dec. 2007, doi: 10.1016/S1003-6326(07)60266-0.

[66] T. DOI, K. MIZUMOTO, M. KAYASHIMA, and S. TANAKA, "Nickel Electroplating Bath Using Citric Acid.," *J. Surf. Finish. Soc. Japan*, vol. 52, no. 6, pp. 462–466, 2001, doi: 10.4139/sfj.52.462.

[67] P. Calleja, J. Esteve, P. Cojocaru, L. Magagnin, E. Vallés, and E. Gómez, "Developing plating baths for the production of reflective Ni-Cu films," *Electrochim. Acta*, vol. 62, pp. 381–389, 2012, doi: 10.1016/j.electacta.2011.12.049.

[68] A. Afshar, A. . Dolati, and M. Ghorbani, "Electrochemical characterization of the Ni–Fe alloy electrodeposition from chloride–citrate–glycolic acid solutions," *Mater. Chem. Phys.*, vol. 77, no. 2, pp. 352–358, Jan. 2003, doi: 10.1016/S0254-0584(02)00017-2.

[69] Y. Li, J. Yao, and X. Huang, "Effect of Saccharin on the Process and Properties of Nickel Electrodeposition from Sulfate Electrolyte," *Int. J. Metall. Mater. Eng.*, vol. 2, no. 1, pp. 0–4, Apr. 2016, doi: 10.15344/2455-2372/2016/123.

[70] M. R. Vaezi, S. K. Sadrnezhaad, and L. Nikzad, "Electrodeposition of Ni-SiC nano-composite coatings and evaluation of wear and corrosion resistance and electroplating characteristics," *Colloids Surfaces A Physicochem. Eng. Asp.*, vol. 315, no. 1–3, pp. 176–182, 2008, doi: 10.1016/j.colsurfa.2007.07.027.

[71] U. S. Waware, A. M. S. Hamouda, B. Bajaj, T. Borkar, and A. K. Pradhan, "Synthesis and characterization of electrodeposited Ni-B-Tl2O3 composite coatings," *J. Alloys Compd.*, vol. 769, pp. 353–359, Nov. 2018, doi: 10.1016/j.jallcom.2018.08.017.

[72] A. K. Chaudhari and V. B. Singh, "A review of fundamental aspects, characterization and applications of electrodeposited nanocrystalline iron group metals, Ni-Fe alloy and oxide ceramics reinforced nanocomposite coatings," *J. Alloys Compd.*, vol. 751, pp. 194–214, Jun. 2018, doi: 10.1016/j.jallcom.2018.04.090.

[73] A. ASHOK, H. S. MAHARANA, and A. BASU, "Effect of electro-co-deposition parameters on surface mechanical properties of Cu–TiO2 composite coating," *Bull. Mater. Sci.*, vol. 38, no. 2, pp. 335–342, Apr. 2015, doi: 10.1007/s12034-015-0884-1.

[74] L. Chen, L. Wang, Z. Zeng, and T. Xu, “Influence of pulse frequency on the microstructure and wear resistance of electrodeposited Ni–Al2O3 composite coatings,” *Surf. Coatings Technol.*, vol. 201, no. 3–4, pp. 599–605, Oct. 2006, doi: 10.1016/j.surfcoat.2005.12.008.

[75] A. D. Pingale, S. U. Belgamwar, and J. S. Rathore, “The influence of graphene nanoplatelets (GNPs) addition on the microstructure and mechanical properties of Cu-GNPs composites fabricated by electro-co-deposition and powder metallurgy,” *Mater. Today Proc.*, vol. 28, pp. 2062–2067, 2020, doi: 10.1016/j.matpr.2020.02.728.

[76] W. Wang, F.-Y. Hou, H. Wang, and H.-T. Guo, “Fabrication and characterization of Ni–ZrO2 composite nano-coatings by pulse electrodeposition,” *Scr. Mater.*, vol. 53, no. 5, pp. 613–618, Sep. 2005, doi: 10.1016/j.scriptamat.2005.04.002.

[77] G. Meng, F. Sun, S. Wang, Y. Shao, T. Zhang, and F. Wang, “Effect of electrodeposition parameters on the hydrogen permeation during Cu–Sn alloy electrodeposition,” *Electrochim. Acta*, vol. 55, no. 7, pp. 2238–2245, Feb. 2010, doi: 10.1016/j.electacta.2009.11.075.

[78] F. Nasirpouri *et al.*, “An investigation on the effect of surface morphology and crystalline texture on corrosion behavior, structural and magnetic properties of electrodeposited nanocrystalline nickel films,” *Appl. Surf. Sci.*, vol. 292, pp. 795–805, Feb. 2014, doi: 10.1016/j.apsusc.2013.12.053.

[79] T. Borkar and S. P. Harimkar, “Effect of electrodeposition conditions and reinforcement content on microstructure and tribological properties of nickel composite coatings,” *Surf. Coatings Technol.*, vol. 205, no. 17–18, pp. 4124–4134, May 2011, doi: 10.1016/j.surfcoat.2011.02.057.

[80] V. Torabinejad, M. Aliofkhazraei, A. Sabour Rouhaghdam, and M. H. Allahyarzadeh, “Functionally Graded Coating of Ni-Fe Fabricated by Pulse Electrodeposition,” *J. Mater. Eng. Perform.*, vol. 25, no. 12, pp. 5494–5501, Dec. 2016, doi: 10.1007/s11665-016-2376-x.

[81] A. Zoikis-Karathanasis, E. A. Pavlatou, and N. Spyrellis, “Pulse electrodeposition of Ni–P matrix composite coatings reinforced by SiC particles,” *J. Alloys Compd.*, vol. 494, no. 1–2, pp. 396–403, Apr. 2010, doi: 10.1016/j.jallcom.2010.01.057.

[82] K. R. Sriraman, S. Ganesh Sundara Raman, and S. K. Seshadri, “Corrosion

behaviour of electrodeposited nanocrystalline Ni–W and Ni–Fe–W alloys," *Mater. Sci. Eng. A*, vol. 460–461, pp. 39–45, Jul. 2007, doi: 10.1016/j.msea.2007.02.055.

[83] K.-L. Lin, C.-J. Hsu, I.-M. Hsu, and J.-T. Chang, "Electroplating of Ni-Cr on steel with pulse plating," *J. Mater. Eng. Perform.*, vol. 1, no. 3, pp. 359–361, Jun. 1992, doi: 10.1007/BF02652390.

[84] M. Metikoš-Huković, I. Škugor, Z. Grubač, and R. Babić, "Complexities of corrosion behaviour of copper–nickel alloys under liquid impingement conditions in saline water," *Electrochim. Acta*, vol. 55, no. 9, pp. 3123–3129, 2010, doi: https://doi.org/10.1016/j.electacta.2010.01.066.

[85] W.-C. Lin, C.-C. Chuang, P.-T. Wang, and C.-M. Tang, "A Comparative Study on the Direct and Pulsed Current Electrodeposition of Cobalt-Substituted Hydroxyapatite for Magnetic Resonance Imaging Application," *Materials (Basel).*, vol. 12, no. 1, p. 116, Dec. 2018, doi: 10.3390/ma12010116.

[86] S. Roy, "Effect of Off-Time on the Composition of Pulse-Plated Cu-Ni Alloys," *J. Electrochem. Soc.*, vol. 142, no. 9, p. 3021, 1995, doi: 10.1149/1.2048679.

[87] C. L. P. Pavithra, B. V Sarada, K. V Rajulapati, T. N. Rao, and G. Sundararajan, "Process Optimization for Pulse Reverse Electrodeposition of Graphene-Reinforced Copper Nanocomposites," *Mater. Manuf. Process.*, vol. 31, no. 11, pp. 1439–1446, 2016, doi: 10.1080/10426914.2015.1127938.

[88] P. Nath, D. K. Sahu, and A. Mallik, "Physicochemical and corrosion properties of sono-electrodeposited Cu-Ni thin films," *Surf. Coatings Technol.*, vol. 307, pp. 772–780, Dec. 2016, doi: 10.1016/j.surfcoat.2016.09.085.

[89] P. NATH, R. PANDEY, A. DAS, and A. MALLIK, "Effect of deposition potential and copper concentration on the phase transformation mechanism and structural distribution during electrodeposition of Ni-Cu magnetic alloy thin films," *Met. Mater.*, vol. 55, no. 04, pp. 255–265, 2017, doi: 10.4149/km_2017_4_255.

[90] D. Givord, "Introduction to magnetism and magnetic materials," in *Magnetism and Synchrotron Radiation*, Springer, 2001, pp. 3–23.

[91] B. D. Cullity and C. D. Graham, *Introduction to Magnetic Materials*. Hoboken, NJ, USA: John Wiley & Sons, Inc., 2008. doi: 10.1002/9780470386323.

[92] R. Oriňáková, A. Turoňová, D. Kladeková, M. Gálová, and R. M. Smith, “Recent developments in the electrodeposition of nickel and some nickel-based alloys,” *J. Appl. Electrochem.*, vol. 36, no. 9, pp. 957–972, Sep. 2006, doi: 10.1007/s10800-006-9162-7.

[93] A. Turoňová, M. Gálová, M. Šupicová, and L. Lux, “Parameters influencing the electrodeposition of a Ni-Cu coating on Fe powders. II. Effect of particle size fraction, suspension density and rotation speed,” *J. Solid State Electrochem.*, vol. 7, no. 10, pp. 689–693, Oct. 2003, doi: 10.1007/s10008-003-0373-0.

[94] S. M. Silaimani, G. Vivekanandan, and P. Veeramani, “Nano-nickel–copper alloy deposit for improved corrosion resistance in marine environment,” *Int. J. Environ. Sci. Technol.*, vol. 12, no. 7, pp. 2299–2306, 2015, doi: 10.1007/s13762-014-0591-2.

[95] P. Ji, R. Long, L. Hou, R. Wu, J. Zhang, and M. Zhang, “Study on hydrophobicity and wettability transition of Ni-Cu-SiC coating on Mg-Li alloy,” *Surf. Coatings Technol.*, vol. 350, no. February, pp. 428–435, Sep. 2018, doi: 10.1016/j.surfcoat.2018.07.038.

[96] J. Wang, Z. Li, G. Fan, H. Pan, Z. Chen, and D. Zhang, “Reinforcement with graphene nanosheets in aluminum matrix composites,” *Scr. Mater.*, vol. 66, no. 8, pp. 594–597, Apr. 2012, doi: 10.1016/j.scriptamat.2012.01.012.

[97] M. Rashad, F. Pan, H. Hu, M. Asif, S. Hussain, and J. She, “Enhanced tensile properties of magnesium composites reinforced with graphene nanoplatelets,” *Mater. Sci. Eng. A*, vol. 630, pp. 36–44, Apr. 2015, doi: 10.1016/j.msea.2015.02.002.

[98] K. Chu and C. Jia, “Enhanced strength in bulk graphene-copper composites,” *Phys. status solidi*, vol. 211, no. 1, pp. 184–190, Jan. 2014, doi: 10.1002/pssa.201330051.

[99] I. Y. Archakov *et al.*, “Microstructure and mechanical characteristics of nanostructured nickel-graphene composites processed by high pressure torsion,” *Rev. Adv. Mater. Sci.*, vol. 50, no. 1–2, pp. 13–23, 2017.

[100] M. Rashad *et al.*, “Effect of graphene nanoplatelets (GNPs) addition on strength and ductility of magnesium-titanium alloys,” *J. Magnes. Alloy.*, vol. 1, no. 3, pp. 242–248, 2013, doi: 10.1016/j.jma.2013.09.004.

[101] M. Rashad, F. Pan, A. Tang, M. Asif, and M. Aamir, “Synergetic effect of graphene nanoplatelets (GNPs) and multi-walled carbon nanotube (MW-CNTs) on mechanical properties of pure magnesium,” *J. Alloys Compd.*, vol. 603, pp. 111–118, 2014, doi: 10.1016/j.jallcom.2014.03.038.

[102] J. Hwang *et al.*, “Enhanced Mechanical Properties of Graphene/Copper Nanocomposites Using a Molecular-Level Mixing Process,” *Adv. Mater.*, vol. 25, no. 46, pp. 6724–6729, Dec. 2013, doi: 10.1002/adma.201302495.

[103] W. J. Kim, T. J. Lee, and S. H. Han, “Multi-layer graphene/copper composites: Preparation using high-ratio differential speed rolling, microstructure and mechanical properties,” *Carbon N. Y.*, vol. 69, pp. 55–65, 2014, doi: 10.1016/j.carbon.2013.11.058.

[104] J. Dutkiewicz *et al.*, “Microstructure and properties of bulk copper matrix composites strengthened with various kinds of graphene nanoplatelets,” *Mater. Sci. Eng. A*, vol. 628, pp. 124–134, 2015, doi: 10.1016/j.msea.2015.01.018.

[105] X. Gao *et al.*, “Mechanical properties and thermal conductivity of graphene reinforced copper matrix composites,” *Powder Technol.*, vol. 301, pp. 601–607, Nov. 2016, doi: 10.1016/j.powtec.2016.06.045.

[106] C. Ayyappadas, A. Muthuchamy, A. Raja Annamalai, and D. K. Agrawal, “An investigation on the effect of sintering mode on various properties of copper-graphene metal matrix composite,” *Adv. Powder Technol.*, vol. 28, no. 7, pp. 1760–1768, Jul. 2017, doi: 10.1016/j.apt.2017.04.013.

[107] N. V. Ponraj *et al.*, “Effect of milling on dispersion of graphene nanosheet reinforcement in different morphology copper powder matrix,” *Surfaces and Interfaces*, vol. 9, no. June, pp. 260–265, 2017, doi: 10.1016/j.surfin.2017.10.006.

[108] N. V. Ponraj, A. Azhagurajan, S. C. Vettivel, X. Sahaya Shajan, P. Y. Nabhiraj, and M. Sivapragash, “Graphene nanosheet as reinforcement agent in copper matrix composite by using powder metallurgy method,” *Surfaces and Interfaces*, vol. 6, pp. 190–196, 2017, doi: 10.1016/j.surfin.2017.01.010.

[109] S. C. Tjong, “Recent progress in the development and properties of novel metal matrix nanocomposites reinforced with carbon nanotubes and graphene nanosheets,” *Mater. Sci. Eng. R Reports*, vol. 74, no. 10, pp. 281–350, Oct. 2013, doi: 10.1016/j.mser.2013.08.001.

[110] H. Yue *et al.*, “Effect of ball-milling and graphene contents on the mechanical properties and fracture mechanisms of graphene nanosheets reinforced copper matrix composites,” *J. Alloys Compd.*, vol. 691, pp. 755–762, 2017, doi: 10.1016/j.jallcom.2016.08.303.

[111] P. Bakhshaei, A. Ataie, and H. Abdizadeh, “Effect of CNT Addition on the Characteristics of Cu-Ni / CNT Nanocomposite,” *J. Nanostructures*, vol. 3, no. 2013, pp. 403–409, 2014, doi: 10.7508/jns.2013.04.003.

[112] A. Ghazaly, B. Seif, and H. G. Salem, “Mechanical and tribological properties of AA2124-graphene self lubricating nanocomposite,” *Miner. Met. Mater. Ser.*, no. 210869, pp. 411–415, 2013, doi: 10.1007/978-3-319-65136-1_71.

[113] B. Ebinezar, “Engineering Analysis of hardness test for aluminium carbon nanotube metal matrix and graphene,” *Indian J. Eng.*, vol. 10, no. 21, pp. 33–39, 2014.

[114] J. LI, L. ZHANG, J. XIAO, and K. ZHOU, “Sliding wear behavior of copper-based composites reinforced with graphene nanosheets and graphite,” *Trans. Nonferrous Met. Soc. China*, vol. 25, no. 10, pp. 3354–3362, Oct. 2015, doi: 10.1016/S1003-6326(15)63970-X.

[115] B. W. Wei *et al.*, “Synthesis and Physical Properties of Graphene Nanosheets Reinforced Copper Composites,” *Adv. Mater. Res.*, vol. 833, pp. 310–314, Nov. 2013, doi: 10.4028/www.scientific.net/AMR.833.310.

[116] J. Jiang, X. He, J. Du, X. Pang, H. Yang, and Z. Wei, “In-situ fabrication of graphene-nickel matrix composites,” *Mater. Lett.*, vol. 220, no. March, pp. 178–181, Jun. 2018, doi: 10.1016/j.matlet.2018.03.039.

[117] S. Wang *et al.*, “High-quality graphene directly grown on Cu nanoparticles for Cu-graphene nanocomposites,” *Mater. Des.*, vol. 139, pp. 181–187, Feb. 2018, doi: 10.1016/j.matdes.2017.11.010.

[118] G. Yasin *et al.*, “Synthesis of spheres-like Ni/graphene nanocomposite as an efficient anti-corrosive coating; effect of graphene content on its morphology and mechanical properties,” *J. Alloys Compd.*, vol. 755, pp. 79–88, Jul. 2018, doi: 10.1016/j.jallcom.2018.04.321.

[119] R. Pérez-Bustamante, D. Bolaños-Morales, J. Bonilla-Martínez, I. Estrada-Guel,

and R. Martínez-Sánchez, “Microstructural and hardness behavior of graphene-nanoplatelets/aluminum composites synthesized by mechanical alloying,” *J. Alloys Compd.*, vol. 615, no. S1, pp. S578–S582, Dec. 2014, doi: 10.1016/j.jallcom.2014.01.225.

[120] S. Rengifo, C. Zhang, S. Harimkar, B. Boesl, and A. Agarwal, “Tribological Behavior of Spark Plasma Sintered Aluminum-Graphene Composites at Room and Elevated Temperatures,” *Technologies*, vol. 5, no. 1, p. 4, Jan. 2017, doi: 10.3390/technologies5010004.

[121] M. Rashad *et al.*, “Development of magnesium-graphene nanoplatelets composite,” *J. Compos. Mater.*, vol. 49, no. 3, pp. 285–293, Feb. 2015, doi: 10.1177/0021998313518360.

[122] A. Jabbar *et al.*, “Electrochemical deposition of nickel graphene composite coatings: effect of deposition temperature on its surface morphology and corrosion resistance,” *RSC Adv.*, vol. 7, no. 49, pp. 31100–31109, 2017, doi: 10.1039/C6RA28755G.

[123] R. Gao *et al.*, “Paper-like graphene-Ag composite films with enhanced mechanical and electrical properties,” *Nanoscale Res. Lett.*, vol. 8, no. 1, p. 32, 2013, doi: 10.1186/1556-276X-8-32.

[124] A. Owhal, A. D. Pingale, S. U. Belgamwar, and J. S. Rathore, “Preparation of novel Zn/Gr MMC using a modified electro-co-deposition method: Microstructural and tribo-mechanical properties,” *Mater. Today Proc.*, Nov. 2020, doi: 10.1016/j.matpr.2020.09.459.

[125] F. Catania *et al.*, “A Review on Recent Advancements of Graphene and Graphene-Related Materials in Biological Applications,” *Appl. Sci.*, vol. 11, no. 2, p. 614, Jan. 2021, doi: 10.3390/app11020614.

Chapter 3

Experimental Details

Chapter 2 was concerned primarily with the various types of fabrication methods of Cu-Ni composites and provides an insight into the fabrication of Cu-Ni alloy matrix composites through electrodeposition and powder metallurgy methods. As well as the need and the scope for future research are discussed in detail. In this chapter, the discussion is devoted to the development of synthesis methods. Two synthesis methods are developed for the Cu-Ni/Gr composite coatings using the electro-co-deposition method and for the Cu-Ni/Gr composites powder using a modified electro-co-deposition method. Then, powder metallurgy method is used to fabricate Cu-Ni/Gr composite pellets (diameter = 25 mm) from Cu-Ni/Gr composite powder. The detailed instrumentation and methodology is discussed in this chapter.

3.1 Electro-co-deposition of Cu-Ni/Gr composite coatings

3.1.1 Preparation of substrates

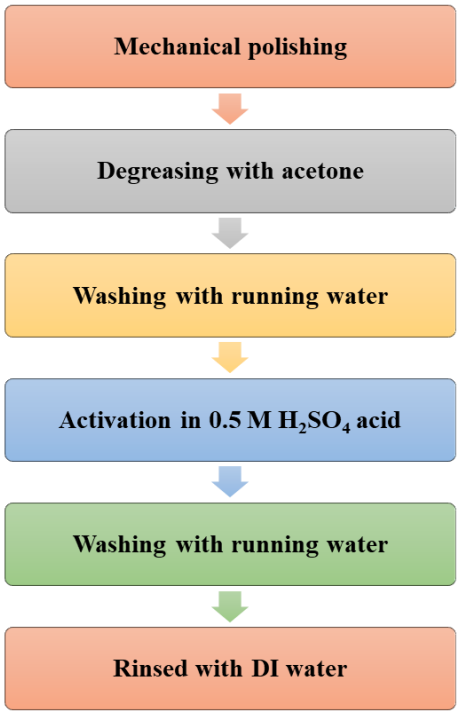

Figure 3.1: Flowchart for pretreatment of stainless-steel substrate

Substrate plays a significant role in the electrodeposition of metal and alloy composite coatings. Substrate material should have good electrical conductivity and mechanical

strength. At present, the substrate should be stable in the electrolyte bath. The substrate surface should be smooth and scratch-free. In the present work, we have used stainless steel as a substrate material. Normally, the stainless-steel substrate surface is covered with dirt, grease, oil, oxide layers. The pre-treatment of the stainless-steel substrate involved steps are shown in Figure 3.1. Initially, the stainless-steel substrate was polished using mechanically polished with different grades (150#, 600#, 1000# and 2500#) of silicon carbide papers to get a bright and smooth surface. Then, degreased in acetone to remove oil, dirt, and grease, etc. After this, the substrate was washed with running water. Subsequently, substrate was activated by dipping in a 5.0 M H_2SO_4 solution for about 3 minutes. Activation of substrate slightly increases the roughness substare to obtain good adhesion for the coatings onto the substrate. Again, the substrate was washed using running water and finally rinsed with DI water before the deposition process.

3.1.2 Materials

Analytical grade chemicals and deionized (DI) water were used to prepare the bath solution. The chemicals and particulates used for the synthesis of Cu-Ni/Gr composite coatings are shown in Figure 3.2.

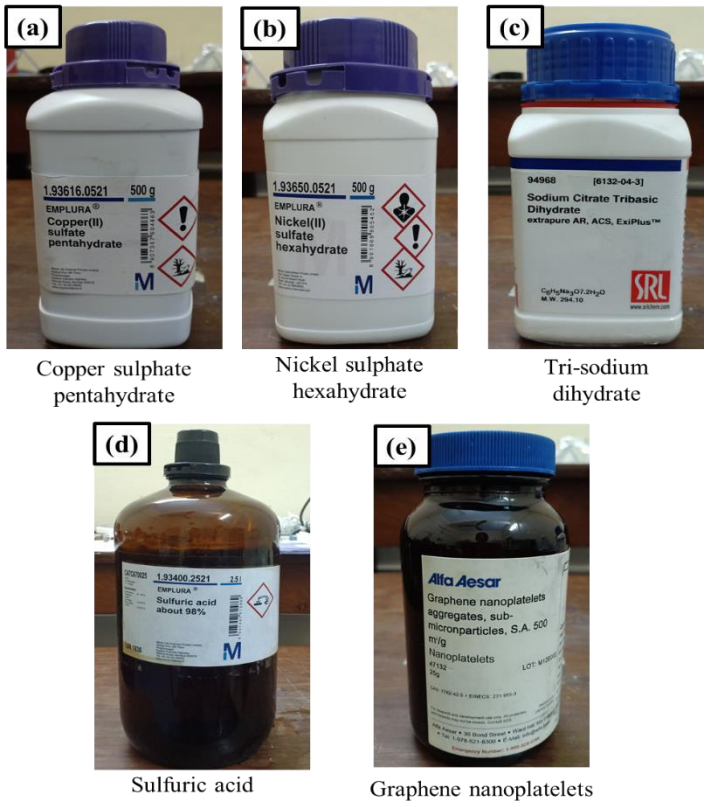

Figure 3.2: Chemicals and particulates used for electro-co-deposition of Cu-Ni/Gr composite coatings

A. Chemicals

Reagents of all analytical grades with a purity of 99% were supplied by Merck Specialties Pvt. Ltd. and SRL Chemical Pvt. Ltd. All electrolyte solutions were formed using deionized (DI) water. A volume of 250 cm^3 of citrate bath was composed of copper sulfate pentahydrate ($CuSO_4.5H_2O$) as the copper source, nickel sulfate hexahydrate ($NiSO_4.6H_2O$) as the nickel source and trisodium citrate dihydrate ($Na_3C_6H_5O_7.2H_2O$) as a complex agent. Sulfuric acid (H_2SO_4) was used to adjust the pH value of the electrolyte solution.

B. Particulates

Graphene nanoplatelets (Gr) were used as a reinforcing element without any further purification in the electrolyte bath for the synthesis of Cu-Ni/Gr composite coatings. The graphene nanoplatelets (thickness 5-15 nm with surface area 500 m^2/g) used in the coatings were reduced graphene oxide procured from Alfa Aesar.

3.1.3 Preparation of Cu-Ni/Gr composite coatings

The experimental setup to prepare composite coatings is shown in Figure 3.3. Pure nickel plate anode (99.9 %) and stainless-steel plate cathode of dimensions 20 × 20 × 1.5 mm were used. The prepared electrolyte solution was filled in a borosilicate glass beaker of 500 ml. The anode and cathode electrodes were immersed vertically into the electrolyte solution.

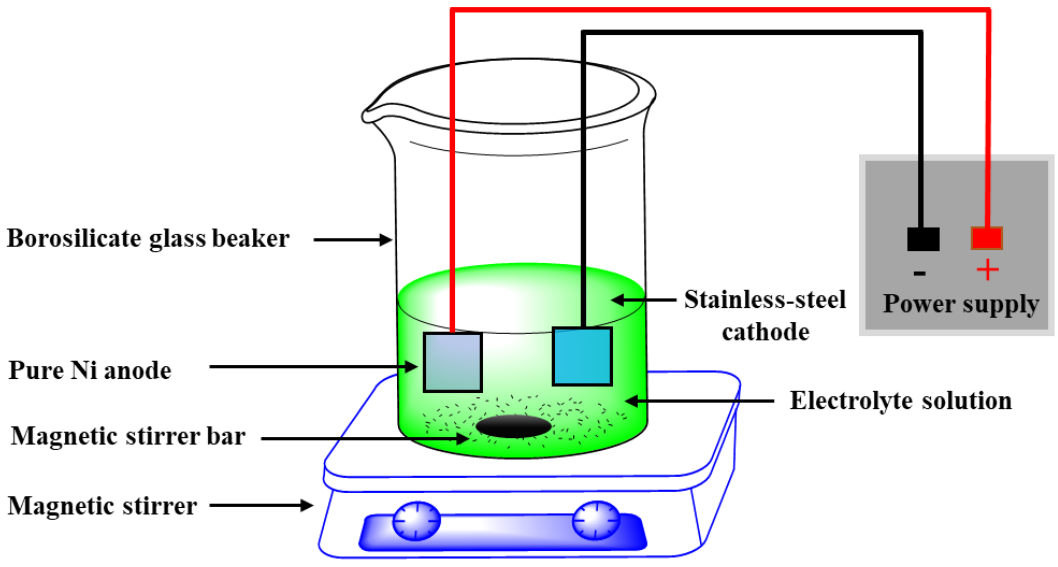

Figure 3.3: Schematic for electro-co-deposition system

A D.C. power supply was employed as a constant current source. The electrolyte solution was prepared using DI water by the addition of a known amount of metal salts, complexing agent and nanoparticles. The concentration of metal salts and electrodeposition process parameters were optimized by evaluating the composition of the alloy coating. Initially, the effective current density was fixed based on the performance of the composite. Then, effective nanoparticle concentration in the electrolyte bath was fixed based on the performance of the composite coatings. In order to achieve uniform dispersion of nanoparticles in the electrolyte bath, ultrasonication treatment was provided to the electrolyte solution to break down the agglomeration of nanoparticles. Electro-co-deposition of coatings was carried out under magnetic stirring to maintain the uniform concentration of metal ions in the electrolyte bath. Each experiment was performed using a new solution. After the deposition process, prepared coating samples were rinsed with DI water and dried in an inert atmosphere. The flowchart of the composite coating process sequence is shown in Figure 3.4.

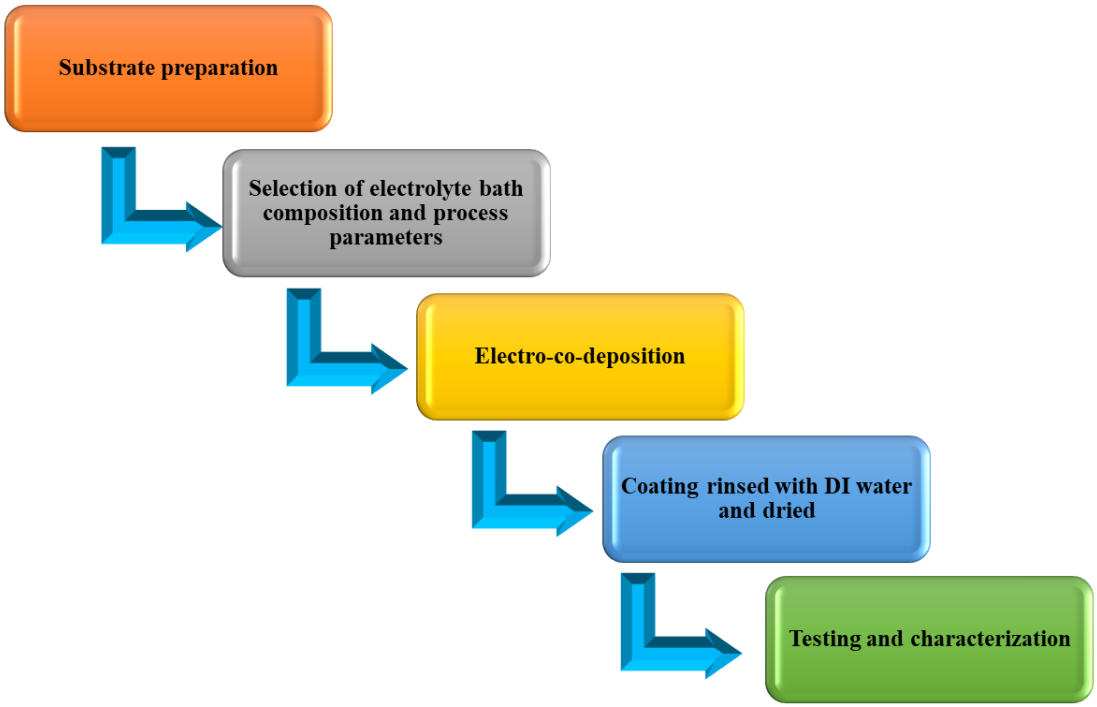

Figure 3.4: Flowchart of composite coating process sequence

3.1.4 Processing of Cu-Ni/Gr composite coatings

The processing of Cu-Ni/Gr composite coatings mainly consists of (a) Substrate preparation and (b) Electro-co-deposition process. Schematic representation of the production process of Cu-Ni/Gr composite coating on stainless steel is shown in Figure 3.5.

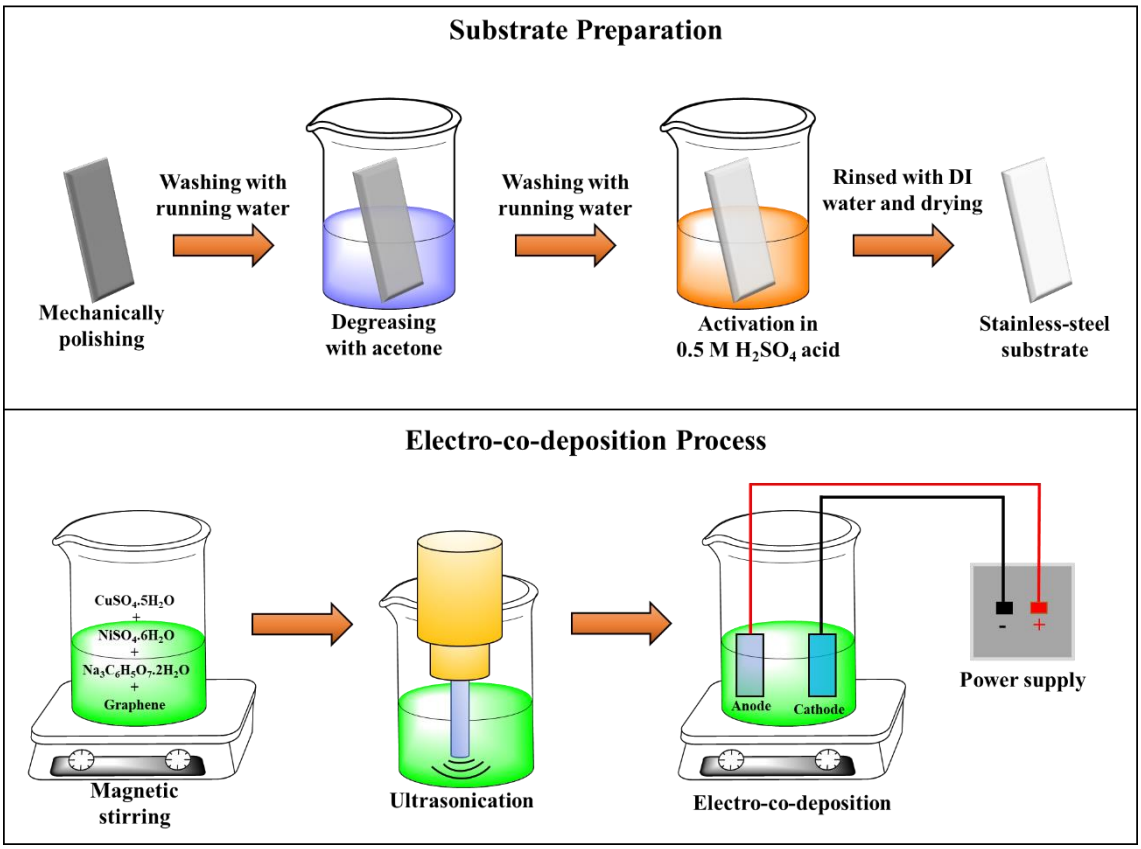

Figure 3.5: Schematic representation of the production process of Cu-Ni/Gr composite coating on a stainless-steel substrate

A. Variation of current density

In order to study the effect of current density on microstructure and properties of Cu-Ni/Gr composite coatings, various current densities (2, 4, 6 and 8 A/dm^2) were used to synthesize Cu-Ni/Gr composite coatings. However, remaining process parameters such as temperature, pH, stirring speed and plating time were kept constant during the electrodeposition process. Cu–Ni/Gr composite coatings were electrodeposited at various current densities in a citrate bath. A volume of 250 cm^3 of citrate bath was composed of $CuSO_4.5H_2O$ (21 g/L), $NiSO_4.6H_2O$ (105 g/L) and $Na_3C_6H_5O_7.2H_2O$ (59 g/L) as a complex agent. For comparison, pure Cu–Ni coating was also prepared. The citrate bath composition and operating conditions are given in Table 3.1. All electrolyte solutions were formed by reagent grade chemicals and deionized water. The vacuum filtration was used to remove insoluble impurities from the electrolyte solution. Then, 100 mg/L graphene nanoplatelets were added to the electrolyte solution. A magnetic stirrer was used for agitation of the electrolyte solution with 300 rpm for 15 min. After stirring, ultrasonic treatment was given for 1 h to

disperse the graphene nanoplatelets uniformly in the solution. A stainless-steel plate of 20 × 20 × 1.5 mm was used as a cathode (substrate) and a nickel plate was used as an anode.

Table 3.1: Used bath composition and operating conditions for electrodeposition of Cu-Ni/Gr composite coatings

Bath composition and operating conditions	Quantity
$CuSO_4.5H_2O$	21 g/L
$NiSO_4.6H_2O$	105 g/L
$Na_3C_6H_5O_7.2H_2O$	59 g/L
pH	4
Temperature	35±1 °C
Steering	300 rpm-using magnetic stirrer
Graphene nanoplatelets	100 mg/L
Current density	2, 4, 6 and 8 A/dm^2
Plating Time	90 min

B. Variation of reinforcement content

In order to study the effect of graphene nanoplatelets on microstructure and properties of Cu-Ni/Gr composite coatings, various graphene nanoplatelets concentration in the electrolyte bath (100, 200, 300, 400 and 500 mg/L) were used. However, remaining process parameters such as temperature, pH, stirring speed and plating time were kept constant during the electrodeposition process.

The Cu-Ni/Gr composite coatings were prepared by electro-co-deposition method, and plating bath solution consisted of $CuSO_4.5H_2O$ (21 g/L), $NiSO_4.6H_2O$ (105 g/L), $Na_3C_6H_5O_7.2H_2O$ (59 g/L) and graphene nanoplatelets (100, 200, 300, 400 or 500 mg/L). Before electrodeposition, the plating solution was agitated using a magnetic stirrer at 500 rpm for 2 h. Subsequently, ultrasonic treatment (20 kHz, 500 W) was given for 1 h to ensure uniform dispersion of graphene nanoplatelets in the plating solution. The electrodeposition was done at 6 A/dm^2 for 60 min on stainless steel substrate (20 × 20 × 1.5 mm), and the nickel plate acted as an anode. The used bath composition and operating parameters during the electrodeposition process are shown in Table 3.2. For comparison, pure Cu–Ni coating was also prepared.

Table 3.2: Used plating bath composition and operating conditions for electrodeposition of Cu-Ni/Gr composite coatings

Bath composition and operating conditions	Quantity
$CuSO_4.5H_2O$	21 g/L
$NiSO_4.6H_2O$	105 g/L
$Na_3C_6H_5O_7.2H_2O$	59 g/L
pH	4
Temperature	40 °C
Agitation	250 rpm
Graphene nanoplatelets	0, 100, 200, 300, 400 and 500 mg/L
Current density	6 A/dm^2
Plating Time	60 min

3.1.5 Characterization of Cu-Ni/Gr composite coatings

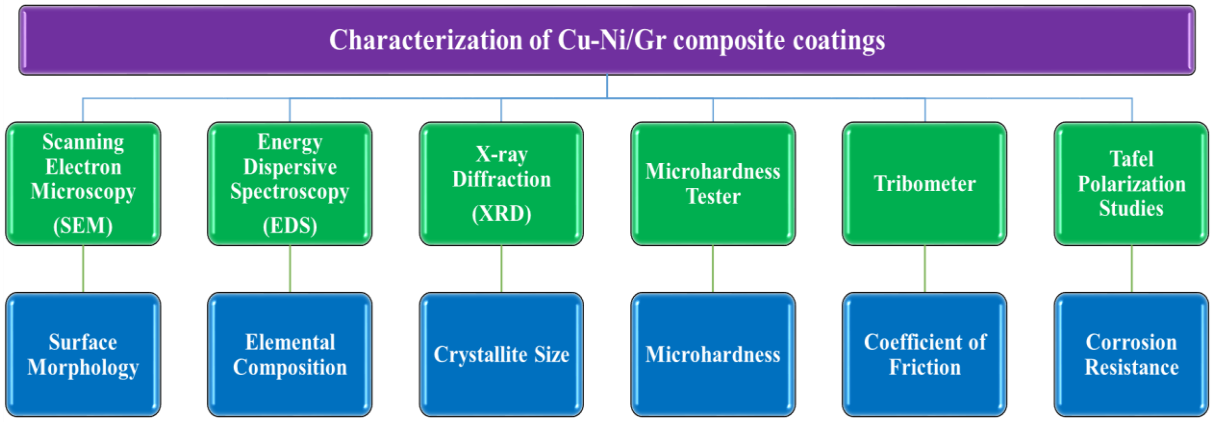

Figure 3.6: Characterization of Cu-Ni/Gr composite coatings

Cu-Ni alloy and its composite coatings are widely used in automobile, marine, chemical and metallurgical applications to enhance the surface properties of components. However, these coatings have been exposing to wear and corrosion during their service life. Hence, surface properties of coatings, such as hardness, wear resistance, and corrosion resistance are mostly considered because they directly affect the lifetime of engineering components. For this reason, the characterization of composite coatings has great importance in the field of materials science. Nowadays, several techniques are used to characterize and evaluate the performance of composite coatings, such as scanning electron microscopy (SEM), energy dispersive spectroscopy (EDS), X-ray diffraction spectroscopy (XRD), microhardness

tester, tribometer, and potentiostat, etc. Different techniques employed to characterize and evaluate the performance of Cu-Ni/Gr composite coatings are shown in Figure 3.6.

3.1.5.1 Surface morphology and elemental composition

Scanning electron micrograph and elemental compositional analysis of prepared samples were done by using FEI-Apreo-S field emission scanning electron microscopy (FESEM) fitted with an energy dispersive spectroscopy (EDS). FESEM attached with EDS is shown in Figure 3.7.

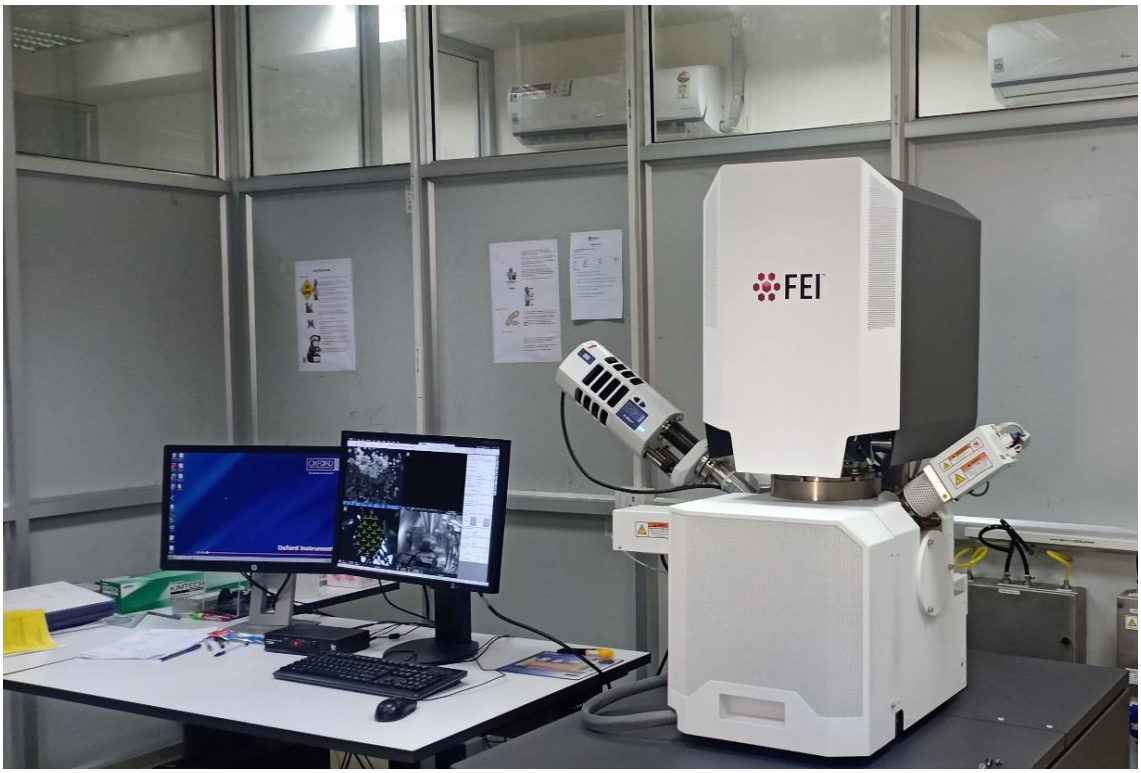

Figure 3.7: Field emission scanning electron microscopy (FESEM) attached with energy dispersive spectroscopy (EDS)

3.1.5.2 Phase structure analysis

X-ray diffractograms of prepared samples were taken using RIGAKU MiniFlex-II X-ray diffractometer (XRD) with Cu Ka radiation (see Figure 3.8). The rate of scanning for 2θ (40°–80°) was 0.05/s. The average crystallite size of the prepared samples was measured using the Scherrer equation (3.1) as follows,

$$D = \left(\frac{0.9\lambda}{\alpha \times \cos\theta} \right) \tag{3.1}$$

where, D is crystallite size, λ is the x-ray wavelength (λ = 0.154 nm), α is FWHM of (111) reflection and θ indicates Bragg's angle.

Also, lattice strain is calculated for the prepared coatings by using the following equation (3.2) as follows [1],

$$\varepsilon = \left(\frac{\alpha}{4 \times \tan\theta} \right) \tag{3.2}$$

where α is FWHM of (111) reflection and θ indicates Bragg's angle.

Figure 3.8: X-ray diffractometer

3.1.5.3 Microhardness Testing

Microhardness was measured using INNOVATEST NEXUS 4303 microhardness testing machine by applying a 20 g load with a duration of 10 s. The Microhardness tester is shown in Figure 3.9.

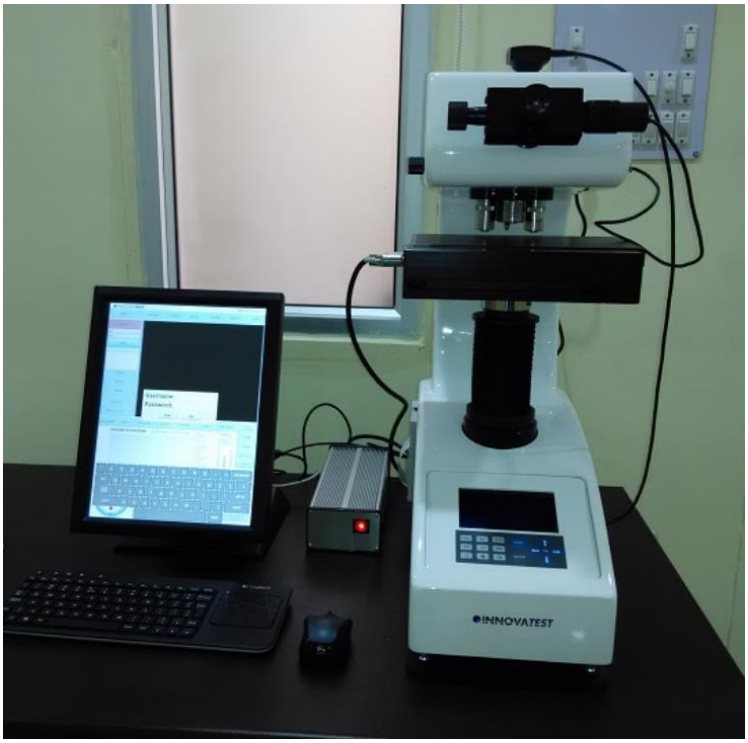

Figure 3.9: Microhardness tester

3.1.5.4 Tribological Testing

The wear test was done using a reciprocating tribometer (CETR) with a ball-on-disk arrangement at an amplitude of 5 mm and 4 N load with 5 Hz frequency. The steel ball of 3 mm diameter was used for testing. The average friction coefficient was calculated from the frictional forces for 300 cycles. The reciprocating tribometer is shown in Figure 3.10.

Figure 3.10: Reciprocating tribometer

3.1.5.5 Corrosion Testing

To estimate the corrosion performance of prepared samples in 3.5 wt.% of NaCl aqueous solution at room temperature, CHI604E potentiostat/galvanostat instrument based on the usual three electrodes cell configuration was used.

3.2 Modified electro-co-deposition method for Cu-Ni/Gr composite powder

In this method, we have combined good features of electro-co-deposition method and convectional powder metallurgy method to develop a modified electro-co-deposition method for the simple, economical and bulk production of Cu-Ni/Gr composites.

Currently, many different methods are adopted to prepare graphene reinforced metal composites like powder metallurgy and electrodeposition [2]–[5]. Powder metallurgy is an efficient and versatile to fabricate metal composites, and it has great potential for enhancing the properties of the composites [6]–[9]. On the other hand, the main disadvantage of this method is that during the high-energy ball milling, the graphene structure will be damaged, and it may deteriorate the properties of the resulting composite [10]. The common coating methods include sputtering, electrodeposition, flame spraying, and chemical vapor deposition. However, the electrodeposition method is widely used for the synthesis of pure, alloy, and composite coatings due to several advantages such as simplicity of operation, cost-effectiveness, scalability, and high production rate [11]. Also, the properties of prepared composites can be controlled by optimizing the process parameters such as current density, pH, temperature, amount of reinforcement, and bath composition [9], [11]–[15]. To achieve the co-deposition of two metals, the standard reduction potentials of these metals need to be similar. The standard reduction potentials for nickel and copper are -0.25 V and +0.34 V, respectively. For the co-deposition of Cu and Ni metals, the standard reduction potential difference can be decreased by adding a suitable complexing agent [16]. In this work, the electro-co-deposition is carried out from a sulfate electrolyte with the addition of sodium citrate as a complexing agent. Sodium citrate can act as a buffering agent, hence eliminating the need for additional additives [17]. In the present work, Cu-Ni/Gr composites were prepared using a modified electrochemical-co-deposition method followed by the conventional powder metallurgy method. In a modified electro-co-deposition method, Cu-Ni/Gr composite powder samples are synthesized by simultaneous deposition of Gr, Ni and Cu atoms on the tip of the

insulated cathode to ensure the uniform distribution of Gr in the Cu-Ni alloy matrix. The use of a modified electro-co-deposition method eliminates the ball-milling step in the powder metallurgy method, and thus prevents the structural damage of Gr. The effects of different concentrations of Gr in the electrolyte bath on the microstructural, mechanical and tribological properties of Cu-Ni/Gr composites were systematically studied.

3.2.1 Experimental setup

In a modified electro-co-deposition method, co-deposition of Cu, Ni atoms and Gr was carried out on the tip of an insulated cathode electrode. The actual experimental setup for a modified electro-co-deposition method is shown in Figure 3.11. Anode electrode was Pt coated titanium fixed at the center of 6 mm thick Perspex sheet. Also, four Pt coated titanium anodes (length 10 mm and diameter 10 mm) were fixed circumferentially in the same Perspex sheet. All four cathode electrodes are connected in series. All experiments were carried out in a 500 ml borosilicate container. A magnetic stirrer with a hot plate (0-1500 rpm, 0-200°C) was used to agitate and maintain the temperature of the electrolyte solution. Arduino (UNO R3 ATmega 16U2) controlled DC stepper motor mechanism was connected to the central cathode electrode to seperate the co-deposited composite powder from the tip of cathode. D.C. Power supply (TESTRONIX 92 D, 0-30 V and 0-10 Amp) was employed to achieve co-deposition of Cu, Ni atoms and Gr to form Cu-Ni/Gr composite powder.

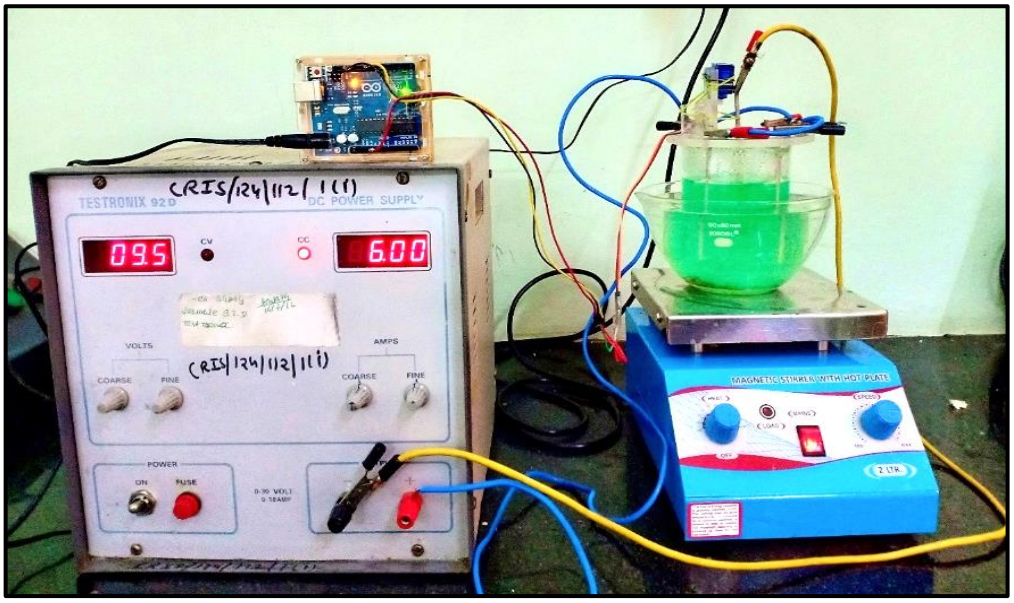

Figure 3.11: Actual experimental setup for a modified electro-co-deposition method

3.2.2 Materials

A. Chemicals

Reagents of all analytical grades with a purity of 99% were supplied by Merck Specialties Pvt. Ltd. All electrolyte solutions were formed using deionized (DI) water. A volume of 450 cm^3 of citrate bath was composed of copper sulfate pentahydrate ($CuSO_4.5H_2O$) as the copper source, nickel sulfate hexahydrate ($NiSO_4.6H_2O$) as the nickel source and trisodium citrate dihydrate ($Na_3C_6H_5O_7.2H_2O$) as a complex agent.

B. Particulates

Graphene nanoplatelets were used as a reinforcing element without any further purification in the electrolyte bath to synthesize Cu-Ni/Gr composite powder samples. The graphene nanoplatelets (thickness 5-15 nm and surface area ≈ 500 m^2/g) used in the coatings were reduced graphene oxide procured from Alfa Aesar.

C. Electrodes

Platinum coated Titanium electrodes with 10 µm thickness and 3 mm diameter were obtained from Titanium tantalum Product limited Chennai, India.

3.2.3 Experimental procedure

Gr reinforced Cu-Ni alloy matrix composite powder samples were prepared under a direct current condition from citrate type bath. First, 0.36 M nickel sulfate hexahydrate ($NiSO_4.6H_2O$), 0.09 M copper sulfate pentahydrate ($CuSO_4.5H_2O$) and 0.38 M trisodium citrate dihydrate ($Na_3C_6H_5O_7.2H_2O$) were dissolved in deionized (DI) water to prepare 450 ml of electrolyte. Then, graphene nanoplatelets (obtained from Alfa Aesar with surface area ≈ 500 $m^2.g^{-1}$ and thickness ≈ 5-10 nm) were added (0, 50, 100 or 200 mg/L) in the electrolyte bath under magnetic stirring with 300 rpm for 15 min. Subsequently, an ultrasonic agitation (20 kHz frequency and 500 watts power) was given for 2 h to uniformly disperse the Gr in the electrolyte bath just before the electrochemical-co-deposition process. The chemical composition and process parameters used for electro-co-deposition of Cu-Ni/Gr composite powder samples are listed in Table 3.3.

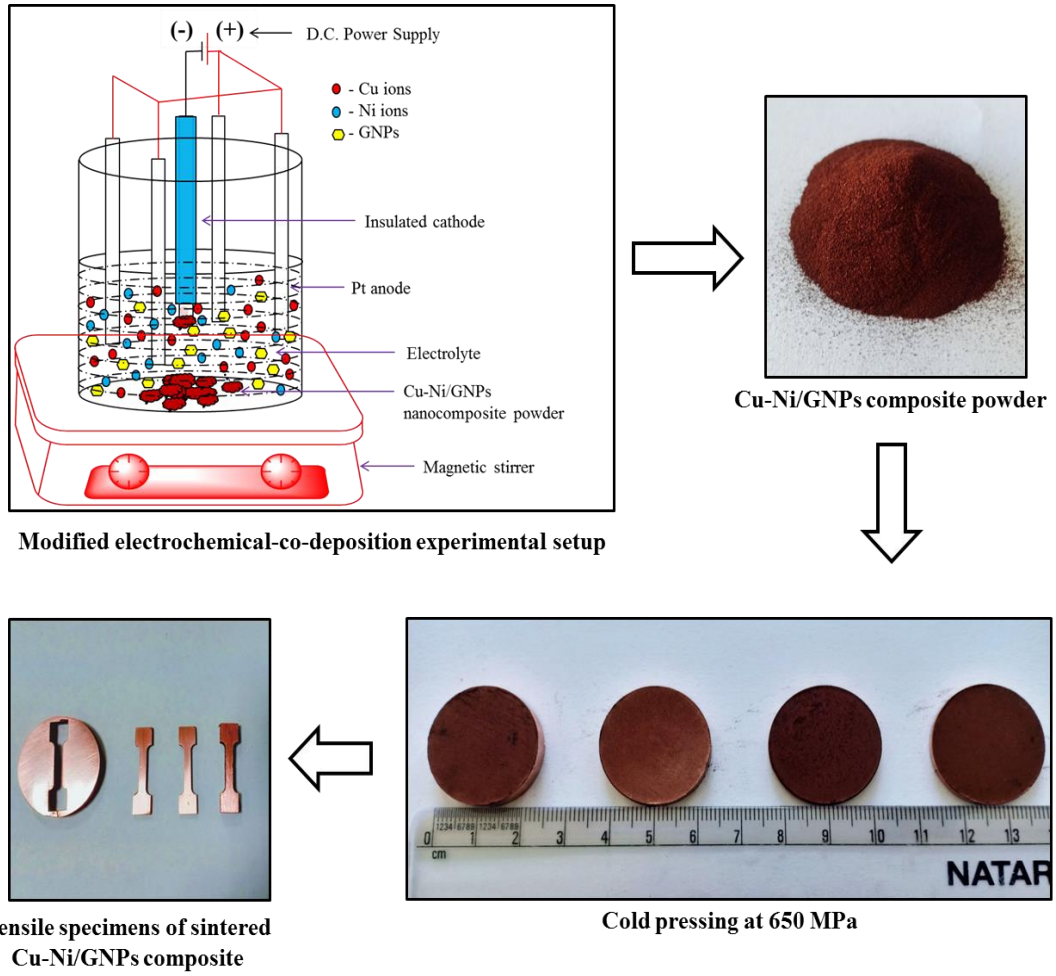

Figure 3.12: Experimental procedure of Cu-Ni/Gr composite fabrication

Table 3.3: The chemical composition and process parameters

Chemical composition and process parameters	Quantity
$NiSO_4.6H_2O$	0.36 M
$CuSO_4.5H_2O$	0.09 M
$Na_3C_6H_5O_7.2H_2O$	0.38 M
Gr	0, 50, 100 and 200 mg/L
pH	4 ± 0.1
D.C. current	6 Amp
Temperature	35 ± 1 °C
Agitation	350 rpm
Time	120 min

The experimental procedure for Cu-Ni/Gr composite fabrication are presented in Figure 3.12. Four platinum (Pt) coated electrodes (length 10 cm and diameter 3 mm) were used as an anode, and one insulated Pt electrode (excluding the tip surface) was used as a

cathode. The electrolyte glass beaker was kept on a magnetic stirrer and the electrolyte was agitated with 350 rpm throughout the experiment. A constant direct current of 6 Amp was applied to the electrodes to facilitate the simultaneous deposition of Gr, Cu and Ni atoms on the tip of the cathode electrode. Arduino (UNO R3 ATmega 16U2) controlled stepper motor mechanism was used to tap the cathode electrode continuously throughout the process to drop down the co-deposited Gr reinforced Cu-Ni alloy powder. The obtained Cu-Ni/Gr composite powder was washed by DI water to remove residual electrolyte solution and dried in an inert atmosphere at 80 ºC using a rotary evaporator. Subsequently, the uniaxial die pressing (at 650 MPa for the 30s) was employed for obtaining Cu-Ni/Gr compacts (diameter = 25 mm and thickness = 6 mm) and then sintered in a muffle furnace at 950 ºC for 2 h in Ar atmosphere. During the heating process, the temperature ramp rate was set to 5 °C/min to avoid deformation or cracking of the samples. Finally, the furnace was switched off, and samples were allowed to cool down in the furnace itself.

3.2.4 Characterization of Cu-Ni/Gr composites

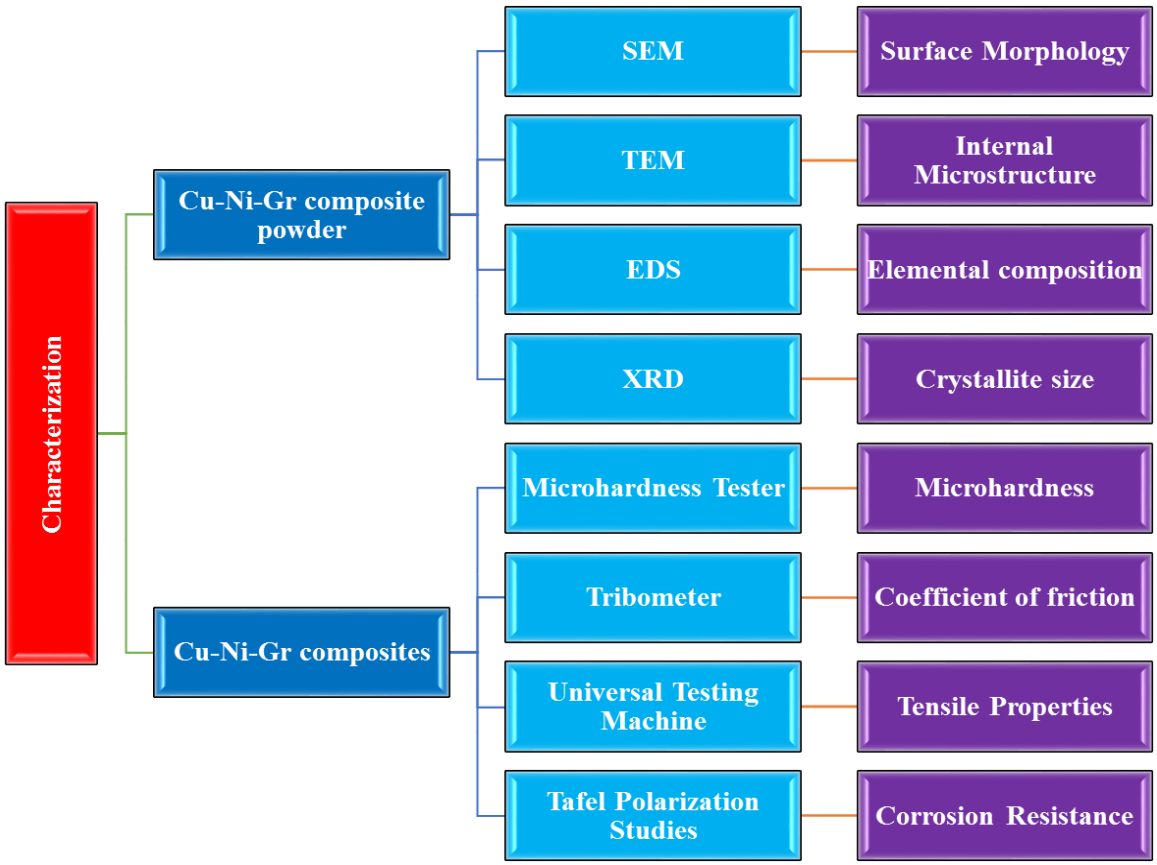

Figure 3.13: Characterization of Cu-Ni/Gr composite powder and the sintered Cu-Ni/Gr composites

In order to study the surface morphology, internal microstructure, elemental composition, and crystallite size of the Cu-Ni/Gr composite powder sample SEM, TEM, EDS, and XRD analysis techniques were used. Also, to determine the microhardness, coefficient of friction, tensile properties and corrosion resistance of sintered Cu-Ni/Gr composites microhardness tester, tribometer, universal testing machine and potentiostat were used. The characterization of Cu-Ni/Gr composite powder and the sintered Cu-Ni/Gr composites is shown in Figure 3.13.

The surface morphology and internal microstructure of prepared powder samples were examined using field emission scanning electron microscopy (FESEM, FEI-Apreo-S) and high-resolution transmission electron microscopy (HRTEM, Tecnai G220 FEI, S-Twin operating at 200 kV). FESEM equipped with electron dispersive spectroscopy (EDS) was employed to examine the composition and distribution of elements in the prepared powder samples. X-ray diffractometer (XRD, RIGAKU MiniFlex-II) was employed to analyze the phase constituents of powder samples using Cu Kα radiation $\lambda = 1.5418$ Å. The 2θ ranged from 40 to 80° at a scan rate of 0.05°/s. The Scherrer equation was used to estimate the average crystallite size of the prepared powder samples.

The Vickers hardness tester (INNOVATEST) was used to measure the hardness using an load of 300 g for 10 s on polished surfaces. The uniaxial tensile tests were performed using a universal testing machine (BISS UNO 100) at room temperature. The tensile rate was 0.6 mm/ min. Each test was conducted three times to reduce human error and check the repeatability. A wire cutting machine (DK7725) was used to cut the tensile specimens. The dog-bone-shaped tensile specimens had a gauge length = 12 mm and a section of 3 mm × 2 mm.

Ball-on-disk configuration (DUCOM Tribometer) was used to investigate the tribological performance of the prepared samples. The counterpart ball was a 6 mm diameter GCr15 steel ball. The disks were prepared samples with a diameter of 25 mm and a thickness of 3 mm. the wear test was performed at a constant load of 10 N (applied using GCr15 steel ball) and rotational velocity of 320 rpm. The average radius of the wear track was 5 mm, thus the average sliding linear speed was 167.46 mm/s, and the test continued for 10 min. The total sliding distance covered for each test was about 100 m. All tribological tests were conducted under the dry condition at room temperature (about 24 °C) and humidity 35%. The wear rate was calculated according to Eq. (1) as follows:

$$W = \left(\frac{AL}{PS} \right) \tag{3.3}$$

where A refers to the cross-section area of the worn scar in mm^2, L is the perimeter of the worn track in mm, P is the applied load in N and the total sliding distance S in m. Each test was performed at least five times for each sample to assure the reproducibility of experimental results. The surface morphologies of worn tracks were examined using FESEM.

3.3 Conclusion

The conclusions based on the work carried out at this point are as follows:

1. In the present chapter, we have discussed the electro-co-deposition method to synthesize Cu-Ni/Gr composite coatings. The electrodeposition of Cu-Ni/Gr composite coatings was carried out at (a) various current densities and (b) various concentrations of Gr in the electrolyte bath. In addition, the ultrasonication treatment was given to the electrolyte before the deposition process to achieve uniform dispersion of Gr in the electrolyte bath.
2. The bulk production of Cu-Ni/Gr composite powder was carried out using a modified electro-co-deposition method. Then convectional powder metallurgy method was used to fabricate Cu-Ni/Gr composites. Before the deposition process, prolonged ultrasonication was employed to break the agglomeration of Gr and achieve Gr's uniform dispersion in the electrolyte bath.
3. In the modified electro-co-deposition method, co-deposition of Gr, copper and nickel occurs at the cathode electrode's tip surface. Arduino-controlled stepper motor mechanism was employed to tap the cathode electrode during the deposition process to drop down the Gr reinforced Cu-Ni matrix powder from the tip surface of the cathode. This method provides facile, economical and bulk production of Cu-Ni/Gr composite powder with a uniform dispersion of Gr into the Cu-Ni matrix.
4. The convectional powder metallurgy method was employed to prepare Cu-Ni/Gr composites from Cu-Ni/Gr composite powder obtained from a modified electro-co-deposition method. A modified electro-co-deposition method eliminates the ball milling step in the powder metallurgy method, which helps prevent Gr from structural damage during processing.

In the next chapter, detailed characterization of (a) Cu-Ni/Gr composite coatings synthesized by electro-co-deposition method and (b) Cu-Ni/Gr composite powder synthesized by a modified electro-co-deposition method are discussed in detail. The characterization of Cu-Ni/Gr composite coatings includes SEM. EDS and XRD analysis. The characterization of Cu-Ni/Gr composite powder includes SEM, EDS, XRD and TEM analysis.

References

[1] M. Boubatra, A. Azizi, G. Schmerber, and A. Dinia, “Morphology, structure, and magnetic properties of electrodeposited Ni films obtained from different pH solutions,” *J Mater Sci Mater Electron*, vol. 22, no. 12, pp. 1804–1809, 2011.

[2] J. Wang, Z. Li, G. Fan, H. Pan, Z. Chen, and D. Zhang, “Reinforcement with graphene nanosheets in aluminum matrix composites,” *Scr. Mater.*, vol. 66, no. 8, pp. 594–597, Apr. 2012.

[3] D. Kuang, L. Xu, L. Liu, W. Hu, and Y. Wu, “Graphene–nickel composites,” *Appl. Surf. Sci.*, vol. 273, pp. 484–490, May 2013.

[4] S. U. Belgamwar and N. N. Sharma, “Synergistic electro-co-deposition and molecular mixing for reinforcement of multi-walled carbon nanotube in copper,” *Mater. Sci. Eng. B*, vol. 178, no. 20, pp. 1452–1457, Dec. 2013.

[5] S. U. Belgamwar, A. D. Pingale, and N. Nipun Sharma, “Investigation on electrical properties of Cu matrix composite reinforced by multi-walled carbon nanotubes,” *Mater. Today Proc.*, vol. 18, pp. 3201–3208, 2019.

[6] S. J. Niteesh Kumar, R. Keshavamurthy, M. R. Haseebuddin, and P. G. Koppad, “Mechanical Properties of Aluminium-Graphene Composite Synthesized by Powder Metallurgy and Hot Extrusion,” *Trans. Indian Inst. Met.*, vol. 70, no. 3, pp. 605–613, 2017.

[7] N. V. Ponraj *et al.*, “Effect of milling on dispersion of graphene nanosheet reinforcement in different morphology copper powder matrix,” *Surfaces and Interfaces*, vol. 9, no. October, pp. 260–265, 2017.

[8] C. Yang *et al.*, “Microstructures and tensile properties of ultrafine-grained Ni-(1-3.5) wt% SiCNP composites prepared by a powder metallurgy route,” *Acta Metall. Sin. (English Lett.*, vol. 28, no. 7, pp. 809–816, 2015.

[9] X. Gao *et al.*, “Mechanical properties and thermal conductivity of graphene reinforced copper matrix composites,” *Powder Technol.*, vol. 301, pp. 601–607, Nov. 2016.

[10] M. Bastwros *et al.*, “Effect of ball milling on graphene reinforced Al6061 composite fabricated by semi-solid sintering,” *Compos. Part B Eng.*, vol. 60, pp. 111–118, Apr. 2014.

[11] A. D. Pingale, S. U. Belgamwar, and J. S. Rathore, “Effect of Graphene Nanoplatelets Addition on the Mechanical, Tribological and Corrosion Properties

of Cu–Ni/Gr Nanocomposite Coatings by Electro-co-deposition Method," *Trans. Indian Inst. Met.*, vol. 73, no. 1, pp. 99–107, Jan. 2020.

[12] A. D. Pingale, S. U. Belgamwar, and J. S. Rathore, "Synthesis and characterization of Cu–Ni/Gr nanocomposite coatings by electro-co-deposition method: effect of current density," *Bull. Mater. Sci.*, vol. 43, no. 1, p. 66, Dec. 2020.

[13] A. D. Pingale, S. U. Belgamwar, and J. S. Rathore, "A novel approach for facile synthesis of Cu-Ni / GNPs composites with excellent mechanical and tribological properties," *Mater. Sci. Eng. B*, vol. 260, no. July, p. 114643, 2020.

[14] A. R. Shelke, J. Balwada, S. Sharma, A. D. Pingale, S. U. Belgamwar, and J. S. Rathore, "Development and characterization of Cu-Gr composite coatings by electro-co-deposition technique," *Mater. Today Proc.*, vol. 28, pp. 2090–2095, Apr. 2020.

[15] A. D. Pingale, S. U. Belgamwar, and J. S. Rathore, "The influence of graphene nanoplatelets (GNPs) addition on the microstructure and mechanical properties of Cu-GNPs composites fabricated by electro-co-deposition and powder metallurgy," *Mater. Today Proc.*, vol. 28, pp. 2062–2067, Mar. 2020.

[16] A. Turoňová, M. Gálová, and M. Šupicová, "Parameters influencing the electrodeposition of a Ni-Cu coating on Fe powders. I. Effect of the electrolyte composition and current density," *J. Solid State Electrochem.*, vol. 7, no. 10, pp. 684–688, Oct. 2003.

[17] R. Oriňáková, A. Turoňová, D. Kladeková, M. Gálová, and R. M. Smith, "Recent developments in the electrodeposition of nickel and some nickel-based alloys," *J. Appl. Electrochem.*, vol. 36, no. 9, pp. 957–972, Sep. 2006.

Chapter 4

Characterization of Cu-Ni/Gr composites

In the previous chapter, the synthesis of Cu-Ni/Gr composite coatings using the electro-co-deposition method and Cu-Ni/Gr composites synthesized by a modified electro-co-deposition method followed by powder metallurgy method were discussed. In this chapter, surface morphology, elemental composition, and microstructure of synthesized Cu-Ni/Gr composite coatings and Cu-Ni/Gr composite powder samples are studied and presented in detail.

4.1 Characterization results of Cu-Ni/Gr composite coatings

For primary characterization purpose, Cu-Ni/Gr composite coatings are synthesized with (i) variation in the current density from 2 A/dm^2 to 8 A/dm^2 and (ii) variation in the Gr content from 0 mg/L to 500 mg/L by electro-co-deposition method. In this section we have studied the effect of variation in current densities on surface morphology, elemental analysis and microstructure of the coating.

4.1.1 Surface morphology of Cu-Ni/Gr composite coatings

4.1.1.1 Effect of current density

We studied the effect of current density on the Cu-Ni/Gr composite coating in order to observe the change in surface morphology of Cu-Ni/Gr coating and coating thickness with respect to the current density. The effect of various current densities on the surface morphology of electrodeposited Cu-Ni/Gr composite coatings is shown in Figure 4.1. At the low current densities, a smooth and compact morphology of produced Cu-Ni/Gr coatings is clearly noticed, as shown in Figures 4.1(a-d). A discernible change is observed in the surface morphology of Cu-Ni/Gr coatings with less compactness due to the increase of current density from 6 to 8 A/dm^2 as shown in Figures 4.1(e-h). Prominently at increased current densities, the rate of deposition is high (like 6 and 8 A/dm^2), which results in less compactness and rough morphology [1]. The reinforced graphene nanoplatelets increase active nucleation sites and hence inhibit crystal growth. The incorporation of graphene nanoplatelets serves as a mechanism for grain refinement of electrodeposited composite coatings. Also, the coating has low graphene content at the current density of 4 A/dm^2, and the coating has a larger crystallite size. Hence, the morphology of sample 4.1 (c) is relatively different from other samples' morphology.

Figure 4.2(a-d) shows SEM cross-sectional of Cu-Ni/Gr composite coatings. From the figure, it is observed that there is sufficient continuity between the deposited coatings and the substrate. The thickness of Cu-Ni/Gr composite coatings electrodeposited at various current densities is measured. The effect of various current densities on the thickness of the Cu-Ni/Gr composite coating is shown in Figure 4.2(e). It is noticed that the thickness increases with an increase in current density. The increase in the thickness of Cu-Ni/Gr composite coating is mainly due to the increase in rate of deposition of metallic ions with increase in the current density.

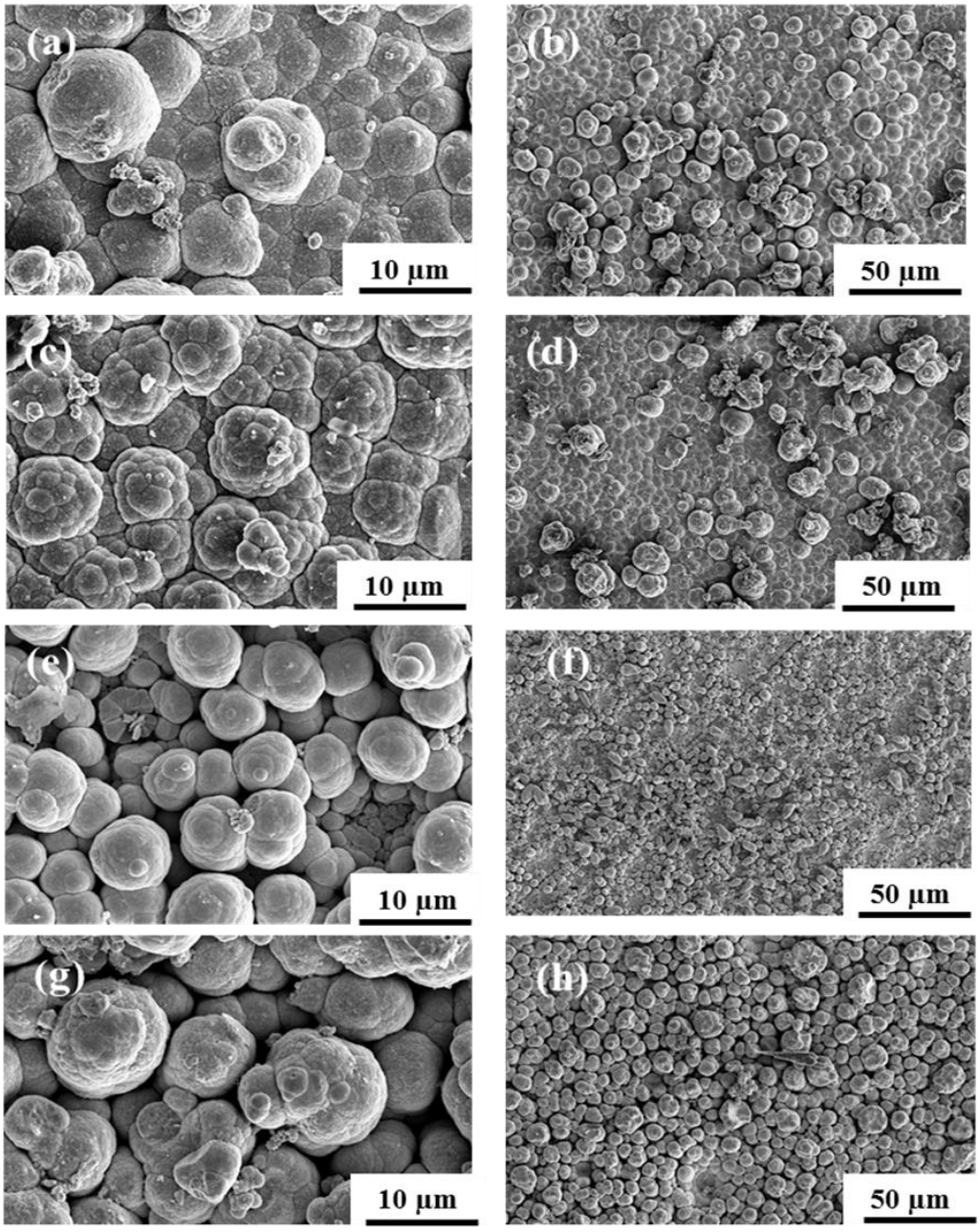

Figure 4.1: Surface morphology of the Cu-Ni/Gr composite coatings electrodeposited at (a, b) 2 A/dm^2, (c, d) 4 A/dm^2, (e, f) 6 A/dm^2 and (g, h) 8 A/dm^2

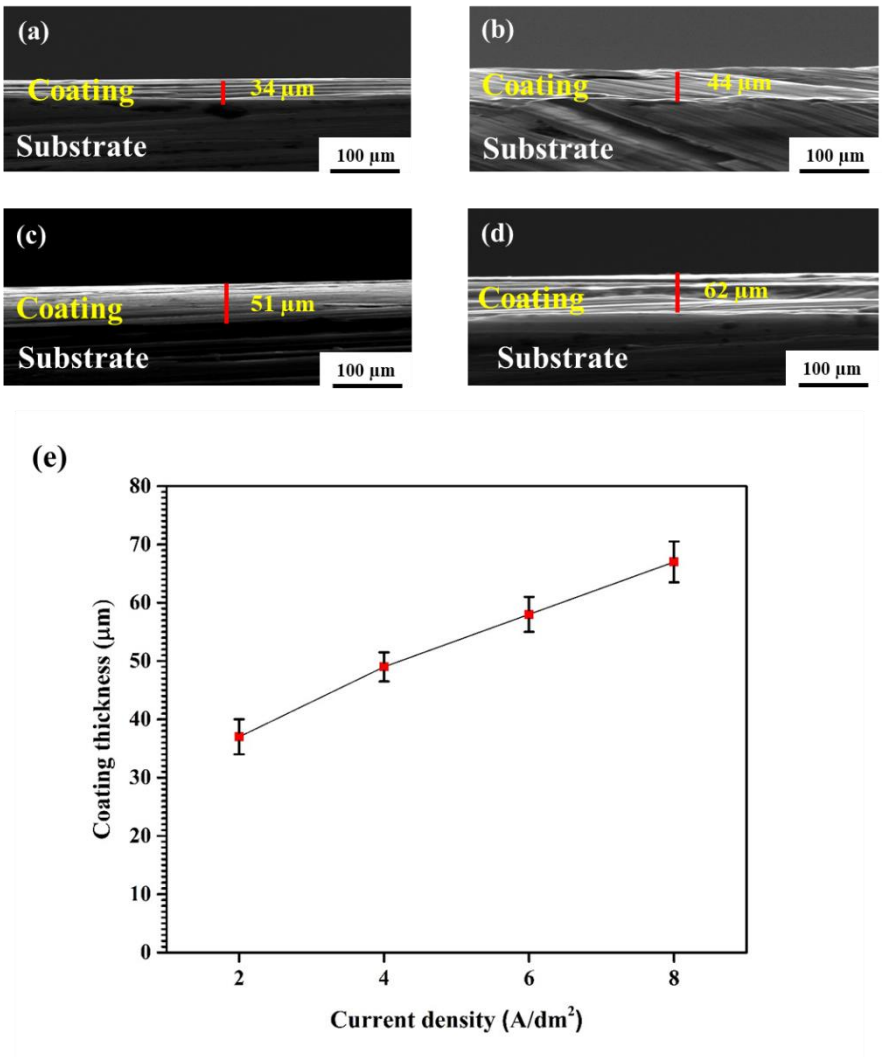

Figure 4.2: (a-d) SEM Cross-sectional of Cu-Ni/Gr composite coatings electrodeposition and (e) is the thickness of Cu-Ni/Gr composite coatings electrodeposited at various current densities

4.1.1.2 Effect of Gr content

In order to study the effect of Gr content on the surface morphology and coating thickness, the SEM analysis of prepared coatings has been carried out. Surface SEM images of Cu-Ni/Gr composite coatings produced at various concentrations of Gr in the plating bath are presented in Figure 4.3(a-h). Figure 4.3(a, b) shows SEM micrographs of pure Cu-Ni coating and it has a nodular structure. Figure 4.3(c-h) shows the change in surface morphology of Cu-Ni/Gr composite coatings by the incorporation of graphene nanoplatelets in the Cu-Ni alloy coating. Also, Figure 4.3 depicts the average size of nodules in the Cu-Ni/Gr composite coatings is decreased with an increase in the concentration of graphene nanoplatelets in the plating bath. During electrodeposition process, graphene nanoplatelets contribute to an increase in the active surface area of the

cathode, which leads to the increase in preferential sites for crystal growth; therefore, the average size of nodules is reduced [2]. The thickness of Cu-Ni/Gr composite coatings electrodeposited at various concentrations of graphene nanoplatelets in the plating bath is presented in Figure 4.4(a-d). From Figure 4.4, the thickness of Cu-Ni/Gr composite coatings are more than pure Cu-Ni alloy coating and it is increased with increase in the concentration of graphene nanoplatelets in the plating bath. This is mainly due to the addition of highly conductive Gr in the plating bath.

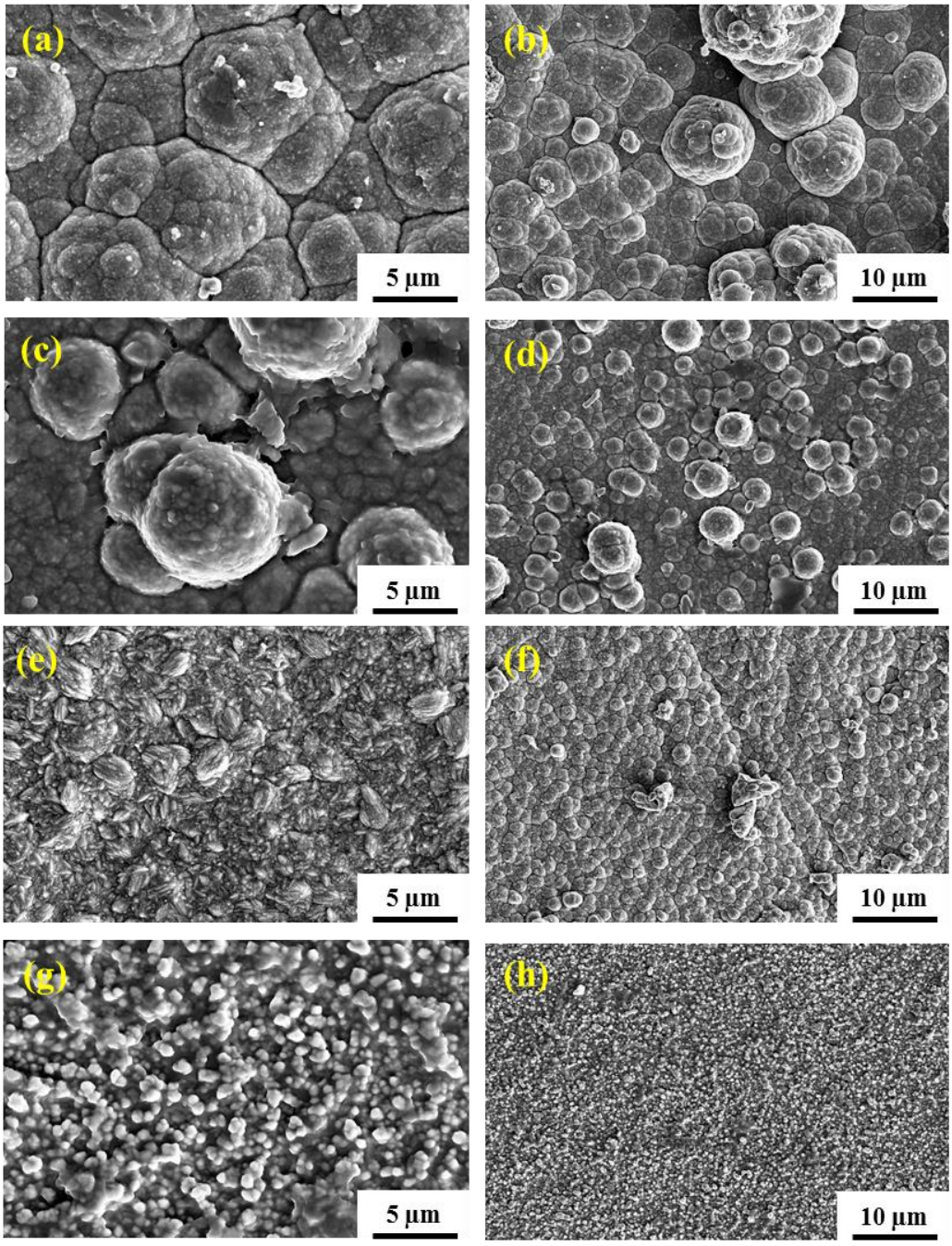

Figure 4.3: SEM images of Cu-Ni/Gr composite coatings (a, b) 0 mg/L, (c, d) 100 mg/L, (e, f) 200 mg/L and (g, h) 400 mg/L

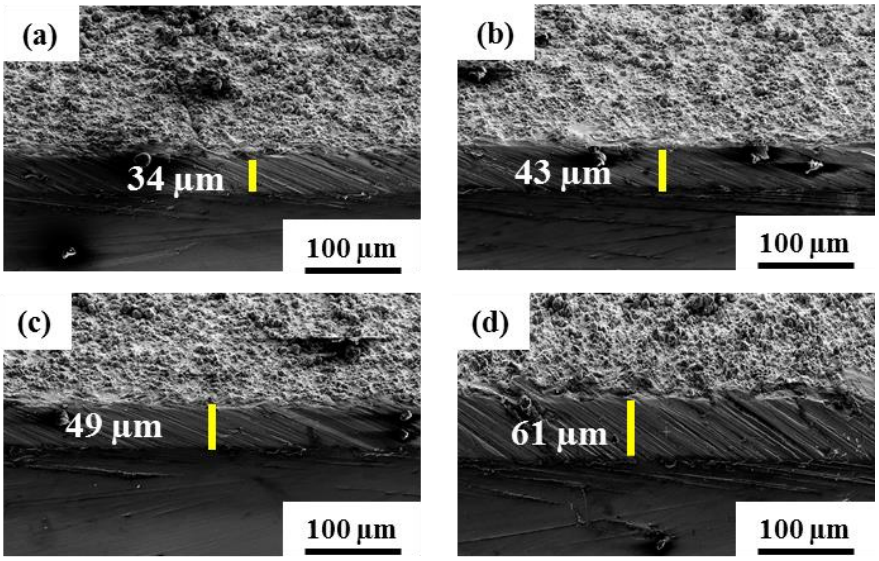

Figure 4.4: Thickness of Cu-Ni/Gr composite coatings (a) 0 mg/L (b) 100 mg/L (c) 200 mg/L and (d) 400 mg/L

4.1.2 Elemental compositional of Cu-Ni/Gr composite coatings

4.1.2.1 Effect of current density

In order to study the effect of various current densities on elemental composition of Cu-Ni/Gr composite coating, EDS analysis has been carried out. The EDS mapping of the Cu-Ni/Gr coatings electrodeposited at various current densities is shown in Figure 4.5. EDS mapping confirms the presence of Cu, Ni and C in the prepared coatings. The C maps in Figure 4.5 shows the presence of graphene platelets in the composite. It is observed that the graphene nanoplatelets and the nickel elements are distributed uniformly in the copper matrix. The EDS results are listed in Table 4.1 shows that the Cu-Ni/Gr composite coating electrodeposited at the current densities of 6 and 8 A/dm^2 has lower copper content, in comparison to the 2 and 4 A/dm^2. On the other hand, by increasing current density, the content of nickel in the electrodeposited coatings is increased. In the presence of citrate as a complexing agent, Cu^{2+} species are discharged with mass transport control, and Ni^{2+} species are discharged with activation control within a wide potential range. In mass transport control, mass transfer coefficient mainly depends on rotation rates, temperature and Cu^{2+} concentration [3], [4]. Therefore, an increase in the overvoltage promotes nickel discharge and, ultimately, leads to deposits with higher nickel contents. Hence, with the increase in the current density from 2 to 8 A/dm^2, the relative content of nickel in the electrodeposited Cu-Ni/Gr coating increases. The enhancement in the characteristics of the electrodeposited coating relies on a homogeneous distribution of the graphene nanoplatelets in the coating [5]. The highest graphene nanoplatelets content and the

homogeneous distribution of the elements are at 6 A/dm^2 coating deposition is seen in Table 4.1 and Figure 4.5(c), respectively.

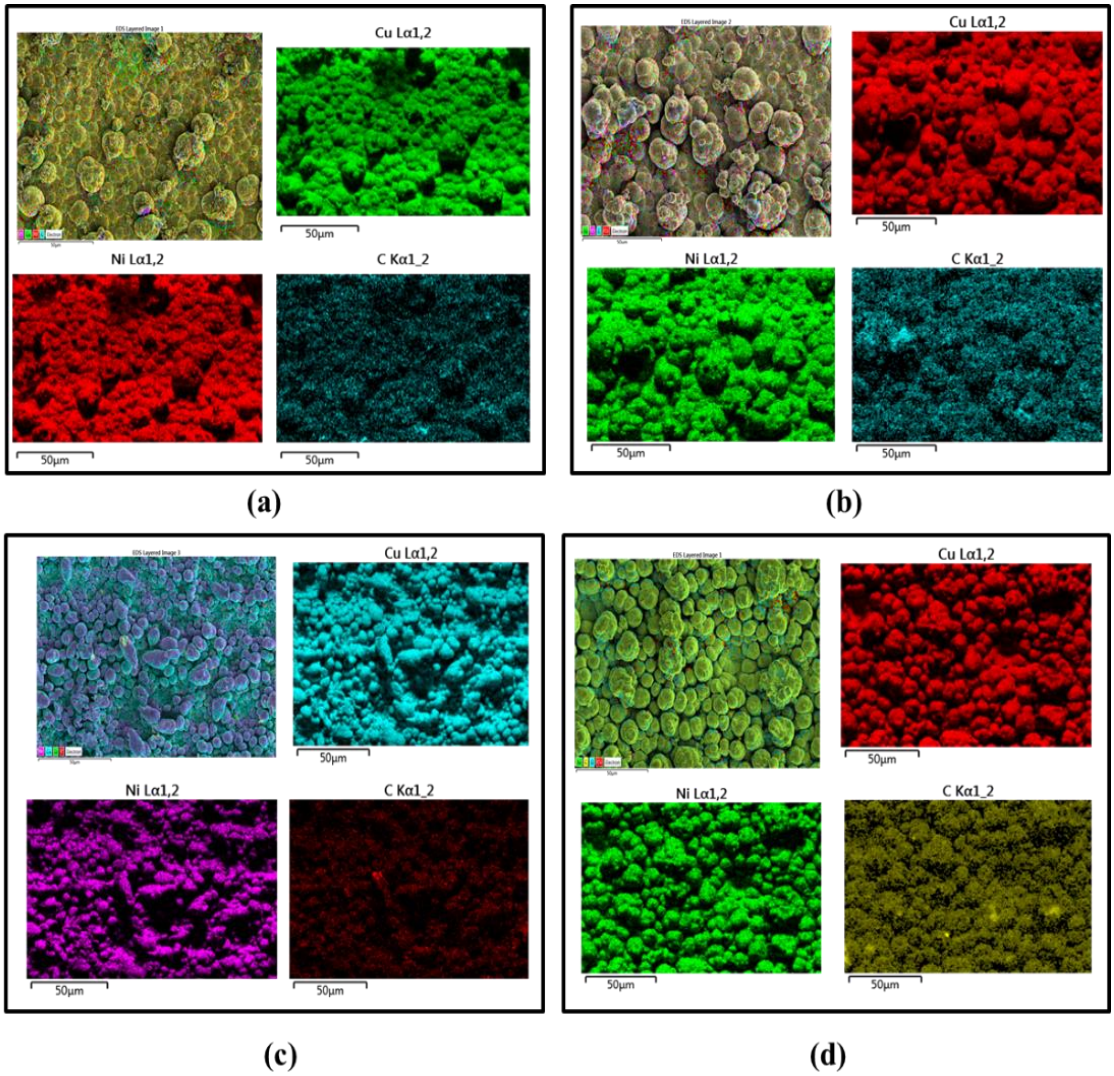

Figure 4.5: EDS mapping of the Cu-Ni/Gr coatings electrodeposited at (a) 2 A/dm^2, (b) 4 A/dm^2, (c) 6 A/dm^2 and (d) 8 A/dm^2

As seen in Table 4.1, as the current density is increased the graphene content of the Cu-Ni/Gr composite coatings is also increased gradually up to 6 A/dm^2 and then started decreasing with further increase in current density. At low current densities, there are less metallic ions that would be embedded with graphene nanoplatelets and deposited on a substrate. At high current densities, metallic ion shows a high deposition rate compared to graphene nanoplatelets [6]. Hence, experimentally it has been observed that the graphene nanoplatelets content in Cu-Ni/Gr composite coatings is gradually increased from 2 to 6 A/dm^2 and then decreased at 8 A/dm^2. However, Cu-Ni/Gr composite coating electrodeposited at 6 A/dm^2 has higher graphene nanoplatelets content.

Table 4.1: EDS data of Cu-Ni and Cu-Ni/Gr composite coatings electrodeposited at various current densities

Coating sample	Cu (wt.%)	Ni (wt.%)	C (wt.%)
Cu-Ni	68.72	31.28	0
Cu-Ni/Gr (2 A/dm^2)	65.92	28.76	5.32
Cu-Ni/Gr (4 A/dm^2)	64.68	29.34	5.98
Cu-Ni/Gr (6 A/dm^2)	63.84	29.55	6.61
Cu-Ni/Gr (8 A/dm^2)	66.18	29.84	3.98

4.1.2.2 Effect of Gr content

The EDS analysis has been carried out to study the effect of various Gr content on elemental composition of Cu-Ni/Gr composite coatings. The elemental composition of Cu-Ni/Gr composite coatings with the various concentrations of graphene nanoplatelets in the plating bath is shown in Figure 4.6. In Figure 4.6, the C maps represent the graphene nanoplatelets. The existence of carbon element confirms the presence of graphene nanoplatelets in the Cu-Ni matrix. Also, from Figure 4.6, it is noticeable that Cu, Ni and graphene nanoplatelets are uniformly distributed in the Cu-Ni/Gr composite coatings surface.

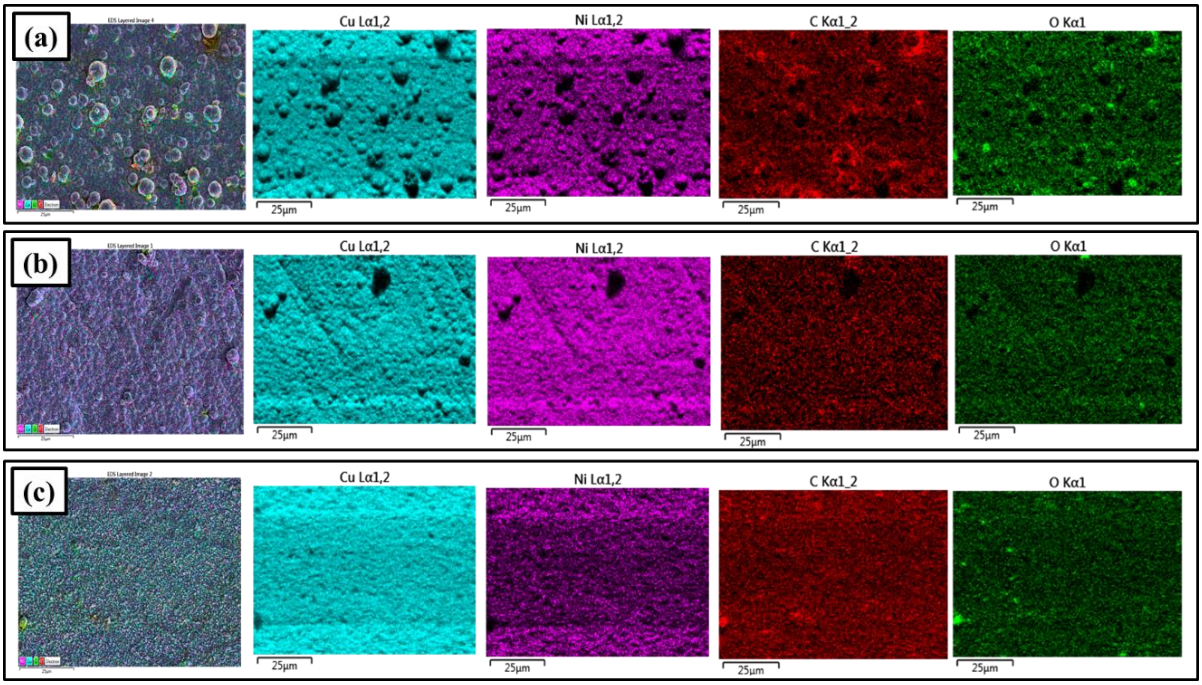

Figure 4.6: EDS mapping of Cu-Ni/Gr composite coatings (a) 100 mg/L (b) 200 mg/L and (c) 400 mg/L

The elemental composition of electrodeposited Cu-Ni/Gr composite coatings at various concentrations of graphene nanoplatelets in the plating bath is given in Table. 4.2. The content of graphene nanoplatelets in the composite coatings depends on different process parameters like pH, current density, temperature, stirring rate, plating time, and concentration of graphene in the plating bath. In this work, the influence of graphene nanoplatelets concentration in the plating bath is studied and the remaining process parameters were kept constant. Table 4.2 shows that graphene nanoplatelets content in the composite coatings is increased from 5.32 to 11 wt. % with the increase in the concentration of graphene nanoplatelets in the plating bath from 100 mg/L to 400 mg/L and then decreased with further increase in Gr concentration of Gr to 500 mg/L. The reduction in Gr content of Cu-Ni/Gr (500 mg/L) composite coating is mainly due to the agglomeration of Gr caused by degraded wettability. When the concentration of graphene nanoplatelets in the plating bath increased upto 400 mg/L, the entrapment of graphene nanoplatelets in the Cu-Ni matrix is increased [7].

Table 4.2: EDS data of Cu-Ni and Cu-Ni/Gr composite coatings electrodeposited at various Gr content

Coating sample	Cu (wt. %)	Ni (wt. %)	C (wt. %)
Cu-Ni	68.72	31.28	0
Cu-Ni/Gr (100 mg/L)	68.25	25.39	6.36
Cu-Ni/Gr (200 mg/L)	64.67	25.92	9.41
Cu-Ni/Gr (400 mg/L)	62.14	26.53	11.33
Cu-Ni/Gr (500 mg/L)	65.12	25.76	9.12

4.1.3 Microstructure of Cu-Ni/Gr composite coatings

4.1.3.1 Effect of current density

The XRD analysis has been carried out to study the effect of current density on structural properties of Cu-Ni/Gr composite coatings. The XRD spectrum of graphene nanoplatelets, Cu-Ni, and Cu-Ni/Gr composite coatings electrodeposited at various current densities is shown in Figure 4.7. On XRD spectrum of Cu-Ni, only one peak of Cu-Ni is observed instead of two separate peaks of Cu and Ni, which confirms the formation of Cu-Ni alloy in all the coatings [8], [9]. The major peak (111) corresponding to Cu-Ni has been observed at $2\theta = 43.6^{o}$, which is between the 2θ values of pure copper at 43.35^{o} (American Mineralogist Crystal Structure Database (AMCSD 0012903)) and pure nickel at 44.53^{o}

(AMCSD 0011153) [10]. The peaks in the XRD pattern of Cu-Ni and Cu-Ni/Gr composite coatings are corresponding to the plane (111), (200) and (220), which confirms the FCC structure of the electrodeposited coatings. The carbon peaks belong to graphene nanoplatelets (around $2\theta = 26°$) are not observed in XRD spectrum of Cu-Ni/Gr composite coatings electrodeposited at various current densities, which is due to very low graphene nanoplatelets content [11]. However, the peak intensity of the Cu-Ni/Gr composite coatings has been weakened with the increase in current density due to the lattice distortion of electrodeposited coatings by the incorporation of graphene nanoplatelets. In Figure 4.7, the width of the FCC reflections peaks are changed across the distinct samples due to the presence of graphene nanoplatelets. Moreover, peak broadening indicative of the small crystallite size of the coatings [12]. However, no impurity (such as Cu_2O) is observed in the XRD spectrum of Cu-Ni and Cu-Ni/Gr composite coatings.

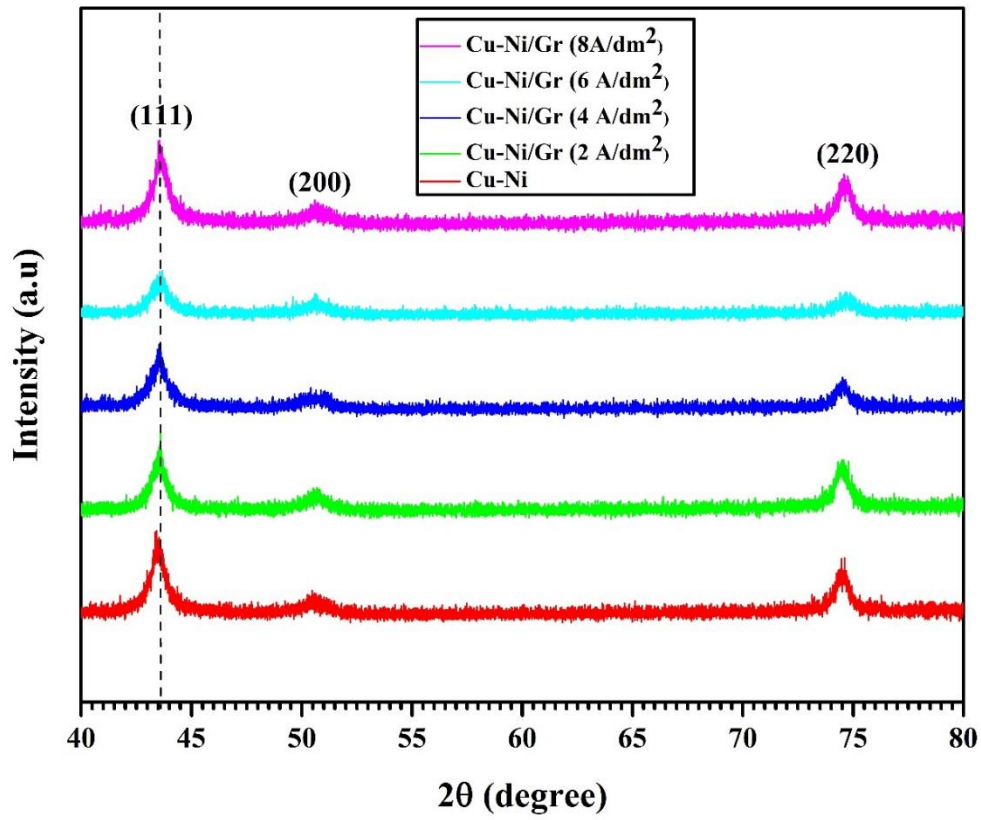

Figure 4.7: X-ray diffraction spectrum of Cu-Ni and Cu-Ni/Gr composite coatings electrodeposited at various current densities

Also, there is a slight decrease in crystallite size of Cu-Ni/Gr composite coatings with the rise in current density upto certain limit, due to the increase in the deposition rate. The crystal growth is inhibited significantly due to the higher deposition rate. Variation in

crystallite size of Cu-Ni and Cu-Ni/Gr composite coatings electrodeposited at various current densities is depicted in Table 4.3. According to the Scherrer equation and XRD pattern, the crystallite size for the (111) reflection was calculated [13]. Moreover, Cu-Ni/Gr composite coating electrodeposited at 6 A/dm^2 has the least crystallite size of about 8 nm. The embedded graphene nanoplatelets increase active nucleation sites and hence inhibit crystal growth. Hence, the incorporation of graphene nanoplatelets serves as a mechanism for grain refinement of electrodeposited composite coatings [2]. Also, the coating has high graphene content at the current density of 6 A/dm^2, and the coating has the least crystallite size. With further incrae in current density to 8 A/dm^2, the crystallite size of the coating is decreased mainly due to reduction in the Gr content of the coating.

The change in the lattice strain of Cu-Ni and Cu-Ni/Gr composite coatings at various current densities is presented in Table 4.3. The lattice strain was calculated with the help of XRD results by using equation (4.1) [14]:

$$\varepsilon = \left(\frac{\alpha}{4 \times \tan\theta} \right) \tag{4.1}$$

where α is full width at half maximum (FWHM) and θ is the Bragg's angle corresponding to FCC (111) peak. As shown in Table 4.3, the lattice strain increases up to 6 A/dm^2 and then decreases. Also, the smaller the crystallite size higher the lattice strain [15]. The generation of defects, such as voids, twins, vacancies, and dislocations, can increase the lattice strain [14].

Table 4.3: Change in the crystallite size and lattices strain of Cu-Ni and Cu-Ni/Gr composite coatings electrodeposited at various current densities

Sr. No.	Coating sample	Crystallite size (nm)	Lattice strain
1	Cu-Ni	10.36	0.0091
2	Cu-Ni/Gr (2 A/dm^2)	10.23	0.0098
3	Cu-Ni/Gr (4 A/dm^2)	9.32	0.0107
4	Cu-Ni/Gr (6 A/dm^2)	7.84	0.0128
5	Cu-Ni/Gr (8 A/dm^2)	8.36	0.0120

4.1.3.2 Effect of Gr content

In order to study the effect of Gr content on structural properties of Cu-Ni/Gr composite coatings, the XRD analysis has been carried out. The X-ray diffraction spectrum of XRD

micrographs for pure Cu, Ni, Cu-Ni, and Cu-Ni/Gr composite coatings with the various concentrations of graphene nanoplatelets in the plating bath is presented in Figure 4.8. No typical peak belonged to Ni was found. It indicates that Cu and Ni atoms have formed a single-phase solid solution [16]. The pure Cu-Ni coating shows a peak at a 2θ value of 43.65º, which is shifted in-between the 2θ values of pure copper (43.3º) and pure nickel (44.5º). The XRD pattern for pure Cu, Cu-Ni and Cu-Ni/Gr composite coatings shows (111), (200) and (220) diffraction peaks, which indicates FCC. crystal structure of the coatings. Also, Figure 4.8 shows the peak intensity of the Cu-Ni reflection peaks (111) has reduced and widths of the corresponding peaks are increased with increasing the concentration of graphene nanoplatelets in the plating bath. It is observed that due to the incorporation of the polycrystalline nature of graphene nanoplatelets, diffraction peaks shift towards the right side with the increase in graphene concentration in the plating bath. Cu-Ni/Gr composite coatings consist of grains with a strong (111) plane and a weak (200) plane orientation. This indicates that the favored crystallographic orientation of all Cu-Ni/Gr composite coatings electrodeposited at various concentration of graphene nanoplatelets in the plating bath is in the (111) direction.

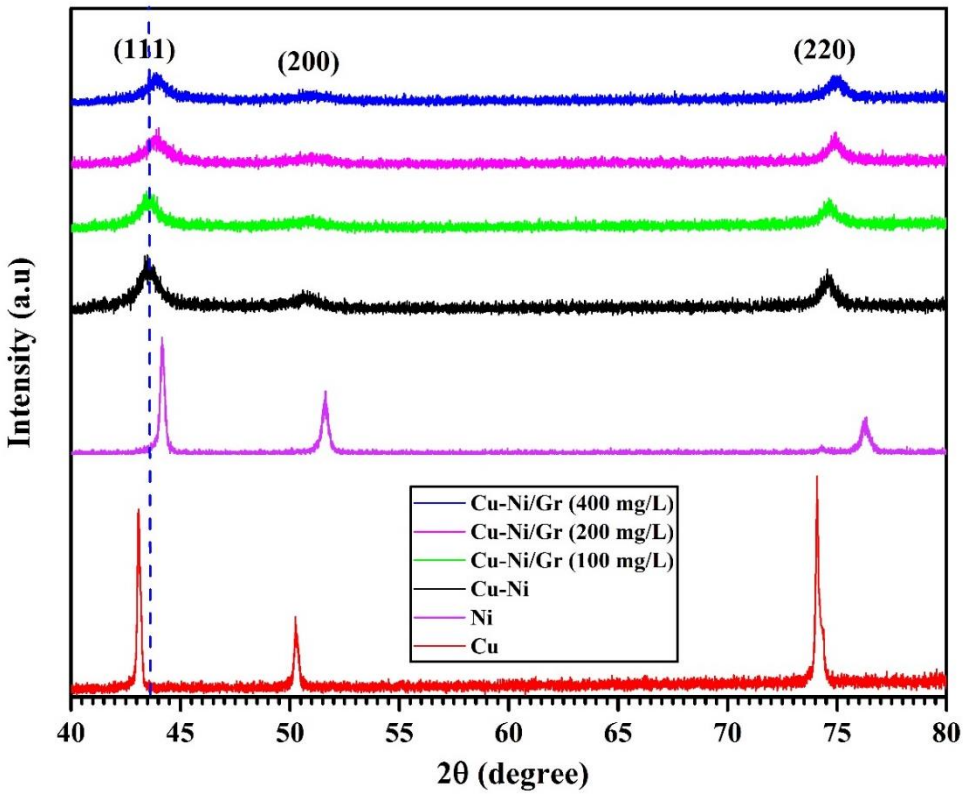

Figure 4.8: X-ray diffraction spectrum of prepared Cu, Ni, Cu-Ni and Cu-Ni/Gr composite coatings

The measured crystallite size and lattice strain of Cu-Ni/Gr composite coatings are depicted in Table 4.4. By using the Scherrer's equation crystallite size of prepared coatings is calculated from the full width at half maximum (FWHM) and XRD data associated (111) reflection [17]. Also, lattice strain is calculated for the prepared coatings by using the following equation (4.1). From Table 4.4, it is observed that increase in lattice strain and decrease in crystallite size with the increase in the concentration of graphene nanoplatelets in the plating bath up to certain limit. Cu-Ni/Gr (400 mg/L) composite coating has a minimum crystallite size of about 7 nm due to the maximum content of graphene nanoplatelets, as shown in Table 4.4 [2]. With the further increase in Gr concentration to 500 mg/L, the crystallite size of the coating is not decreased. The reason for this result is that Gr is adsorbed less on the cathode due to the agglomeration of Gr in the electrolyte bath.

Table 4.4: The change in the crystallite size and lattices strain of Cu-Ni/Gr composite coatings electrodeposited at various Gr content in the electrolyte bath

Sr. No.	Coating sample	Crystallite size (nm)	Lattice strain
1	Cu-Ni	10.36	0.0091
2	Cu-Ni/Gr (100 mg/L)	7.4	0.0132
3	Cu-Ni/Gr (200 mg/L)	7.14	0.0137
5	Cu-Ni/Gr (400 mg/L)	6.87	0.0144
6	Cu-Ni/Gr (500 mg/L)	6.88	0.0142

4.2 Characterization results of Cu-Ni/Gr composite powder

For primary characterization purpose, six different samples with variation in the concentration of Gr were prepared by the modified electro-co-deposition method. In this section we have studied the effect of variation in graphene nanoplatelets content on surface morphology, elemental analysis and microstructure of the Cu-Ni/Gr composite coating.

4.2.1 Surface morphology of Cu-Ni/Gr composite powder

FESEM analysis has been carried out to study the effect of Gr reinforcement on surface morphology of Cu-Ni alloy powder. The external morphology of the pure Cu-Ni alloy and Cu-Ni/Gr composite powder samples were examined by FESEM. The image of electrochemical-co-deposited pure Cu-Ni (Figure 4.9(a-b)) and Cu-Ni/Gr (200 mg/L) composite powder samples (Figure 4.9(c-d)) shows the dendritic structure with clearly

distinguishable tip-splitting and hierarchy. The average particle size of pure Cu-Ni alloy and Cu-Ni/Gr (200 mg/L) composite powder samples was in the range of 5-15 µm.

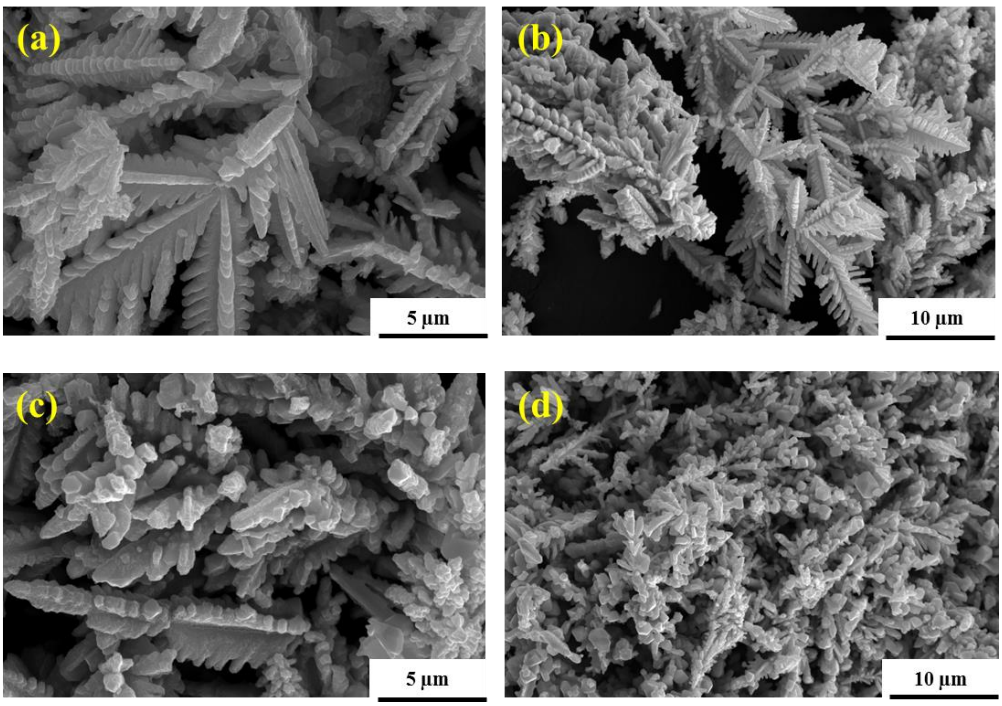

Figure 4.9: FESEM images of electrochemical-co-deposited (a-b) pure Cu-Ni alloy and (c-d) Cu-Ni/Gr (200 mg/L) composite powder samples

4.2.2 Elemental composition of Cu-Ni/Gr composite powder

In order to study the elemental composition of Cu-Ni/Gr composite powder, EDS analysis has been carried out. Figure 4.10(a-b) exhibits the element distribution map of pure Cu-Ni alloy and Cu-Ni/Gr (200 mg/L) composite powder samples measured by the EDS method and corresponding elemental composition are presented in Table 4.5. Table 4.5 presents the Cu-Ni/Gr composite powder sample contains 79.63-84.67 wt.% Cu, 9.91-10.78 wt.% Ni, 3.70-7.85 wt.% Gr and about 1.53-1.74 wt.% O elements. It revealed that the content of copper, nickel, and carbon in the Cu-Ni/Gr composite powder samples was significantly affected by the concentration of Gr in the electrolyte bath. In all prepared Cu-Ni/Gr composite powder samples, Cu content is much higher than Ni content because copper is nobler than nickel. In the electrodeposition process, Cu^{2+} has a greater attraction of electrons than Ni^{2+} thus Cu is more easily deposited than Ni. Cu enriched alloy is also forms due to the presence of high concentration of sodium citrate in the electrolyte bath [18], [19]. It is noteworthy that with the increase in Gr into the Cu-Ni alloy matrix, the content of Ni in the Cu-Ni/Gr composite powder sample is increases and Cu decreases, suggesting that during the deposition process Gr slightly affected on the Cu-Ni ratio.

Table 4.5: Elemental composition of pure Cu-Ni alloy and Cu-Ni/Gr composite powder samples

Samples	Cu (wt. %)	Ni (wt. %)	C (wt. %)	O (wt. %)
Cu-Ni	87.39	10.75	-	1.86
Cu-Ni/Gr (50 mg/L)	84.67	9.91	3.70	1.72
Cu-Ni/Gr (100 mg/L)	83.04	10.29	5.14	1.53
Cu-Ni/Gr (200 mg/L)	79.63	10.78	7.85	1.74
Cu-Ni/Gr (250 mg/L)	81.95	10.34	5.98	1.73

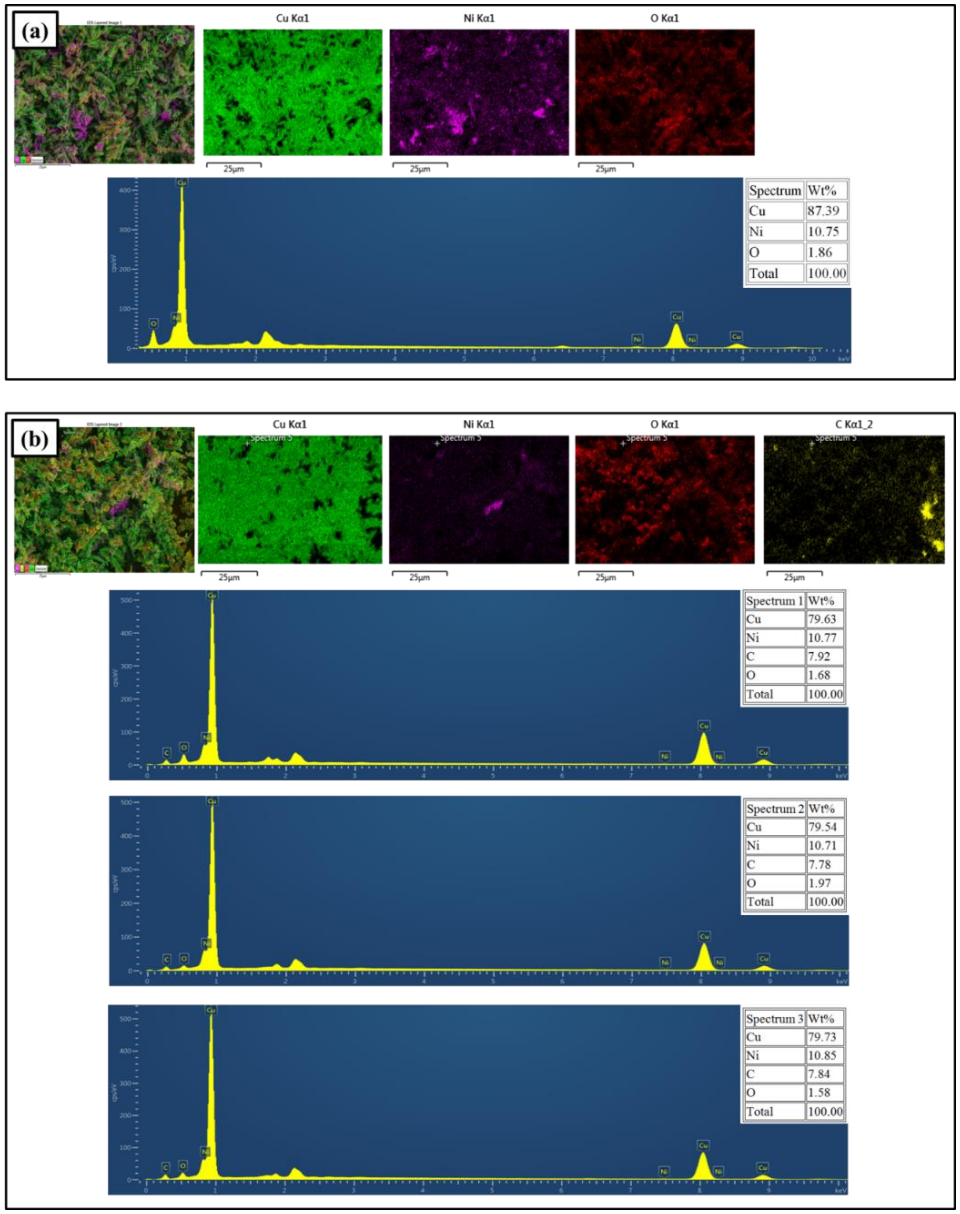

Figure 4.10: Elemental distribution map of (a) pure Cu-Ni alloy composite powder sample and (b) Cu-Ni/Gr (200 mg/L) composite powder sample at three different points (Spectrum 1, Spectrum 2, Spectrum 3)

Previous research has shown that nickel ions can be easily deposited on the defective sites of the graphene [2]. The slight increase in Ni content is attributed to the increase in Gr concentration in the electrolyte bath. The EDS analysis of Cu-Ni/Gr (200 mg/L) composite powder sample was carried out at three different points to ensure even dispersion of Gr. From EDS spectrums presented in Figure 4.10(b), it is observed that the wt. % of Cu is 79.63 ± 0.09, wt. % of Ni is 10.78 ± 0.08, wt. % of C is 7.85 ± 0.07 and the wt. % of O is 1.74 ± 0.18, which confirms the even dispersion of Gr in the Cu-Ni alloy matrix. The Gr serves as an effective reinforcing element which may provide a barrier to the movement of the dislocations. The most important feature of this technique is the simultaneous deposition of Gr, Ni^{2+} and Cu^{2+} on the tip of the cathode surface, which provides an even dispersion of Gr in the Cu-Ni alloy matrix as shown in Figure 4.10(b).

4.2.3 TEM analysis of Cu-Ni/Gr composite powder

In order to study the interaction of metal particles with Gr and elemental distributions in greater detail, TEM-EDS analysis was carried out. TEM image of Cu-Ni/Gr (200 mg/L) composite powder is presented in Figure 4.11(a), where quite a spherical shape (minimum diameter ≈ 10 nm) produced Cu-Ni nanoparticles are visible. The interface between the Gr and Cu-Ni alloy matrix is presented in Figure 4.11(b). It shows that Cu and Ni atoms deposited on Gr and producing transition region. Figure 4.11(c) displays the HRTEM image of the Gr area with a lattice fringe 0.36 nm. In Figure 4.11(c) inserted image shows the typically selected area electron diffraction (SAED) pattern of Gr. The SAED pattern of Gr shows circular rings originated from diffraction of an electron from (100) and (110) planes. Figure 4.11(d) shows the HRTEM image of the Cu-Ni alloy matrix area with a lattice fringe of 0.205 nm and the inserted image is the SAED pattern of Cu-Ni alloy matrix. The SAED pattern of Cu-Ni alloy shows circular rings originated from the diffraction of an electron from (111), (200), and (220) planes. TEM-EDS images of Cu-Ni/Gr (200 mg/L) composite powder are shown in Figure 4.11(e). The TEM-EDS results indicate that Gr nanoplatelets tightly adhere to the Cu-Ni alloy matrix.

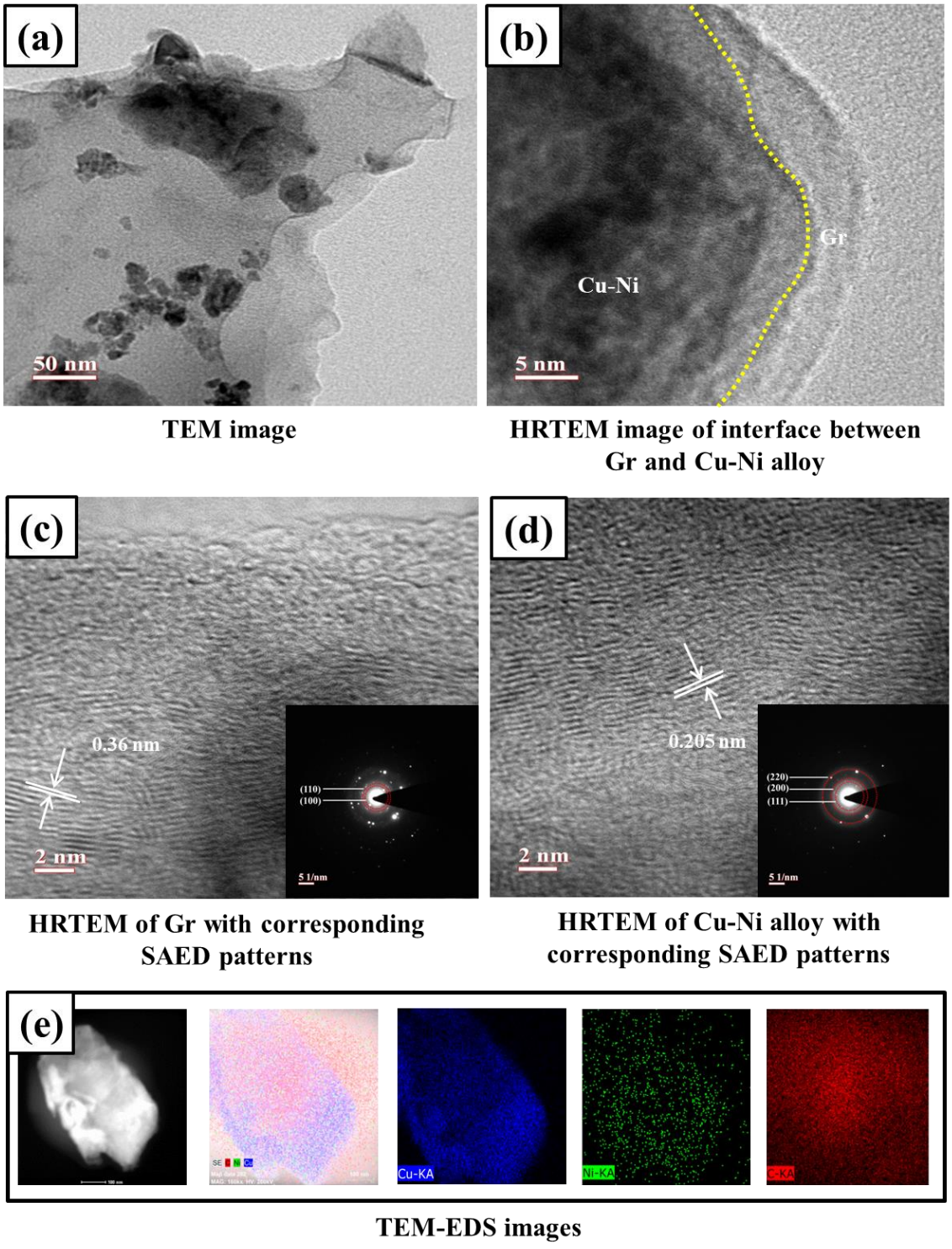

Figure 4.11: TEM-EDS analysis of Cu-Ni/Gr (200 mg/L) composite powder

4.2.4 XRD analysis of Cu-Ni/Gr composite powder

The XRD analysis has been carried out to study the effect of various Gr content on structural properties of Cu-Ni/Gr composite powder in more detail. Figure 4.12 displays the XRD patterns of pure Cu-Ni alloy and Cu-Ni/Gr composite powder samples. In Figure 4.12, characteristic peaks corresponding to (111), (200), and (220) crystallographic planes

are related to FCC structure. The pure Cu-Ni alloy powder sample shows a major peak (111) at a 2θ angle of 43.6º (JCPDS file No. 47-1406 [20]). No separate peaks corresponding to pure Cu and Ni are observed in the XRD spectrum of Cu-Ni alloy powder sample, and this confirms that modified electrochemical-co-deposition allows the formation of Cu-Ni alloy rather than distinct Cu and Ni particles. Comparing the XRD spectrums of Cu-Ni alloy and Cu-Ni/Gr composite powder samples, the Gr incorporated Cu-Ni alloy matrix powder sample shows shifted and widened peaks, which is due to the polycrystalline nature of Gr [2]. It is a well-known fact that the shifting of XRD peaks positions of electrodeposited samples is mainly associated with the lattice distortion due to defects. The incorporation of Gr in the Cu-Ni alloy structure generates lattice strain [21]. Hence, as the Gr content is increased in the Cu-Ni alloy matrix, the intensity of (111) peak is decreased and slightly shifted towards a higher 2θ angle. During the electrochemical-co-deposition process, Gr develop new nucleation sites accelerating the nucleation process while impeding Cu and Ni crystals growth; consequently, the presence of Gr leads to grain refinement.

The crystallite size of the pure Cu-Ni alloy and Cu-Ni/Gr composite powder samples are represented in Table 4.6. In this figure, the crystallite size of the Cu-Ni/Gr composite powder sample shows a diminishing trend from about 39 nm to 26 nm with an increase in the Gr concentration in the electrolyte bath.

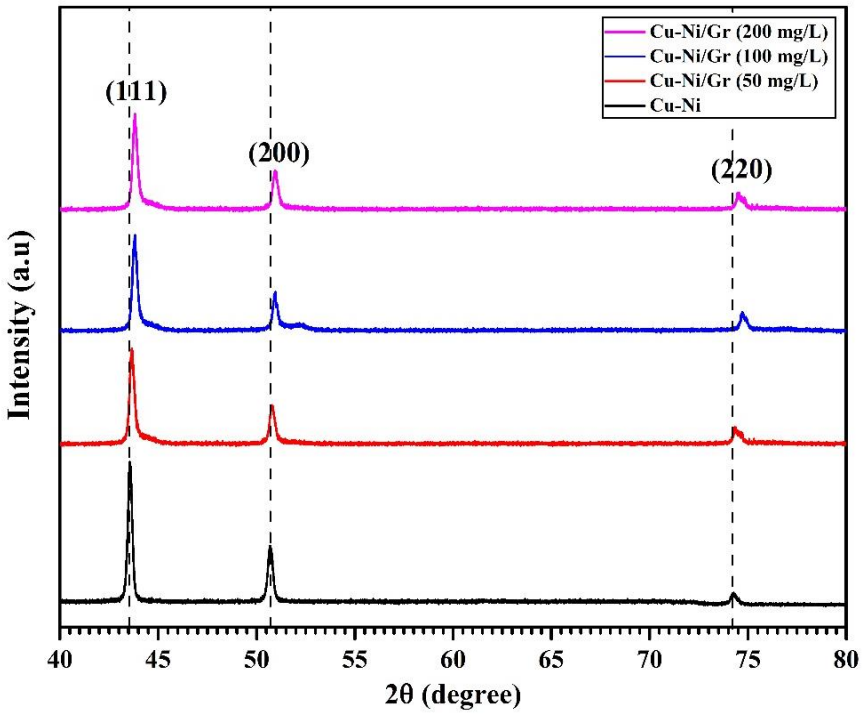

Figure 4.12: XRD patterns of pure Cu-Ni alloy and Cu-Ni/Gr composite powder

Table 4.6: Crystallite size of pure Cu-Ni alloy and Cu-Ni/Gr composite powder

Sr. No.	Coating sample	Crystallite size (nm)	Lattice strain
1	Cu-Ni	39.56	0.0025
2	Cu-Ni/Gr (50 mg/L)	37.12	0.0026
3	Cu-Ni/Gr (100 mg/L)	32.33	0.0030
5	Cu-Ni/Gr (200 mg/L)	25.72	0.0038
6	Cu-Ni/Gr (250 mg/L)	31.56	0.0031

4.3 Conclusion

1. Cu-Ni/Gr composite coatings are successfully electrodeposited using various current densities (such as 2, 4, 6 and 8 A/dm^2). The influence of various current densities on the surface morphology, elemental composition and microstructure of Cu-Ni/Gr composite coatings was examined by FESEM, EDS and XRD analysis.
2. The EDS analysis showed that the content of Gr in the Cu-Ni/Gr composite coating is increased with an increase in current density from 2 A/dm^2 to 6 A/dm^2 and then decreased with further increase in the current density to 8 A/dm^2.
3. The XRD analysis showed that the incorporation of Gr in Cu-Ni alloy coating influenced the crystallite size. The crystallite size of the Cu-Ni/Gr composite coating was decreased with an increase in current density from 2 A/dm^2 to 6 A/dm^2 and then increased with further increase in the current density to 8 A/dm^2.
4. Cu-Ni/Gr composite coatings are successfully electrodeposited using various concentrations of Gr (such as 0, 100, 200, 300, 400 and 500 mg/L) in the electrolyte bath. The influence of various concentrations Gr in the electrolyte bath on the surface morphology, elemental composition and microstructure of Cu-Ni/Gr composite coatings was examined by FESEM, EDS and XRD analysis.
5. The EDS analysis showed that the content of Gr in the Cu-Ni/Gr composite coating was increased with an increase in Gr concentration in the electrolyte bath from 100 mg/L to 400 mg/L and then decreased with further increase in the Gr concentration in the electrolyte bath to 500 mg/L.
6. The XRD analysis showed that the incorporation of Gr in Cu-Ni alloy coating influenced the crystallite size. The crystallite size of the Cu-Ni/Gr composite coating was decreased with an increase in Gr concentration in the electrolyte bath from 100

mg/l to 400 mg/L and then increased with further increase in the Gr concentration in the electrolyte bath to 500 mg/L.

7. The Gr reinforced Cu-Ni alloy matrix composite powder samples are successfully synthesized through a modified electro-co-deposition method using various concentrations of Gr in the electrolyte bath. GNPs were added in concentrations of 0, 50, 100, 150, 200 and 250 mg/L and uniformly dispersed by ultra-sonication treatment (20 kHz frequency and 500 W power). This composite powder is comprised of pure copper and nickel extracted from their 98% pure metal salts and Gr.
8. The reinforcement of Gr into the Cu-Ni alloy matrix is confirmed from FESEM, EDS, XRD and HRTEM analysis. The uniform dispersion of Gr into the Cu-Ni alloy matrix was observed from EDS and TEM analysis. The Gr and Cu-Ni alloy particles interact at a molecular level and hence dispersion takes place at a molecular level.
9. The SEM analysis showed that the average particle size of pure Cu-Ni alloy and Cu-Ni/Gr composite powder samples are in the range of 5-15 μm. The XRD analysis revealed that the crystallite size of the Cu-Ni alloy powder sample was decreased by the addition of Gr in the electrolyte bath up to 200 mg/L.
10. The facile, economical and bulk production of Cu-Ni/Gr composite powder has been achieved using a modified electro-co-deposition method with a uniform dispersion of Gr into the Cu-Ni alloy matrix without damaging its structure.

References

[1] V. F. C. Lins *et al.*, "Effect of the Current Density on Morphology , Porosity , and Tribological Properties of Electrodeposited Nickel on Copper," *J. Mater. Eng. Perform.*, vol. 17, no. 5, pp. 741–745, 2008, doi: 10.1007/s11665-008-9205-9.

[2] G. Yasin *et al.*, "Synthesis of spheres-like Ni/graphene nanocomposite as an efficient anti-corrosive coating; effect of graphene content on its morphology and mechanical properties," *J. Alloys Compd.*, vol. 755, pp. 79–88, Jul. 2018, doi: 10.1016/j.jallcom.2018.04.321.

[3] E. Pellicer *et al.*, "A comparison between fine-grained and nanocrystalline electrodeposited Cu–Ni films. Insights on mechanical and corrosion performance," *Surf. Coatings Technol.*, vol. 205, no. 23–24, pp. 5285–5293, Sep. 2011, doi: 10.1016/j.surfcoat.2011.05.047.

[4] S. Rode, C. Henninot, C. Vallières, and M. Matlosz, "Complexation Chemistry in Copper Plating from Citrate Baths," *J. Electrochem. Soc.*, vol. 151, no. 6, p. C405, 2004, doi: 10.1149/1.1715092.

[5] I. S. A. Laszczyńska, J. Winiarski, B. Szczygieł, "Electrodeposition and characterization of Ni–Mo–ZrO2 composite coatings," *Appl. Surf. Sci.*, vol. 369, pp. 224–231, 2016, doi: 10.1016/j.apsusc.2016.02.086.

[6] Z. Xu, "Graphene Composites," in *Graphene*, Y. F. Hongwei Zhu, Zhiping Xu, Dan Xie, Ed. Elsevier, 2018, pp. 201–214. doi: 10.1016/B978-0-12-812651-6.00008-2.

[7] J. P. Celis, J. Roos, and C. Buelens, "A Mathematical Model for the Electrolytic Codeposition of Particles with a Metallic Matrix," *J. Electrochem. Soc.*, vol. 134, no. 6, pp. 1402–1408, 1987, doi: 10.1149/1.2100680.

[8] P. Q. Dai, C. Zhang, J. C. Wen, H. C. Rao, and Q. T. Wang, "Tensile Properties of Electrodeposited Nanocrystalline Ni-Cu Alloys," *J. Mater. Eng. Perform.*, vol. 25, no. 2, pp. 594–600, Feb. 2016, doi: 10.1007/s11665-016-1881-2.

[9] I. Bakonyi, E. Tóth-Kádár, J. Tóth, T. Becsei, T. Tarnóczi, and P. Kamasa, "Magnetic and electrical transport properties of electrodeposited Ni-Cu alloys and multilayers," *J. Phys. Condens. Matter*, vol. 11, no. 4, pp. 963–973, 1999, doi: 10.1088/0953-8984/11/4/004.

[10] R. T. Downs and M. Hall-Wallace, "The American Mineralogist crystal structure database," *Am. Mineral.*, vol. 88, no. 1, pp. 247–250, Jan. 2003, [Online]. Available: https://doi.org/

[11] H. Algul *et al.*, “The effect of graphene content and sliding speed on the wear mechanism of nickel-graphene nanocomposites,” *Appl. Surf. Sci.*, vol. 359, pp. 340–348, 2015, doi: 10.1016/j.apsusc.2015.10.139.

[12] B. Szczygieł and M. Kołodziej, “Composite Ni/Al2O3 coatings and their corrosion resistance,” *Electrochim. Acta*, vol. 50, no. 20, pp. 4188–4195, 2005,

[13] P. S. Related, “On Variance as a Measure of Line Broadening in Diffractometry General Theory and Small Particle Size,” *Proc. Phys. Soc.*, vol. 80, p. 286, 1962.

[14] M. Boubatra, A. Azizi, G. Schmerber, and A. Dinia, “Morphology, structure, and magnetic properties of electrodeposited Ni films obtained from different pH solutions,” *J Mater Sci Mater Electron*, vol. 22, no. 12, pp. 1804–1809, 2011, doi: 10.1007/s10854-011-0366-1.

[15] S. K. Ghosh, A. K. Grover, G. K. Dey, and M. K. Totlani, “Nanocrystalline Ni-Cu alloy plating by pulse electrolysis,” *Surf. Coatings Technol.*, vol. 126, no. 1, pp. 48–63, 2000, doi: 10.1016/S0257-8972(00)00520-X.

[16] B. Li, S. Du, and T. Mei, “Pulse electrodepsoited Ni-Cu/TiN-ZrO 2 nanocomposite coating: microstructural and electrochemical properties,” *Mater. Res. Express*, vol. 6, no. 9, p. 096433, Jul. 2019, doi: 10.1088/2053-1591/ab31e9.

[17] A. L. Patterson, “The Scherrer Formula for X-Ray Particle Size Determination,” *Phys. Rev.*, vol. 56, no. 10, pp. 978–982, Nov. 1939, doi: 10.1103/PhysRev.56.978.

[18] C. R. Thurber *et al.*, “Metal Matrix Composite Coatings of Cupronickel Embedded with Nanoplatelets for Improved Corrosion Resistant Properties,” *Int. J. Corros.*, vol. 2018, pp. 1–11, Jun. 2018, doi: 10.1155/2018/5250713.

[19] A. D. Pingale, S. U. Belgamwar, and J. S. Rathore, “Synthesis and characterization of Cu–Ni/Gr nanocomposite coatings by electro-co-deposition method: effect of current density,” *Bull. Mater. Sci.*, vol. 43, no. 1, p. 66, Dec. 2020.

[20] V. Zin, K. Brunelli, and M. Dabalà, “Characterization of Cu–Ni alloy electrodeposition and synthesis of nanoparticles by pulsed sonoelectrochemistry,” *Mater. Chem. Phys.*, vol. 144, no. 3, pp. 272–279, Apr. 2014, doi: 10.1016/j.matchemphys.2013.12.028.

[21] A. D. Pingale, S. U. Belgamwar, and J. S. Rathore, “Effect of Graphene Nanoplatelets Addition on the Mechanical, Tribological and Corrosion Properties of Cu–Ni/Gr Nanocomposite Coatings by Electro-co-deposition Method,” *Trans. Indian Inst. Met.*, vol. 73, no. 1, pp. 99–107, Jan. 2020, doi: 10.1007/s12666-019-01807-9.

Chapter 5

Mechanical, Tribological and Corrosion Performance of Cu-Ni/Gr Composites

In previous chapter, Cu-Ni/Gr composite coatings are characterized by FESEM, EDS and XRD techniques to study the (i) effect of various current densities and (ii) various concentrations of Gr in the electrolyte bath on surface morphology, elemental composition and microstructure of coatings. Also, Cu-Ni/Gr composites powder was characterized by FESEM, EDS, HRTEM and XRD techniques in order to confirm the proper reinforcement of Gr in the Cu-Ni alloy matrix using a modified electro-co-deposition method.

In this chapter, the effect of various current densities and various concentrations of graphene nanoplatelets in the electrolyte bath on the mechanical, tribological and corrosion properties of Cu-Ni/Gr composite coatings are investigated in detail. Also, the effect of various concentrations of graphene nanoplatelets in the electrolyte bath on mechanical, tribological and corrosion properties of Cu-Ni/Gr composites prepared by a modified electro-co-deposition method followed by powder metallurgy method are discussed.

5.1 Mechanical, tribological and corrosion performance of Cu-Ni/Gr composite coatings synthesized by the electro-co-deposition method

5.1.1 Microhardness of Cu-Ni/Gr composite coatings

The Vickers microhardness test is widely used to measure the hardness of metal, alloys and composite coatings. In this work microhardness of Cu-Ni/Gr composite coatings was measured using INOVATEST microhardness tester. The microhardness measurement was carried out on the surface of prepared coatings. A diamond pyramid indenter with a square base (angle between opposite faces = 136°) was used. To measure the microhardness, test sample is placed on anvil. The anvil is raised up close to the point of the indenter with the help of screw threads arrangement. Then values of applied load and dwell time are feed to the microhardness tester. The applied load was 20 g for a dwell time of 10 s. During test, the applied load was 20 g for a dwell time of 10 s. The values of applied load and dwell time are optimized during the test to minimize the errors in the measurement. Due to the application of load, the diamond pyramid indenter is pressed into the surface of the coating. After this, the load is released and the anvil with the test sample is lowered. The two

diagonals of the indentation were measured with the help of a microscope and their average was calculated to measure the microhardness of the coating. The schematic of indentation mark for diamond pyramid indenter is shown in Figure 5.1.

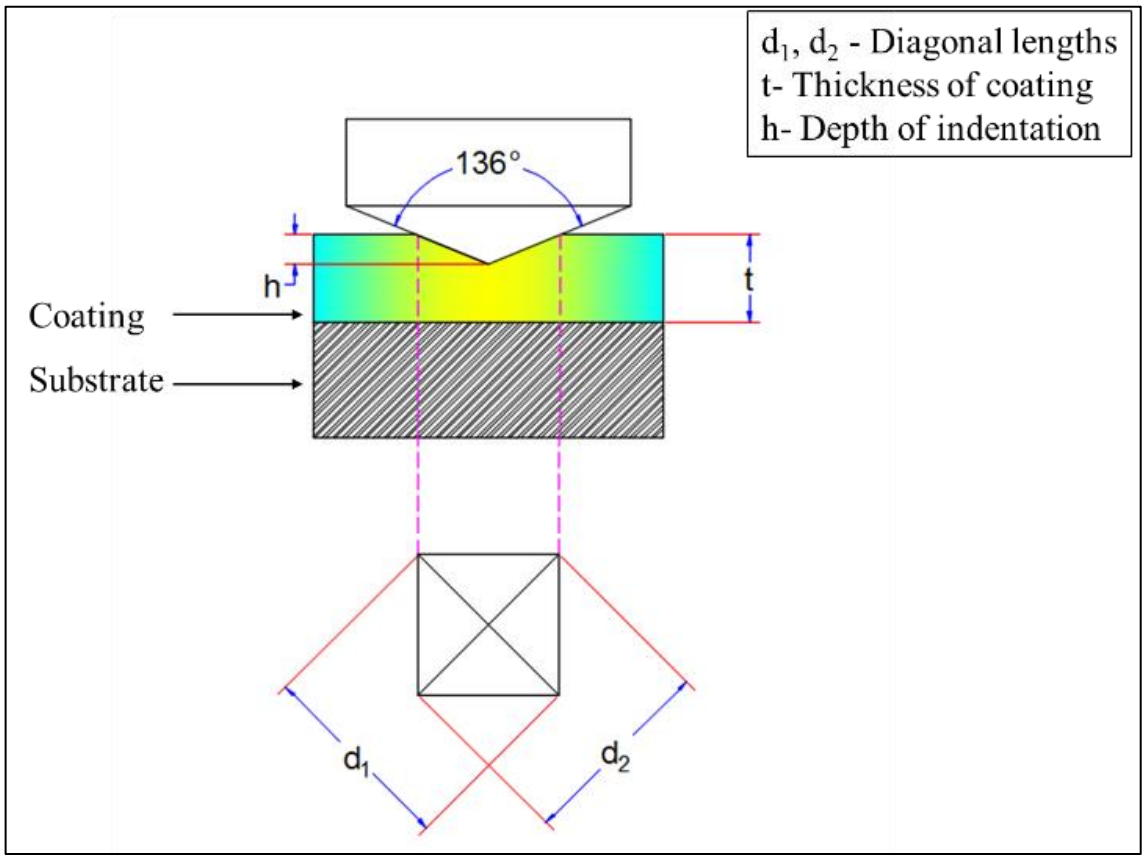

Figure 5.1: Schematic of indentation mark for diamond pyramid indenter

From Figure 5.1, we can calculate indentation depth using the following equation (5.1):

$$h = \frac{d_{avg}}{2\sqrt{2}\tan\left(\frac{136}{2}\right)} = \frac{d_{avg}}{7.0006} \tag{5.1}$$

where,

$$d_{avg} = \frac{(d_1 + d_2)}{2} \tag{5.2}$$

The Vickers hardness is the quotient obtained by dividing the kgf load by the square mm area of indentation.

$$HV = \frac{2F\sin\left(\frac{136°}{2}\right)}{d_{avg}^2}\pi r^2 = \frac{1.8544F}{d_{avg}^2} \quad (5.3)$$

where, F is applied load in kgf and d_{avg} is an arithmetic mean of two diagonals d_1 and d_2 in mm. The thickness of the layer shall be at least 1.5 times the diagonal of the indentation[1].

$$t > 1.5\, d_{avg} \quad (5.4)$$

The calculation for indentation depth and of Cu-Ni/Gr composite coating:

The indentation mark of the diamond pyramid indenter on Cu-Ni alloy coating surface is shown in Figure 5.2. The two diagonal lengths were measured using a microscope attached with the microhardness tester.

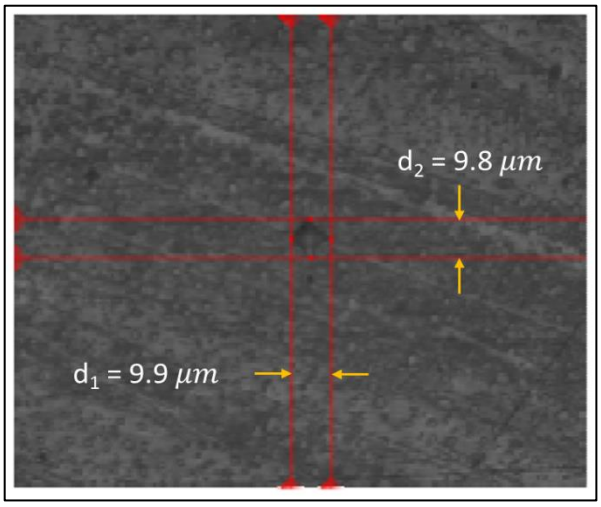

Figure 5.2: Indentation mark of diamond pyramid indenter of microhardness tester on Cu-Ni/Gr (100 mg/L) composite coating

1. Calculation of average diagonal length (d_{avg}) using equation (5.2):

$$d_{avg} = \frac{(d_1 + d_2)}{2}$$

$$d_{avg} = \frac{(9.9 + 9.8)}{2}$$

$$d_{avg} = 9.85\,\mu m$$

[1] https://archive.org/details/gov.in.is.1501.2002/page/n7/mode/1up

2. Calculation of indentation depth using equation (5.1):

$$h = \frac{d_{avg}}{7.0006}$$

$$h = \frac{9.85}{7.0006}$$

$$h = 1.4\,\mu m$$

Indentation depth for Cu-Ni/Gr composite coating is $h = 1.4\,\mu m$.

3. Calculation of Microhardness for Cu-Ni/Gr (100 mg/L) composite coating using equation (5.3):

$$HV = \frac{2F\sin\left(\frac{136°}{2}\right)}{d_{avg}^2}\pi r^2 = \frac{1.8544F}{d_{avg}^2}$$

$$HV = \frac{1.8544 \times (20 \times 10^{-3})}{(9.85 \times 10^{-3})^2}$$

$$HV = 382.26$$

Microhardness for Cu-Ni/Gr (100 mg/L) composite coating is 382.26 HV. Also, the measured thicknesses for all Cu-Ni/Gr composite coatings are higher than 30 µm. Here, the thickness of Cu-Ni/Gr (100 mg/L) composite coating 43 ± 3 µm is much higher than the indentation depth of 1.4 µm. Also, it satisfies equation (5.4). A similar observation is found for all prepared coatings, i.e. the thickness of the coating was much higher than the indentation depth. Hence, it is confirmed that the measured microhardness of the coating is not dominated by the substrate.

5.1.1.1 Effect of current density

In order to study the effect of various current densities on microhardness of Cu-Ni/Gr composite coatings, microhardness testing of prepared coatings was carried out. The microhardness variation of Cu-Ni/Gr composite coatings electrodeposited at various current densities is represented in Figure 5.3. The measured microhardness of Cu-Ni/Gr composite coatings is higher than Cu-Ni alloy coating. The microhardness of Cu-Ni/Gr composite coating deposited at 2 A/dm^2, 4 A/dm^2, 6 A/dm^2 and 8 A/dm^2 of current density are 362 HV, 375 HV, 388 HV and 351 HV, respectively. The improved microhardness of

Cu-Ni/Gr composite coatings is mainly due to the crystallite size refinement and an increase in the percentage of grain boundaries after incorporation of graphene nanoplatelets, as well as extraordinary mechanical properties of graphene nanoplatelets [1]. The movement of dislocations in the Cu-Ni/Gr composite coating is hindered by graphene nanoplatelets, which tends to increase the deformation resistance and lattice distortion energy [2], [3]. As shown in Figure 5.3, the microhardness of Cu-Ni/Gr composite coating first increases up to 6 A/dm^2 then decreases with an increase in current density. The adsorption force of graphene nanoplatelets surrounded by positive ion cloud (Cu^{2+} and Ni^{2+}) in the bath is increased with an increase in current density within a certain range [4]. Hence, the content of graphene nanoplatelets in the coatings is gradually increased up to 6 A/dm^2 as observed from Table 4.1. However, with further increase in current density to 8 A/dm^2, independent metal ions (Cu^{2+} and Ni^{2+}) are quickly attracted to the substrate, the content of incorporated graphene nanoplatelets decreases [5], [6]. Thus, the microhardness of Cu-Ni/Gr composite coating decreases at the current density 8 A/dm^2.

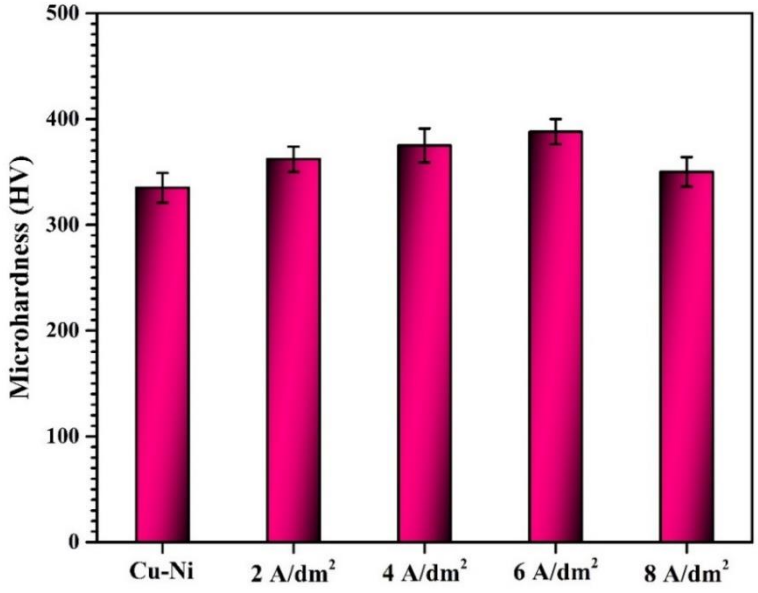

Figure 5.3: Variation in microhardness of Cu-Ni/Gr composite coatings electrodeposited at various current densities.

5.1.1.2 Effect of Gr content

In order to study the effect of Gr content on microhardness of Cu-Ni/Gr composite coatings, microhardness testing of prepared coatings was carried out. The dependence of the microhardness of Cu-Ni/Gr nanocomposite coatings on the concentration of graphene

nanoplatelets in the plating bath is depicted in Figure 5.4. The microhardness of Cu-Ni alloy matrix composite coatings mainly depends upon the microstructure of the alloy matrix and the content of the reinforcing element embedded into the alloy matrix. From Figure 5.4, it is clearly visible that the microhardness of Cu-Ni/Gr nanocomposite coatings is higher than Cu-Ni coating and in general, it increases with an increase in the concentration of Gr in the plating bath upto 400 mg/L and starts decreasing with further increase in Gr concentration to 500 mg/L. The microhardness of Cu-Ni/Gr composite coating deposited at 100 mg/L, 200 mg/L, 400 mg/L and 500 mg/L concentration of Gr in the electrolyte bath are 390 HV, 442 HV, 484 HV and 432 HV, respectively. The decrease in the microhardness of Cu-Ni/Gr (500 mg/L) composite coating is attributed to the decrease of the Gr content in the composite coating. At higher concentration of Gr in the electrolyte bath, the agglomeration of the Gr is enhanced, and agglomerated Gr are settled at in the electrolyte bath because of gravity. Hence, the absorption of Gr into Cu-Ni alloy matrix is decreased. In addition to this, at higher concentration of Gr in the electrolyte bath, the viscosity of the electrolyte bath is increased, and gas bubbles cannot easily be removed from the cathode surface.

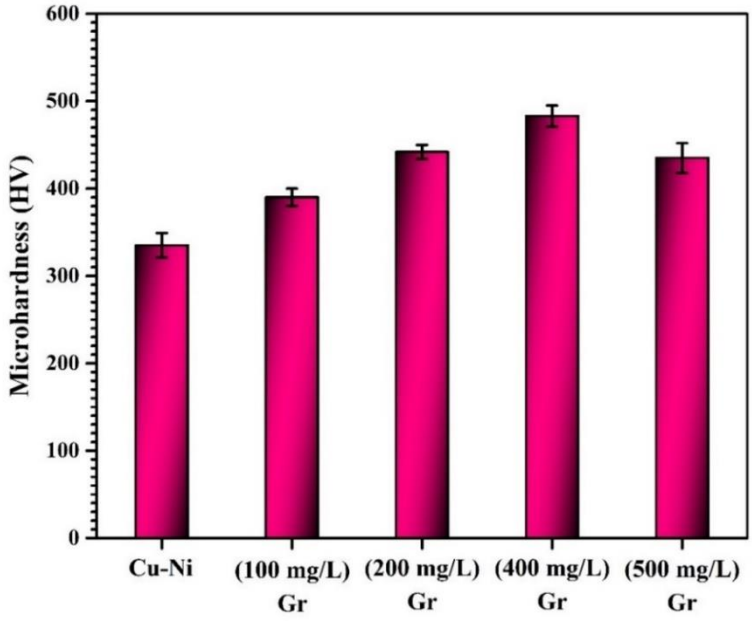

Figure 5.4: Microhardness of Cu-Ni/Gr composite coatings prepared at various concentrations Gr in the plating bath

These bubbles affect the absorption of Gr particles into the Cu-Ni alloy matrix; hence, the Gr content in Cu-Ni/Gr (500 mg/L) coating is reduced. Cu-Ni/Gr (400 mg/L) composite coating shows a maximum microhardness value of 483 HV. Increase in microhardness of composite coatings is attributed to particle strengthening, dispersion strengthening and

solid solution strengthening [7]. In the present work, improvement in microhardness is mainly due to the crystallite size refinement and dispersion strengthening by the incorporation of graphene nanoplatelets in the Cu-Ni matrix.

5.1.2 Tribological performance of Cu-Ni/Gr composite coatings

Tribological performance focus on wear, friction and lubrication of sliding surfaces in relative motion. The most common cause for the replacement of materials in the automobile, marine and aerospace industries is the wearing of materials. Applications of protective coatings on base materials is the most suitable approach, which provides good wear resistance. In marine applications, the use of copper-based alloy coatings provides superior wear resistance. The wear test is usually carried out to obtain fundamental information on the wear mechanism and to study how material microstructure affects on wear performance. In the view of engineering applications, the tribological performance of Cu-Ni/Gr composite coatings has great importance to increase the service life of the base materials in harsh working conditions. In the last decade, the tribological performance of different composite coatings prepared by the electro-co-deposition method has been studied extensively. However, only few studies are available on Cu-Ni alloy matrix composite coatings. Also, the effect of graphene nanoplatelet reinforcement on the tribological performance of Cu-Ni alloy matrix composite coatings is not studied. Graphene nanoplatelets are considered as an excellent solid lubricant due to the presence of weak Van der Walls bonds between the graphene layers and strong interlayer covalent bonds between carbon atoms [8]. To study the tribological performance of Cu-Ni/Gr composite coatings CETR reciprocating tribometer is used.

The schematic diagram for the wear test setup is represented in Figure 5.5. During the test, the sample is fixed into a table using a holding clamp. Then, a steel ball of 3 mm diameter is pressed against a flat coating sample that is moved backwards and forwards in a reciprocating motion. The wear test is carried out at an amplitude of 5 mm and 4 N load with 5 Hz frequency. Friction is usually measured by measuring the force required to restrain the pin or ball against the direction of travel. The average friction coefficient is calculated from the frictional forces for 300 cycles. Before the wear tests, the weight of the Cu-Ni/Gr composite coatings was measured by a digital balance with an accuracy of 0.0001 g. Also, after the wear tests, the coatings were weighted, and then the wear weight loss was calculated. Also, the worn surface of the Cu-Ni/Gr composite coatings was examined by scanning electron microscopy (SEM) (FEI-Apreo S) attached with energy

dispersive spectroscopy (EDS). SEM images of worn surface help to understand the state and characteristics of friction interface. Also, EDS mapping of wear track helps to understand the elemental distributions on the worn surface.

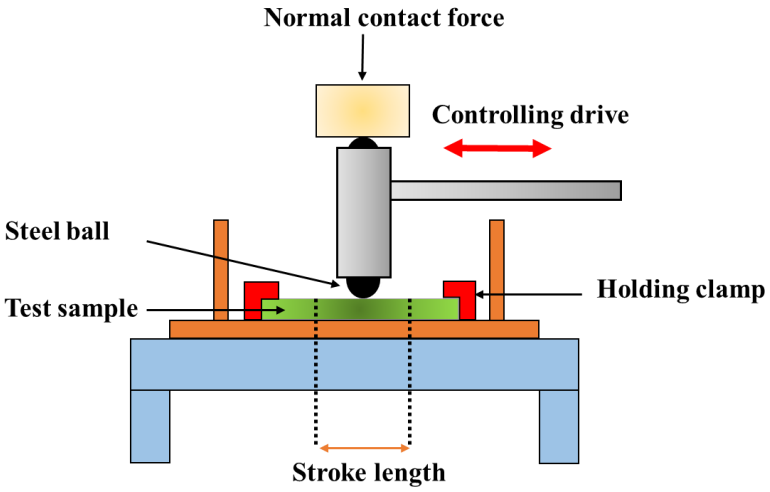

Figure 5.5: The schematic diagram for wear test setup

5.1.2.1 Effect of current density

The average coefficient of friction graph of Cu-Ni and Cu-Ni/Gr composite coatings electrodeposited at various current densities is given in Figure 5.6. The semiconductor strain gauges measured the frictional forces for 500 cycles. From the ratio of tangent force to the normal force, the coefficient of friction was calculated. The measured average coefficient of friction for Cu-Ni/Gr composite coatings is lower than Cu-Ni coating. The Cu-Ni/Gr composite coating electrodeposited at 6 A/dm^2 has a lower value of the average coefficient of friction compared to the remaining current densities. The reduction of coefficient of friction is attributed to the role of graphene nanoplatelets in the Cu-Ni/Gr composite coatings. The graphene nanoplatelets present in the coating acts as a lubricant and mating surface slides easily over each other [9]. In addition, according to Archard's equation, the wear rate of a material is inversely proportional to its hardness [10]. The Cu-Ni/Gr composite coating electrodeposited at 6 A/dm^2 has higher microhardness; thus, it restrains the plastic deformation of coating and helps to reduce the coefficient of friction. However, the increase in the coefficient of friction in the other electrodeposited coatings is due to the decrease of graphene nanoplatelet content in the coatings. It is clearly seen that when current density increases up to 6 A/dm^{2,} the graphene contents in the coating

increase gradually and hence the average coefficient of friction also decreases with an increase in graphene contents which can be seen from Figure 5.6.

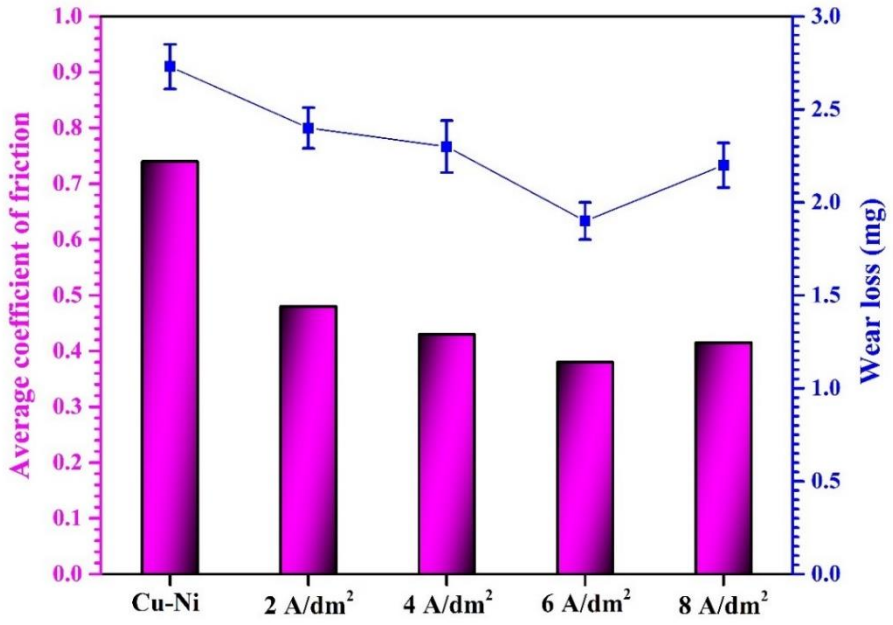

Figure 5.6: The average coefficient of friction and wear loss of Cu-Ni/Gr composite coatings electrodeposited at various current densities

5.1.2.2 Effect of Gr content

The average coefficient of friction and wear loss data of all the electrodeposited samples in terms of variation in the concentration of graphene nanoplatelets in the plating bath is presented in Figure 5.7. Based on the obtained results, it is clearly visible that average coefficient of friction of Cu-Ni/Gr composite coatings is lesser than pure Cu-Ni coating and it decreases with an increase in the concentration of graphene nanoplatelets in the plating bath upto 400 mg/L. The measured average coefficient of friction of Cu-Ni/Gr composite coating deposited at 100 mg/L, 200 mg/L, 400 mg/L and 500 mg/L concentration of Gr in the electrolyte bath are 0.49, 0.41, 0.27, and 0.45, respectively. During the sliding process, graphene nanoplatelets act as a solid lubricant in-between the mating surfaces, therefore the average friction coefficient of the prepared coatings is decreased. Graphene nanoplatelets are known as the strongest, gas-impermeable and thermally and chemically stable nanomaterial. Also, graphene nanoplatelets possess high shear strength hence acts as solid lubricant. Also, Cu-Ni/Gr (400 mg/L) composite coating has the lowest average coefficient of friction due to the higher microhardness [11].

In the present work, based on the results and above discussion, wear mechanism for Cu-Ni/Gr composite coating is proposed, as shown in Figure 5.8. Graphene nanoplatelets, nanostructured material, are homogeneously distributed into the Cu-Ni alloy matrix (Figure 5.8(a)). During the wear, a continuous metallic film can be retained on the coating surface because of the strengthening and pinning effects of graphene nanoplatelets (Figure 5.8(b)). As the sliding process continues, a thin layer of the lubricating film of metal comprising graphene nanoplatelets is formed on the wear track (Figure 5.8(c)). Also, there is a possibility of graphene nanoplatelets sheets peeled by the steel ball and formed nanorolls, which decrease the friction coefficient.

Figure 5.7 shows the measured wear loss of Cu-Ni/Gr composite coatings prepared at various concentration of graphene nanoplatelets in the electrolyte bath. Figure 5.7 reveals that Cu-Ni film has the highest wear loss as compared to other coatings. The measured wear loss of Cu-Ni/Gr composite coating deposited at 100 mg/L, 200 mg/L, 400 mg/L and 500 mg/L concentration of Gr in the electrolyte bath are 2.3 mg, 1.94 mg, 1.32 mg and 2.15 mg, respectively. The wear loss of Cu-Ni/Gr composite coatings decreases with the increase in graphene nanoplatelets content in the electrolyte bath upto 400 mg/L and then start increasing with further increase in Gr concentration of in the electrolyte bath to 500 mg/L. This is attributed to the decrease in the microhardness at of Cu-Ni/Gr composite coating at 500 mg/L due to the decrease in the content of Gr.

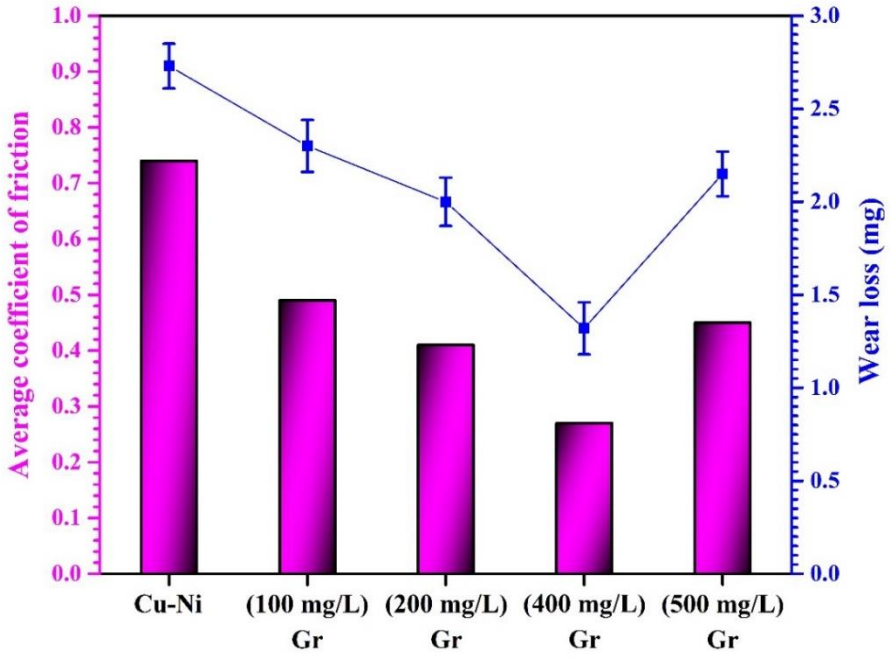

Figure 5.7: Average coefficient of friction and wear loss of Cu-Ni/Gr composite coatings prepared at various concentrations Gr in the plating bath

At higher concentration (500 mg/L) of graphene nanoplatelets in the electrolyte bath, the absorption of graphene nanoplatelets on the cathode surface decreases due to the agglomeration of graphene. Hence, wear loss of Cu-Ni/Gr composite coating is increased at 500 mg/L of graphene nanoplatelets concentration in the electrolyte bath.

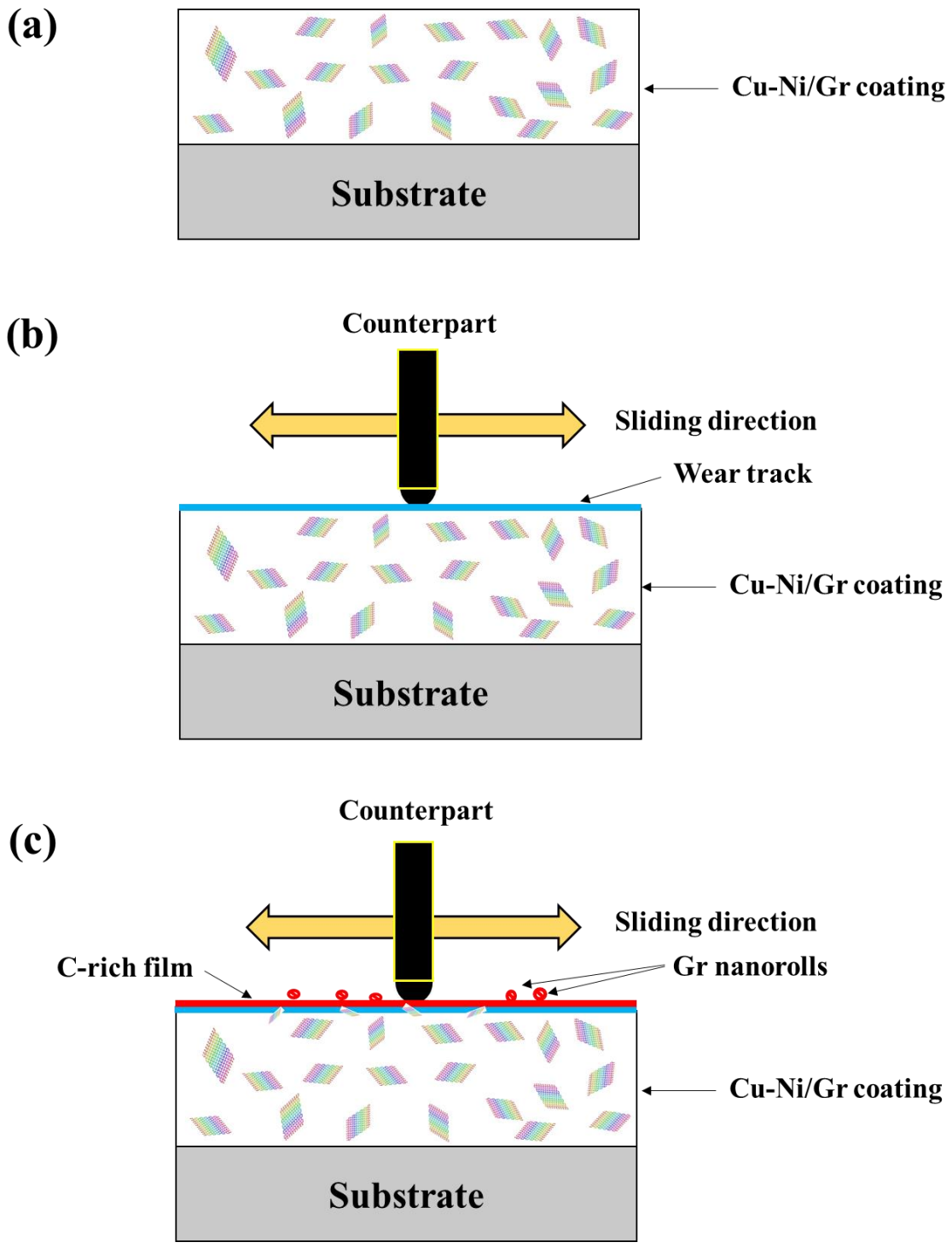

Figure 5.8: Illustrations of the wear mechanism for (a-c) Cu-Ni/Gr composite coatings

5.1.3 Corrosion performance of Cu-Ni/Gr composite coatings

Reports on corrosion failure of metallic hardware used in marine, automobile, and chemical industries have been increasing in the past two decades. Corrosion is defined as the natural process due to which pure metal is converted into its stable forms such as metal oxides, metal sulfides, or metal hydroxides. The degradation of materials due to corrosion is a serious problem faced by several industries. Corrosion of metals is generally considered as an undesirable phenomenon because it causes damage and disintegration of the metallic parts starts from the surface of metallic parts exposed to the environment and extends to the entire bulk of the metal part. Metals of higher reactivity series such as iron, zinc will react more and easily get corroded. In order to increase the corrosion resistance of such metals in the marine environment, the application of the protective coating is very important.

Over the past several years, composite coatings have been extensively used to increase the corrosion resistance of metals at a reduced cost. The application of alloy coatings such as Zn-Ni, Cu-Ni and Ni-Mo is considered as one of the important routes to increase corrosion resistance. However, Cu-Ni alloy coating is most suitable to provide high corrosion resistance in the marine environment. In the marine environment, the 70-30 Cu-Ni alloy has been employed in high flow conditions because of the increased hardness and high corrosion resistance provided by the higher amount of Ni. In Cu-Ni alloy coating, when the amount of nickel is less than 40 wt.%, a dense inner layer of Cu_2O and an outer layer of $Cu_2(OH)_3Cl$ develop a passivating layer in seawater (high chloride environment). Initially, Cu_2O later is formed and then the $Cu_2(OH)_3Cl$ layer is developed. During the formation of the Cu_2O layer, several Ni ions can be embedded into the Cu_2O layer then $Cu_2(OH)_3Cl$ layer is produced by precipitation from the dissolution of Cu^{2+} ions [12].

Graphene nanoplatelets are being widely used in composite coatings to increase the corrosion resistance due to its extraordinary properties, such as chemically inert to the acidic solution, impermeable to most of the gases and liquids, so it shows huge potential for the application of high corrosion resistance coating. In this work, graphene nanoplatelets are incorporated into the Cu-Ni alloy matrix to synthesize Cu-Ni/Gr composite coating by electro-co-deposition method. The corrosion performance of Cu-Ni/Gr composite coatings are studied by varying deposition current density and by varying graphene nanoplatelets concentration in the electrolyte bath. The anti-corrosion performance of deposited Cu-Ni/Gr composite coatings is evaluated using CH604E

potentiostat/galvanostat instrument based on the usual three electrodes cell configuration. This instrument is widely employed to study corrosion at the surface. Corrosion of metals generally occurs at a rate calculated by an equilibrium between opposing electrochemical reactions. There are two electrochemical reactions one is a cathodic electrochemical reaction, and another is anodic electrochemical reaction. In cathodic electrochemical reaction, solution species (such as O_2 or H_2) is reduced by removing electrons from metal. Also, in anodic electrochemical reaction, metal is oxidized due to the releasing electrons into the metal. When cathodic and anodic reactions are in equilibrium, the electron flow from each reaction is balance and hence there is no flow of electrons.

The determination of electrochemical parameters by the Tafel extrapolation method for Cu-Ni alloy coating is shown in Figure 5.9. The potentiostat records the current value across the applied potential range. The horizontal axis is an electrical potential and the vertical axis is the logarithmic current density. The open-circuit potential (OCP) is the potential at which the total cathodic current is equal to the total anodic current. The corrosion current (I_{corr}) is the value of cathodic or anodic current at OCP. The rate of corrosion is directly related to polarization resistance (R_p). The R_p is the resistance offered by the test sample to oxidation during the application of an external potential. The R_p (polarization resistance) is calculated for all deposited coatings by using extracted electrochemical parameters such as E_{corr} (corrosion potential), I_{corr} (corrosion current density), β_a (anodic tafel slope) and β_c (cathodic tafel slope).

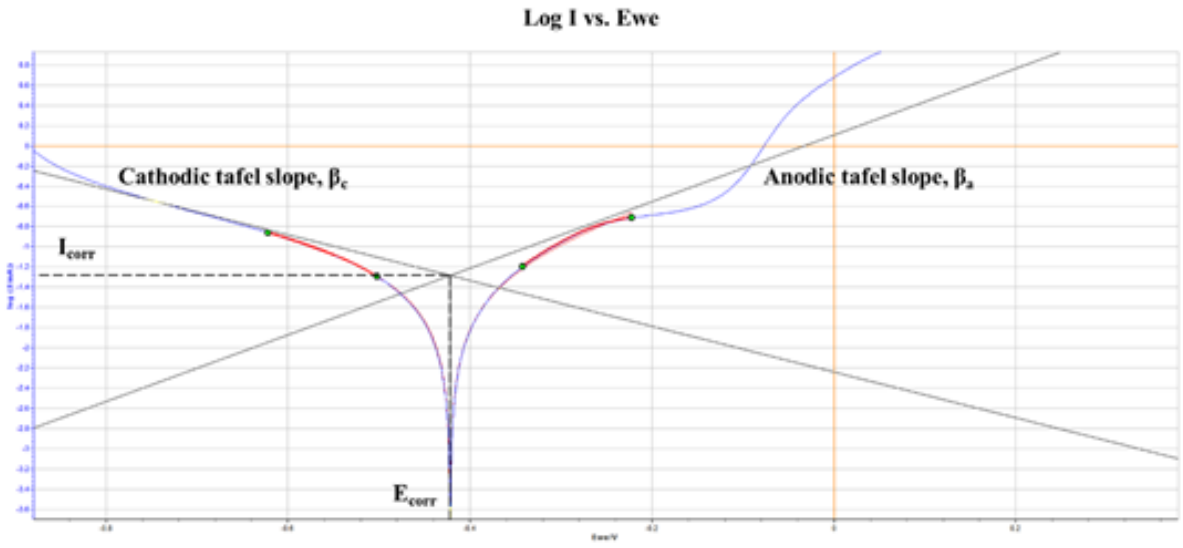

Figure 5.9: The determination of electrochemical parameters by Tafel extrapolation method for Cu-Ni alloy coating

The R_p (kΩ.cm^2) value for prepared coatings is calculated using the Stern-Geary equation 5.5:

$$R_p = \frac{\beta_a \beta_c}{2.303(\beta_a + \beta_c)} \left(\frac{1}{I_{corr}} \right) \quad (5.5)$$

where I_{corr} is the corrosion current density (μA/cm^2), β_a is anodic tafel slope (mV/decade) and β_c is cathodic tafel slope (mV/decade).

5.1.3.1 Effect of current density

The potentiodynamic linear polarization graphs of Cu-Ni and Cu-Ni/Gr composite coatings electrodeposited at various current densities are given in Figure 5.10 and the corresponding calculation are shown in Table 5.1. In a potential range of + 0.4 V to - 0.9 V at the scan rate of 0.01 V/s, the electrode kinetics of the electrodeposited coatings was examined. The corrosion resistance of the Cu-Ni/Gr composite coatings is affected by the current density of electro-co-deposition, which is displayed in Table 5.1 and Figure 5.10.

Table 5.1: Calculated corrosion results of Cu-Ni and Cu-Ni/Gr composite coatings electrodeposited at various current densities.

Sample	E_{corr} (V)	I_{corr} (A)	R_p (kΩ.cm^2)
Cu-Ni	-0.432	96×10^{-6}	83.26
Cu-Ni/Gr (2 A/dm^2)	-0.426	52×10^{-6}	189.86
Cu-Ni/Gr (4 A/dm^2)	-0.424	63×10^{-6}	194.16
Cu-Ni/Gr (6 A/dm^2)	-0.411	31×10^{-6}	198.22
Cu-Ni/Gr (8 A/dm^2)	-0.428	87×10^{-6}	195.88

All Cu-Ni/Gr composite coatings exhibited lower corrosion current and higher corrosion potential as compared to the pure Cu-Ni alloy coating. This is mainly due to the reinforcement of graphene nanoplatelets into the Cu-Ni alloy matrix. Graphene nanoplatelets possess extraordinary chemical inertness. Graphene nanoplatelets on the surface of coatings act as an isolation barrier in between metal and the medium to delay the rate of corrosion and hence enhance the corrosion resistance of the coating. Also, the incorporated Gr at the surface decrease the exposed metallic area that could undergo corrosion attack. The Cu-Ni/Gr composite coatings electrodeposited at 6 A/dm^2 shows lower corrosion current and higher corrosion potential. The low rate of corrosion is the

cause of lower corrosion current, and high rate of corrosion is the cause of lower corrosion potential. At 6 A/dm^2 current density, the Cu-Ni/Gr composite coating gives a lower anodic current, which shows the higher corrosion resistance of the prepared coating. There are many reasons for enhancement in the corrosion resistance of the nanoparticles reinforced composite coatings [13]–[15]. Incorporated graphene nanoplatelets avoid the initiation and growth of corrosion by filling the gaps and micro holes in the composite coatings [16]. Cu-Ni/Gr composite coating deposited at 6 A/dm^2 has high graphene contents; therefore, it shows higher corrosion resistance. Moreover, the composite coating deposited at 8 A/dm^2 has high surface roughness, and less graphene content results in high surface area exposed to the corrosive environment and decrease in corrosion resistance [14].

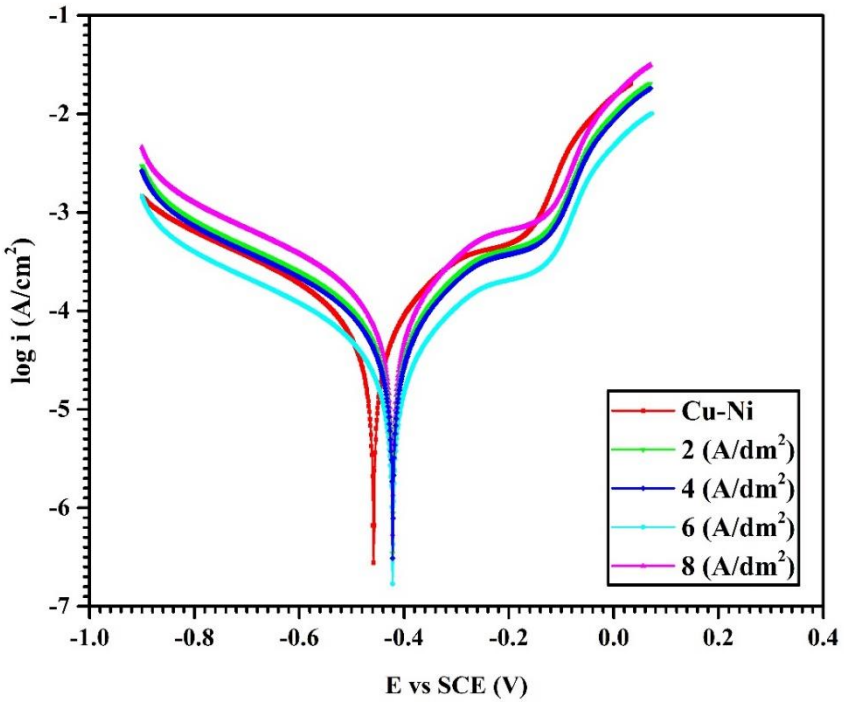

Figure 5.10: Potentiodynamic linear polarization graph of Cu-Ni and Cu-Ni/Gr composite coatings electrodeposited at various current densities

5.1.3.2 Effect of Gr content

A. Immersion Study

Figure 5.11 shows the immersion test curves of Cu-Ni/Gr composite coatings electrodeposited at various concentrations of graphene nanoplatelets in the plating bath. From Figure 5.11, in 3.5 wt. % NaCl solution, the open circuit potential (OCP) for pure Cu-Ni, Cu-Ni/Gr (100 mg/L), Cu-Ni/Gr (200 mg/L), and Cu-Ni/Gr (500 mg/L) composite

coatings were shifted negatively after four, six, nine and seven days respectively. The Cu-Ni/Gr (400 mg/L) composite coating was remained stable over an extended period of 16 days and shifted negatively after 35 days. The pure Cu-Ni coating has a higher rate of corrosion compared to other films and then the rate decreases as protective cuprous oxide layer forms over time. The Cu-Ni/Gr (500 mg/L) composite coating is less stable than Cu-Ni/Gr (400 mg/L) composite coating mainly due to the decrease in the graphene nanoplatelets content in the coating. The results of the immersion test revealed that the higher the content of graphene nanoplatelets in the Cu-Ni coating provides the additional barrier type protection against corrosion.

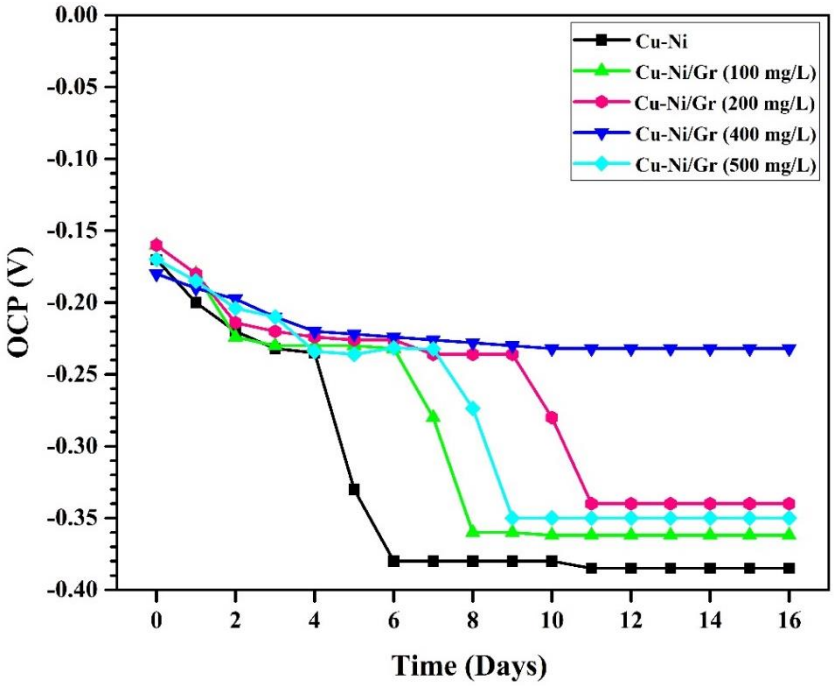

Figure 5.11: Immersion test curves of Cu-Ni/Gr composite coatings in 3.5 wt.% NaCl solution

B. Potentiodynamic Polarization

Figure 5.12 illustrates the polarization curves of Cu-Ni/Gr composite coatings prepared at various concentrations of graphene nanoplatelets in the plating bath. The polarization resistance (R_p), corrosion potentials (E_{corr}) and corrosion current densities (I_{corr}) values calculated from the polarization curves are represented in Table 5.2. The E_{corr} values for prepared coatings increased, -0.382 V to -0.224 V, as the concentration of graphene nanoplatelets increased from 100 mg/L to 400 mg/L in the plating bath and the decreased to -0.358 V with further increase in the graphene nanoplatelets concentration to 50 mg/L, as seen in Table 5.2. At the same time, I_{corr} values of Cu-Ni/Gr composite coatings were

significantly decreased compared to pure Cu-Ni coating. The R_p value of the prepared coatings is determined using the Stern-Geary equation. In Table 5.2, the R_p value of the pure Cu-Ni coating was 85.71 kΩ·cm^2, however, the Cu-Ni/Gr (400 mg/L) increased to 229.36 kΩ·cm^2. The graphene nanoplatelets were well distributed in Cu-Ni matrix and serve as barriers to the initiation of corrosion defects by a reduction in micro-void in the coatings. It has been reported that $CuCl_2^-$ species (shown in equation 5.6 and 5.7) creates by the dissolution of copper and then it forms Cu_2O (shown in equation 5.8) as the pH at the interface increases during the corrosion of Cu alloys [17]–[19]. The formation of the Cu_2O layer on the surface of coatings after 30 days soaking in the 3.5 wt.% of NaCl solution is confirmed by XRD analysis. Figure 5.13 is the XRD result for the Cu-Ni/Gr (100 mg/L) composite coating, after 30 days soaking in the 3.5 wt.% of NaCl solution. Casey et al. also presented similar XRD result for Cu_2O in the corrosion products of Cu-Ni-0.15% Mt sample left in simulated seawater [12].

$$Cu^+ + Cl^- \rightarrow CuCl \quad (5.6)$$

$$CuCl + Cl^- \rightarrow CuCl_2^- \quad (5.7)$$

$$2CuCl_2^- + 2H_2O \rightarrow Cu_2O + 2H^+ + 4Cl^- \quad (5.8)$$

After the formation of Cu_2O layer, a $Cu_2(OH)_3Cl$ layer is formed by the precipitation from the dissolution of Cu^{2+} ions [19], [20]. The study also showed that the protective cuprous oxide layer has a low electronic conductivity, thereby increasing the corrosion resistance.

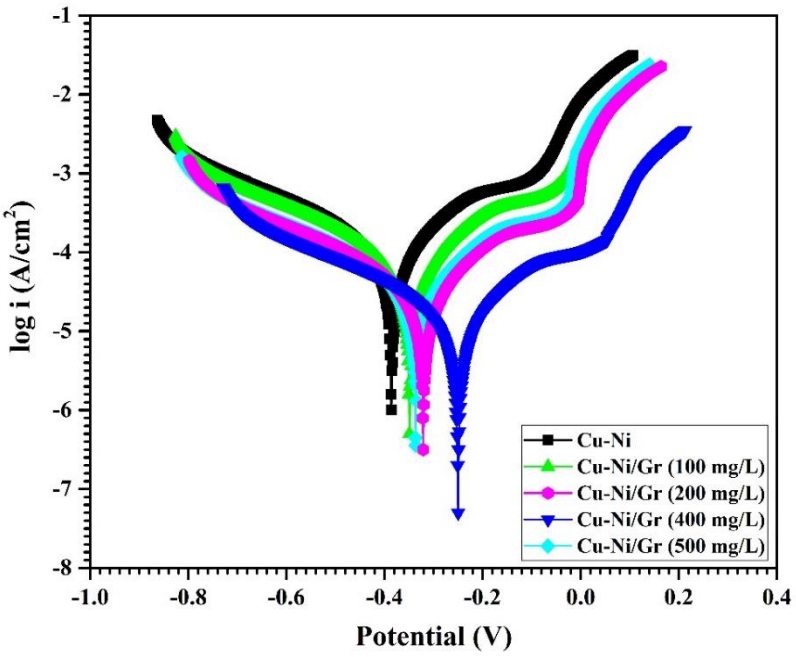

Figure 5.12: Polarization curves of Cu-Ni/Gr composite coatings prepared at various concentrations graphene nanoplatelets in the plating bath

Table 5.2: E_{corr}, I_{corr} and R_p of Cu-Ni/Gr composite coatings.

Sample	E_{corr} (V)	I_{corr} (A)	R_p (kΩ.cm^2)
Cu-Ni	-0.382	2.74×10^{-6}	85.71
Cu-Ni/Gr (100 mg/L)	-0.368	1.52×10^{-6}	128.34
Cu-Ni/Gr (200 mg/L)	-0.346	6.36×10^{-7}	173.22
Cu-Ni/Gr (400 mg/L)	-0.224	8.43×10^{-7}	229.36
Cu-Ni/Gr (500 mg/L)	-0.358	5.45×10^{-7}	147.36

These observations reveal that the corrosion performance of pure Cu-Ni coating is enhanced by the incorporation of graphene nanoplatelets in the Cu-Ni matrix. Incorporated graphene nanoplatelets change the microstructure of pure Cu-Ni coating, resulting in an increase in the corrosion resistance of the Cu-Ni/Gr composite coatings. Also, reinforcement of graphene nanoplatelets into the Cu-Ni alloy matrix significantly improves the surface morphology by increasing compactness of coating and decreasing the structural defect of deposits. The Cu-Ni/Gr (400 mg/L) composite coating has higher corrosion resistance due to the presence of high graphene content.

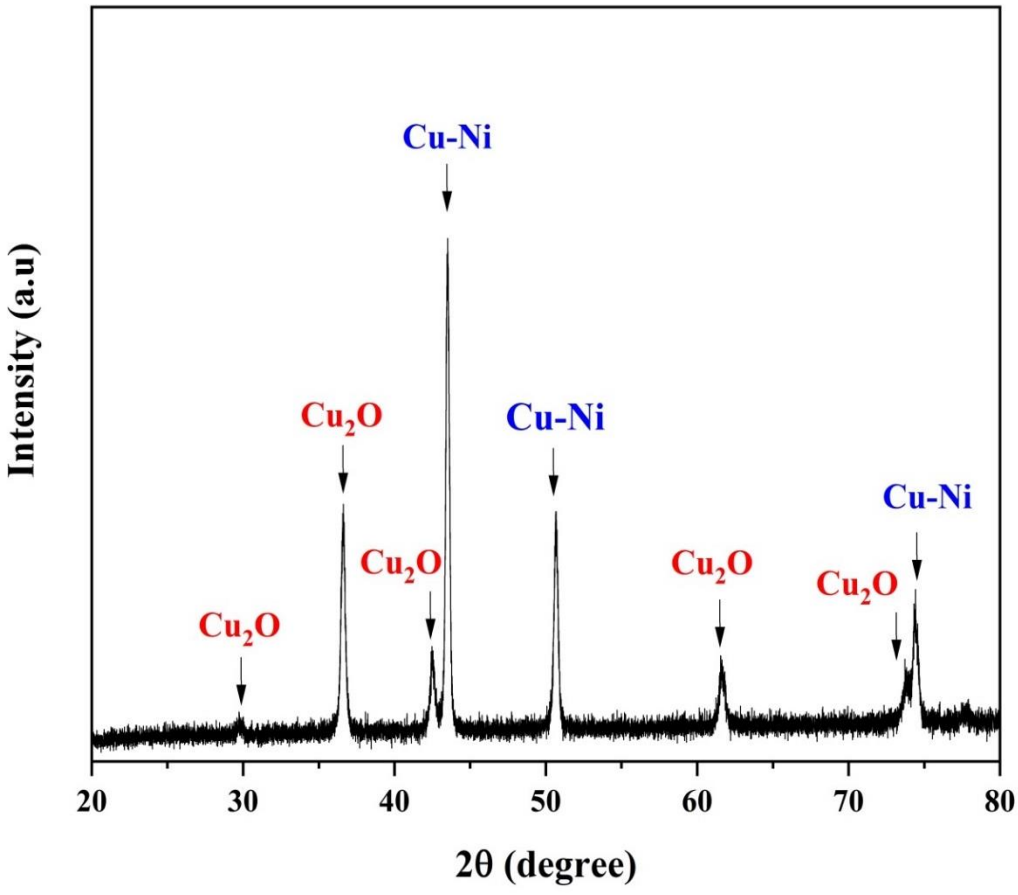

Figure 5.13: XRD result for the Cu-Ni/Gr (100 mg/L) composite coating after 30 days soaking in the 3.5 wt. % of NaCl solution

5.2 Characterization results of Cu-Ni/Gr composite synthesized from powder

Mechanical, tribological and corrosion properties of Cu-Ni/Gr composites synthesized by modified electro-co-deposition method followed by powder metallurgy method are discussed. Mechanical characterization includes microhardness, yield strength, ultimate tensile strength, hardness and percentage elongation of Cu-Ni/Gr composites. Tribological characterization includes a coefficient of friction, wear rate and surface morphology and elemental composition of worn surface. In corrosion characterization, Tafel plots are obtained to measure corrosion parameters such as corrosion current corrosion voltage and polarization resistance of composites.

5.2.1 Microhardness of Cu-Ni/Gr composites

The Vickers microhardness for pure Cu-Ni alloy and Cu-Ni/Gr composites is represented in Figure 5.14. The microhardness of Cu-Ni/Gr composites is significantly higher than that of the pure Cu-Ni alloy. The measured average microhardness for Cu-Ni/Gr composite prepared at 50 mg/L, 100 mg/L, 200 mg/L and 250 mg/L are 68 HV, 91 HV, 107 HV and 101 HV, respectively. The hardness of Cu-Ni/Gr composites is increased with an increase in the graphene nanoplatelets content in the electrolyte bath upto 200 mg/L and then decreased further increase in graphene nanoplatelets content in the electrolyte bath to 250 mg/L.

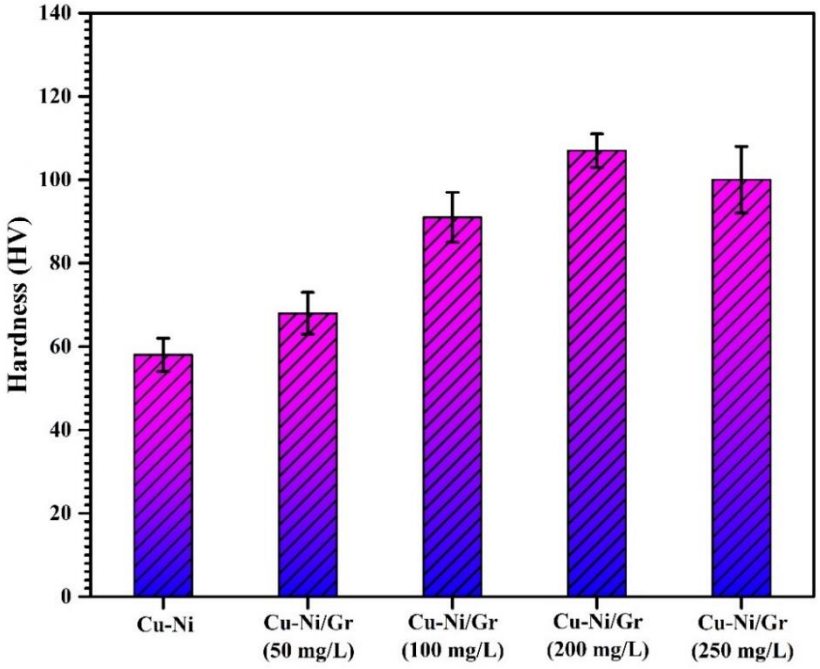

Figure 5.14: Vickers hardness of pure Cu-Ni alloy and Cu-Ni/Gr composites

Graphene nanoplatelets have shown the ability to improve the hardness significantly in a pure Ni [16] and Cu matrix [21]. The result indicates that after adding graphene nanoplatelets, the hardness increases from 58 HV to 107 HV. Among the composites, Cu-Ni/Gr (200 mg/L) composite shows the highest hardness of 107 HV, which is about 84.5% higher than that of pure Cu-Ni alloy. This suggests that when graphene nanoplatelets concentration in the electrolyte bath is minimum, the content of graphene nanoplatelets in the Cu-Ni/Gr composite is less, which results in uniform dispersion of graphene nanoplatelets into the Cu-Ni alloy matrix with less agglomeration. The improvement in hardness of Cu-Ni/Gr composites is mainly due to the resistance offered by Gr for the dislocations movement and their even distribution in the Cu-Ni alloy matrix. In Cu-Ni/Gr composites, the graphene nanoplatelets have very high shear strength that effectively impedes dislocation motion across a grain boundary. As shown in Table 4.6, graphene nanoplatelets decreased the crystallite size of the Cu-Ni/Gr composite powder samples, and according to the Hall-Petch equation [22], the microhardness of fabricated Cu-Ni/Gr composites increases with decrease in the crystallite size.

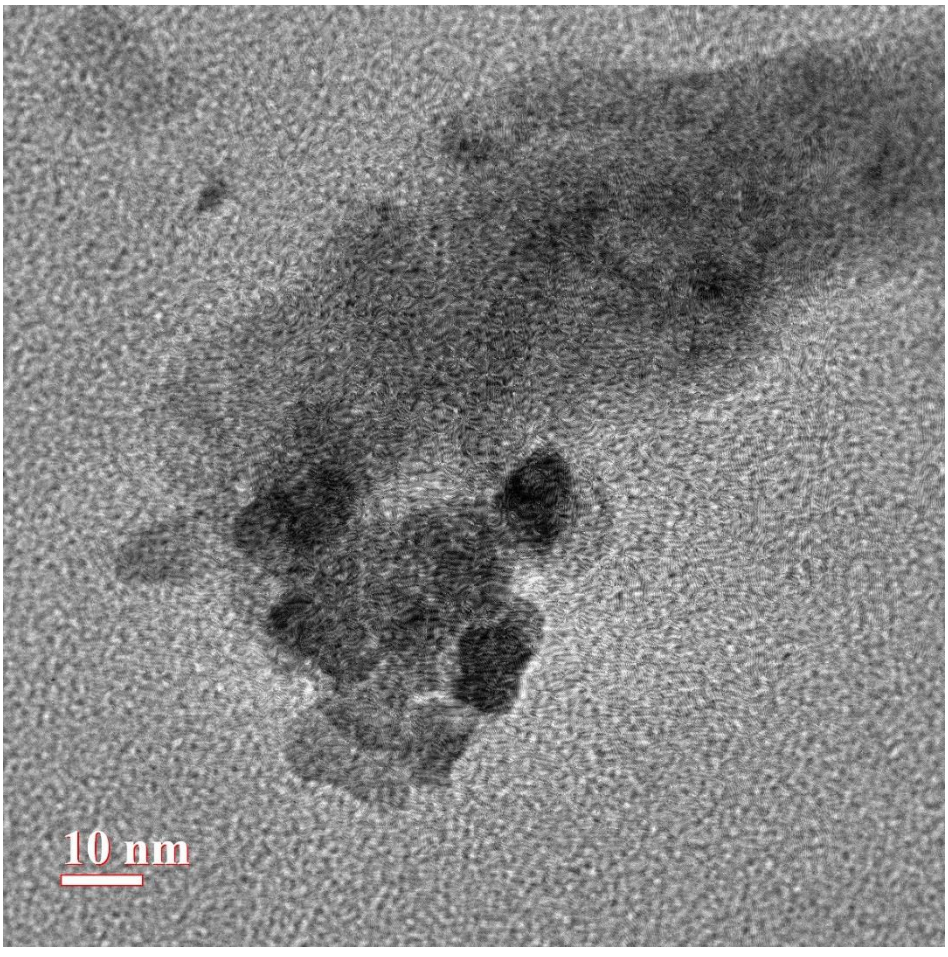

Figure 5.15: HRTEM images of Cu-Ni/Gr composite powder.

The interaction between Cu-Ni alloy and graphene nanoplatelets is shown in Figure 5.15. From Figure 5.15, it is clearly seen that Cu-Ni alloy particles are nucleated on the surface of graphene nanoplatelets. Due to the nucleation and growth of Cu-Ni alloy particles on graphene nanoplatelets surface, graphene occupies the grain boundary position and graphene nanoplatelets will not cause any substitutional or interstitial defect. In case of plastic deformation, grain boundaries act as a barrier to dislocation movement because grains are arranged in a different orientation. In Cu-Ni/Gr composite, in addition to randomly arranged grains, graphene nanoplatelets are also presents at grain boundaries. The graphene nanoplatelets have a different crystal structure and chemical properties than the Cu-Ni alloy crystal structure. Hence, misorientation grains and two different phases altogether impede the movement of dislocations, which results in the hardening of Cu-Ni/Gr composites. As the concentration of the graphene nanoplatelets in the electrolyte bath increased from 200 mg/L to 250 mg/L, more graphene nanoplatelets were dispersed in the Cu-Ni alloy matrix. However, as the amount of graphene nanoplatelets increases in the Cu-Ni/Gr composite, agglomeration of the graphene nanoplatelets initiates. The agglomeration was mainly due to the presence of high Van der Waals force among the graphene nanoplatelets. Under applied loading conditions this agglomeration bond would have failed and therefore, there is decrease in the microhardness.

5.2.2 Tensile testing of Cu-Ni/Gr composites

Tensile tests are conducted for Cu-Ni/Gr composites having various concentrations of graphene nanoplatelets in the electrolyte bath to study the strengthening behavior of Gr. Figure 5.16 presents the tensile curves of pure Cu-Ni alloy and Cu-Ni/Gr composites. The YS, UTS and fracture elongation of pure Cu-Ni alloy and Cu-Ni/Gr composites are listed in Table 5.3. The YS and UTS of the Cu-Ni/Gr composites are increased with increasing Gr concentration in the electrolyte bath upto 200 mg/L. The pure Cu-Ni alloy shows a YS of 111 MPa and UTS of 157 MPa. Also, Cu-Ni/Gr (200 mg/L) composite has YS of 265 MPa and the UTS of 299 MPa, which are 138.7% and 90.5% greater than that of pure Cu-Ni alloy. Also, fracture elongation is decreased from 44% to 5%, with an increase in the Gr concentration in the electrolyte bath. The enhancement of YS and UTS in the composites is associated with (i) aspect ratio of reinforcement (ii) interfacial bonding between reinforcement and matrix and (iii) reinforcement distribution in the matrix [23]. In this work, enhancement in the YS and UTS has been attributed to the homogeneous dispersion of Gr and the strong interfacial bonding between Gr and Cu-Ni alloy matrix,

which results in efficient interfacial load-transfer ability. Also, due to the extraordinary strength and stiffness of Gr prevent the shearing and rupture of the composite by impeding the dislocation propagation during plastic deformation [24].

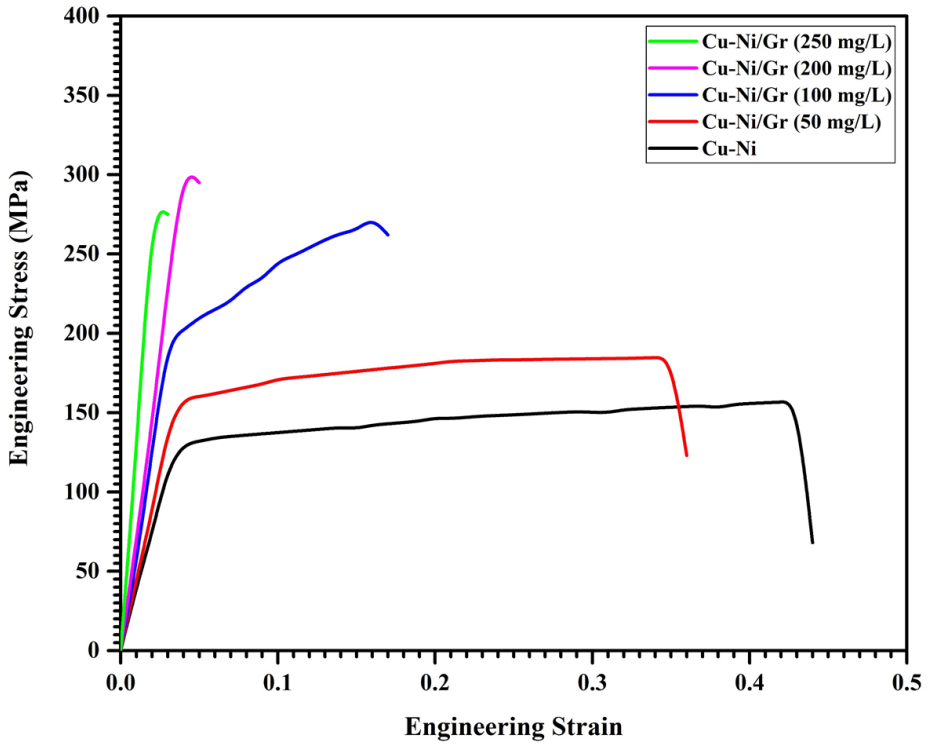

Figure 5.16: Stress and strain curve of pure Cu-Ni alloy and Cu-Ni/Gr composites

Table 5.3: The YS, UTS and fracture elongation of pure Cu-Ni alloy and Cu-Ni/Gr composites

Samples	YS (MPa)	UTS (MPa)	Fracture elongation (%)
Cu-Ni	111 ± 4	157 ± 4	44 ± 3
Cu-Ni/Gr (50 mg/L)	137 ± 4	185 ± 5	36 ± 3
Cu-Ni/Gr (100 mg/L)	175 ± 5	271 ± 4	17 ± 2
Cu-Ni/Gr (200 mg/L)	265 ± 4	299 ± 5	5 ± 2
Cu-Ni/Gr (250 mg/L)	234 ± 5	278 ± 5	3 ± 2

The graphene nanoplatelets are mainly distributed along the boundary of Cu-Ni alloy grains. When the content of graphene nanoplatelets increases, the associativity among Cu-Ni alloy grains decreases while the associativity among the Gr increases. Cracks nucleation occurs at the interface and propagates through the Cu-Ni alloy matrix. In addition, incorporated Gr are composed of few-layer graphene, thus cracks also easily

develop in the layers of graphene. Therefore, the fracture elongation of the Cu-Ni/Gr composite gradually decreases with an increase in the graphene nanoplatelet content.

Images of tensile fracture surfaces were taken using Scanning electron microscopy for analysis of fracture surface. Figure 5.17(a-d) shows SEM images of the tension-induced fracture morphology of pure Cu-Ni alloy and Cu-Ni/Gr composites with different Gr concentrations in the electrolyte bath. Pure Cu-Ni alloy (Figure 5.17(a-b)) fracture has many tear ridges and dimples, which are due to the ductile nature of the material. However, with an increase in the graphene nanoplatelets concentration in the electrolyte bath, the amount of dimples decreases and the fracture surface becomes slightly flat. Also, a large number of pores and cracks are observed on the fracture surface of the Cu-Ni/Gr (200 mg/L) composite (Figure 5.17(c-d)). These cavities and pores are responsible for the crack and fracture initiation and thus leading to low ductility of Cu-Ni/Gr (200 mg/L) composite.

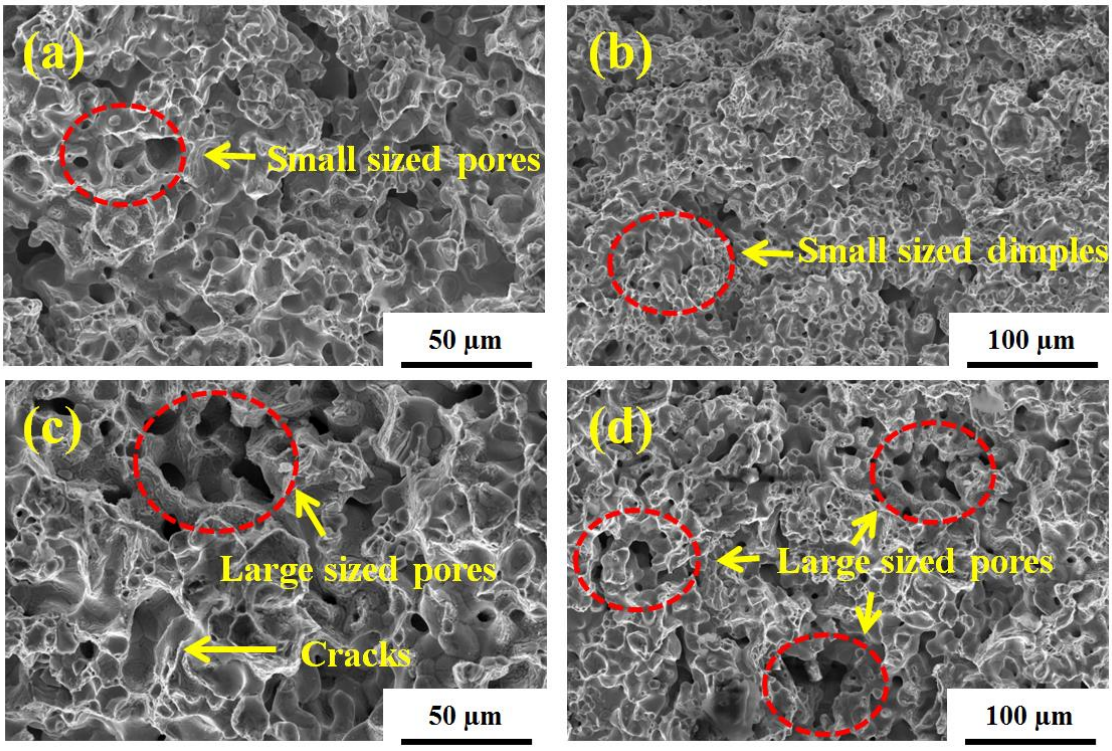

Figure 5.17: SEM images of the tension-induced fracture morphology of (a, b) pure Cu-Ni alloy, (c, d) Cu-Ni/Gr (200 mg/L) composite

5.2.3 Tribological performance of Cu-Ni/Gr composites

Figure 5.18 illustrates the measured friction coefficient curves of pure Cu-Ni alloy and Cu-Ni/Gr composites. It can be seen from Figure 5.18 that at the beginning time, all

friction coefficient curves increase rapidly and then attained a fairly stable behavior. After 200 seconds, all friction coefficient curves become stable and smooth. Also, the friction coefficient decreases from 0.56 to 0.25 when the graphene nanoplatelets concentration in the electrolyte bath increases from 0 to 200 mg/L. According to Figure 5.18, the friction coefficient of pure Cu-Ni alloy is 0.54. However, the friction coefficient of Cu-Ni/Gr (200 mg/L) is 0.29, which is significantly lower than that of pure Cu-Ni alloy. The enhancement in the friction coefficient Cu-Ni/Gr composites is ascribed to the introduction of Gr in the Cu-Ni alloy matrix. The graphene nanoplatelets play a crucial role in the friction-reduction properties as an ideal solid lubricant due to its surface properties and graphitic structure [25].

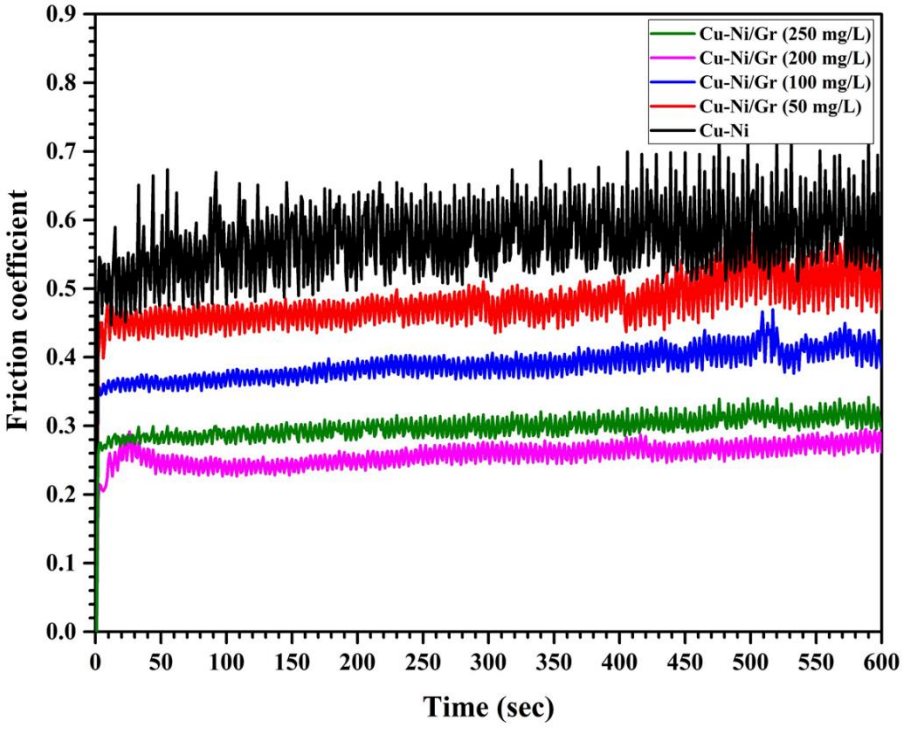

Figure 5.18: Friction coefficient curves of pure Cu-Ni alloy and Cu-Ni/Gr composites

The wear rates of pure Cu-Ni alloy and Cu-Ni/Gr composites are represented in Figure 5.19. As shown in Figure 5.19, the wear rate of Cu-Ni/Gr composites is lower than that of the pure Cu-Ni alloy and it decreases with further increase in Gr concentration in the electrolyte bath. According to Archard's equation, the wear rate of the composites depends upon its hardness and it decreases with an increase in the hardness of the composites [26]. Cu-Ni/Gr (200 mg/L) composite shows a minimum wear rate of 0.2798×10^{-4} mm^3 $N^{-1}m^{-1}$ due to its higher microhardness (Figure 5.14).

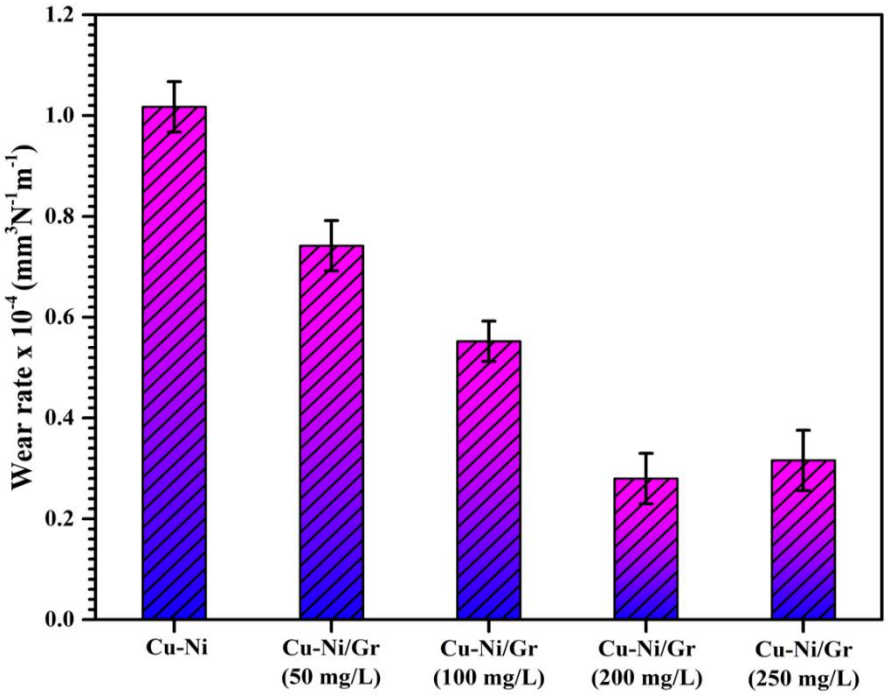

Figure 5.19: Wear rate of Cu-Ni alloy and Cu-Ni/Gr composites

Figure 5.20(a-d) shows the FESEM morphologies analysis belonging to the wear tracks of the sintered samples, Figure 5.20(e) illustrates the EDS spectrum taken from the red marked region in Figure 5.20(d) and Figure 5.20(f) depicts a schematic representation of the wear mechanism for Cu-Ni/Gr composites. From Figure 5.20(a) pure Cu-Ni alloy shows a rougher surface as compared to Cu-Ni/Gr composites. Also, the worn surface of pure Cu-Ni alloy has several delamination caused due to plastic deformation. Large fluctuations in the friction coefficient of pure Cu-Ni are observed due to the rough surface (Figure 5.19). Cu-Ni/Gr composites have negligible delamination, and it decreases with an increase in the concentration of graphene nanoplatelets in the electrolyte bath, as shown in Figure 5.20(b-d). Based on the EDS spectrum taken from the red marked region in wear track of Cu-Ni/Gr (200 mg/L) composite (Figure 5.20(e)) confirms that graphene nanoplatelets are present within the wear track. Graphene nanoplatelets can provide a lubricating effect due to significantly low shear strength. During the sliding process, Gr are squeezed out from the composites and formed the Gr rich films on the worn surface and change the sliding friction mode to rolling friction mode (Figure 5.20(f)). Also, with an increase in graphene nanoplatelets content in the composite, these films become more continuous [27]. This trend indicates that a higher concentration of Gr (upto 200 mg/L) is promising in the reduction of friction coefficient and the wear rate of Cu-Ni/Gr composites.

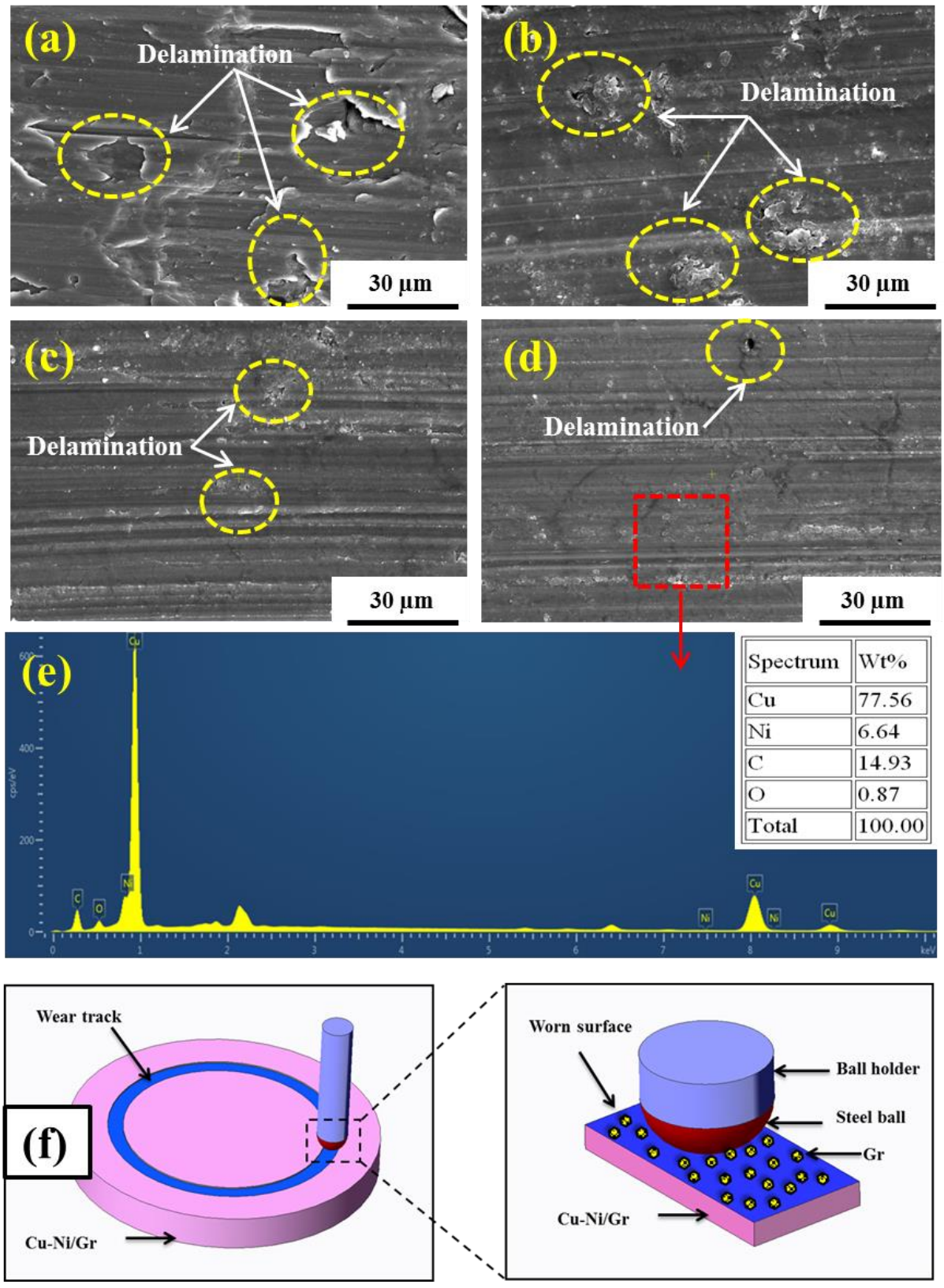

Figure 5.20: FESEM morphologies analysis belonging to the wear tracks of the sintered samples: (a) Cu-Ni alloy, (b) Cu-Ni/Gr (50 mg/L), (c) Cu-Ni/Gr (100 mg/L), (d) Cu-Ni/Gr (200 mg/L), (e) EDS spectrum taken from the red marked region, (f) A schematic representation of the wear mechanism for Cu-Ni/Gr composite

5.2.4 Corrosion performance of Cu-Ni/Gr composites

The polarization test is one of the techniques to measure the anticorrosion performance of composites, which provides the corrosion potential (E_{corr}), corrosion current density (I_{corr}), anode polarization resistance (R_p). The potentiodynamic polarization curves of Cu-Ni alloy and Cu-Ni/Gr composites with different content of Gr in the electrolyte bath is represented in Figure 5.21. The values of E_{corr}, I_{corr} and R_p of Cu-Ni alloy and Cu-Ni/Gr composites are listed in Table 5.4. As shown in Table 5.4, the Cu-Ni/Gr composites showed positive I_{corr} and E_{corr} than that of Cu-Ni alloy. The values of E_{corr} for Cu-Ni/Gr composites prepared at 50 mg/L, 100 mg/L, 200 mg/L and 250 mg/L are -0.143 V, -0.117 V, -0.056 V and -0.087 V respectively, while the I_{corr} values are 5.824×10^{-6} A, 3.731×10^{-6} A, 2.486×10^{-6} A and 3.137×10^{-6} A, respectively. Also, it is observed that the corrosion resistance of the Cu-Ni/Gr composite increased with the increase in the concentration of Gr in the electrolyte bath upto 200 mg/L and then decreased with further increase in the concentration of Gr in the electrolyte bath to 250 mg/L. The measured R_p values for Cu-Ni/Gr composite prepared at 50 mg/L, 100 mg/L, 200 mg/L and 250 mg/L are 4.177 kΩ.cm^2, 7.632 kΩ.cm^2,12.862 kΩ.cm^2 and 11.465 kΩ.cm^2, respectively.

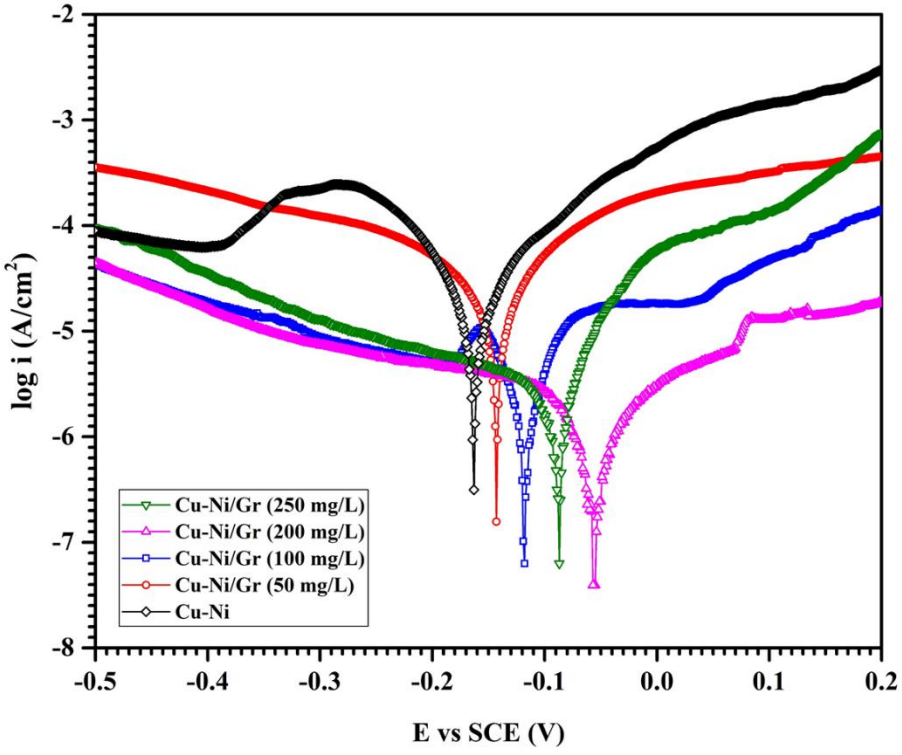

Figure 5.21: Potentiodynamic polarization curves of Cu-Ni alloy and Cu-Ni/Gr composites with different content of Gr in the electrolyte bath

Table 5.4: E_{corr}, I_{corr} and R_p of Cu-Ni alloy and Cu-Ni/Gr composite coatings

Sample	E_{corr} (V)	I_{corr} (A)	R_p (kΩ.cm^2)
Cu-Ni	-0.162	8.263×10^{-6}	1.298
Cu-Ni/Gr (50 mg/L)	-0.143	5.824×10^{-6}	4.177
Cu-Ni/Gr (100 mg/L)	-0.117	3.731×10^{-6}	7.632
Cu-Ni/Gr (200 mg/L)	-0.056	2.486×10^{-6}	12.862
Cu-Ni/Gr (250 mg/L)	-0.087	3.137×10^{-6}	11.465

The obtained results reveal that the incorporation of graphene nanoplatelets in the Cu-Ni alloy matrix enhanced the corrosion resistance of prepared Cu-Ni/Gr composites. The best corrosion resistance of Cu-Ni/Gr composite obtained at 200 mg/L concentration of Gr in the electrolyte bath. The anodic portion of the polarization curve is related to the formation of $CuCl^-$ on the surface of composite (equation 5.9) and by the dissolution of Cu^+, CuCl is produced (equation 5.10). Also, at higher concentration of chloride, $CuCl_2^-$ species are developed.

$$Cu^+ + Cl^- \rightarrow CuCl + e^- \quad (5.9)$$

$$Cu^+ + Cl^- \rightarrow CuCl \quad (5.10)$$

$$CuCl + Cl^- \rightarrow CuCl_2^- \quad (5.11)$$

$$O_2 + 2H_2O + e^- \rightarrow 4OH^- \quad (5.12)$$

$$2CuCl_2^- + 2H_2O \rightarrow Cu_2O + 2H^+ + 4Cl^- \quad (5.13)$$

The corrosion of Cu-Ni/Gr composite in chloride environments takes place through the anodic reactions as given in equation (5.9-5.11) and the cathodic reaction (equation 5.12). The transport rate of $CuCl_2^-$ is slowed by an increase in pH close to the surface, which results in the formation of Cu_2O layer on the surface of the composite (equation 5.12). After the formation of Cu_2O layer, the $Cu_2(OH)_3Cl$ layer forms by precipitation from the dissolution of Cu^{2+}. During the formation of the Cu_2O layer several Ni ions can be embedded into the Cu_2O layer then $Cu_2(OH)_3Cl$ layer is produced by precipitation from the dissolution of Cu^{2+} ions [12]. The reinforcement of graphene nanoplatelets in the Cu-Ni alloy matrix fill the defects such as several voids, gaps and cracks owing to its nano size, which contribute to the outstanding resistance to the Cu-Ni/Gr composite to undergo corrosion. At 250 mg/L concentration of Gr in the electrolyte bath, the polarization resistance starts decreasing. This may be due to the agglomeration of Gr nanoplatelets in the Cu-Ni alloy matrix.

5.3 Conclusion

1. The effect of different current densities (such as 2, 4, 6 and 8 A/dm^2) on mechanical, tribological and corrosion properties of Cu-Ni/Gr composite coatings are investigated. Based on the experimental results, the coatings prepared at 6 A/dm^2 exhibit a reduced crystallite size with enhanced mechanical properties and corrosion resistance.
2. The amount of graphene nanoplatelets in Cu–Ni/Gr composites coatings was increased up to 6 A/dm^2 and then decreased. The incorporation of graphene nanoplatelets in Cu-Ni coating influenced the crystallite size. As the graphene nanoplatelets content was increased, the crystallite size of the coating decreased, which in turn increased the microhardness, corrosion resistance and decreased the coefficient of friction of the coating. The Cu–Ni/Gr composite coating reached the maximum values of desirable properties at 6 A/dm^2 of current density.
3. The effect of different concentrations of Gr (such as 100, 200, 300, 400 and 500 mg/L) in the electrolyte bath on the mechanical, tribological and corrosion properties of the Cu-Ni/Gr composite coatings are investigated. The incorporation of graphene nanoplatelets in the Cu-Ni matrix by electro-co-deposition process enhanced the tribological, mechanical and corrosion properties.
4. The 400 mg/L concentration of graphene nanoplatelets in the plating bath provided the best increase in the microhardness and corrosion resistance. The measured microhardness for Cu–Ni/Gr (400 mg/L) composite coating increases by 44.17% compared to pure Cu–Ni coating. Also, the average friction coefficient of Cu–Ni coating was decreased from 0.74 to 0.27 when it was incorporated with graphene nanoplatelets. The immersion study indicates that the incorporation of graphene nanoplatelets stabilizes the corrosion potential and enhances the corrosion resistance.
5. The Cu-Ni/Gr composites were synthesized through a modified electrochemical-co-deposition method followed by convectional powder metallurgy method at different concentrations of Gr (such as 50, 100, 200 and 250 mg/L) in the electrolyte bath. The hardness, YS, and UTS of the Cu-Ni/Gr composite were increased with an increase in the concentration of Gr in the electrolyte bath. When Gr concentration in the electrolyte bath was 200 mg/L, the microhardness of 107 HV, YS of 265 MPa and UTS of 299 MPa were achieved in Cu-Ni/Gr composite, which were 84.5%, 138.7% and 90.5% improvement over pure Cu-Ni alloy. The fracture mode of Cu-Ni/Gr composite transforms from ductile fracture to brittle fracture with an increase in Gr concentration

in the electrolyte bath. For tribological performance, both the friction coefficient and wear rate were decreased when Gr concentration in the electrolyte bath increased. We believed that the Cu-Ni/Gr composites synthesized by the proposed method could be employed in the automobile, aerospace, and marine industries due to enhanced mechanical and tribological properties.

References

[1] C. M. P. Kumar, T. V. Venkatesha, and R. Shabadi, "Preparation and corrosion behavior of Ni and Ni-graphene composite coatings," *Mater. Res. Bull.*, vol. 48, no. 4, pp. 1477–1483, 2013.

[2] Z. Shahri and S. R. Allahkaram, "Effect of particles concentration and current density on the cobalt/hexagonal boron nitride nano-composite coatings properties," *Iran. J. Mater. Sci. Eng.*, vol. 9, no. 4, pp. 1–7, 2012.

[3] Y. Tang, X. Yang, R. Wang, and M. Li, "Enhancement of the mechanical properties of graphene–copper composites with graphene–nickel hybrids," *Mater. Sci. Eng. A*, vol. 599, pp. 247–254, 2014.

[4] M. R. R. Vaezi, S. K. K. Sadrnezhaad, and L. Nikzad, "Electrodeposition of Ni–SiC nano-composite coatings and evaluation of wear and corrosion resistance and electroplating characteristics," *Colloids Surfaces A Physicochem. Eng. Asp.*, vol. 315, no. 1–3, pp. 176–182, Feb. 2008.

[5] I. Jo *et al.*, "Low-Frequency Acoustic Phonon Temperature Distribution in Electrically Biased Graphene," *Nano Lett.*, vol. 11, no. 1, pp. 85–90, Jan. 2011.

[6] M. Haerifar and M. Zandrahimi, "Effect of current density and electrolyte pH on microstructure of Mn–Cu electroplated coatings," *Appl. Surf. Sci.*, vol. 284, pp. 126–132, 2013.

[7] A. L. Patterson, "The Scherrer Formula for X-Ray Particle Size Determination," *Phys. Rev.*, vol. 56, no. 10, pp. 978–982, Nov. 1939.

[8] M. HE, W. HU, C. ZHONG, J. WENG, B. SHEN, and Y. WU, "Effect of wear conditions on tribological properties of electrolessly-deposited Ni-P-Gr-SiC hybrid composite coating," *Trans. Nonferrous Met. Soc. China*, vol. 22, no. 10, pp. 2586–2592, 2012.

[9] Y. Lei, J. Jiang, T. Bi, J. Du, and X. Pang, "Tribological behavior of *in situ* fabricated graphene–nickel matrix composites," *RSC Adv.*, vol. 8, no. 39, pp. 22113–22121, 2018.

[10] B. Han and X. Lu, "Tribological and anti-corrosion properties of Ni–W–CeO2

coatings against molten glass," *Surf. Coatings Technol.*, vol. 202, no. 14, pp. 3251–3256, 2008.

[11] J. Chen, J. Li, D. Xiong, Y. He, Y. Ji, and Y. Qin, "Preparation and tribological behavior of Ni-graphene composite coating under room temperature," *Appl. Surf. Sci.*, vol. 361, pp. 49–56, 2016.

[12] C. R. Thurber *et al.*, "Metal Matrix Composite Coatings of Cupronickel Embedded with Nanoplatelets for Improved Corrosion Resistant Properties," *Int. J. Corros.*, vol. 2018, pp. 1–11, Jun. 2018.

[13] A. Jabbar *et al.*, "Electrochemical deposition of nickel graphene composite coatings effect of deposition temperature on its surface morphology and corrosion resistance," *RSC Adv.*, vol. 7, no. 49, pp. 31100–31109, 2017.

[14] R. A. Shakoor, R. Kahraman, U. S. Waware, Y. Wang, and W. Gao, "Properties of electrodeposited Ni-B-ZrO2 composite coatings," *Int. J. Electrochem. Sci.*, vol. 10, no. 3, pp. 2110–2119, 2015.

[15] M. Alizadeh and H. Safaei, "Characterization of Ni-Cu matrix, Al2O3reinforced nano-composite coatings prepared by electrodeposition," *Appl. Surf. Sci.*, vol. 456, pp. 195–203, 2018.

[16] G. Yasin *et al.*, "Synthesis of spheres-like Ni/graphene nanocomposite as an efficient anti-corrosive coating; effect of graphene content on its morphology and mechanical properties," *J. Alloys Compd.*, vol. 755, pp. 79–88, Jul. 2018.

[17] S. Colin, E. Beche, R. Berjoan, H. Jolibois, and A. Chambaudet, "An XPS and AES study of the free corrosion of Cu-, Ni- and Zn-based alloys in synthetic sweat," *Corros. Sci.*, vol. 41, no. 6, pp. 1051–1065, 1999.

[18] M. Metikoš-Huković, I. Škugor, Z. Grubač, and R. Babić, "Complexities of corrosion behaviour of copper–nickel alloys under liquid impingement conditions in saline water," *Electrochim. Acta*, vol. 55, no. 9, pp. 3123–3129, 2010.

[19] I. Milošev and M. Metikoš-Huković, "The behaviour of Cu-xNi (x = 10 to 40 wt%) alloys in alkaline solutions containing chloride ions," *Electrochim. Acta*, vol. 42, no. 10, pp. 1537–1548, 1997.

[20] A. L. Ma, S. L. Jiang, Y. G. Zheng, and W. Ke, “Corrosion product film formed on the 90/10 copper–nickel tube in natural seawater: Composition/structure and formation mechanism,” *Corros. Sci.*, vol. 91, pp. 245–261, Feb. 2015.

[21] L. Wang *et al.*, “Graphene-copper composite with micro-layered grains and ultrahigh strength,” *Sci. Rep.*, vol. 7, no. 1, p. 41896, Mar. 2017.

[22] D. Sobha Jayakrishnan, “Electrodeposition: the versatile technique for nanomaterials,” in *Corrosion Protection and Control Using Nanomaterials*, Elsevier, 2012, pp. 86–125.

[23] Z. Hu *et al.*, “Graphene-reinforced metal matrix nanocomposites – a review,” *Mater. Sci. Technol.*, vol. 32, no. 9, pp. 930–953, Jun. 2016.

[24] Y. Tang, X. Yang, R. Wang, and M. Li, “Enhancement of the mechanical properties of graphene-copper composites with graphene-nickel hybrids,” *Mater. Sci. Eng. A*, vol. 599, pp. 247–254, 2014.

[25] Y. Peng, Z. Wang, and K. Zou, “Friction and Wear Properties of Different Types of Graphene Nanosheets as Effective Solid Lubricants,” *Langmuir*, vol. 31, no. 28, pp. 7782–7791, Jul. 2015.

[26] M. Alizadeh and A. Cheshmpish, “Electrodeposition of Ni-Mo/Al2O3 nano-composite coatings at various deposition current densities,” *Appl. Surf. Sci.*, vol. 466, no. October 2018, pp. 433–440, Feb. 2019.

[27] Z. Xu, X. Shi, W. Zhai, J. Yao, S. Song, and Q. Zhang, “Preparation and tribological properties of TiAl matrix composites reinforced by multilayer graphene,” *Carbon N. Y.*, vol. 67, pp. 168–177, Feb. 2014.

Chapter 6

Process Parameters Optimization

In the previous chapter, (i) the effect of various current densities and (ii) the effect of various concentrations of Gr in the electrolyte bath on mechanical, tribological and corrosion properties of Cu-Ni/Gr composite coatings is investigated. Also, the effect of various concentrations of Gr in the electrolyte bath on mechanical, tribological and corrosion properties of Cu-Ni/Gr composites prepared by a modified electro-co-deposition method followed by powder metallurgy method is also discussed.

In this chapter, the effect of electrolysis parameters such as pH, current density, graphene nanoplatelets concentration and amount of nickel sulfate on microhardness and polarization resistance of Cu-Ni/Gr composite coatings prepared by the electro-co-deposition method are briefly discussed. Similarly, the effect of electrolysis parameters such as pH, current, graphene nanoplatelets concentration and amount of nickel sulfate on microhardness and polarization resistance of Cu-Ni/Gr composites prepared by a modified electro-co-deposition method followed by powder metallurgy method are discussed. The set of experiments was performed based on the design developed by Taguchi method.

6.1 Effect of electrolysis parameters on microhardness and corrosion resistance of Cu-Ni/Gr composite coatings

6.1.1 Experimental design of Cu-Ni/Gr composite coatings

In the current investigation, pH, current density, Gr concentration and amount of nickel sulfate have been selected as process variables. The fixed electrolysis parameter for the experimental study is listed in Table 6.1. The respective process variable range selected for this study is listed in Table 6.2. The experiments have been designed based on the Taguchi method, and the results have been analyzed for the microhardness value of composite coating. Based on the results of the above studies, the significances of the parameters are ranked by order. Analysis of variances (ANOVA) studies is performed to recognize the significances of process parameters and the percentage of contributions is identified. In the present work, we have investigated as the maximum hardness and high

polarization resistance (R_p) as performance index and have chosen a larger-the-better S/N ratio for microhardness and polarization resistance.

$$\frac{S}{N} = -10\log\frac{1}{N_i}\sum\frac{1}{y_i^2} \tag{6.1}$$

where, y_i denotes the N_i observations of response variables.

Table 6.1: Fixed electrolysis parameter for experimental study

Fixed Parameters	Quantity
Amount of $CuSO_4.5H_2O$	21 g/L
Electrodeposition Time	60 min
Magnetic stirring	350 rpm
Ultrasonication time	60 min
Temperature	35°C

Table 6.2: Input variables and their levels

Parameter No.	Description	Level 1	Level 2	Level 3	Level 4
A	pH	3	3.5	4	4.5
B	Current density (A/dm^2)	2	4	6	8
C	Gr concentration (mg/L)	100	200	300	400
D	$NiSO_4.6H_2O$ (g/L)	42	63	84	105

In electro-co-deposition method, major parameters, which influence the quality of prepared Cu-Ni/Gr composite coating are 1) pH, 2) current density, 3) Gr concentration in the electrolyte and 4) amount of nickel sulfate. With the four parameters as variables and considering four levels of each variable, a fractional factorial design of 16 experiments is done with L_{16} orthogonal array. Table 6.2 presents the respective process variable with their corresponding levels with which the composite coatings have been experimented and optimization of microhardness and polarization resistance using Taguchi was performed using MINITAB software. The experiments have been conducted using Taguchi experimental design (L_{16} orthogonal array) and are shown in Table 6.3.

Table 6.3: The basic Taguchi L_{16} orthogonal array

Exp. No.	Parameters				Notation	Microhardness (HV)	R_p ($k\Omega.cm^2$)
	A	B	C	D			
1	1	1	1	1	$A_1B_1C_1D_1$	374	94.23
2	1	2	2	2	$A_1B_2C_2D_2$	423	151.65
3	1	3	3	3	$A_1B_3C_3D_3$	454	188.87
4	1	4	4	4	$A_1B_4C_4D_4$	482	223.35
5	2	1	2	3	$A_2B_1C_2D_3$	432	156.87
6	2	2	1	4	$A_2B_2C_1D_4$	388	123.74
7	2	3	4	1	$A_2B_3C_4D_1$	458	204.41
8	2	4	3	2	$A_2B_4C_3D_2$	435	177.85
9	3	1	3	4	$A_3B_1C_3D_4$	458	190.41
10	3	2	4	3	$A_3B_2C_4D_3$	475	217.32
11	3	3	1	2	$A_3B_3C_1D_2$	368	112.65
12	3	4	2	1	$A_3B_4C_2D_1$	398	145.45
13	4	1	4	2	$A_4B_1C_4D_2$	466	205.14
14	4	2	3	1	$A_4B_2C_3D_1$	427	169.43
15	4	3	2	4	$A_4B_3C_2D_4$	430	172.34
16	4	4	1	3	$A_4B_4C_1D_3$	372	115.73

Table 6.4: The basic Taguchi L_{16} orthogonal array

Exp. No.	A	B	C	D	Notation	Microhardness 1	Microhardness 2	Microhardness 3	Microhardness (HV)
1	1	1	1	1	$A_1B_1C_1D_1$	328	320	318	322
2	1	2	2	2	$A_1B_2C_2D_2$	395	385	378	386
3	1	3	3	3	$A_1B_3C_3D_3$	439	459	440	446
4	1	4	4	4	$A_1B_4C_4D_4$	455	466	468	463
5	2	1	2	3	$A_2B_1C_2D_3$	396	390	381	389
6	2	2	1	4	$A_2B_2C_1D_4$	376	376	388	380
7	2	3	4	1	$A_2B_3C_4D_1$	458	452	446	452
8	2	4	3	2	$A_2B_4C_3D_2$	399	404	415	406
9	3	1	3	4	$A_3B_1C_3D_4$	444	445	425	438
10	3	2	4	3	$A_3B_2C_4D_3$	461	481	468	470
11	3	3	1	2	$A_3B_3C_1D_2$	367	351	371	363
12	3	4	2	1	$A_3B_4C_2D_1$	359	375	361	365
13	4	1	4	2	$A_4B_1C_4D_2$	444	427	434	435
14	4	2	3	1	$A_4B_2C_3D_1$	412	388	406	402
15	4	3	2	4	$A_4B_3C_2D_4$	415	422	429	422
16	4	4	1	3	$A_4B_4C_1D_3$	341	358	339	346

Table 6.5: The basic Taguchi L_{16} orthogonal array

Exp. No.	A	B	C	D	Notation	R_p 1	R_p 2	R_p 3	R_p ($k\Omega.cm^2$)
1	1	1	1	1	$A_1B_1C_1D_1$	91.52	93.25	97.92	94.23
2	1	2	2	2	$A_1B_2C_2D_2$	148.35	154.22	152.38	151.65
3	1	3	3	3	$A_1B_3C_3D_3$	189.25	185.22	192.14	188.87
4	1	4	4	4	$A_1B_4C_4D_4$	220.52	224.74	224.79	223.35
5	2	1	2	3	$A_2B_1C_2D_3$	154.25	157.65	158.71	156.87
6	2	2	1	4	$A_2B_2C_1D_4$	121.54	126.54	123.14	123.74
7	2	3	4	1	$A_2B_3C_4D_1$	202.58	207.85	202.8	204.41
8	2	4	3	2	$A_2B_4C_3D_2$	178.54	176.22	178.79	177.85
9	3	1	3	4	$A_3B_1C_3D_4$	188.245	192.21	190.775	190.41
10	3	2	4	3	$A_3B_2C_4D_3$	217.85	219.35	214.76	217.32
11	3	3	1	2	$A_3B_3C_1D_2$	113.25	112.85	111.85	112.65
12	3	4	2	1	$A_3B_4C_2D_1$	148.25	144.85	143.25	145.45
13	4	1	4	2	$A_4B_1C_4D_2$	204.52	206.25	204.65	205.14
14	4	2	3	1	$A_4B_2C_3D_1$	171.25	166.25	170.79	169.43
15	4	3	2	4	$A_4B_3C_2D_4$	173.98	171.25	171.79	172.34
16	4	4	1	3	$A_4B_4C_1D_3$	113.25	115.75	118.19	115.73

6.1.2 Statistical analysis of experimental results

The statistical modelling for the microhardness and polarization resistance of Cu-Ni/Gr composite coatings synthesized by electro-co-deposition method has been done. General first-order models are developed for estimating the microhardness and polarization resistance of the coatings. The models are developed by regression analysis of the experimental data as listed in Table 6.3. The microhardness obtained for the coatings in all three sets of sixteen experiments has been subjected to statistical analysis. The analysis done for the microhardness is given in Table 6.6. The microhardness of coatings is analyzed by using variance analysis. The analysis is carried out by using the Taguchi method with significant values of process parameters. The data obtained by this analysis are shown in Table 6.6.

The model was obtained after performing regression analysis which is given as Equation (6.2):

$$\text{Microhardness} = 275.6 - 1.35\,A + 0.41\,B + 0.3392\,C + 0.651\,D \quad (6.2)$$

where, microhardness in HV, A is the pH, B is the current density (A/dm^2), C is the amount of Gr concentration (mg/L) and D is the amount of nickel sulfate (g/L).

The main effect plot and the effect of the process parameters in terms of percentage contribution are shown in Figure 6.1(a, b).

Table 6.6: Analysis of variance for microhardness

Source	DF	Adj SS	Adj MS	F-Value	P-Value	R^2
Regression	4	26780.9	6695.2	37.57	0.000	93.18%
A	1	9.1	9.1	0.05	0.825	
B	1	13.6	13.6	0.08	0.787	
C	1	23018.1	23018.1	129.15	0.000	
D	1	3740.1	3740.1	20.99	0.001	
Error	11	1960.5	178.2			
Total	15	28741.4				

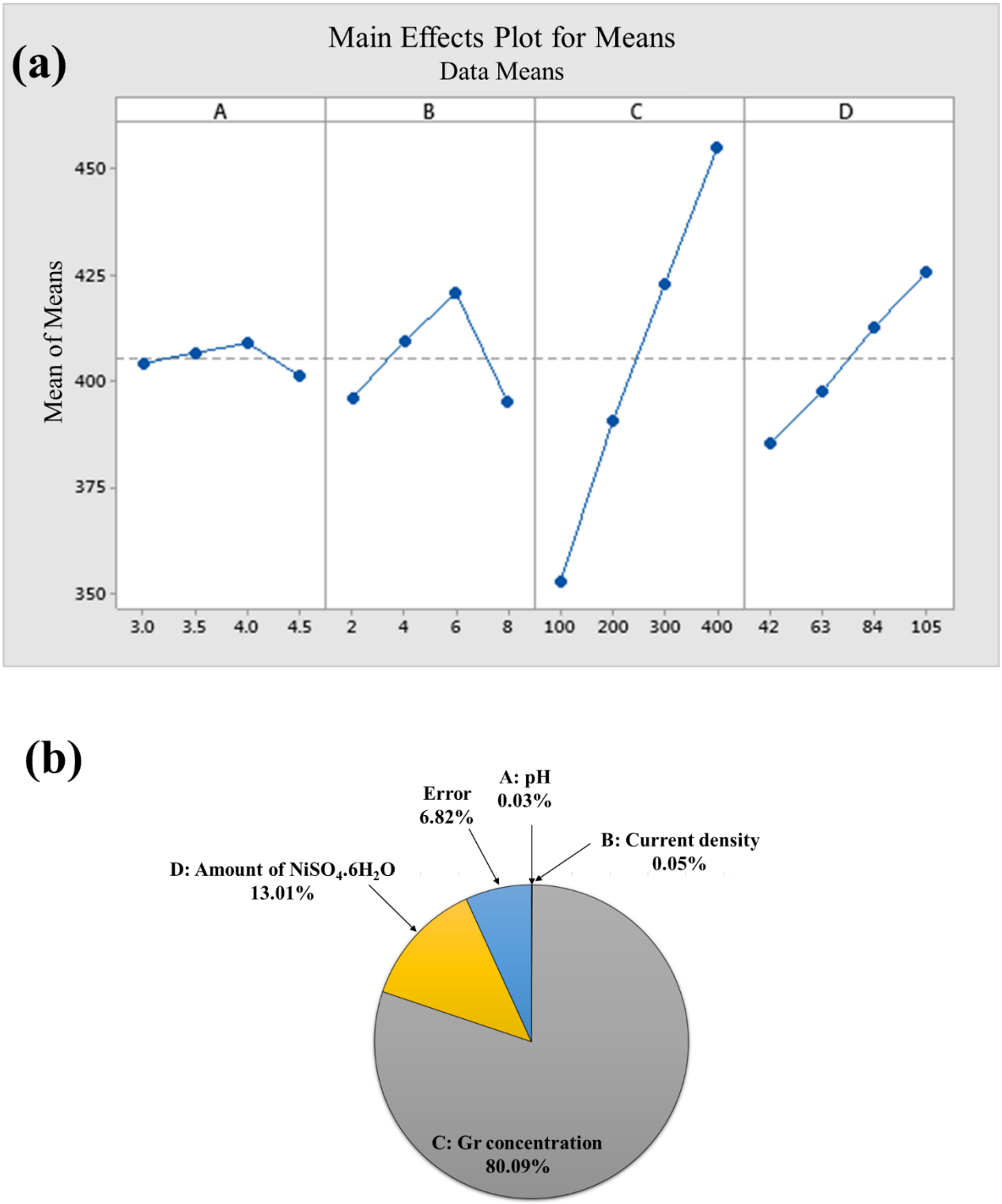

Figure 6.1: (a) Main effect plot showing effect of process parameters on change in microhardness (HV), (b) Percentage contribution of process parameters on change in microhardness (HV)

The analysis done for the polarization resistance is shown in Table 6.7. The polarization resistance has been investigated by variance analysis. The study is carried out by using the Taguchi method with significant values of process parameters. The data obtained by this analysis are shown in Table 6.7. The great value of R^2 of 93.18% gave a convinced justification to the reliability of regression models for microhardness of Cu-Ni/Gr composite coating. A small error of 6.82% is mainly due to uncontrollable fluctuations in current density, electrolyte temperature, magnetic stirring rate, and pH.

The model was obtained after performing regression analysis which is given as Equation (6.4):

$$R_p = 48.5 + 0.83\ A + 0.791\ B + 0.3280\ C + 0.3815\ D \quad (6.3)$$

where, R_p represents polarization resistance in $k\Omega.cm^2$, A is the pH, B is the current density (A/dm^2), C is the amount of Gr concentration (mg/L) and D is the amount of nickel sulfate (g/L). The main effect plot and the effect of the process parameters in terms of percentage contribution are shown in Figure 6.2(a, b).

Table 6.7: Analysis of variance for polarization resistance

Source	DF	Adj SS	Adj MS	F-Value	P-Value	R^2
Regression	4	22849.4	5712.4	152.93	0.00000	98.23%
A	1	3.4	3.4	0.09	0.76732	
B	1	50.1	50.1	1.34	0.27126	
C	1	21512.2	21512.2	575.92	0.00000	
D	1	1283.7	1283.7	34.37	0.00011	
Error	11	410.9	37.4			
Total	15	23260.3				

It can be seen from the main effect plot that for the considered range of process parameters used pH, current density and amount of nickel sulfate have an insignificant effect on microhardness and polarization resistance. It can be observed from the main effect plots that Gr concentration in the electrolyte bath was found to be the most significant process parameter for microhardness and polarization resistance of Cu-Ni/Gr composite coatings.

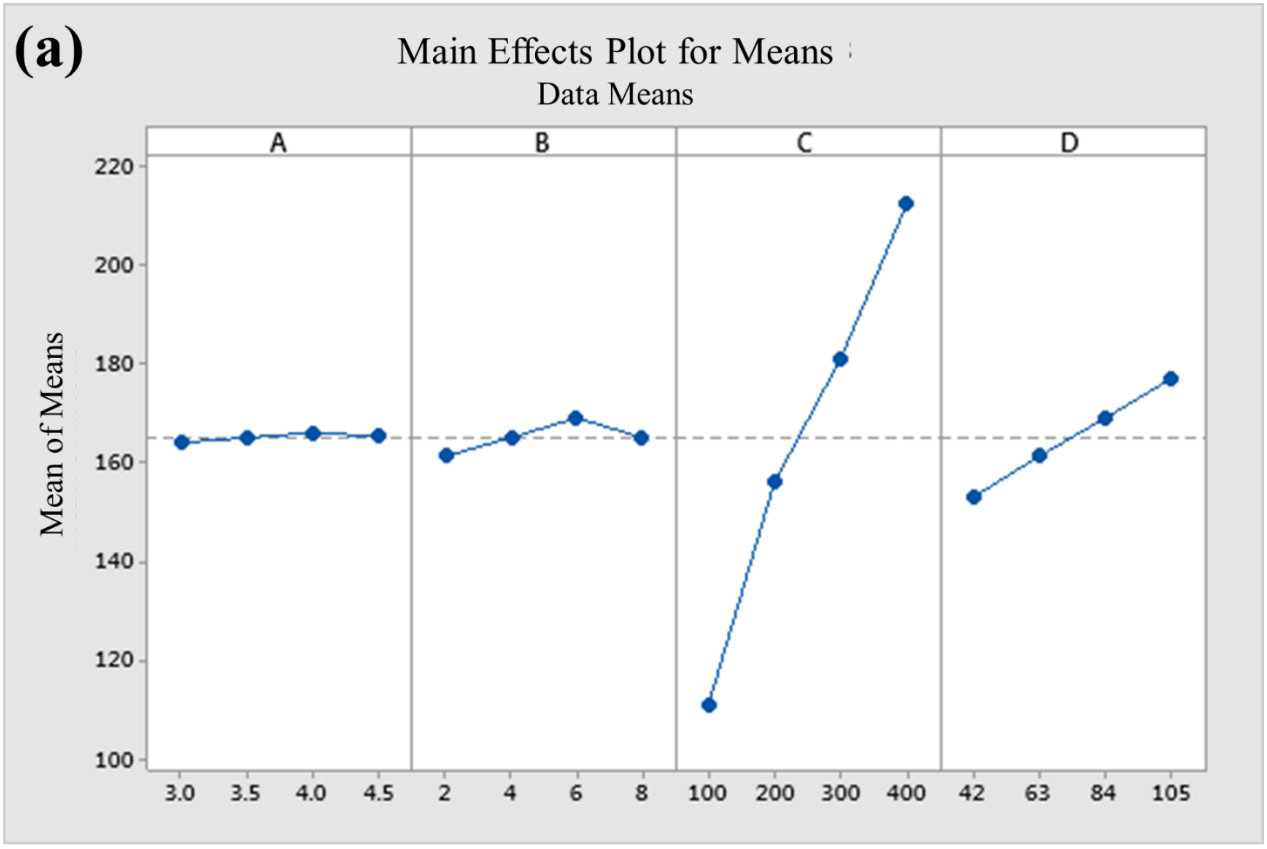

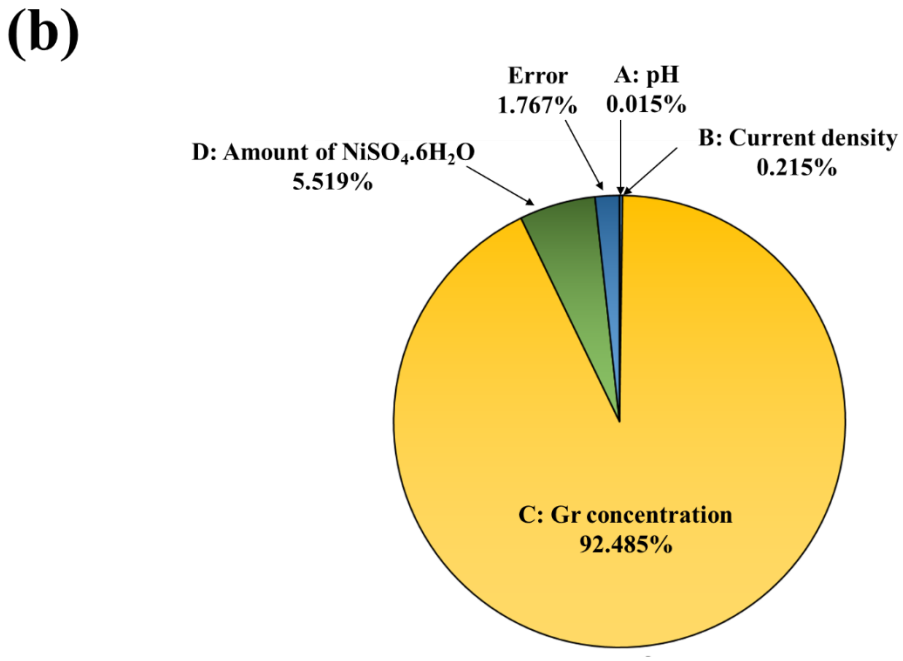

Figure 6.2: (a) Main effect plot showing effect of process parameters on change in polarization resistance (kΩ.cm^2), (b) Percentage contribution of process parameters on change in polarization resistance (kΩ.cm^2)

For the validation of the developed regression model, three sets of experiments have been carried out at random values of process parameters. The data for these set of experiments are shown in **Table 6.8.**

Table 6.8: Experiments for the validation of the regression model developed by variance analysis

Sr. No.	Process Parameters				Microhardness (HV)		R_p (kΩ.cm^2)	
	A	B	C	D	Regression predicted	Experimental	Regression predicted	Experimental
1	3	2	100	63	347 ± 23	356	109.40 ± 1.9	113.12
2	4	8	300	42	402 ± 24	412	172.52 ± 3.0	169.25
3	4.5	4	200	84	393 ± 23	381	153.04 ± 2.7	156.46

The optimized values of process parameters for the maximum value of the microhardness and polarization resistance are shown in **Table 6.9.**

Table 6.9: The optimized values of process parameters for the maximum value of the microhardness and polarization resistance of Cu-Ni/Gr composite coatings

Parameter No.	Description	Value
A	pH	4
B	Current density (A/dm^2)	6
C	Gr concentration (mg/L)	400
D	$NiSO_4.6H_2O$ (g/L)	105

Cu-Ni/Gr composite coatings are fabricated by electro-co-deposition method and tested for microhardness and polarization resistance. The microhardness and polarization resistance of coatings are investigated by using a microhardness tester and potentiostat, respectively. All prepared coatings are tested under the identical conditions in the controlled environment. From the results, it is revealed that the microhardness and polarization resistance of the Cu-Ni/Gr composite coating increases with increase in the Gr concentration in the electrolyte bath. By Taguchi and regression analysis, it is found that the Gr concentration in the electrolyte is the most influencing parameter of the process for microhardness and polarization resistance of the Cu-Ni/Gr composite coatings. The

addition of Gr decreases the crystallite size of the coating and hence requires more power for penetration, which results in a rise in microhardness [9]. More concentration of the nickel sulfate in the electrolyte results in an increase in the amount of Ni in the Cu-Ni/Gr composite coatings and improves the microhardness value. Also, graphene nanoplatelets act as an inert physical barrier to the initiation and growth of corrosion defects and hence improving the corrosion resistance [10].

6.2 Effect of electrolysis parameters on microhardness and corrosion resistance of Cu-Ni/Gr composites prepared by modified electro-co-deposition method followed by powder metallurgy method

We also studied the effect of electrolysis parameters such as pH, current, Gr concentration and amount of nickel sulfate on the microhardness and polarization resistance of the Cu-Ni/Gr composite pellets. The Taguchi's statistical method has been employed to design the experiments. The available literature on Cu-Ni/Gr composite lacks any statistical investigation to conclude on parameter, which may significantly influence mechanical and corrosion properties of the Cu-Ni/Gr composite.

6.2.1 Experimental design of Cu-Ni/Gr Composites

In the current investigation, pH, current, Gr concentration and amount of nickel sulfate have been selected as process variables. The fixed electrolysis parameter for the experimental study is listed in Table 6.10. The experiments have been designed based on the Taguchi method, and the results have been analyzed for microhardness and polarization resistance values of Cu-Ni/Gr composites. Based on the results of the above studies, the significances of the parameters are ranked by order. Analysis of variances (ANOVA) studies are performed to recognize the significances of process parameters and the percentage of contributions is identified. In the present work, we have investigated as the maximum hardness and high polarization resistance (R_p) as performance index and have chosen a larger-the-better S/N ratio for hardness and polarization resistance.

$$\frac{S}{N} = -10\log\frac{1}{N_i}\sum\frac{1}{y_i^2} \tag{6.4}$$

where, y_i denotes the N_i observations of response variables.

In electro-co-deposition method, major parameters, which influence the quality of formed Cu-Ni/Gr composite powder are 1) pH 2) current density 3) Gr concentration in the electrolyte and 4) amount of nickel sulfate. With the four parameters as variables and considering four levels of each variable, a fractional factorial design of 16 experiments is done with L_{16} orthogonal array. Table 6.11 shows the respective process variable with their corresponding levels with which the composite coatings have been experimented and optimization of microhardness and polarization resistance using Taguchi was performed using MINITAB software. The L_{16} orthogonal array having four parameters with four levels is selected to conduct experiments. The optimal level of the process parameters is obtained by using Taguchi optimization technique and a mathematical model is developed using regression analysis to predict the output from a selected range of process parameters. The experimental output values are used to find the best combination of optimal parameters. Here the objective is to maximize the microhardness and polarization resistance of Cu-Ni/Gr composite coatings. The higher the value of microhardness and polarization resistance better is the result. For the optimization of the process parameters using the Taguchi method, the objective is taken as larger is better.

Table 6.10: Fixed electrolysis parameter for experimental study

Fixed Parameters	Quantity
Amount of $CuSO_4.5H_2O$	23 g/L
Electrodeposition Time	120 min
Magnetic stirring	350 rpm
Ultrasonication time	120 min
Temperature	35°C

Table 6.11: Input variables and their levels

Parameter No.	Description	Level 1	Level 2	Level 3	Level 4
A	pH	3	3.5	4	4.5
B	Current (A)	4	5	6	7
C	Gr concentration (mg/L)	50	100	150	200
D	$NiSO_4.6H_2O$ (g/L)	65	75	85	95

Table 6.12: The basic Taguchi L_{16} orthogonal array

Exp. No.	Parameters				Notation	Microhardness (HV)	R_p ($k\Omega.cm^2$)
	A	B	C	D			
1	1	1	1	1	$A_1B_1C_1D_1$	69	4.237
2	1	2	2	2	$A_1B_2C_2D_2$	92	6.723
3	1	3	3	3	$A_1B_3C_3D_3$	100	8.198
4	1	4	4	4	$A_1B_4C_4D_4$	110	9.725
5	2	1	2	3	$A_2B_1C_2D_3$	93	6.766
6	2	2	1	4	$A_2B_2C_1D_4$	74	5.487
7	2	3	4	1	$A_2B_3C_4D_1$	109	8.984
8	2	4	3	2	$A_2B_4C_3D_2$	99	7.452
9	3	1	3	4	$A_3B_1C_3D_4$	100	8.354
10	3	2	4	3	$A_3B_2C_4D_3$	110	9.532
11	3	3	1	2	$A_3B_3C_1D_2$	73	4.956
12	3	4	2	1	$A_3B_4C_2D_1$	92	6.384
13	4	1	4	2	$A_4B_1C_4D_2$	108	9.124
14	4	2	3	1	$A_4B_2C_3D_1$	98	7.356
15	4	3	2	4	$A_4B_3C_2D_4$	96	7.584
16	4	4	1	3	$A_4B_4C_1D_3$	73	5.211

Table 6.13: The basic Taguchi L_{16} orthogonal array

Exp. No.	A	B	C	D	Notation	Microhardness 1	Microhardness 2	Microhardness 3	Microhardness (HV)
1	1	1	1	1	$A_1B_1C_1D_1$	67	72	68	69
2	1	2	2	2	$A_1B_2C_2D_2$	94	95	87	92
3	1	3	3	3	$A_1B_3C_3D_3$	103	101	96	100
4	1	4	4	4	$A_1B_4C_4D_4$	113	108	109	110
5	2	1	2	3	$A_2B_1C_2D_3$	96	94	89	93
6	2	2	1	4	$A_2B_2C_1D_4$	77	76	69	74
7	2	3	4	1	$A_2B_3C_4D_1$	106	112	109	109
8	2	4	3	2	$A_2B_4C_3D_2$	103	104	90	99
9	3	1	3	4	$A_3B_1C_3D_4$	99	103	98	100
10	3	2	4	3	$A_3B_2C_4D_3$	108	112	110	110
11	3	3	1	2	$A_3B_3C_1D_2$	74	71	74	73
12	3	4	2	1	$A_3B_4C_2D_1$	93	92	91	92
13	4	1	4	2	$A_4B_1C_4D_2$	107	106	111	108
14	4	2	3	1	$A_4B_2C_3D_1$	96	101	97	98
15	4	3	2	4	$A_4B_3C_2D_4$	94	97	97	96
16	4	4	1	3	$A_4B_4C_1D_3$	71	71	77	73

Table 6.14: The basic Taguchi L_{16} orthogonal array

Exp. No.	A	B	C	D	Notation	R_p 1	R_p 2	R_p 3	R_p (kΩ.cm^2)
1	1	1	1	1	$A_1B_1C_1D_1$	4.123	4.254	4.334	4.237
2	1	2	2	2	$A_1B_2C_2D_2$	6.524	6.854	6.791	6.723
3	1	3	3	3	$A_1B_3C_3D_3$	8.145	8.235	8.214	8.198
4	1	4	4	4	$A_1B_4C_4D_4$	9.801	9.758	9.616	9.725
5	2	1	2	3	$A_2B_1C_2D_3$	6.654	6.798	6.846	6.766
6	2	2	1	4	$A_2B_2C_1D_4$	5.354	5.452	5.655	5.487
7	2	3	4	1	$A_2B_3C_4D_1$	8.851	9.012	9.089	8.984
8	2	4	3	2	$A_2B_4C_3D_2$	7.354	7.548	7.454	7.452
9	3	1	3	4	$A_3B_1C_3D_4$	8.265	8.368	8.429	8.354
10	3	2	4	3	$A_3B_2C_4D_3$	9.547	9.658	9.391	9.532
11	3	3	1	2	$A_3B_3C_1D_2$	4.825	5.012	5.031	4.956
12	3	4	2	1	$A_3B_4C_2D_1$	6.245	6.425	6.482	6.384
13	4	1	4	2	$A_4B_1C_4D_2$	9.125	9.254	8.993	9.124
14	4	2	3	1	$A_4B_2C_3D_1$	7.254	7.456	7.358	7.356
15	4	3	2	4	$A_4B_3C_2D_4$	7.452	7.654	7.646	7.584
16	4	4	1	3	$A_4B_4C_1D_3$	5.154	5.354	5.125	5.211

6.2.2 Statistical analysis of experimental results

The statistical modelling for the microhardness and polarization resistance of Cu-Ni/Gr composites prepared by modified electro-co-deposition followed by powder metallurgy method has been studied and discussed. General first-order models are developed for estimating the microhardness and polarization resistance of the coatings. The models are developed by regression analysis of the experimental data as listed in Table 6.12. The microhardness obtained for the coatings in all the three sets of sixteen experiments have been subjected to statistical analysis as given in Table 6.13. The analysis done for the microhardness is given in Table 6.15. The microhardness of coatings is analyzed by using variance analysis. The analysis is carried out by using the Taguchi method with significant values of process parameters. The data obtained by this analysis are shown in Table 6.15.

Table 6.15: Analysis of variance for microhardness

Source	DF	Adj SS	Adj MS	F-Value	P-Value	R^2
Regression	4	2761.80	690.45	38.13	0.000	93.27%
A	1	0.80	0.80	0.04	0.837	
B	1	3.20	3.20	0.18	0.682	
C	1	2737.80	2737.80	151.18	0.000	
D	1	20.00	20.00	1.10	0.316	
Error	11	199.20	18.11			
Total	15	2961.00				

The model was obtained after performing regression analysis which is given as Equation (6.5):

$$\text{Microhardness} = 52.3 + 0.40\,A + 0.40\,B + 0.2340\,C + 0.100\,D \quad (6.5)$$

where, microhardness in HV, A is the pH, B is the current (A), C is the amount of Gr concentration (mg/L) and D is the amount of nickel sulphate (g/L).

The main effect plot and the effect of the process parameters in terms of percentage contribution are shown in Figure 6.3(a, b).

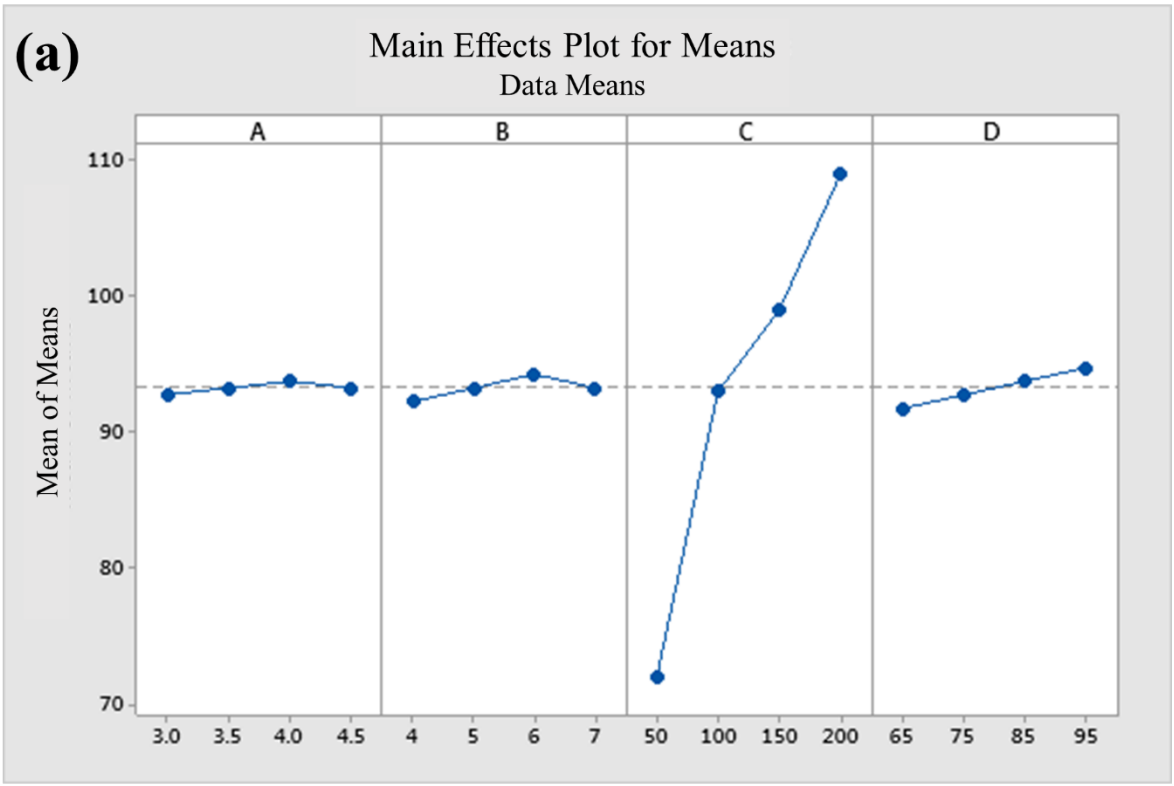

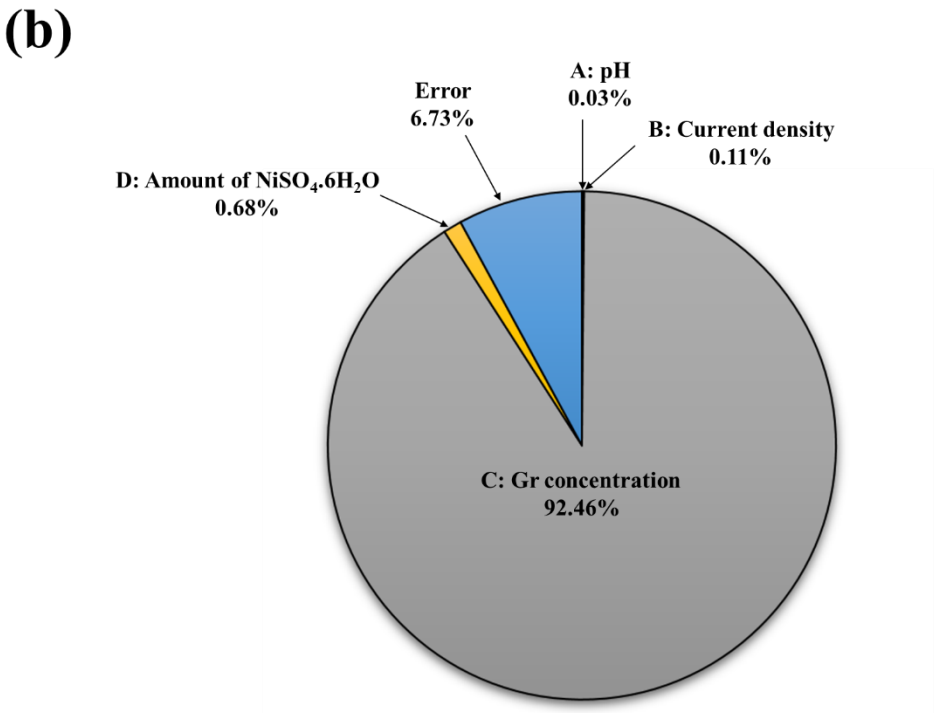

Figure 6.3: (a) Main effect plot showing effect of process parameters on change in microhardness (HV), (b) Percentage contribution of process parameters on change in microhardness (HV)

The analysis done for the polarization resistance is shown in Table 6.16. The polarization resistance has been investigated by variance analysis. The study is carried out by using the Taguchi method with significant values of process parameters. The data obtained by this analysis are shown in Table 6.16.

Table 6.16: Analysis of variance for polarization resistance

Source	DF	Adj SS	Adj MS	F-Value	P-Value	R^2
Regression	4	42.1777	10.5444	140.91	0.00000	98.09%
A	1	0.0367	0.0367	0.49	0.49839	
B	1	0.0280	0.0280	0.37	0.55308	
C	1	39.6563	39.6563	529.95	0.00000	
D	1	2.4567	2.4567	32.83	0.00013	
Error	11	0.8231	0.0748			
Total	15	43.0008				

The model was obtained after performing regression analysis which is given as Equation (6.6):

$$R_p = 0.403 + 0.086\ A + 0.0374\ B + 0.02816\ C + 0.03505\ D \quad (6.6)$$

where, R_p represents polarization resistance in $k\Omega.cm^2$, A is the pH, B is the current (A), C is the amount of Gr concentration (mg/L) and D is the amount of nickel sulfate (g/L).

The analysis done for the polarization resistance is shown in Table 5. The deposition height has been analyzed by using variance analysis. The study has been carried out by using the Taguchi method with significant values of process parameters. The data obtained by this analysis are shown in Table 5.

The main effect plot and the effect of the process parameters in terms of percentage contribution are shown in Figure 6.4(a, b).

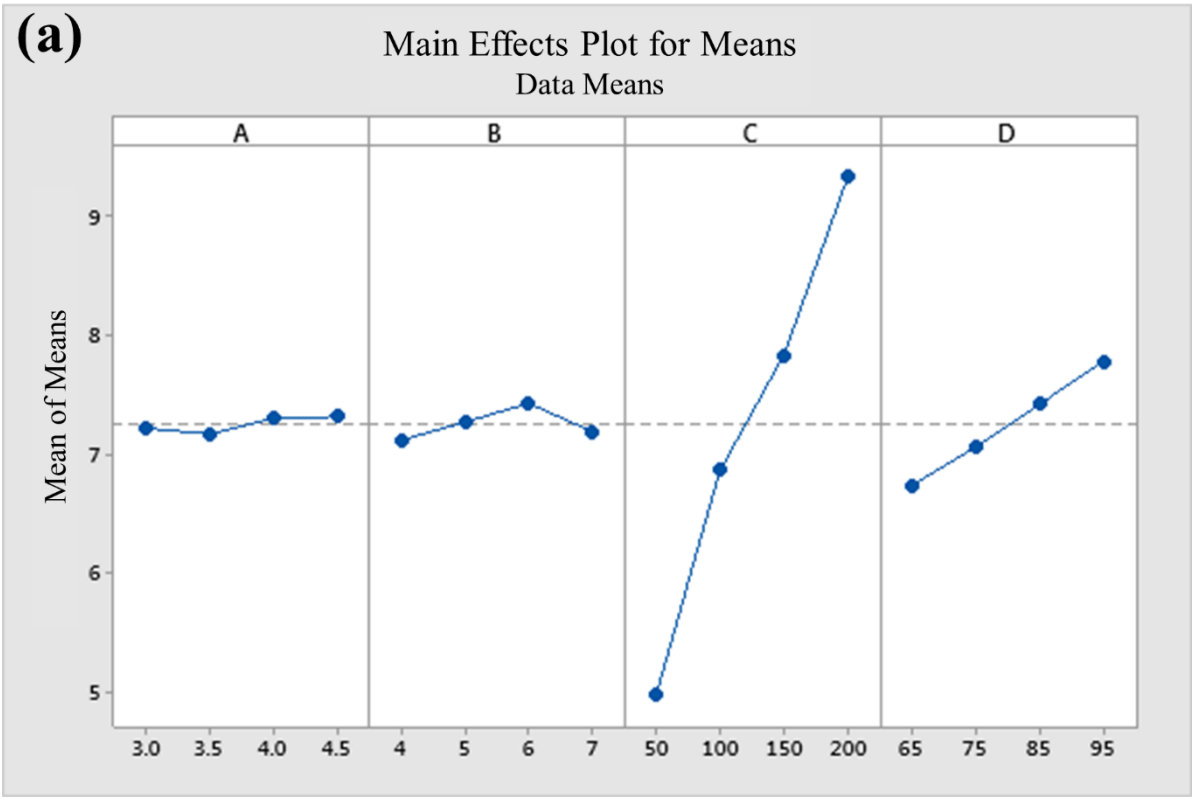

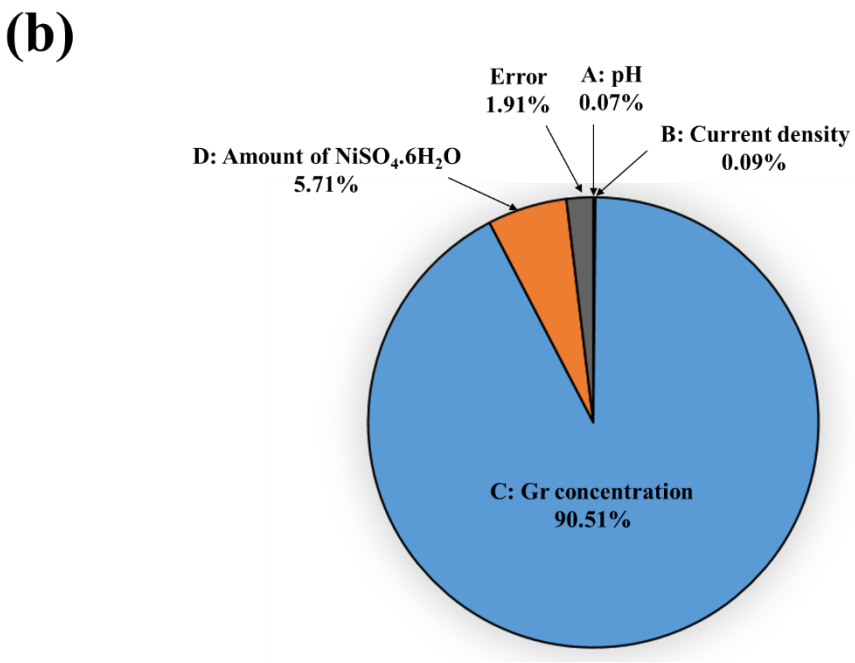

Figure 6.4: (a) Main effect plot showing effect of process parameters on change in polarization resistance (kΩ.cm^2), (b) Percentage contribution of process parameters on change in polarization resistance (kΩ.cm^2)

For the validation of the developed regression model, three sets of experiments have been carried out at random values of process parameters. The data for these set of experiments are shown in **Table 6.8.**

Table 6.8: Experiments for the validation of the regression model developed by variance analysis

Sr. No.	Process Parameters				Microhardness (HV)		R_p (kΩ.cm^2)	
	A	B	C	D	Regression predicted	Experimental	Regression predicted	Experimental
1	3.5	7	150	65	92 ± 6.17	96	7.46 ± 0.14	7.44
2	4	6	50	85	68 ± 4.58	73	5.35 ± 0.10	5.36
3	4.5	4	100	95	79 ± 5.35	86	7.12 ± 0.13	7.13

The optimized values of process parameters for the maximum value of the microhardness and polarization resistance are shown in **Table 6.9.**

Table 6.9: The optimized values of process parameters for the maximum value of the microhardness and polarization resistance of Cu-Ni/Gr composites.

Parameter No.	Description	Value
A	pH	4
B	Current density (A/dm^2)	6
C	Gr concentration (mg/L)	200
D	$NiSO_4.6H_2O$ (g/L)	95

Cu-Ni/Gr composites are fabricated by a modified electro-co-deposition method followed by powder metallurgy method and tested for microhardness and polarization resistance. The microhardness and polarization resistance of prepared Cu-Ni/Gr composites were investigated by using microhardness tester and potentiostat, respectively. All prepared Cu-Ni/Gr composites are tested under identical conditions in the controlled environment. From the obtained results, it is revealed that the microhardness and polarization resistance of the Cu-Ni/Gr composites increases with increasing the Gr concentration in the electrolyte bath. By Taguchi and regression analysis, it is found that the Gr concentration in the electrolyte is the most influencing parameter of the process for microhardness and

polarization resistance of the Cu-Ni/Gr composites. The addition of Gr reduced the crystallite size of the Cu-Ni alloy powder and hence required more power for penetration; hence the microhardness is improved. A higher concentration of nickel sulfate in the electrolyte results in an increase in the amount of Ni in the Cu-Ni/Gr composite and improves the microhardness value [11]–[13]. However, the reinforcement of graphene nanoplatelets in the Cu-Ni alloy matrix fills the defects such as several voids, gaps and cracks owing to its nano size, which contribute to the outstanding resistance to the Cu-Ni/Gr composite to undergo corrosion [14].

6.3 Conclusion

1. Cu-Ni/Gr composite coatings were fabricated by electro-co-deposition method and characterized for microhardness and corrosion resistance. The statistical study of the effect of electrolysis parameters on the microhardness and polarization resistance was carried out using Taguchi statistical method.
2. The obtained results revealed that the Gr concentration in the electrolyte bath and amount of nickel sulfate in the electrolyte had a significant influence on the synthesis of Gr reinforced Cu-Ni alloy matrix composite coatings.
3. The other process parameters such as pH of the solution and current density supplied showed less significance on the microhardness and corrosion resistance of the Cu-Ni/Gr composite coatings.
4. Also, Cu-Ni/Gr composites were produced by a modified electro-co-deposition method followed by powder metallurgy method and characterized for microhardness and corrosion resistance.
5. The statistical study showed that the Gr concentration in the electrolyte bath and amount of nickel sulfate in the electrolyte had the greatest influence on the synthesis of Cu-Ni/Gr composites.
6. The other electrolysis parameters such as the current supplied and pH of the electrolyte exhibited less significant effect on the microhardness and corrosion resistance.
7. The optimized values of pH, current density, Gr concentration and amount of $NiSO_4.6H_2O$ for the maximum value of the microhardness and polarization resistance of Cu-Ni/Gr composite are 4, 6 A/dm^2, 200 mg/L and 95 g/L, respectively.

References

[1] M. Haciismailoglu and M. Alper, “Effect of electrolyte pH and Cu concentration on microstructure of electrodeposited Ni-Cu alloy films,” *Surf. Coatings Technol.*, vol. 206, no. 6, pp. 1430–1438, 2011.

[2] S. K. Ghosh, A. K. Grover, G. K. Dey, and M. K. Totlani, “Nanocrystalline Ni-Cu alloy plating by pulse electrolysis,” *Surf. Coatings Technol.*, vol. 126, no. 1, pp. 48–63, 2000.

[3] S. Roy, “Effect of Corrosion on the Composition of Pulse-Plated Cu-Ni Alloys,” *J. Electrochem. Soc.*, vol. 141, no. 6, p. 1509, 1994.

[4] M. Cherkaoui, E. Chassaing, and K. Vu Quang, “Pulse plating of Ni-Cu alloys,” *Surf. Coatings Technol.*, vol. 34, no. 3, pp. 243–252, Apr. 1988.

[5] A. D. Pingale, S. U. Belgamwar, and J. S. Rathore, “Synthesis and characterization of Cu–Ni/Gr nanocomposite coatings by electro-co-deposition method: effect of current density,” *Bull. Mater. Sci.*, vol. 43, no. 1, p. 66, Dec. 2020.

[6] A. D. Pingale, S. U. Belgamwar, and J. S. Rathore, “A novel approach for facile synthesis of Cu-Ni/GNPs composites with excellent mechanical and tribological properties,” *Mater. Sci. Eng. B*, vol. 260, no. July, p. 114643, Oct. 2020.

[7] A. Pingale, A. Owhal, S. Belgamwar, and J. Rathore, “Electro-co-deposition and properties of Cu-Ni-MWCNTs composite coatings,” *Trans. IMF*, 2020.

[8] A. D. Pingale, A. Owhal, A. S. Katarkar, S. U. Belgamwar, and J. S. Rathore, “Facile synthesis of graphene by ultrasonic-assisted electrochemical exfoliation of graphite,” *Mater. Today Proc.*, no. xxxx, Nov. 2020.

[9] A. D. Pingale, S. U. Belgamwar, and J. S. Rathore, “Effect of Graphene Nanoplatelets Addition on the Mechanical, Tribological and Corrosion Properties of Cu–Ni/Gr Nanocomposite Coatings by Electro-co-deposition Method,” *Trans. Indian Inst. Met.*, vol. 73, no. 1, pp. 99–107, Jan. 2020.

[10] M. E. Turan, Y. Sun, Y. Akgul, Y. Turen, and H. Ahlatci, “The effect of GNPs on

wear and corrosion behaviors of pure magnesium," *J. Alloys Compd.*, vol. 724, pp. 14–23, 2017.

[11] U. Sarac and M. C. C. Baykul, "Morphological and microstructural properties of two-phase Ni–Cu films electrodeposited at different electrolyte temperatures," *J. Alloys Compd.*, vol. 552, pp. 195–201, Mar. 2013.

[12] M. S. Safavi, M. Fathi, S. Mirzazadeh, A. Ansarian, and I. Ahadzadeh, "Perspectives in corrosion-performance of Ni–Cu coatings by adding Y 2 O 3 nanoparticles," *Surf. Eng.*, vol. 0, no. 0, pp. 1–10, Jan. 2020.

[13] I. Mizushima, "Microstructure of Electrodeposited Cu-Ni Binary Alloy Films," *J. Electrochem. Soc.*, vol. 143, no. 6, p. 1978, 1996.

[14] A. T. Lawal, "Graphene-based nano composites and their applications. A review," *Biosens. Bioelectron.*, vol. 141, p. 111384, Sep. 2019.

Chapter 7

Overall Conclusions and Future Scope

7.1 Overall Conclusion

The overall conclusion of the thesis is presented based on work done in the individual chapters. In the present thesis, two synthesis methods have been developed for the Cu-Ni/Gr composite coatings using the electro-co-deposition method and for the Cu-Ni/Gr composite powder using a modified electro-co-deposition method. The later method is followed by the powder metallurgy method to fabricate Cu-Ni/Gr composite pellets. The surface morphology, elemental composition, and microstructure of synthesized Cu-Ni/Gr composite coatings and Cu-Ni/Gr composite powder samples have been studied in detail. The effect of electrolysis parameters such as pH, current density, graphene nanoplatelets concentration and amount of nickel sulfate on microhardness and polarization resistance of Cu-Ni/Gr composite coatings prepared by the electro-co-deposition method are briefly discussed. Also, the statistical modeling for the microhardness and polarization resistance of Cu-Ni/Gr composites prepared by modified electro-co-deposition followed by powder metallurgy method has been studied and discussed. The important results of present study are summarized in the following paragraphs:

The Cu-Ni/Gr composite coatings have been successfully prepared by electro-co-deposition method. The main conclusion can be stated as follows:

1. In chapter 4 and 5, the effect of various current densities (2, 4, 6 and 8 A/dm^2) on surface morphology, elemental composition, microstructure, mechanical, tribological and corrosion properties of composite coatings was investigated. The EDS analysis showed that the content of Gr in the Cu-Ni/Gr composite coating was increased with an increase in current density from 2 A/dm^2 to 6 A/dm^2 and then decreased with further increase in the current density to 8 A/dm^2. The XRD analysis showed that the incorporation of Gr in Cu-Ni alloy coating influenced the crystallite size. The crystallite size of the Cu-Ni/Gr composite coating was decreased with an increase in current density from 2 A/dm^2 to 6 A/dm^2 and then increased with further increase in the current density to 8 A/dm^2. As the graphene nanoplatelets content was increased, the crystallite size of the coating decreased, which in turn increased the microhardness, corrosion resistance and decreased the

coefficient of friction of the coating. The Cu–Ni/Gr composite coating reached the maximum values of desirable properties at 6 A/dm2 of current density.

2. In chapter 4 and 5, the effect of various Gr concentrations (0, 100, 200, 300, and 500 mg/L) in the electrolyte bath on surface morphology, elemental composition, microstructure, mechanical, tribological and corrosion properties of composite coatings were investigated. The EDS analysis showed that the content of Gr in the Cu-Ni/Gr composite coating was increased with an increase in Gr concentration in the electrolyte bath from 100 mg/L to 400 mg/L and then decreased with a further increase in the Gr concentration in the electrolyte bath to 500 mg/L. The XRD analysis showed that the incorporation of Gr in Cu-Ni alloy coating influenced the crystallite size. The crystallite size of the Cu-Ni/Gr composite coating was decreased with an increase in Gr concentration in the electrolyte bath from 100 mg/l to 400 mg/L and then increased with further increase in the Gr concentration in the electrolyte bath to 500 mg/L. The measured microhardness for Cu–Ni/Gr (400 mg/L) composite coating increases by 44.17% compared to pure Cu–Ni coating. Also, the average friction coefficient of Cu–Ni coating was decreased from 0.74 to 0.27 when it was incorporated with graphene nanoplatelets. The immersion study indicates that the incorporation of graphene nanoplatelets stabilizes the corrosion potential and enhances the corrosion resistance.
3. In Chapter 6, the effect of electrolysis parameters on mechanical and corrosion properties of Cu-Ni/Gr composite coatings was studied by statistical method using Taguchi and variance analysis. By Taguchi and regression analysis, it was found that the Gr concentration in the electrolyte is the most influencing parameter of the process for microhardness and polarization resistance of the Cu-Ni/Gr composite coatings. The other process parameters such as pH of the solution and current density supplied showed less significance on the microhardness and corrosion resistance of the Cu-Ni/Gr composite coatings. The addition of Gr decreases the crystallite size of the coating and hence requires more power for penetration, which results in a rise in microhardness. More concentration of the nickel sulfate in the electrolyte results in increase in the amount of Ni in the Cu-Ni/Gr composite coatings and improves the microhardness value. Also, graphene nanoplatelets act as an inert physical barrier to the initiation and growth of corrosion defects and hence improving the corrosion resistance

The Cu-Ni/Gr composites have been successfully prepared by a modified electro-co-deposition method followed by powder metallurgy method. The main conclusion can be stated as follows:

4. In chapter 3, the co-deposition of Gr, copper and nickel was carried out on the tip surface of the cathode electrode during the modified electro-co-deposition method. Arduino-controlled stepper motor mechanism was employed to tap the cathode electrode during the deposition process to drop down the Gr reinforced Cu-Ni matrix powder from the tip surface of the cathode. A modified electro-co-deposition method eliminates the use of the ball milling step in the powder metallurgy method, which helps to prevent Gr from structural damage during processing.
5. In chapter 4, the effect of different concentrations of Gr (0, 50, 100, 150, 200 and 250 mg/L) in the electrolyte bath on the surface morphology, elemental composition, microstructure, mechanical, tribological and corrosion properties of the composites were systematically investigated. The reinforcement of Gr into the Cu-Ni alloy matrix was confirmed from FESEM, EDS, XRD and HRTEM analysis. The SEM analysis showed that the average particle size of pure Cu-Ni alloy and Cu-Ni/Gr nanocomposite powder samples are in the range of 5-15 µm. The uniform dispersion of Gr into the Cu-Ni alloy matrix was observed from EDS and TEM analysis. The Gr and Cu-Ni alloy particles interact at a molecular level and hence dispersion takes place at a molecular level. The XRD analysis revealed that the crystallite size of the Cu-Ni alloy powder sample was decreased by the addition of Gr in the electrolyte bath up to 200 mg/L. When Gr concentration in the electrolyte bath was 200 mg/L, the microhardness of 107 HV, friction coefficient of 0.25, YS of 265 MPa and UTS of 299 MPa were achieved in Cu-Ni/Gr composite, which were 84.5%, 55.3% 138.7% and 90.5% improvement over pure Cu-Ni alloy. The fracture mode of Cu-Ni/Gr composite transforms from ductile fracture to brittle fracture with an increase in Gr concentration. The reinforcement of graphene nanoplatelets in the Cu-Ni alloy matrix fill the defects such as several voids, gaps and cracks owing to its nano size, which contribute the outstanding resistance to the Cu-Ni/Gr composite to undergo corrosion.
6. In chapter 6, the statistical study showed that the Gr concentration in the electrolyte bath and amount of nickel sulfate in the electrolyte had the greatest influence on the synthesis of Cu-Ni/Gr composites. The other electrolysis parameters such as the

current supplied and pH of the electrolyte exhibited less significant effect on the microhardness and corrosion resistance.

7.2 Future Scope of the Work

No research concludes with an absolute end. The proposed work can be extended in many directions, which may lead to further investigations about Cu-Ni/Gr composites. From the perspectives of present work, the following aspects can be investigated further:

1. The enhancement of mechanical, tribological and corrosion properties due to the addition of Gr have been discussed. It would be of both academic and technical interest to study the effect of Gr addition on the electrical and thermal properties of Cu-Ni/Gr composites.
2. Study on computational techniques in Cu-Ni/Gr composites are not yet reported. Computational techniques will help in predicting the properties of the composites without even fabrication.

❖ International Journal Publications

[1] **A. D. Pingale**, S. U. Belgamwar, and J. S. Rathore, "Effect of Graphene Nanoplatelets Addition on the Mechanical, Tribological and Corrosion Properties of Cu–Ni/Gr Nanocomposite Coatings by Electro-co-deposition Method," *Trans. Indian Inst. Met.*, vol. 73, no. 1, pp. 99–107, Jan. 2020, doi: 10.1007/s12666-019-01807-9. **(Springer)**

[2] **A. D. Pingale**, S. U. Belgamwar, and J. S. Rathore, "A novel approach for facile synthesis of Cu-Ni/GNPs composites with excellent mechanical and tribological properties," *Mater. Sci. Eng. B*, vol. 260, no. July, p. 114643, Oct. 2020, doi: 10.1016/j.mseb.2020.114643. **(Elsevier)**

[3] **A. D. Pingale**, S. U. Belgamwar, and J. S. Rathore, "Synthesis and characterization of Cu–Ni/Gr nanocomposite coatings by electro-co-deposition method: effect of current density," *Bull. Mater. Sci.*, vol. 43, no. 1, p. 66, Dec. 2020, doi: 10.1007/s12034-019-2031-x. **(Springer)**

❖ International Conference Publications

[1] **A. D. Pingale**, A. Owhal, A. S. Katarkar, S. U. Belgamwar, and J. S. Rathore, "Recent researches on Cu-Ni alloy matrix composites through electrodeposition and powder metallurgy methods: A review," *Mater. Today Proc.*, vol. 47, pp. 3301–3308, Jul. 2021, doi: 10.1016/j.matpr.2021.07.145. **(Elsevier)**

❖ Book chapter Publications

[1] **A. D. Pingale**, A. Owhal, A. S. Katarkar, S. U. Belgamwar, and J. S. Rathore, "Cupronickel Composites: An Overview of Recent Progress and Applications, RAMMML (2022), ISBN 9781032416311. **(CRC Press)**

Brief biography of the Candidate

Pingale Ajay Dadabhau joined Birla Institute of Technology and Science, Pilani, Pilani Campus, Rajasthan, India in Jan 2018 with broad expertise in material & mechanical characterization, structural design and CAD-Modelling. He completed a B.E. degree in Mechanical engineering from Ajeenkya D Y Patil School of Engineering, Pune, India in 2015, and a M.E. degree in Mechanical Design Engineering from the Ajeenkya D Y Patil School of Engineering, Pune, India in 2017. His research activities focused on composite fabrication, composite characterization, development of composite fabrication methods, synthesis of nanomaterials, pool boiling heat transfer and finite element simulation of various composites.

Brief biography of the Supervisor

Dr. Sachin U Belgamwar received his B.E. degree in Mechanical Engineering from Anuradha Engineering College, Chikhli, Amaravati University, India in 1999, and the M.E. and Ph.D. degree in Mechanical Engineering from Birla Institute of Technology and Science, Pilani India, in 2001 and 2014 respectively. His Ph.D. research was on "Investigations on Multiwalled Carbon Nanotube Reinforced Copper". After working for six years in different engineering colleges, he joined the Mechanical Engineering Department, Birla Institute of Technology and Science, BITS-Pilani, Pilani Campus, in January 2007 as a Lecturer. Currently he is working as Assistant Professor in Mechanical Engineering Department and he also holds the position of Faculty-in-Charge, First Degree (FD) Admission at Birla Institute of Technology and Science, Pilani Campus, India. His area of research is on

- Electrochemical synthesis of carbon nanotube reinforced metal matrix composites.
- Quantification of carbon nanotube distribution in composite and microstructure property correlations.
- Thermo-physical properties and characterization of the nanocomposite.
- MEMS

He has 15+ years teaching expertise on MEMS, Thermodynamics, Power Plant Engineering, Transport Phenomena, Mechanics of Solids, Fluid Mechanics, Computer Aided Design and Kinematics and dynamics of Machines. He has supervised several Ph.D., master and undergraduate students for thesis and project work.

Dr. Belgamwar has been served as Principal Investigator and Co-Principal Investigator in many projects based on CNT reinforced Metal Matrix Composites, Electrical characterizations of nanocomposites, Dynamic modelling and Experimental Analysis of Double Row Deep Groove Ball Bearing with Multiple Localized Defects funded by BITS-Pilani Seed Grant, Research Initiation Grant and Aerodynamics R&D Board respectively, Currently he is Principal Investigator of an on-going project based on "Powder assistive hybrid e-trike (PAH e-trike) for disabled person in rural and urban region of India". He has more than 30 national and International publications and one granted patent on "method of producing uniform mixture of copper and carbon nanotube in bulk for copper metal composites".

Brief biography of the Co-Supervisor

Prof. Jitendra Singh Rathore completed his B.E. (Mechanical) from M. B. M. Engineering College, Jodhpur, M. Tech. (Machine Design) from Indian Institute of Technology, Roorkee, and Ph.D. from Birla Institute of Technology and Science (BITS), Pilani. After working for four years in Indian Ordnance Factories Organization, he joined the Mechanical Engineering Department, BITS, Pilani, India, in December 2006. Currently, He is a faculty in Mechanical Engineering Department, BITS, Pilani for over 15 years and serving as an Associate Professor. His research interests include nanorobotics, low Reynolds number hydrodynamics, skin tribology and bio materials.